Combustion Research Facility
Energy Laboratory
Massachusetts Institute of Technology
Cambridge, MA 02139

Transformation of Coal Mineral Matter During Pulverized Coal Combustion

Principal Investigators

Prof. János M. Beér and Prof. Adel F. Sarofim

Associate Investigators

Dr. László E. Barta
Dr. Majed A. Toqan
Valerie J. Wood
Dr. J. Derek Teare

Final Report
December 1992

Sponsored by

New England Power Service Co.
ABB-Combustion Engineering
Public Service Electric & Gas Co.
Empire State Electric Energy Research Corp.
ENEL S.p.A.
Electric Power Research Institute

DISCLAIMER

Prepared by the Massachusetts Institute of Technology, Cambridge, Massachusetts

ABSTRACT

The theoretical development of a sequence of mathematical sub-models capable of calculating the fouling tendency of a coal based on microscopic analysis of the coal mineral matter is described. The sub-models interpret computer controlled-scanning electron microscope analysis data in terms of mineral size and chemical composition distributions; follow the transformation of these mineral property distributions during the combustion of the coal; determine the probability of the resultant fly ash particles impacting on boiler-tube surfaces and of their sticking upon impaction. The sub-models are probabilistic, and take account of the particle-to-particle variation of coal mineral matter and fly ash properties by providing mean values and variances for particle size, chemical composition and viscosity. The various sub-models are combined into a Coal Fouling Tendency (CFT) computer code. Comparison of CFT modeling results obtained for any coal or coal blend with those obtained for a coal whose behavior in a given boiler plant is known, can give useful information on their relative fouling tendencies.

The report also includes data on the deposition characteristics of five coals or coal blends, obtained from combustion experiments in the 1-2 MW flame tunnel at MIT. The measurement data were used for validation of the CFT calculations, and for ranking the five fuels with respect to their fouling behavior. Similar ranking of other coals, without combustion testing, can be based solely on results from the CFT model, and examples are given in the report.

ACKNOWLEDGEMENTS

Most of the information presented in this report has been supported by a consortium of private companies from the energy and electric utility fields. The authors gratefully acknowledge the support from ABB-Combustion Engineering, Inc., Electric Power Research Institute, Empire State Electric Energy Research Corporation, New England Power Service Company, and Public Service Electric and Gas Co. Support for earlier phases of the project was also provided by AMAX Coal Co., American Electric Power, Canadian Electrical Association, Detroit Edison Co., Northeast Utilities Service Co., Nova Scotia Power Corp, and Shell Development Co.

The authors also acknowledge the major role played by Dr. Peter M. Walsh. As one of the original co-principal investigators on the program, he made key contributions to both the experimental and the theoretical investigations which had laid the foundations for the model development discussed in this report. David O. Loehden and Dr. Larry S. Monroe also made significant contributions during the course of the research.

One of the authors, László E. Barta thanks his institute in Hungary (EGI) and the U.S. Fulbright Foundation for financial support. All the drafts and the final version of this report were typed and edited with the excellent assistance of Ms. Bonnie Caputo of the MIT Energy Laboratory.

As indicated in the text, some data used in the validation of the modeling were generated during the combustion of coal-water-fuels during a US-DOE project under Contract Number DE-AC22-89PC88654 in which MIT was a subcontractor of ABB-Combustion Engineering, Inc.

TABLE OF CONTENTS

LIST OF FIGURES

LIST OF FIGURES (continued)

LIST OF FIGURES (continued)

LIST OF FIGURES (continued)

LIST OF FIGURES (continued)

LIST OF FIGURES (continued)

LIST OF FIGURES (continued)

LIST OF TABLES

LIST OF TABLES (Continued)

NOMENCLATURE

A : surface area of the inner char core (of radius δ); *or* total tube surface area (m^2)
A_i : surface area of i^{th} cross-sectioned inclusion particle; *or* surface area of cross-sectioned inclusion particle after distribution of the ion-exchangeable mineral matter (m^2)
A_{ij} : cross-sectional area of particle of size x_i, having concentration of a chemical compound c_j (m^2)
A_t : clean tube surface (m^2); *or* total air/fuel mass ratio
A_{st} : sticky surface of tube (m^2)
A_{nst} : non-sticky surface of tube (m^2)
a_{inc} : inclusion content of a coal particle, random variable
a_{ion} : ion-exchangeable mineral matter content of a coal particle, random variable
a : projected area of fly ash particle (m^2)
B : constant calculated from particle chemical composition (Section 2.3, viscosity)
C_D : drag coefficient
c_{air} : specific heat coefficient of air (kJ/kg-K)
c_i : concentration of a chemical compound of "total" mineral inclusions, random variable
c_i : recalculated concentration of chemical compound after sulfur removal
c_i^{ion} : concentration of a chemical compound in the ion-exchangeable mineral matter
$c_{p\ air}$ and $c_{p\ flue\ gas}$: heat capacity of air and flue gas (kJ/kg-K)
D_c, D_{coal} : coal particle diameter (m)
d, d_p : diameter of a fly ash particle (m)
d_t : tube outer diameter (m)
$E(\eta)$: mean impaction efficiency
F : constant calculated from particle chemical composition (Section 2.3, viscosity)
$F_{chem}(t)$, $F(t)$: distribution of chemical composition of fly ash, with t being the concentration of a chemical compound
$F_{size}(y)$: size distribution function of fly ash
$f(D)$: probability density function of actual size, D
$f(c)$: distribution of chemical composition of "total" inclusions
$f(x)$: size distribution of "total" minerals
$f(x,c)$: joint size-chemical composition of "total" minerals
$f_a(y)$: two-dimensional distribution function of particle size
$f_v(y)$: three-dimensional distribution function of particle size
$f_m(\rho,x)$: joint size and density distribution of fly ash, mass-based
$f(c_i,x_j)$: joint size-chemical composition distribution function
$g(A)$: probability density of measured section area, A
$g(c,y,t)$: special probability function (Section 3.3.16)
g_{ash} : fly ash mass flux ($kg/m^2/s$)
H : deposition thickness (m)
H_i : lower calorific value of coal (kJ/kg)
h_{air}, h_{gas} : heat conduction coefficient of air and flue gas (kJ/m^2 -s-K)
K : value of the ratio of n/n_o (Section 3.3.12)
K_{dep} : specific heat conductivity of deposit (kJ/m-s-K)
K_{tube} : specific heat conductivity of tube (kJ/m-s-K)

K_{gas} : specific heat conductivity of gas (kJ/m-s-K)
k_{imp} : constant for impaction efficiency (m^{-1})
k_{st} : constant for surface sticking efficiency (m^{-1})
k : number of eroded particles per impacting particle
L : length of tube investigated (m)
M : total mass deposited (kg)
M_i : the i^{th} moment of size distribution
$M_i(c)$: the i^{th} moment of "total" inclusion size distribution of a chemical composition c
M_{3inc} : third moment of inclusion size distribution
m_{air} : mass flow of cooling air (kg/s)
m : mass of a fly ash particle (kg)
$\tilde{N}_{inc}$: number of inclusions in a coal particle, random variable
N_{inc} : mean value of N_{inc}
N : number of fly ash particles
n_o, n : number of inclusion particles in a coal particle before and after coalescence of mineral matter
Δn : the value of n_o - n
P_i : perimeter of the i^{th} cross-sectioned inclusion particle (m)
Pr_{gas} : Prandtl number of gas
Pr_{air} : Prandtl number of air
p(A/D) : probability of measuring a section area, A from a particle size of D
Re_{air} : Reynolds number of air
Re_{gas} : Reynolds number of gas
Re_p^o : particle Reynolds number at relative velocity of U
Re_p : actual particle Reynolds number
Stk : Stokes number
Stk_{eff} : effective Stokes number, $\psi \times$ Stk
T : temperature (K or °C)
T^* : surface temperature of deposit (K)
T_{air}^o : initial temperature of cooling air (K)
ΔT_{air} : inlet combustion air temperature (K)
U : flue gas velocity, free flow (m/s)
V_t : total flue gas/fuel mass ratio
w : event of writing a data record into a random computer file
X : clean tube surface area fraction
Y_n : random variable of a particle property (e.g., size) after n^{th} time step
ΔY_n : transition random variable at n^{th} time step
Y : non-sticky tube surface area fraction
Z : sticky tube surface area fraction
α : parameter used in Section 2.9.4 (s^{-1})
$\alpha_{1,2}(t)$: special functions for the calculation of the chemical composition distribution of fly ash (Section 3.3.15)
β : parameter used in Section 2.9.4 (m/s)
Γ^* : incomplete gamma function

δ : transition radius (m)
η : viscosity (poise)
η_{crit} : critical viscosity for particle stickiness (poise)
η_{st} : sticking fraction of impacting fly ash particles at flue gas temperature
η°_{st} : sticking fraction of impacting fly ash particles at initial tube temperature
η^{*}_{st} : sticking fraction of impacting fly ash particles at deposition surface temperature
η_{imp} : impacting fraction of fly ash particles at clean tube surface
η^{*}_{imp} : impacting fraction of fly ash particles at actual deposition surface
$\eta_{imp}(\rho,x)$: impaction efficiency of a particle of size x, and of density ρ
$\lambda_{1,2}(t)$: special functions for the calculation of the chemical composition distribution of fly ash (Section 3.3.15)
μ_g : gas viscosity (poise)
ρ_d : bulk density of deposit (kg/m^3)
ρ_{ij} : density of particle of size x_i, with chemical compound concentration c_j (kg/m^3)
ρ_{inc} : mean density of the mineral inclusions (kg/m^3)
ρ_p : fly ash particle density (kg/m^3)
ψ : correction factor for derivation of Stk_{eff} (Section 2.7)

EXECUTIVE SUMMARY

Advances in our understanding of the details of chemical and physical processes of deposit formation in pulverized coal-fired boiler plant have led to the development at MIT of a Coal Fouling Tendency (CFT) computer code. Through utilization of a number of mathematical models and computer sub-codes, the CFT is capable of predicting the *relative* fouling tendency of coals. The analytical input data to the code are the ultimate analyses of the coal, extended by the size and chemical composition distributions of mineral inclusions determined by CCSEM, and the amount and type of organically-bound minerals in the coal.

The procedural steps in the CFT model include:

- interpretation of CCSEM data on size and chemical composition of coal mineral matter.
- sub-model to account for particle-to-particle variation of mineral matter properties in the coal.
- fly ash generation sub-model capable of predicting fly ash size and composition distributions for sub-bituminous and bituminous coals.
- sub-model to obtain the impaction and sticking efficiency of the resulting fly ash as a function of temperature via the determination of the statistical variation of particle size and viscosity.
- calculation of the fly ash deposition rate for a range of flue gas temperature.

Through the combined use of these sub-models, the relative fouling tendencies of a coal or a blend of different coals can be assessed.

Validation of the predictions of the CFT code is based on experimental data obtained in the MIT Combustion Research Facility, a 1-2 MW flame tunnel capable of simulating the combustion conditions in a utility boiler. Using various pulverized coals and coal blends as fuel, measurements were taken of the fly ash deposition on tubes inserted with the flame tunnel. Deposit formations were monitored for periods up to two hours in duration on stainless steel tubes. Throughout this report the combustion gas temperature in the vicinity of a tube surface is characterized as the "flue gas temperature." Deposition data were obtained at two flue gas temperatures for each type of coal or coal blend.

Based on comparisons with the experimental data, the CFT model has yielded a number of both qualitative and quantitative conclusions. Following are the qualitative conclusions:

- The distributions of both particle size and chemical composition of mineral matter are modified by the same random coalescence process during the coal burnout.

Therefore the changes of these mineral matter properties are inter-dependent. The rate of change depends on the number of mineral particles within the coal particle, the first and second moment of the inclusion size distribution and the radius of transition from diffusion-controlled to kinetically-controlled combustion;

- While both the mean value and the standard deviation of the mineral size distribution are increased, the standard deviations of the chemical composition and the particle viscosity are decreased by the random coalescence process of the coal mineral matter.

- The increase of mineral particle size contributes to higher fly ash impaction efficiency, and the decrease of the variance of particle viscosity lowers the variance of the sticking efficiency as the flue gas temperature increases.

- At constant initial surface temperature of the target tube, the deposition mass per unit projected tube surface area increased linearly with time. The deposition rate (mass of accumulated deposit per unit projected tube surface area per unit time) increased with increasing flue gas temperature.

- The sensitivity of the fly ash deposition rate to flue gas temperature increases with increasing gas temperature due mainly to the decreasing standard deviation of the sticking efficiency with increasing gas temperature.

The quantitative predictions of the CFT model were tested experimentally on five coals of different characteristics. The measured size and chemical composition distributions of fly ash were compared with predictions and good agreement was obtained. CFT predictions were also made for fly ash deposition rates over a wide temperature range that included the two experimental temperatures for each coal, and in all cases the predictions were in good agreement with the experiments.

The deposition predictions provide data that can be used to rank the five coals with respect to their deposition behavior. Such ranking can be made for a given combustion system or boiler without any details of the combustion system being available *a priori*, as long as an appropriate comparison temperature is used for each coal. For ranking purposes, in this report we assign to each coal a "comparison flue gas temperature" that is calculated by taking 62% of the adiabatic flame temperature for that coal. Based on the CFT deposition prediction at the appropriate comparison temperature for each coal, the fouling tendency of the five coals (ranked from low to high) is summarized below:

1./ Mapco bituminous coal: low fly ash mass flux due to low ash content/heating value; low impaction efficiency was measured due to fine distribution of fly ash size distribution; the fly ash deposition rate at the comparison flue gas temperature was low.

2./ Blend coal of 70% Wyoming lignite and 30% Oklahoma bituminous coal: the blending of Oklahoma coal with Wyoming lignite changed the behavior of the fly ash sticking efficiency with temperature, *relative to the unblended lignite,* in two significant ways. i) Blending increased the minimum flue gas temperature at which fly ash deposition occurred, ii) When appropriate comparison temperatures are selected for the two cases, the coal blend exhibited lower fly ash sticking efficiency.

3./ Wyoming lignite: large standard deviation of fly ash particle viscosity caused a relatively high sticking efficiency of the fly ash even at relatively low flue gas temperature, which resulted in a higher fly ash deposition rate than for the blended coal discussed above.

4./ Island Creek bituminous coal: a coarse size distribution of fly ash was generated due to the coarse coal size distribution which resulted in high impaction efficiency.

5./ Jader bituminous coal: high proportion of extraneous mineral matter of coarse size distribution gave high impaction efficiency. Also the high fly ash flux contributed to high fly ash deposition rate.

The report also contains a similar ranking of five different coals, based solely on CCSEM measurements of pulverized samples of each coal, coupled with ultimate analysis data and a characterization of the organically-bound mineral contents. Recommendations are presented for future research to enhance the usefulness of the CFT predictions. One such enhancement to the CFT code would address deposit hardness through inclusion of a submodel of the process of sintering within the deposited fly ash material.

SECTION 1

INTRODUCTION

Research has been moving steadily to relate ash chemistry of different coal gravity fractions to the deposition potential of coals (Bryers and Taylor, 1976). Borio and Narcisco (1979) suggested that the composition of ash fractions of higher specific gravity be used for the calculation of the slagging index, while that of the lower specific gravity be used for the fouling index. However, the correlation between data of standard (ASTM) bulk chemical analyses of coal ash and deposition characteristics has been rather poor.

The application of computer-controlled scanning electron microscopy with automated image analysis (CCSEM) for the analysis of the coal, pioneered by Huggins et al. (1980), provides a powerful tool for the determination of the compositions and sizes of individual mineral inclusions in the coal. In particular, CCSEM makes it possible to collect statistically significant amounts of data on individual mineral particles in a reasonable period of time and at an affordable cost.

For the past decade, a research project has been conducted at MIT under sponsorship of an industrial consortium that has included electric utilities and utility research organizations, coal supply companies, and a boiler manufacturer. The goal has been the attainment of improved understanding of the deposition of ash on heat exchanger surfaces in pulverized coal combustion. Much of the experimental work was carried out in the MIT Combustion Research Facility (CRF), a 1-2 MW pilot-scale flame tunnel. Supplementary experiments were also undertaken in laminar-flow "drop-tube" furnaces. Extensive modeling effort has been invested in support of the experimental work. Prior results have been reported in various ESEERCO reports (see Section 8.1), MIT theses (Loehden, 1988; Monroe 1989), and refereed papers (Loehden et al., 1989; Barta et al., 1990 & 1992; Beér et al., 1992). Other publications include Barta et al. (1989 & 1991) and Beér et al. (1990).

It should be stressed that the rate of deposit accumulation (fouling) on boiler heat exchange surfaces is dependent not only on the coal type but also on the design and operating variables of the boiler-combustion plant. Prediction of absolute values of boiler fouling for different designs and operating conditions extends beyond the scope of the present MIT study. We have established, however, that it is already feasible to determine *relative* fouling tendencies (RFT) for different coals, which can be used for the assessment of the performance of a coal or a blend of coals when compared with that of a coal regularly used in the same plant.

Earlier phases of the MIT research have established a broad data-base on the deposition characteristics of a range of coals, and validated a number of theoretical models of the processes leading to the formation and possible deposition of fly ash particles. The most recent phase, reported here, has two principal objectives -- namely, extension of the data-base for model validation, and integration of a number of computational codes to yield a single "user-friendly" Coal Fouling Tendency (CFT) code.

The various computational segments of the CFT code provide the characterization of coal mineral particles by CCSEM, prediction of the fly ash size and composition distributions, and predictions of the probability of impaction of the fly ash on heat exchange surfaces and of their retention due to the viscous characteristics of the fly ash. The sub-models and their interrelationship in this modeling sequence are illustrated in Figure 1. The following points are noted:

- The only experimental-analytical input needed for the modeling is the computer controlled-scanning electron microscopy of the coal for determining the mineral matter size and chemical composition distributions.

- The stereological correction program is based on a statistical method to generate 3-dimensional size distributions from the 2-dimensional sectioned area size distributions.

- The coalesceable fraction (fraction of sufficiently low viscosity) of the mineral matter is calculated from coal mineral size and chemical composition distributions.

- Probabilistic calculations of particle-to-particle variation of chemical composition of the coalesceable fraction provide mean values and variances of individual chemical species concentrations.

- The framework of a physical model for the coalescence of mineral inclusions during combustion is set by the application of the combustion model and the implications of the char combustion mechanism for the movement and relative positions of the mineral particles in the course of the char burn-out.

- The random coalescence model provides information on fly ash size and chemical composition distributions.

- The fly ash size and density distributions serve as inputs to the fly ash impaction model calculations.

- The fly ash chemical composition can be used to estimate the distribution of slag viscosity for a given temperature and hence the "sticking coefficient".

- The impaction and sticking efficiencies are the most important parameters to calculate the relative fouling tendency (RFT) of the coal or blend of coals in question.

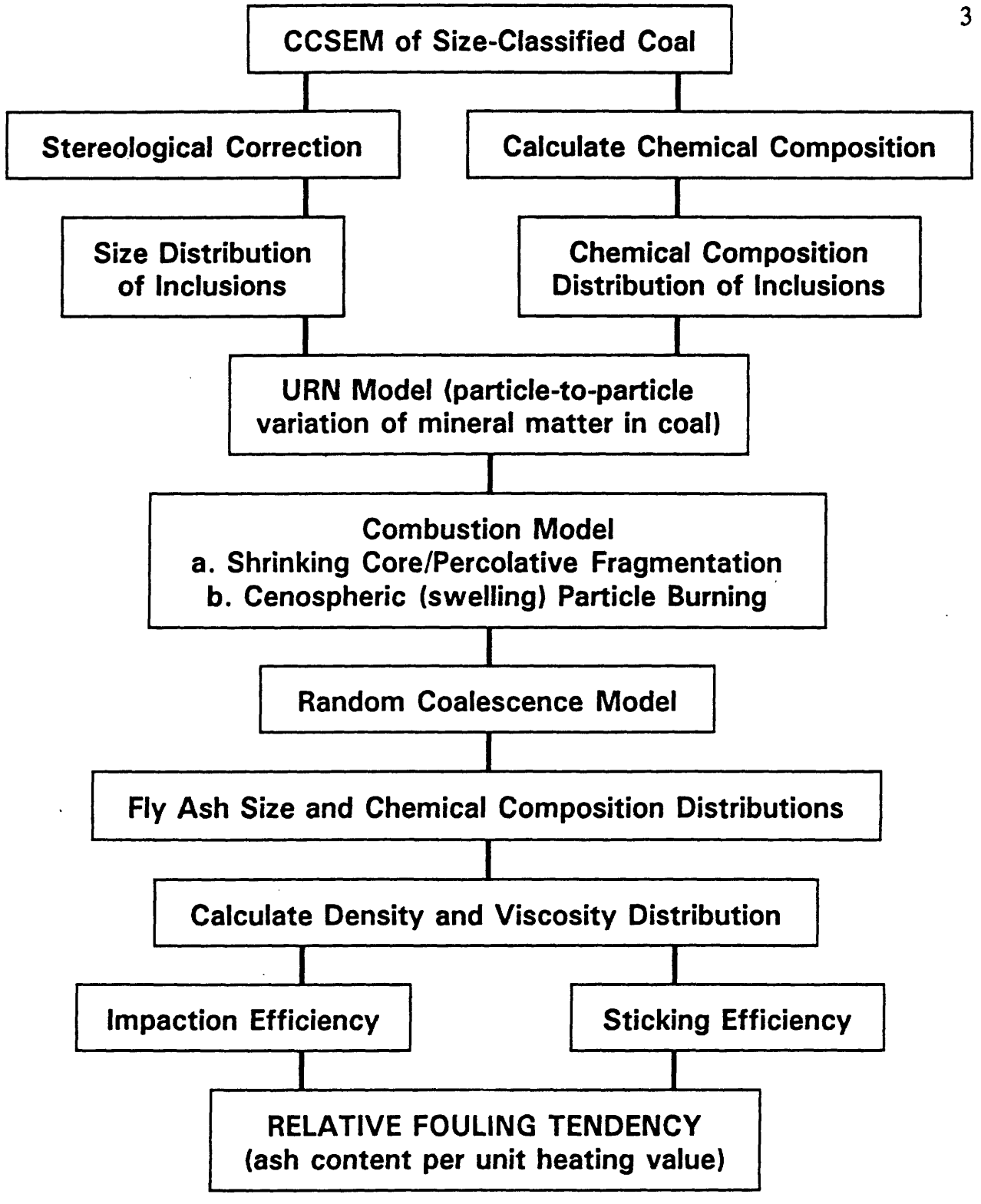

Figure 1. Coal Fouling Tendency Model (CFT)

The elements of this model are based on theoretical and experimental studies carried out on industrial type and size pulverized coal flames in the MIT Combustion Research Facility.

There are caveats. Such a model by the complexity of the process it describes is necessarily incomplete. Deposited fly ash may be eroded by the more abrasive constituents of the fly ash (e.g., quartz). It may slough off when a certain thickness of deposit is reached. There may be further transformations of sintering and crystallization in the deposit over longer periods of time if it is not removed, and this may affect the eventual cleanability of the deposit, etc.

These elements of the state and transformation of the ash are, however, beyond the scope of this work. While they may not be neglected in many cases, e.g., for long-term behavior of deposit, their effect in our investigation is considered to be of second order, unlikely to change the relative fouling tendency of the fly ash determined by the model.

In the balance of this report we will first characterize the various components of the CFT model. Section 2 provides a narrative description of these components, following the flow chart of Figure 1. These descriptions contain the governing equations wherever appropriate, but many of the algebraic details are deferred until Section 3 or Appendix A. The most comprehensive prior descriptions of these components of the CFT model were given by Beér et al. (1992), and by Barta et al. (1992). Figures 1 through 12 are taken from these two published papers, with acknowledgements wherever previous publication had occurred.

Section 3 provides a detailed description of the coupling of these component sub-models into the "Coal Fouling Tendency" code, including the specification for the input data files. A logic diagram is given in Figure 13.

The remaining sections of this report deal with the entire body of experimental and computational work carried out during the most recent phase of the research project. Five coals were studied in the CRF, and the experimental results and data analysis are given in Section 4, with the aid of Figures 14 through 92 and Tables 1 through 26.

Section 5 deals with the comparison of CFT model predictions with the experimental data for these five coals, and makes use of Table 27 and Figures 93 through 110. Finally we move, in Section 6, to a discussion of relative fouling tendency, not only for the five coals tested in the CRF, but also for five additional coals that were ranked purely on the basis of CCSEM measurements of pulverized samples of each coal (coupled, for each sample, with data on the ultimate analysis and with knowledge of the organically bound mineral content). The latter five samples, provided by the consortium member ENEL S.p.A., are identified by individual names, but collectively are referenced as the "ENEL coals" (or coals from Italy), to distinguish them from the "CRF coals" that were the subject of combustion tests. Section 6 includes Figures 111 through 117, and Tables 28 through 32. Conclusions drawn from this body of work are summarized in Section 7, and recommendations are made with respect to further research effort.

SECTION 2

THEORETICAL CONSIDERATIONS

The following subsections describe the components (or sub-models) of the CFT model. Since the intent is to provide a continuous narrative, some of the algebraic details are deferred until Section 3, or treated in Appendix A.

2.1 Automated Image Analysis with the Electron Microprobe

Mineral inclusions in pulverized coal and fly ash particles are analyzed by automated image analysis using a Joel 733 Superprobe with a Tracor Northern TN5500 Mini-Computer as a controller. The procedure for analysis is similar to the methods presented by Lee et al. (1980); Moza et al. (1979); Huggins et al. (1980); and Huffmann and Huggins (1984). Samples of coal or fly ash mixed with epoxy resin are hardened and polished, and the polished surface of the pellet is carbon coated to prepare it for microprobe analysis. The measurement begins with running the Particle Recognition and Characterization (PRC) program on the Tracor Northern Computer. It has been shown by Barta et al. (1989), the statistical error at the two ends of the size distribution function can be significant due to the small number of available particles in the sample. It is therefore necessary that a different number of random fields should be set up at different magnifications to obtain a statistically significant number (mininum of 500) of particles for each size class.

The microprobe is operated using a back scattered electron detector, which provides the best contrast between mineral inclusions/fly ash and the coal or epoxy. The PRC program directs the beam to scan the field until a particle is found as determined by a higher intensity than the background. The area, perimeter, shape factor and the minimum, maximum and average diameters for the particle are determined. After the size of a particle is measured, the beam is placed at its center and energy dispersive x-ray spectral counts (EDS) are accumulated for about five seconds. Total counts on 13 elements (Na, Mg, Al, Si, P, Cr, S, Cl, Ca, K, Ba, Ti and Fe) are obtained and normalized. The information so acquired by the Tracor Northern Computer is sent to an IBM microcomputer for further data processing.

A program has been written (Loehden, 1988 and Horváth, 1989) for the IBM XT microcomputer to read the Tracor Northern data file and convert the EDS counts to oxide weight percents using calibration curves developed for standard materials. The minimum detectability limit is checked for each element. The program then classifies the particles into classes using composition classification limits according to the guidelines published by Huggins et al. (1980). The size and composition distribution for each of the mineral and fly ash categories are stored in separate files for further calculations.

2.2 Correction of Microprobe Size

A single measurement of size (either planar area or linear segment length) taken on a random section of a particle of a given shape has an upper bound of the true value, but is very likely to be smaller. Although it is not possible to determine the size of an individual particle from a single random section, the size distribution of a collection of similarly shaped particles can be determined from the distribution of measured areas. For spherical particles, an Abel transformation can be used to correct the data to give the actual size distribution.

The governing equation for the transformation of actual size and sectioned area was given by King (1982):

$$g(A) = \int_0^\infty p(A/D)\ f(D)\ dD$$

where
- $g(A)$ = probability density of measured sectioned area, A
- $p(A/D)$ = probability of measuring a section, A, from a particle of size D,
- $f(D)$ = probability density of actual size D.

The distribution of sectioned areas from a single-sized particle of a given shape, p(A/D), can be found by analytical methods, experimental determinations, or numerical simulations (King, 1982). Monroe (1989) used a numerical simulation similar to that by Dinger (1975) to develop the kernel functions for a number of shapes: cubes, tetrahedrons, hexagonal prisms, etc.

2.3 Coalesceable Fraction of the Mineral Matter

At this point in the calculations the coalesceable fraction of the coal mineral matter is separated from the rest, mainly quartz, so that further analysis can be focused on the former fraction.

Approximate calculations of mineral particle viscosity variation with temperature can be made from known chemical composition of the mineral matter. Barta and Beér (1990) combined the viscosity relationship by Watt and Fereday (1969) with the probabilistic calculations of the particle-to-particle variation of chemical composition to predict a particle-to-particle variation of the particle viscosity at a given temperature.

Watt and Fereday's relationship is given as:

$$\log \eta = \frac{10^7\ B}{(T-150)^2} + F$$

where
- η is viscosity in poise
- T is temperature °C

and B and F are constants calculated from the composition of the particles.

Since the fractional mineral oxides concentrations are random variables, η is also a random variable. From the chemical compositions of individual mineral particles it is possible to calculate approximate viscosity distribution at any given temperature. As an illustration, results for a Texas lignite are shown for 1773 K and 1273 K, respectively, in Figure 2. It can be seen that the variance of the viscosity distribution decreases with increasing temperature. By calculating the particle viscosity at a given temperature, it is possible to arrange the mineral particles into two groups: one having particle viscosity values lower than a critical value, say 10^6 poise, and the other having particle viscosity values higher than the critical viscosity value. Since the mineral matter is often a physical mixture of different mineral types of different size distributions (e.g., clay and pyrite), it is likely that the previous two groups of mineral particles have two different size distributions. This is shown in Figure 3, where the size distributions of mineral particles of the Texas lignite having viscosities, calculated at 1273 K, lower and higher than 10^6 poise, respectively, are plotted. The results show that the mean value and standard deviation of the size distribution of mineral particles having viscosities lower than the critical value are smaller most likely because of their higher content of low melting point alkali compounds. By assigning a value for a critical viscosity below of which mineral particles will coalescence, an estimate of the coalesceable fraction of the mineral matter can be obtained.

2.4 Urn Model (particle-to-particle variation of mineral matter properties in coal particles)

In order to apply the information gained on a limited number of coal particles to a large number of coal particles in a pulverized coal, it is necessary to know the particle-to-particle variations of mineral particle parameters such as total volume, chemical composition, etc.

Various researchers (e.g., Charon et al., 1990) have used computational approaches to the modeling of the random distribution of mineral inclusions among coal particles. In contrast, Barta et al. (1989 and 1990) developed a probabilistic method, which yields an analytic solution to the problem of the particle-to-particle variation of mineral properties. In this so-called "urn" model, CCSEM information is used on the number-based distributions of inclusion size and mineral oxide content (e.g., SiO_2). The mass of each mineral class found in a narrow mineral particle size range is subdivided into equal size small fractions, and these fractional masses are distributed randomly among coal particles of a narrow size range. In the model, the "urns" represent coal particles of the same size into which fractions of mineral oxides are "thrown" i.e., distributed with equal probability (Figure 4). By summing up the mineral volume in a coal particle, the probabilistic distribution of a mineral oxide in a narrow size range of coal particles can be determined. The distribution can then be integrated over a broad spectrum of particle size range.

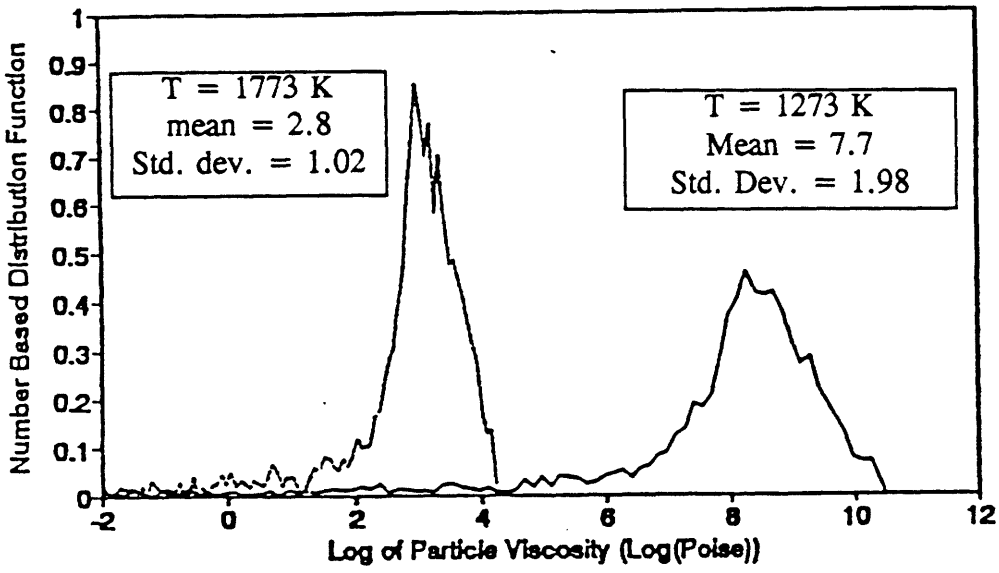

Figure 2. **Mineral Matter Viscosity Distribution**
Texas Lignite of 64-75 μm.
After Barta and Beér (1990).

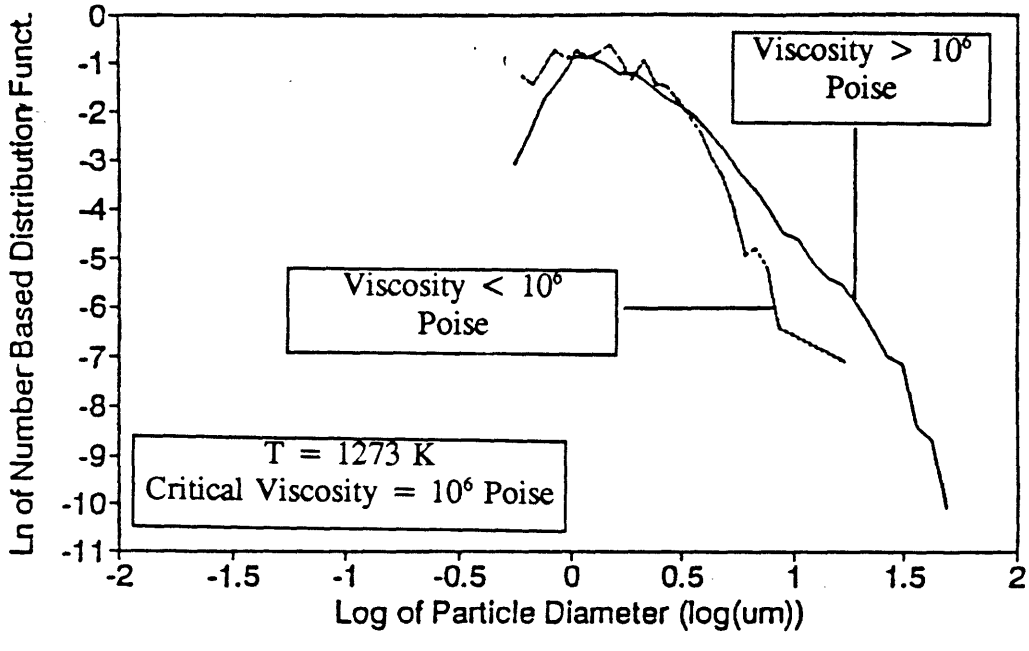

Figure 3. Size Distribution of Mineral Matter
Texas Lignite of 64-75 μm.
After Barta and Beér (1990).

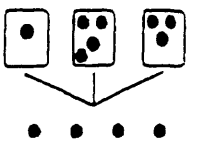

equiprobable
distribution

The probability of finding "j" number of balls in an URN is:

$$P(\nu = j) = \frac{\lambda^j}{j!} * e^{-\lambda}$$

where

$$\nu = \textit{No. of balls per one URN}$$

$$\lambda = \frac{n}{m} = \frac{\textit{No. of mineral particles of size of D}}{\textit{No. of coal particles of volume of V}}$$

Figure 4. Urn Model for Monosize Mineral and Coal Particles. After Barta et al. (1990).

Poisson distribution of mineral particles in the "urns". The distributions of surface or volume (mass) fractions do not directly obey Poisson laws but can be obtained by Fourier transforms of the Poisson distributions.

The Taylor series expansion of these latter functions gives more easily handled approximate expressions (e.g., gamma distribution function) for the distribution of the convoluted random variables (mineral surface or volume fractions in a coal particle). These calculations yield mean values and variances, values that can be directly compared with and tested by experimental data (CCSEM) as seen in Figure 5. Details of the above theory can be found elsewhere (Barta et al., 1989).

The urn model can be used to make prediction of the fly ash viscosity distribution assuming total mineral matter coalescence in each coal particle. The prediction can be tested by calculating from CCSEM measurements the total chemical composition of mineral matter in a single coal particle and by analyzing a sufficient number of coal particles. The results obtained on the Texas lignite can be seen in Figure 6. This figure also shows the comparison of the viscosity distributions of the mineral matter without and with total coalescence. It shows that due to the random allocation of mineral matter into coal particles, the viscosity distribution of an imaginary fly ash particle (total coalescence case) has a smaller standard deviation than the mineral matter obtained for the fly ash with no mineral matter coalescence.

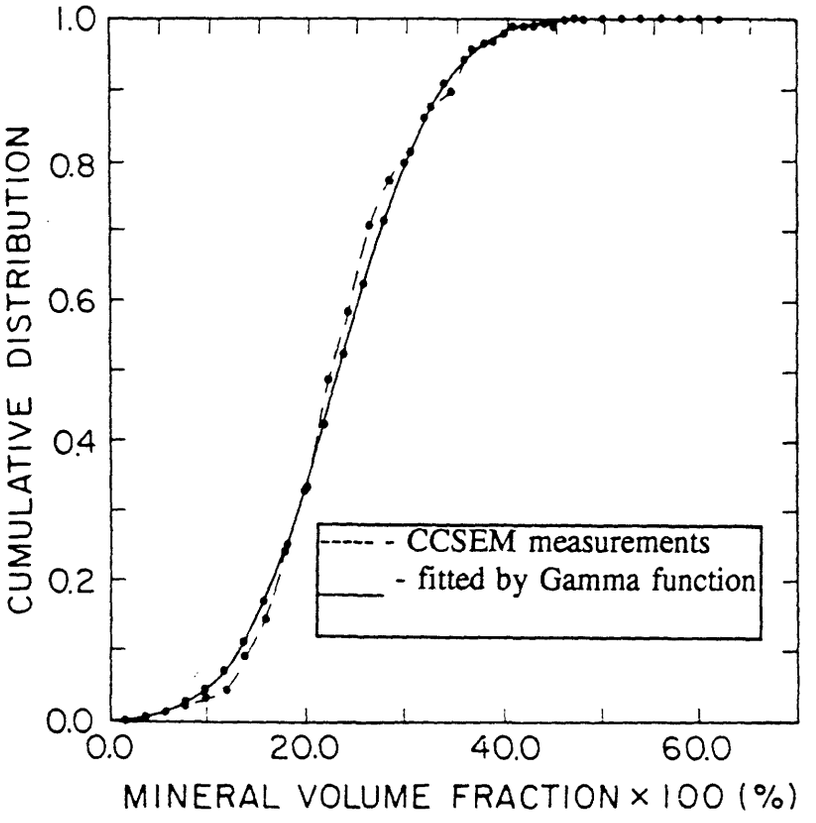

Figure 5. **Mineral Volume Fraction Distribution in Texas Lignite of 64-75 μm.**
After Barta et al. (1990).

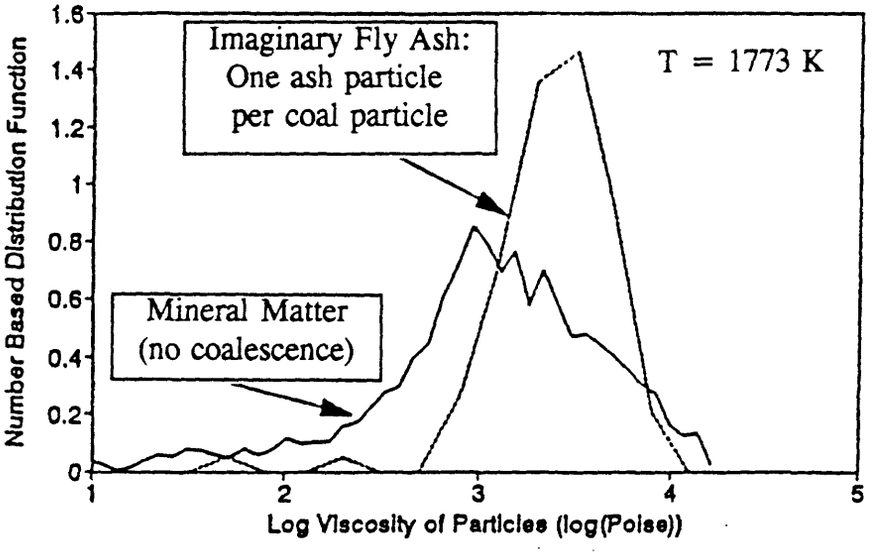

Figure 6. **Viscosity Distributions of Imaginary Fly Ash and Mineral Matter.**
After Barta and Beér (1990).

2.5 Combustion and Mineral Coalescence Models

There are a number of models of particle fragmentation during char combustion (Kerstein and Niksa, 1983; Srinivasachar et al., 1988; Kang et al., 1988) which bear on the problem of coal mineral matter coalescence during combustion and hence the formation of fly ash from the coal mineral matter. While these models make valuable contribution to our insight into the qualitative details of the physical-chemical processes involved, their inclusion into quantitative models of mineral matter coalescence would require at present further assumptions to be made on the relation of coal structure and char fragmentation.

Results of well controlled pilot-scale experiments showed that with the exception of rare coal mineral matter compositions, e.g., very high sodium content, the size distribution of the fly ash formed in the U.S. coals studied in the MIT-CRF resembled closely that of the coal mineral matter (Loehden et al., 1989; Monroe, 1989). This result is important for calculation of fly ash impaction probability on a deposition target.

A comparison of the distributions of the chemical compositions of fly ash and coal mineral particles, however, showed evidence of particle coalescence particularly because the chemical composition is a much more sensitive measure of coalescence than is the particle size (linear vs. cube root proportionality). For purposes of calculating a sticking coefficient, i.e., the fraction of impacted particles captured into the deposit, the changes in the chemical composition of the fly ash particles, due to their coalescence with other particles, is significant because of the effect of this upon the fly ash viscosity.

There is need, therefore, for models of mineral particle coalescence during combustion to be applied. Such models would have to lead to quantitative results in good general agreement with experiments, to be based on technically feasible mechanisms and to be sufficiently simple for their incorporation in the overall deposition model.

The combustion model adopted for our calculations is based on the broadly accepted dual mechanism of char particle burning: external or stagnant boundary layer-type diffusional transport of the reactant oxygen to the outer surface of the particle, pore diffusion into the inside of the particle and surface reaction on active sites of the surface. Values of the kinetic parameters for the diffusional and surface reaction rates were taken from Field et al. (1967).

For mineral matter particle coalescence it was assumed that these particles are retained on the surface of the burning char particle in molten spherical droplet form and that they will coalesce with other particles upon getting in contact with them. This may happen through the recession of the char surface in the course of combustion and the movement of the molten slag droplets towards the center of the char where they may coalesce with mineral inclusions ("volumetric coalescence"), or through the reduction of inter-particle distance on the continually reducing outer surface of the burning char ("surface coalescence"), Figure 7.

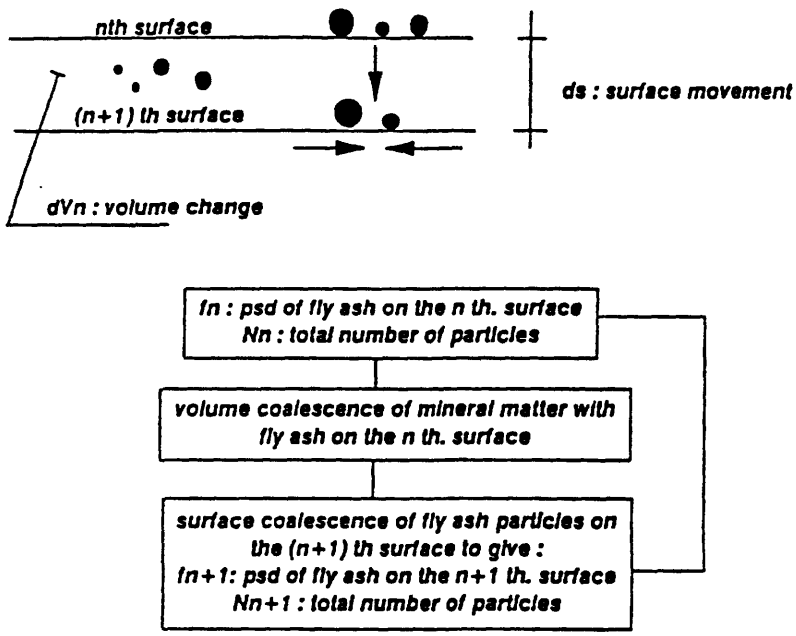

Figure 7. Random Coalescence Model.

The above-described coalescence is assumed to proceed as long as the char particle burns in the shrinking sphere mode. When the char is reduced to the size where the oxygen penetration of the particle becomes significant, combustion increasingly reverts to internal burning with constant outer diameter but decreasing particle density. In the absence of data on internal porosity and intrinsic reactivity, it is reasonable to postulate a changeover in burning mode when the particle size has diminished to the point at which the resistances to external diffusion and surface reaction are equal. During the surface reaction rate controlled internal burning of the particle, it is assumed that coal particle size remains constant and that the mineral particles do not move or coalesce. As a critical value of the porosity of the char particle is reached, the particle disintegrates, preserving the slag (molten ash) particle size reached during the external diffusion-controlled part of the char particle combustion. Upon cooling and solidification of these slag particles, fly ash is formed with size and chemical composition distributions calculable by the "random coalescence model."

2.6 Random Coalescence Model

The formation of fly ash from the mineral matter during the burnout of a char particle is treated as a stochastic process in which the mineral particle size and chemical composition are taken as random variables. The coal char particle burnout is divided into time segments and a transition random variable is chosen to describe the change in the selected properties of the fly ash. If Y_n denotes a random variable of a fly ash property (such as size, or SiO_2 content) on

the char particle surface exposed to oxygen, and Y_{n+1} is the random variable after an infinitesimal time step, then the basic equation which governs the stochastic process can be given as:

$$Y_{n+1} = Y_n + \Delta Y_n$$

where

ΔY_n is the transition random variable.

In the process of volumetric coalescence, fly ash particles situated on the burning char surface coalesce with mineral particles as these become exposed by the receding char surface. The surface-type coalescence of ash particles takes place as they are redistributed onto the newly developed reduced char surface. (Figure 7).

In the case of the burnout sequence described in Section 2.5, the stochastic process is ended by the fragmentation of the char as its porosity reaches a critical value, say 80%, due to internal burning.

By solving the stochastic equation numerically, Monroe (1989) proposed a dimensionless criterion to correlate the fractional coalescence with different values of coal size, mineral size, and mineral mass fraction for similar burning modes of the coal. Figure 8 shows Monroe's results of a series of model predictions for various values of these three variables.

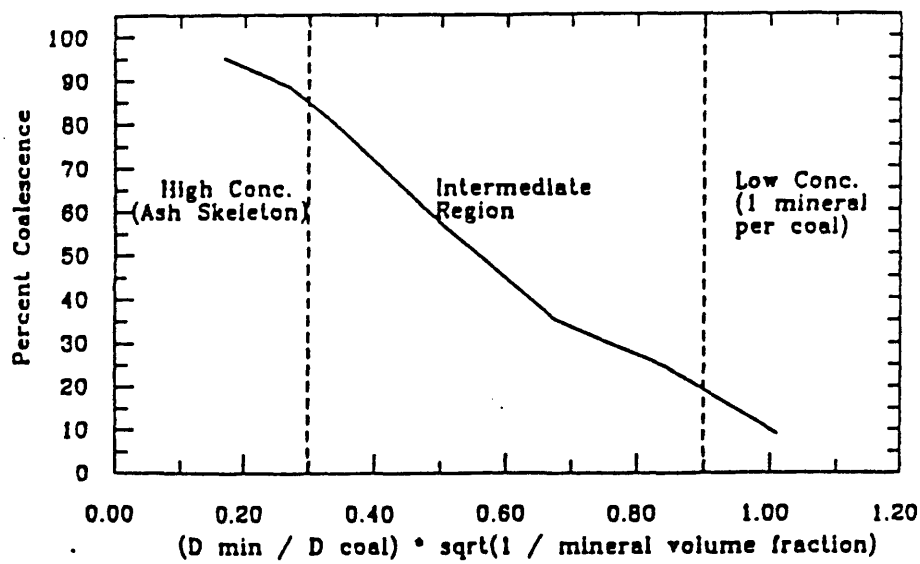

Figure 8. Correlation of Coalescence Behavior of Variations of Coal Particle Size, Mineral Particle Size and Mineral Fraction.
After Monroe (1989).

Due to the random coalescence of mineral matter, the distribution of a chemical compound (e.g., FeO) will change. Results obtained on beneficiated Upper Freeport coal (Figure 9) show that in the course of the transformation of the mineral matter to the fly ash, the variance of the FeO distribution decreased. As a consequence, the viscosity distribution of the fly ash has also a smaller standard deviation than the mineral matter had before the combustion (Figure 10).

2.7 Impaction Model

The bulk of the ash is transported to heat exchange surfaces by inertial impaction. The main forces acting on particles carried by the gas stream are inertial and drag forces. The inertial forces are proportional to the particle mass (and hence the third power of the diameter), and the drag forces to projected surface area of the particle (second power of diameter). The inertial to drag force ratio is therefore proportional to the particle diameter -- smaller particles follow streamlines around obstacles in the flow while larger particles separate from streamlines and impact on obstacles such as heat exchange surfaces. Langmuir and Blodgett (1946) solved the equation of motion for water droplets around a cylinder for the drop trajectories and calculated the limiting droplet size that would just pass the cylinder. They gave the collection efficiency of a cylinder, i.e., the probability of impaction for a particle approaching the cylinder, as a function of two dimensionless quantities, the Stokes number and the Reynolds number:

$$\mathrm{Stk} = \frac{\rho_p d_p^2 U}{9\mu_g d_t} \quad \text{and} \quad \mathrm{Re}_p^{\circ} = \frac{U d_p \rho_g}{\mu_g}$$

Variables are defined in the Nomenclature, with suffixes p, g and t referring to particles, gas and tube, respectively. The Stokes number relates the characteristic stopping time of the particle to the flow time around the cylinder. Israel and Rosner (1983) produced a generalized expression for the collection efficiency allowing also for non-Stokesian behavior of particles by a correction factor ψ. Following Walsh's (1987) experimental and modeling studies, Loehden (1988) developed a computer model to calculate the impaction efficiencies of particles in gas flow around a tube. In the model, the Israel-Rosner correlation is used to calculate the impaction efficiency as:

$$\eta_{imp} = \left[1 - \frac{1.25}{Stk_{eff} - 0.125} - \frac{0.014}{(Stk_{eff} - 0.125)^2} + \frac{0.508 * 10^{-4}}{(Stk_{eff} - 0.125)^3}\right]^{-1}$$

$$\text{where } \mathrm{Stk}_{eff} = \psi\,\mathrm{Stk} \quad \text{and} \quad \psi = \frac{24}{\mathrm{Re}_p^{\circ}} \int_0^{Re_p^{\circ}} \frac{d\mathrm{Re}_p}{C_D(\mathrm{Re}_p)\mathrm{Re}_p}$$

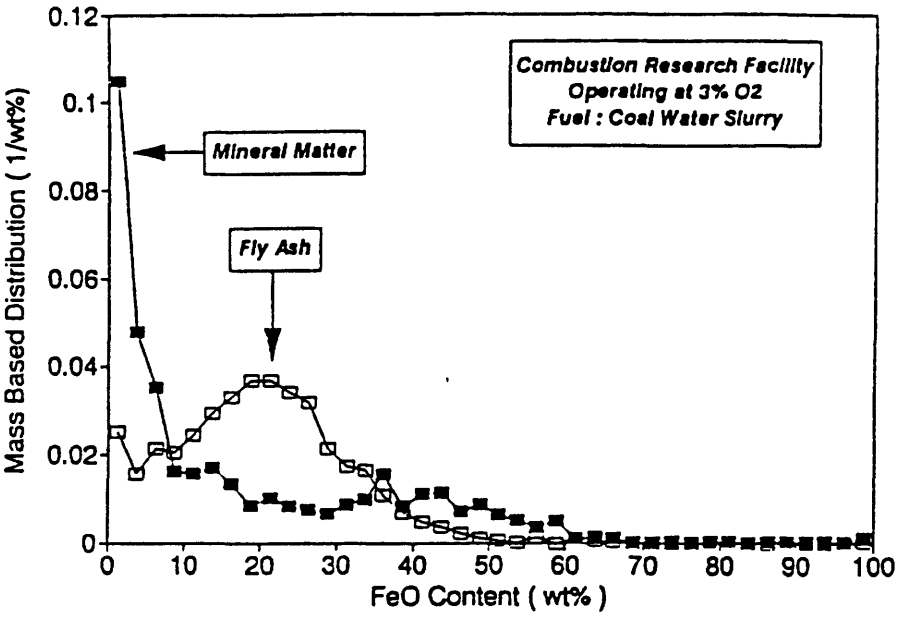

Figure 9. **Redistribution of FeO Compound as a Result of Coal Mineral Transformation to Fly Ash**

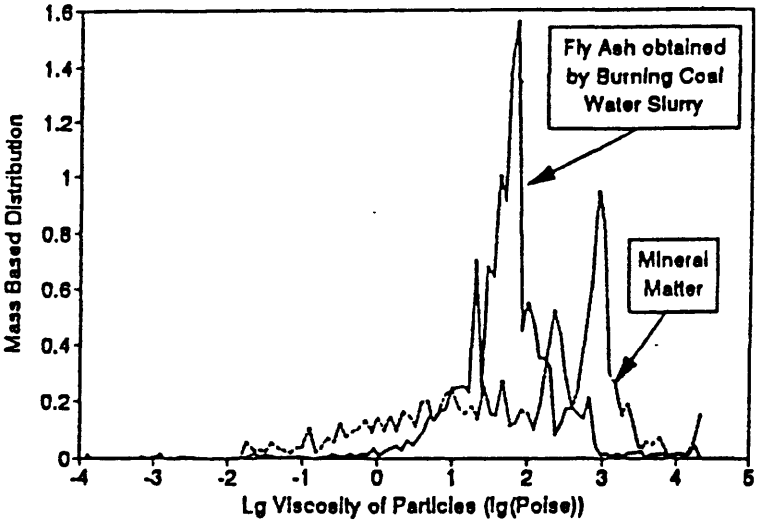

Figure 10. **Viscosity Distributions of Mineral Matter and Fly Ash from Beneficiated Upper Freeport Coal**

Figures above are taken from Barta et al. (1991). The data were obtained under DOE contract number DE-AC22 89PC 88654

Walsh et al. (1987) calculated the Stokes correction factor ψ using the drag correlation proposed by Klyachko (1934):

$$C_D = \frac{24}{Re_p}\left(1 + \frac{1}{6} Re_p^{2/3}\right)$$

The impaction efficiency of a fly ash particle is determined by its size and density at given flue gas parameters and tube geometry. The average impaction efficiency of the total fly ash can be given by

$$E(\eta)=\int_0^\infty\int_0^\infty \eta_{imp}(\rho,x)*f_m(\rho,x)\ dx\ d\rho$$

where

$E(\eta)$: *mean impaction efficiency,*
η_{imp}: *impaction efficiency for a fly ash particle,*
f_m : *mutual size and density distribution of fly ash.*

During experiments with Eagle Butte coal in the MIT-CRF, particulate samples and deposits on mullite tubes were collected (Walsh et al., 1987). The particulate samples were analyzed by CCSEM microprobe measurements to provide input data for impaction model calculations. Predicted and experimentally determined deposition rates on ceramic (mullite) tubes of different diameters at 1545 K gas temperature gave excellent agreement (Figure 11).

2.8 Sticking Efficiency

Another calculation on the probability density distribution of fly ash viscosity at different temperatures provides the basis for incorporating the "sticking efficiency" into the deposition model. The probability of retention in a dry deposit of a particle impacted on a tube depends upon its stickiness, i.e., viscosity. It has been shown (Wibberly, 1980) that, for deposition to occur the kinetic energy of the fly ash particle has to be consumed by the energy of viscous deformation. A critical viscosity value is chosen. Particles which have viscosities lower than this critical value will stick to the tube surface upon impaction, while those having higher viscosities will bounce off. The sticking efficiency is given by the following equation:

$$\eta_{st} = Prob.\ \{\eta\ (T,Chem.) < \eta_{crit}\ \}$$

At a given temperature, the calculated viscosity of a fly ash particle varies from particle-to-particle due to changing particle chemical composition. The mass fraction of particles having a viscosity of smaller than a critical viscosity value is, by definition, the sticking efficiency. The sticking efficiency depends on the particle temperature, since the higher the temperature, the higher the probability of finding a sticky particle. A cumulative distribution function of η_{st} can be obtained by calculating the viscosity of each particle by using a formula (e.g., the

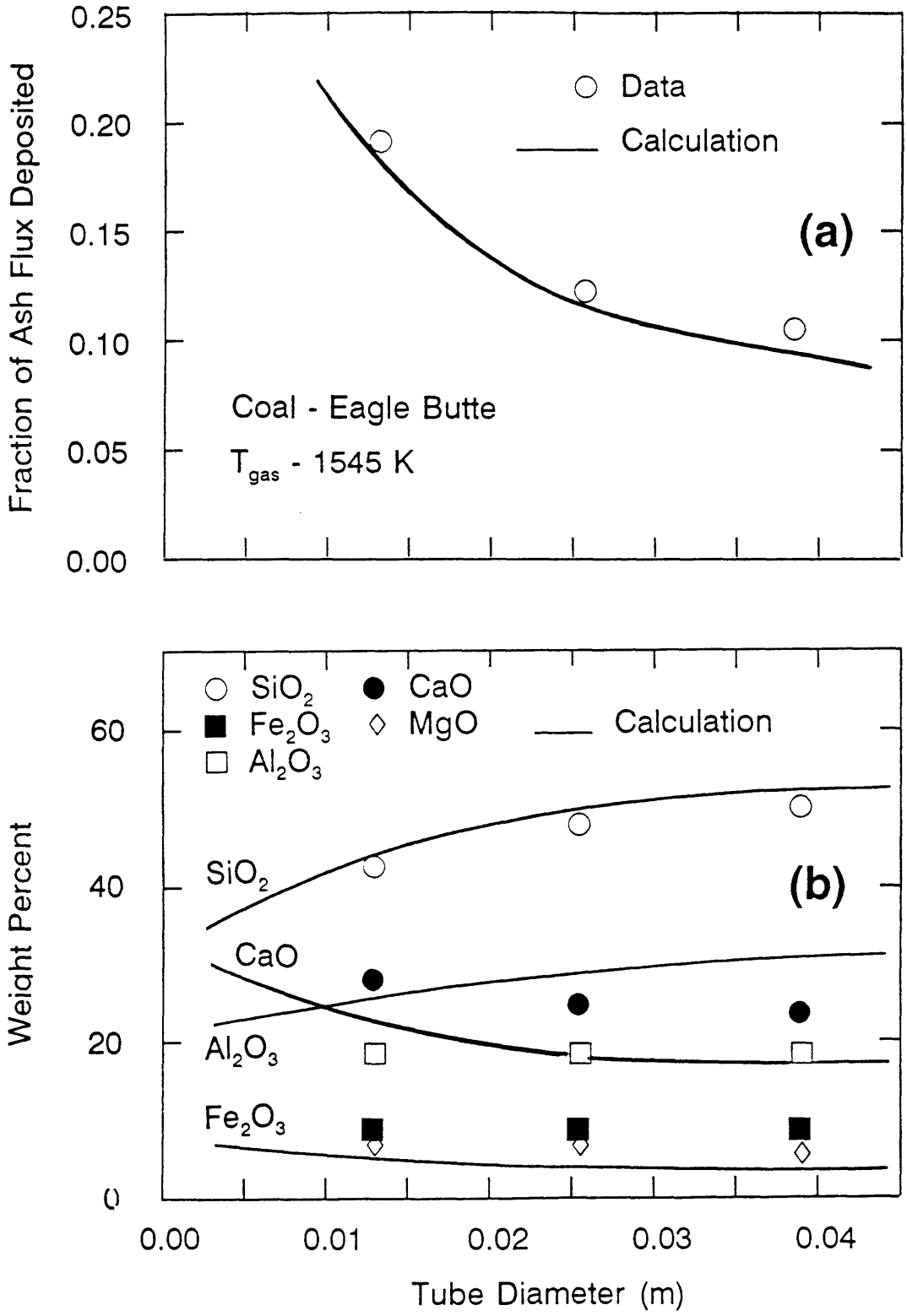

Figure 11. a. Measured Deposition and Impaction Model Prediction for Various Tube Diameters.
b. Predicted and Experimentally Determined Composition of Deposited Ash.
After Loehden et al. (1989).

Watt-Fereday equation) to calculate the viscosity from the chemical composition at the particle temperature at which its deformation occurs. Due to particle cooling in the boundary layer of the target tube and further temperature drop is expected by heat conduction upon particle impaction, the effective particle temperature will be between the flue gas and the deposit surface temperatures.

2.9 Time Resolved Deposition Model

Since this model has not been published before, a detailed description of the model is presented at this point. The time-resolved deposition model is capable of obtaining the projected surface area fractions of the clean tube, the sticky and non-sticky deposit surface, as a function of time. These surface area fractions are used to calculate the average deposit thickness and the deposition rate (mass of deposit per time and unit projected tube surface area) as a function of time. The surface temperature of the deposit is calculated by assuming a stationary heat transfer through the boundary layer of flue gas, the deposit layer, the tube shell and the coolant in the tube. It is assumed that the fly ash particles are sticky below a certain critical viscosity and behave as non-sticky when their viscosity is higher than the critical value. The effect of chemical reaction between deposited particles on the formation of the area fractions is neglected. The cooling of fly ash particles in the flue gas boundary layer around the tube has an effect on the temperature of fly ash particles with a size of lower than 10 μm.

In the following three sub-sections the differential terms are presented for the effect of impaction on the redistribution of total projected surface area between area that remains uncoated and areas on which deposits are either sticky or non-sticky. Section 2.9.4 assembles these differentials into a combined equation for each of the three surface components and then presents the reduced area. The quasi-stationary limit is presented in Section 2.9.5. The definition of the symbols used in these equations is given in the Nomenclature.

2.9.1 Development of the Tube Surface Area Fraction

Let dN denote the number of fly ash particles approaching the deposition tube in a cross section of area A for an infinitesimal period of time. The sticky portion of the impacting fly ash particles will stick to the tube surface, but the non-sticky impacting fly ash particles will bounce off. The deposited fly ash particles will increase the mass of deposit and decrease the clean tube surface. Following the particle deposition, they will cool down to the actual surface temperature. The sticky and non-sticky surface area formed after deposition can be calculated by taking the total surface of sticky and non-sticky particles calculated at the surface temperature. The process is described by the following equations:

Increase of deposition mass:

$$\frac{A_t}{A} * m * \eta_{st} * \eta^*_{imp} * dN$$

Decrease of tube surface:

$$\frac{A_t}{A} * a * \eta_{st} * \eta^*_{imp} * dN$$

Increase of sticky surface:

$$\frac{A_t}{A} * a * \eta_{st} * \eta^*_{imp} * dN * \frac{\eta^*_{st}}{\eta_{st}}$$

Increase of non-sticky surface:

$$\frac{A_t}{A} * a * \eta_{st} * \eta^*_{imp} * dN * \frac{\eta_{st} - \eta^*_{st}}{\eta_{st}}$$

2.9.2 Development of Non-Sticky Deposit Surface Area Fraction

The sticky portion of the impacting fly ash particles will stick to the non-sticky deposit surface. However, each non-sticky impacting particle may erode "k" non-sticky particles. Further discussion of this erosion factor is deferred until Section 5. The surface revealed after erosion will have the same sticky/non-sticky surface area ratio as that of the total deposit surface. The deposit mass will increase by that of the deposited sticky particles and decrease by the mass of the eroded particles. Following the deposition, the newly deposited sticky fly ash particles will cool down to the actual surface temperature. The actual sticky and non-sticky surface is calculated by taking the actual surface temperature. The process is described by the following equations:

Increase of deposition mass:

$$\frac{A_{nt}}{A} * m * \eta_{st} * \eta^*_{imp} * dN - \frac{A_{nt}}{A} * m * \eta^*_{imp} * (1 - \eta_{st}) * k * dN$$

Increase of sticky surface:

$$\frac{A_{nt}}{A} * a * \eta_{st} * \eta^*_{imp} * dN * \frac{\eta^*_{st}}{\eta_{st}} + \frac{A_{nt}}{A} * a * \eta^*_{imp} * (1 - \eta_{st}) * k * \frac{A_{st}}{A_{nt} + A_{st}} * dN$$

2.9.3 Development of the Sticky Surface Area Fraction

The impacting fly ash particles stick to the sticky surface and increase the deposition mass. Following impaction, the particles will cool down to the actual surface temperature and either remain sticky or become non-sticky, depending on the particle viscosity calculated at the surface temperature. The impacting non-sticky fly ash particles will decrease the sticky surface, since after cooling they remain non-sticky.

Increase of deposition mass:

$$\frac{A_{st}}{A} * m * \eta^{*}_{imp} * dN$$

Increase of non-sticky surface:

$$\frac{A_{st}}{A} * a * \eta_{st} * \eta^{*}_{imp} * dN * \frac{\eta_{st} - \eta^{*}_{st}}{\eta_{st}} + \frac{A_{st}}{A} * a * (1 - \eta_{st}) * \eta^{*}_{imp} * dN$$

2.9.4 Derivation of the Governing Differential Equation

The conservation of the fly ash mass can be given in the following form:

$$m * dN = g_{ash} * A * dt$$

The following equations were derived from the results of the previous considerations and from the fact that the total surface area is constant ($dA = d(A_t + A_{st} + A_{nt}) = 0$). Therefore there are only two independent area fractions.

Change in tube surface area:

$$dA_t = -\frac{A_t}{A} * a * \eta_{st} * \eta^{*}_{imp} * dN$$

Change in non-sticky surface area:

$$dA_{nst} = \frac{A_t}{A} * a * (\eta_{st} - \eta_{st}^*) * \eta_{imp}^* * dN +$$
$$+ \frac{A_{st}}{A} * a * (1 - \eta_{st}) * \eta_{imp}^* * dN +$$
$$+ \frac{A_{st}}{A} * a * (\eta_{st} - \eta_{st}^*) * \eta_{imp}^* * dN -$$
$$- \frac{A_{nt}}{A} * a * \eta_{st}^* * \eta_{imp}^* * dN -$$
$$- \frac{A_{nt}}{A} * a * \eta_{imp}^* * (1 - \eta_{st}) * k * \frac{A_{st}}{A_{nt} + A_{st}}$$

Change of sticky surface area:

$$dA_{st} = \frac{A_t}{A} * a * \eta_{st}^* * \eta_{imp}^* * dN -$$
$$- \frac{A_{st}}{A} * a * (1 - \eta_{st}) * \eta_{imp}^* * dN -$$
$$- \frac{A_{st}}{A} * a * (\eta_{st} - \eta_{st}^*) * \eta_{imp}^* * dN +$$
$$+ \frac{A_{nt}}{A} * a * \eta_{st}^* * \eta_{imp}^* * dN +$$
$$+ \frac{A_{nt}}{A} * a * \eta_{imp}^* * (1 - \eta_{st}) * k * \frac{A_{st}}{A_{nt} + A_{st}}$$

Change in deposit mass:

$$dM = \frac{A_t}{A} * m * \eta_{st} * \eta_{imp}^* * dN +$$
$$+ \frac{A_{st}}{A} * m * \eta_{imp}^* * dN +$$
$$+ \frac{A_{nt}}{A} * m * \eta_{st} * \eta_{imp}^* * dN -$$
$$- \frac{A_{nt}}{A} * m * \eta_{imp}^* * (1 - \eta_{st}) * k * dN$$

The surface temperature of the deposit will increase due to increasing deposit thickness. In turn, the sticking portion of the deposited fly ash particles will also increase. It is therefore necessary to calculate the surface temperature as a function of deposit thickness. The average deposit thickness is defined by the following equation:

$$H = \frac{M}{A * \rho_{dep}}$$

The formula to calculate the surface temperature of the deposit can be found in Section 3.3.20. The sticking efficiency of particles on the deposit can be given by the function of the sticking efficiency vs. temperature:

$$\eta_{st}^{*} = \eta_{st}(T^{*})$$

By rearranging the previous equations, the final form of the deposition growth model can be formulated as follows

$$\frac{dX}{dt} = -\eta_{st} * \eta_{imp}^{*} \alpha * X$$

$$\frac{dZ}{dt} = \alpha * \eta_{imp} * (\eta_{st}^{*} * X - (1-\eta_{st}^{*}) * Z + \eta_{st}^{*} * Y + Y * (1-\eta_{st}) * k * \frac{Z}{Y+Z})$$

$$\frac{dY}{dt} = \alpha * \eta_{imp} * ((\eta_{st} - \eta_{st}^{*}) * X + (1-\eta_{st}^{*}) * Z - \eta_{st}^{*} * Y - Y * (1-\eta_{st}) * k * \frac{Z}{Y+Z})$$

$$\frac{dH}{dt} = \eta_{imp} * \beta * ((X+Y) * \eta_{st} + Z - Y * (1-\eta_{st}) * k)$$

$$\eta_{st}^{*} = \eta_{st}(T^{*})$$

$$\eta_{st} = \eta_{st}(T)$$

where

$$\alpha = \frac{3 * g_{ash}}{2 * \rho_{p} * d} \qquad \beta = \frac{g_{ash}}{\rho_{dep}}$$

T = *particle temperature*

2.9.5 Quasi-Stationary Case

The differential equation for the uncoated tube surface area fraction indicates an exponential decay of this fraction, X, and this decay occurs on a time-scale short compared to

the deposit growth times in our experiments. Thus, a quasi-stationary case can be derived by equating the tube surface area fraction and its time derivative to zero. By substituting these conditions into the governing differential equations, a simple Riccati-type of differential equation can be derived for which an analytical solution can be obtained. The results for the surface fractions and for the deposit thickness are as follows:

$$X^* = 0$$

$$Y^* = 1 - Z^*$$

$$Z^* = \frac{1}{2} * \frac{(1-\eta_{st})*k-1}{(1-\eta_{st})*k} + \frac{1}{2} * \sqrt{\left(\frac{(1-\eta_{st})*k-1}{(1-\eta_{st})*k}\right)^2 + \frac{4*\eta_{st}^*}{(1-\eta_{st})*k}}$$

$$\frac{\rho_{dep}}{g_{ash}} * \frac{dH}{dt} = \eta_{imp}^* * (Y^* * \eta_{st} + Z^* - Y^* * (1-\eta_{st}) * k)$$

In the case when erosion is negligible (k=0), the equations of this quasi-stationary case have a simpler form:

$$X^* = 0$$

$$Y^* = 1 - \eta_{st}^*$$

$$Z^* = \eta_{st}^*$$

$$\frac{\rho_{dep}}{g_{ash}} * \frac{dH}{dt} = \eta_{imp}^* * ((1-\eta_{st}^*) * \eta_{st} + \eta_{st}^*)$$

SECTION 3

COAL FOULING TENDENCY (CFT) CODE

3.1 Introduction

The theoretical considerations discussed in Section 2 characterize a set of sub-models that are assembled together into a computer code, called the "Coal Fouling Tendency" code, to assist in the calculations of the relative fouling tendencies of different coals. A key sub-model describes the coal mineral matter (m.m.) transformation into fly ash. This entails the prediction of the fly ash size and chemical composition distributions for given values of the initial parameters of the coal (e.g., coal particle size, density, ash content, included mineral size distribution, organically-bound mineral fraction, etc.), and also prediction of the random particle-to-particle variation of the above parameters. These predictions are obtained by means of a series of weighted integrals, as described in Section 3.2 below.

The code was written in Pascal language and it can be run the under DOS operating system which is widely accessible. To avoid a long running time, a 486 machine is suggested. To run the CFT, an input file has to be created in which the characteristics of the coal, mineral matter and the flue gas are to be listed. The output file contains the size distributions of the mineral matter and the fly ash, the predicted distribution functions of the MgO, Al_2O_3, SiO_2, CaO and FeO concentrations in the fly ash. The deposition rate of fly ash as a function of flue gas temperature is calculated and listed in the output file, too. The last section of the output file contains a copy of the input file for assisting further utilization of the output file.

The CFT code consists of a series of subroutines which are designed to complete certain sub-tasks during the execution of the main program. The code takes the CCSEM data file of a coal sample and calculates both the chemical composition and size of each inclusion and extraneous mineral particle. The calculation of these parameters is made by using correction functions, which calculate the chemical composition of mineral particles from the measured X-ray counts of the preset chemical elements, and which use the Abel function to obtain the correct size distribution function of the mineral particles from that of the cross-sectioned particles.

The size distribution of inclusions and the inclusion content of the coal are used to obtain the most probable number of inclusions in a coal particle. Described by a Poisson distribution, this number varies randomly from coal particle to coal particle. Also, the size distribution of the inclusions varies from coal particle to coal particle. The variation of inclusion size distribution is obtained by randomly choosing different numbers of particles of a given size. These variations are taken into account within the "inclusion loop" of the main code. When there are two mineral matter types in the coal, namely inclusions and ion-exchangeable minerals, the ion-exchangeable mineral matter is distributed onto the inclusions randomly. Due to the large number of ion-exchangeable nuclei per inclusion particle, the random distribution can be approximated by assuming that each inclusion would receive an allocation of ion-exchangeable

mineral matter proportional to its area fraction. After the redistribution of the ion-exchangeable mineral matter, the total number of particles will be the same as that of the inclusions, however, the distribution of size, and concentration of a chemical compound will be altered. The particles formed by the coalescence of non-exchangeable and included minerals are named as "total" inclusions. Following the determination of the total inclusion number and the size distribution of inclusions, the ion-exchangeable mineral content of the coal is calculated by using the assumption that the ion-exchangeable mineral content of the inclusion-free coal matrix is constant.

The effect of coal particle combustion on the size and chemical composition distribution of the mineral matter is taken into account by surface and volumetric type of coalescence of inclusion particles with the ion-exchangeable mineral matter until the coal particle reaches its critical bulk porosity, whereupon total disintegration of the burning char stops any further coalescence between inclusion particles. The random coalescence model is used to determine the effect of inclusion random coalescence on the final distributions of fly ash size and chemical composition. These distributions are inputs of the sub-code to determine the impaction and sticking efficiencies of fly ash.

The impaction efficiency is calculated first, for a pre-selected set of flue gas parameters (temperature, velocity, etc.) and parameters of the target tube (diameter, wall temperature, etc.). A time-resolved deposition model is used to describe the growth of deposit as a function of temperature and time. These results are stored in an output file for further data processing.

3.2 Theoretical Basis of the Coal Fouling Tendency Code

The "logic diagram" of the calculation of the fly ash size and chemical composition distributions formed by the combustion of a single coal particle is plotted in Figure 12. The calculation starts by determining the most probable coal particle and mineral matter (m.m.) properties, followed by the calculation of fly ash properties.

3.2.1 The Most Probable Coal and Mineral Matter Property Distributions

- Select a coal particle of size D_c;
- Determine the mean ash content and density of coal particles of size D_c;
- Calculate the included (a_{inc}) and ion-exchangeable (a_{ion}) m.m. content;
- Take the joint size-chemical composition distribution function of inclusions ($f_{inc}(x,c)$);
- Calculate the inclusion size distribution function and its third moment ($f_{inc}(x)$, M_{3inc});
- Calculate the "total" inclusion number in a coal particle (n_o);
- Calculate the joint size-chemical composition distribution function of the "total" inclusions (f(x,c)) by using the values of a_{inc} and a_{ion};

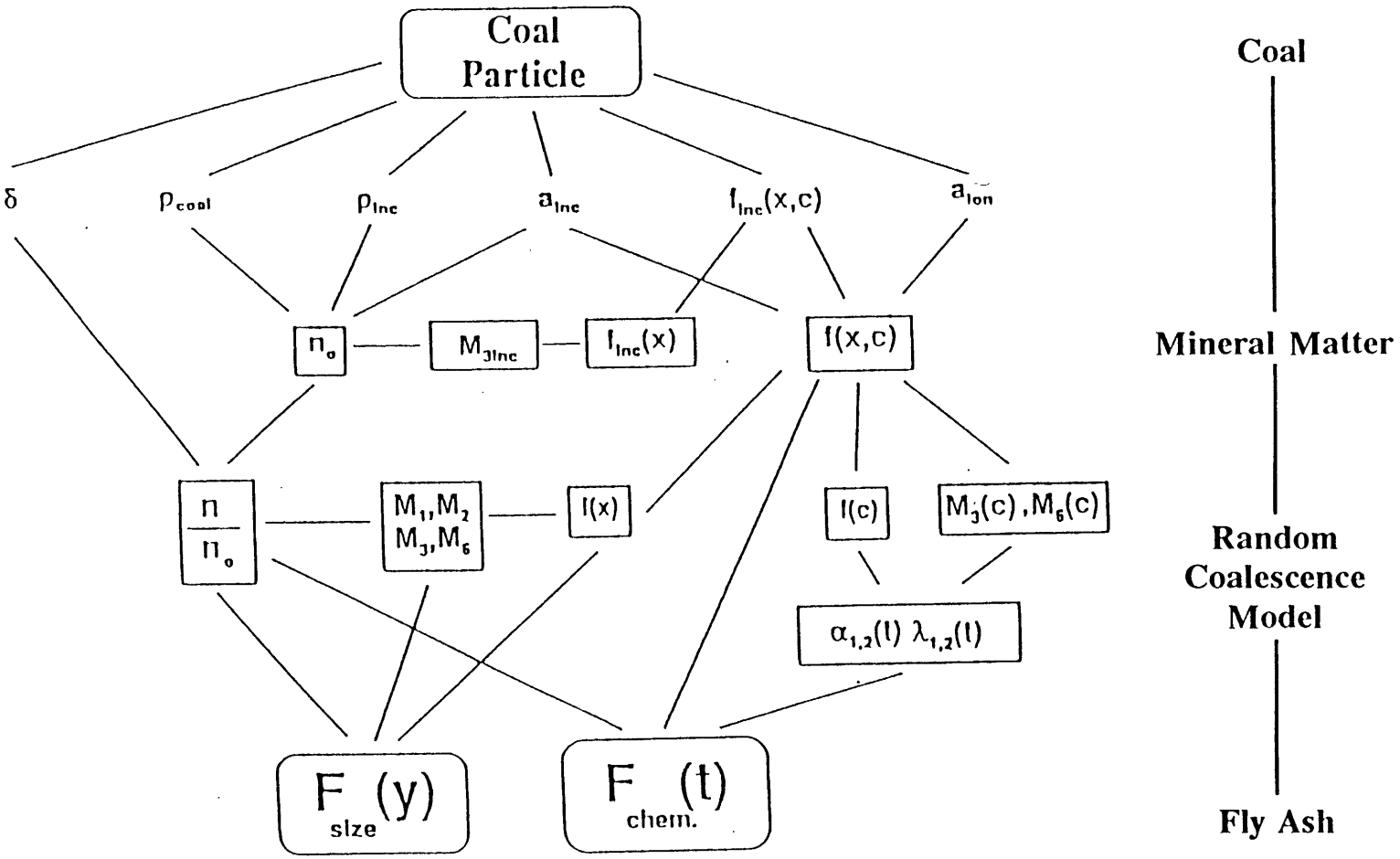

Figure 12. "Logic" Diagram of the CFT Model

3.2.2 The Most Probable Fly Ash Size Distribution

- Calculate the size distribution function of the "total" inclusions (f(x));
- Compute its first, second, third and sixth moments (M_1, M_2, M_3, M_6);
- Calculate the transition radius by using a given value of δ (the ratio of transition radius and coal radius);
- Calculate the number reduction of inclusions due to random coalescence (n/n_o);
- Compute the size distribution function of the fly ash ($F_{size}(y)$);

3.2.3 The Most Probable Fly Ash Chemical Composition Distribution

- Calculate the chemical composition distribution of the "total" inclusions (f(c));
- Obtain the third and sixth moments of the size distribution of the "total" inclusions as a function of the chemical composition ($M_3(c)$,$M_6(c)$);
- Calculate the functions of $\alpha_{1,2}(t)$ and $\lambda_{1,2}(t)$;
- Compute the chemical composition distribution ($F_{chem}(t)$);

In the most comprehensive case, even with mono-size coal particles, the input parameters such as inclusion size distribution, inclusion density, coal ash content and density are varying from coal particle to coal particle. In order to obtain the final distribution functions of the fly ash, all the input parameters have to be considered as random variables. Their distribution functions can be obtained by the application of the urn model.

3.2.4 The Variances of the Fly Ash Size and Chemical Composition Distributions

- Obtain the joint size-chemical composition distribution of the inclusions;
- Calculate the number of inclusions of a given size and chemical composition;
- Consider this value as the mean of a Poisson distribution;
- Create a new random value by using this Poisson distribution for the number of inclusions of the given size and chemical composition;
- Repeat the latter procedure for every possible value of inclusion size and chemical composition; (In this way a new random joint size-chemical composition distribution function can be obtained with a random total number of inclusions.)
- Compute the probability of this new configuration by using the Poisson probabilities of each case;
- Calculate the total mass of the newly developed inclusion particles;
- Obtain the total volume of the coal matrix and the mass of ion-exchangeable m.m.;
- Calculate the new mass ratio of ion-exchangeable m.m. to inclusions; (In this way, a new coal particle is created that

can be used as an input to the calculational procedure.)
- Integrate the Poisson probability weighted fly ash size and chemical composition distribution functions after each run.

3.3 Description of the CFT Subroutines

The description of the CFT Subroutines follows the logic of the "block" diagram shown in Figure 13.

3.3.1 Unit of "Translate" Subroutine

This unit translates the input CCSEM file into a file of random access record type. The chemical composition of each inclusion particle is calculated by using a correction function and the measured X-ray counts for every element. The translated file (named by 'CCSEMname'.DAT) contains a series of records each storing the actual particle chemical composition, average, minimum and maximum diameters, particle perimeter, shape factor, and an assigned density value.

3.3.2 Unit of "Identify" Subroutine

The chemical composition of an inclusion particle supplies the information for identifying it as one of the mineral types (e.g., quartz). The criteria for identification are stored in a file called 'COAL.ID'. After identification, the unit assigns a density value to the particle. This information is stored into the corresponding data record. The output file name of this unit is 'CCSEMname'.dat.

3.3.3 Unit of "SO_3 Correction" Subroutine

The sulfur in the coal is assumed to escape into the flue gas during the coal combustion process. Therefore the chemical composition of inclusion particles has to be changed accordingly. The unit of SO_3 correction removes the sulfur from the inclusion particles and recalculates their new chemical composition by using the following formula:

$$\overline{c_i}=\frac{c_i}{(100-c_{SO_3})}*100 \text{ and } \overline{c_{SO_3}}=0.0$$

where

$\overline{c_i}$ *is the new concentration of compound of i,*
c_i *is the old concentration of compound of i.*

The output file name of this unit is 'work.dat'.

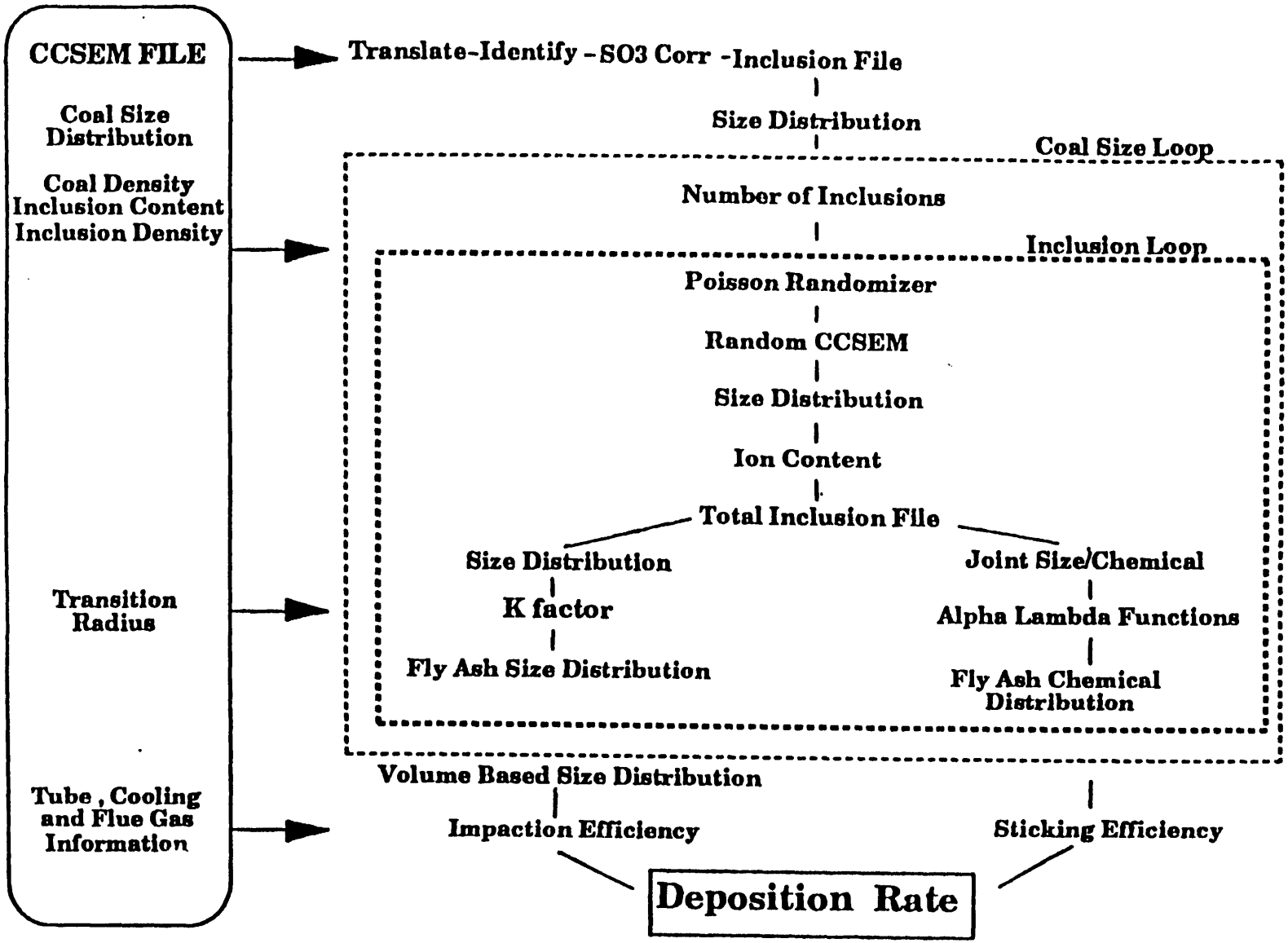

Figure 13. "Network" of Pascal Subroutines

3.3.4 Unit of "Inclusion Size Distribution" Subroutine

After the correction of chemical composition, the size distribution of the included mineral matter is determined. The calculation takes the Abelian transformation to obtain the three-dimensional distribution function from the two-dimensional sectioned area size distribution. The integral transformation is shown as follows:

$$f_v(y) = -\frac{2}{\pi} y_o \frac{d}{dy} \int_y^{\infty} \frac{f_a(x)dx}{\sqrt{(x^2 - y^2)}}$$

where

$f_v(y)$ is the three dimensional distribution function,
$f_a(y)$ is the two dimensional distribution function,

$$y_o = \left(\frac{2}{\pi} \int_0^{\infty} \frac{f_a(x)dx}{x}\right)^{-1}.$$

The moments of the inclusion size distribution are required for latter calculations. The moments are approximated by the following equations:

$$M_1 = \frac{\pi}{2} \frac{N}{\sum_i^N \frac{1}{x_i}} \qquad M_2 = \sqrt{\pi} \frac{\Gamma(2) \sum_i^N x_i}{\Gamma(3/2)\ M_1}$$

$$M_3 = \sqrt{\pi} \frac{\Gamma(5/2) \sum_i^N x_i^2}{\Gamma(2)\ M_1} \qquad M_6 = \sqrt{\pi} \frac{\Gamma(4) \sum_i^N x_i^5}{\Gamma(7/2)\ M_1}$$

where

x_i is the particle diameter in the cross section plane
M_i is the i^{th} moment of the size distribution.

3.3.5 Unit of "Inclusion Number" Subroutine

The number of included mineral particles in a coal particle is calculated by using the size, density and inclusion content of the coal particle and by the third moment of the inclusion size distribution function. The following equation is used for the calculation:

$$N_{inc} = \frac{D_{coal}^3 \, a_{inc}}{\rho_{inc} \, M_3}$$

where D_{coal} is the coal diameter, a_{inc} is the inclusion content of coal, and ρ_{inc} is the average inclusion density.

3.3.6 Unit of "Random Inclusion Number" Subroutine

The mineral inclusion number in a coal particle follows the Poisson distribution. This law is used to calculate a random Poisson number $\tilde{N}_{inc}$ with a mean value of N_{inc}. The probability that $\tilde{N}_{inc}$ equals a value of k is given as follows:

$$Prob.\ (\tilde{N}_{inc}=k) = e^{-N_{inc}} \frac{N_{inc}^k}{k!}$$

3.3.7 Unit of "Random CCSEM File" Subroutine

Not only does the total inclusion number change from coal particle to coal particle but the size distribution of included mineral matter also changes. The change of size distribution can be described by the fact that the number of inclusion particles irrespective of their size will obey the Poisson law. It is therefore possible to derive a size distribution function which changes randomly from coal particle to coal particle. It is obtained by creating a series of random inclusion files into which the records of inclusion properties are written randomly according to the Poisson law. In our case, the Poisson distribution is approximated by a binomial distribution; at each inclusion data record, the probability of writing the record into the new random file or skipping it, can be given by the following equation:

$$Prob.\ (w=k) = \binom{10}{k} 0.1^k \, 0.9^{10-k}$$

where "w" is the event of writing a record into the random file. It has a mean value of 1 and variance of 0.9. It is therefore true that N independent trials of writing a record will have a mean value of N and a variance of 0.9*N which can approximate the needed Poisson distribution. In this way, a new random inclusion file is created, in which the number of included particles of a given size will be a Poisson random variable. The name of the created output file is 'RANINC.DAT'.

3.3.8 Unit of "Random Size Distribution" Subroutine

This segment of the Coal Fouling Tendency (CFT) code uses a random inclusion file and it supplies the inclusion size distribution function and its moments. The calculation is made with the unit of inclusion size distribution, only the input file is different.

3.3.9 Unit of "Ion-Exchangeable Content" Subroutine

The volume of inclusion-free coal particle can be calculated by subtracting the total volume of inclusions from the coal particle volume. The ion-exchangeable mineral matter content of a coal particle is calculated with the assumption that the fraction of ion-exchangeable mineral matter in a coal particle free of included minerals is constant. The formula for the calculation is shown as follows:

$$\tilde{a}_{inc} = \frac{\tilde{N}_{inc}\,\tilde{M}_{3inc}\,\rho_{inc}}{D_c^3\,\rho_{coal}}$$

$$\tilde{a}_{ion} = \left(1 - \tilde{a}_{inc}\,\frac{\rho_{coal}}{\rho_{inc}}\right)\frac{(a_{ion} + a_{inc})\,\dfrac{a_{ion}}{a_{inc}}}{\left(1 + \dfrac{a_{ion}}{a_{inc}} - (a_{ion} + a_{inc})\right)}$$

where N_{inc} is the actual (random) total number of inclusions in the coal particle, M_{3inc} is the third moment of the inclusion size distribution, ρ_{inc} is the average inclusion density, D_c is the coal particle diameter, ρ_{coal} is the coal density, a_{inc} is the actual inclusion content of the coal particle, and a_{ion} is the actual ion-exchangeable mineral content of the coal.

3.3.10 Unit of "Total Inclusion File" Subroutine

The ion-exchangeable mineral matter in the coal particle is distributed onto the included particles proportional to their surface fraction. Another file ('RANTOT.DAT') is generated by this code segment in which the chemical composition and size distribution of the inclusion particles are modified. The following equations are used in the calculations:

$$\tilde{c}_i = \frac{\dfrac{A_i}{\sum A_i}\,c_i + \dfrac{\tilde{a}_{ion}}{\tilde{a}_{inc}}\,\dfrac{P_i}{\sum P_i}\,c_i^{ion}}{\dfrac{A_i}{\sum A_i} + \dfrac{\tilde{a}_{ion}}{\tilde{a}_{inc}}\,\dfrac{P_i}{\sum P_i}}$$

$$\tilde{A}_i = A_i + \frac{\tilde{a}_{ion}}{\tilde{a}_{inc}}\,\frac{P_i}{\sum P_i}\sum A_i$$

where A_i is the surface area of a cross sectioned inclusion particle, P_i is the perimeter of the

cross sectioned inclusion particle, and c_i^{ion} is the concentration of the chemical compound "i".

3.3.11 Unit of "Total Inclusion Size Distribution" Subroutine

The size distribution of the total mineral matter is calculated by taking the randomly created total inclusion file as an input file. The calculation is made with the unit of inclusion size distribution, only the input file is different. The results of this calculation are the number-based total inclusion particle size distribution and its first, second, third and sixth moments.

3.3.12 Unit of "K Factor" Subroutine

The K factor is the ratio of the number of fly ash particles generated from an individual coal particle to the number of inclusions originally contained in that coal particle.

$$K = e^{-\frac{\tilde{N}_{inc}\,\pi}{8A}(M_2 - M_1^2)} \int_0^{\infty} f(x)\, e^{-\frac{\tilde{N}_{inc}\pi}{8A}(x+M_1)^2}\, dx$$

where $\tilde{N}_{inc}$ is the total number of inclusions, and A is the internal surface area in a coal particle over which the inclusion particles are randomly distributed by the process of coalescence during coal particle burnout.

3.3.13 Unit of "Fly Ash Size Distribution" Subroutine

The fly ash cumulative size distribution function is calculated by using that of the total inclusions and the previously determined K factor. The formula for the calculation is as follows:

$$F(y) = \int_0^{y} f(x) * \Gamma^*(\alpha(x), \lambda * \frac{\pi}{6} * (y^3 - x^3))\, dx$$

where

$$\alpha(x) = \frac{(1-K) * x^2 * M_3^2}{K * M_2 * M_6} \qquad \lambda = \frac{6 * M_3}{\pi * M_6}$$

Γ^* : *The Incomplete* Γ *Function*

3.3.14 Unit of "Joint Size and Chemical Compound Distribution Function" Subroutine

This unit uses the randomly created total mineral inclusion file to determine the mass-

based joint size and chemical compound distribution function: where A_{ij} is the measured cross sectional area of a particle characterized by size x_j and concentration c_i of a given chemical compound. The density, ρ_{ij}, is calculated from the chemical composition of the specific particle. The normalization factor is the area-density product, summed over all particles.

$$f(c_i, x_j) = \frac{\sum A_{ij} * \rho_{ij}}{\sum A_k * \rho_k}$$

3.3.15 Unit of "Alpha and Lambda Functions" Subroutine

For the calculation of the distribution functions of chemical compounds in the fly ash, four work functions are to be determined, which can be obtained from the joint size and chemical compound concentration function of total inclusion particles. For the calculation of α_1, λ_1, α_2 and λ_2, the following integral formulas are used:

$$\lambda_1 = \frac{\int_0^t f(c)*(t-c)*M_3(c)*\frac{\pi}{6}\,dc}{\int_0^t f(c)*(t-c)^2*M_6(c)*(\frac{\pi}{6})^2\,dc} \qquad \alpha_1 = \frac{\Delta n * y^2}{n * M_2} * \lambda_1 * \int_0^t f(c)*(t-c)*M_3(c)*\frac{\pi}{6}\,dc$$

$$\lambda_2 = \frac{\int_t^1 f(c)*(c-t)*M_3(c)*\frac{\pi}{6}\,dc}{\int_t^1 f(c)*(c-t)^2*M_6(c)*(\frac{\pi}{6})^2\,dc} \qquad \alpha_2 = \frac{\Delta n * y^2}{n * M_2} * \lambda_2 * \int_t^1 f(c)*(c-t)*M_3(c)*\frac{\pi}{6}\,dc$$

where $\Delta n/n = (1-K)/K$ expresses the number of captured particles as a fraction of the number of acceptors.

3.3.16 Unit of "Chemical Compound Concentration in Fly Ash" Subroutine

This unit calculates the distribution functions of MgO, CaO, FeO, Al_2O_3 and SiO_2 content in the fly ash. The cumulative distribution of the concentration of a specific compound in the fly ash is given by

$$F(t) = \int_0^1 \int_0^\infty f(y,c)*g(c,y,t)\,dydc$$

in which the cumulative distribution of a chemical species after capture by acceptor inclusions of a given size and concentration is expressed as:

$$g(c,y,t) = Prob.(\tau<t) =$$

$$= \begin{cases} 1 - \int_0^{\infty} \frac{\lambda_2^{\alpha_2}}{\Gamma(\alpha_2)} * x^{\alpha_2-1} * e^{-\lambda_2 * x} * \Gamma^*(\alpha_1, \lambda_1 * (x - \frac{y^3 * \pi}{6} * (t-c))) \, dx & when \quad t \le c \\ 1 - \int_{\frac{y^2 * \pi}{6} * (t-c)}^{\infty} \frac{\lambda_2^{\alpha_2}}{\Gamma(\alpha_2)} * x^{\alpha_2-1} * e^{-\lambda_2 * x} * \Gamma^*(\alpha_1, \lambda_1 * (x - \frac{y^3 * \pi}{6} * (t-c))) \, dx & when \quad t > c \end{cases}$$

3.3.17 Unit of "Sticking Efficiency" Subroutine

The sticking efficiency of fly ash is determined by the mass fraction of fly ash particles having calculated viscosities of lower than a critical value. This unit calculates the particle viscosity by the Watt-Fereday equation:

$$\log_{10}(\eta) = \frac{10^7 * m}{(T-150)^2} + c$$

where

$$S = MgO + Al_2O_3 + SiO_2 + CaO + FeO$$

$$m = (0.835 * SiO_2 + 0.601 * Al_2O_3) \; / \; S - 0.109$$

$$c = (4.15 * SiO_2 + 1.92 * Al_2O_3 + 2.76 * FeO + 1.6 * CaO) \; / \; S - 3.92$$

T is the temperature in °C

The sticking efficiency of fly ash is obtained by the calculation of the following probability:

$$\eta_{st} = Prob. \; (\; \eta < \eta_{crit})$$

where

η_{crit} *is the critical viscosity value.*

3.3.18 Unit of "Volume-Based Size Distribution of Fly Ash" Subroutine

This unit takes the number-based cumulative distribution function of the fly ash and calculates the volume-based cumulative distribution function by the following integral equation:

$$F_{vol}(y) = F_{num}(y)\ \frac{y^3}{M_3} - \int_0^y F_{num}(x)\ \frac{3x^2}{M_3}\ dx$$

where

F_{num} is the number based cumulative distribution function,
F_{vol} is the volume based cumulative distribution function.

3.3.19 Unit of "Impaction Efficiency" Subroutine

The impaction efficiency is defined as the impacted mass fraction of particles going through the projected area of a tube. This unit uses the following formulas to calculate the impaction efficiency of fly ash:

$$\eta_{imp} = \int_0^\infty f_{vol}(d_p)\ \eta_{imp}(d_p)\ d\ d_p$$

$$g = Stk_{eff}(d_p) - 0.125$$

$$\eta_{imp}(d_p) = [1 + \frac{1.25}{g} - \frac{0.014}{g^2} + \frac{0.508 * 10^{-4}}{g^3}]^{-1}$$

$$Stk_{eff}(d_p) = \psi * \frac{\rho_p\ d_p^2\ U}{9 \mu_{gas} d_t}$$

$$\psi = \frac{18}{Re_o}(Re_o^{1/3} - \sqrt{6}\ arctg\ (\frac{Re_o^{1/3}}{\sqrt{6}})$$

$$Re_o = \frac{\rho_{gas}\ U\ d_p}{\mu_{gas}}$$

The flue gas density and viscosity are calculated at the actual temperature.

3.3.20 Unit of "Deposition Calculation" Subroutine

The deposition build-up is calculated by considering the impaction and sticking efficiency of the fly ash particles. It is assumed that if a sticky particle impacts the deposit surface, then it sticks to it. Also, if a non-sticky particle impacts a sticky deposit surface, then it sticks to the deposit, too. However, if a non-sticky particle impacts a non-sticky particle on the deposit surface, then it either bounces off or erodes the "k" number of non-sticky surface particles. After erosion, the revealed surface will display a mixture of sticky and non-sticky surface according to the local temperature and the local stickiness of the deposited fly ash particles. The governing differential equations given in Section 2.9.4 are used in the calculations.

The sticking efficiencies of η_{st} and η_{st}^{*} are evaluated at the particle and the actual deposit temperature, respectively. The flue gas temperature is an input of this unit. However, the actual surface temperature is calculated by taking into account a stationary heat extraction by the coolant. In our case, the coolant is air. The equation used for calculation is given as:

$$T_{*} = T - (1-\frac{K_1}{K_2})*(T-T_{air}^{o})*e^{-\frac{K_1*L}{\dot{m}_{air}c_{air}}}$$

where

$$K_1=[\frac{1}{2(r_{out}+H)*\pi*h_{gas}}+\frac{1}{2*\pi*K_{dep}\ln\frac{r_{out}+H}{r_{in}}}+\frac{1}{2*\pi*K_{tube}\ln\frac{r_{out}}{r_{in}}}+\frac{1}{2*\pi*h_{air}}]^{-1}$$

$$K_2=[\frac{1}{2*\pi*K_{dep}\ln\frac{r_{out}+H}{r_{in}}}+\frac{1}{2*\pi*K_{tube}\ln\frac{r_{out}}{r_{in}}}+\frac{1}{2*\pi*h_{air}}]^{-1}$$

$$h_{gas} = \frac{K_{gas}*0.023}{2*(r_{out}+H)}*Re_{gas}^{0.8}*Pr_{gas}^{0.3}$$

$$h_{air} = \frac{K_{air}*0.023}{2*(r_{out}+H)}*Re_{air}^{0.8}*Pr_{air}^{0.3}$$

The Reynolds and Prandtl numbers are calculated at the inlet temperature of the air.

3.4 Structure of the Input Data File

The structure of the input data file (IDF) is shown with an example file given in Appendix B. The second and third lines of the IDF contain the names of the CCSEM files. These files are the output files to the Particle Recognition Program used for microprobe analyses. Both the IDF and CCSEM input file must be in the directory where the main CFT program code is stored.

The seventh line contains an integer number, which determines the number of following lines in which the volume (or mass) based cumulative size distribution function of the coal will be put. In our example it is eight. This number determines also the number of coal size classes to be used in the code. Each of the following lines has two numbers. The first is the coal particle size in micrometer, the second is the value of the volume-based size distribution function of the coal at the specified particle size.

In our example, line 18 contains the mean coal particle density in g/cm^3. The heat input and the elemental chemical composition of the coal are given in lines 19 through 40. Line 42 contains the ratio of the maximal inclusion and the actual coal particle size. The ratio of the transition radius and the initial coal radius is located in line 45. The mean inclusion content of the coal is stored in line 48. If there is ion-exchangeable mineral content in the coal then it has to be stored in line 51. These two fractions are dimensionless numbers. The variation of the total number of included particles in a coal particles can be set by inserting a value in line 54 of the IDF. This value is the ratio of the standard deviation and the mean value of the total number of inclusions in a coal particle, for which the distribution function is approximated by the Poisson distribution.

Line 56 contains an integer number used to determine the number of trials to approximate the joint size and chemical compound distribution in the calculation of the fly ash chemical concentration distribution. The Gaussian numerical integration is used in the calculation of the distribution of a chosen chemical compound in the fly ash. Line 58 contains the number of integral division. A small number would increase the speed of calculation; however, the numerical error in the calculations will be larger. There are also two input data stored in line 60 for the maximum limits of the integration of the distribution function of a given chemical compound. The integration is made in two different ways depending on the magnitude of the α and λ functions, there are two maximum integral limits in this line.

The chemical composition of the ion-exchangeable mineral matter is stored within lines 64 through 93. The concentration values and the symbols of the chemical compounds are stored in separate lines.

The information to calculate the surface temperature of the deposit is stored in the next part of the input file. An approximate value of the cooling air velocity is stored in line 97. This should be a low value (as it is shown in our example), since it is only used as an initial value to adjust the initial tube surface temperature. The inner and outer radius of the target tube are located in lines 99 and 101, respectively. The inlet air temperature is given in line 103. The initial tube surface temperature, the minimum and maximum temperature limits and the number of interval division are stored in line 105. The initial tube surface temperature must be larger than the temperature which can be obtained with the air velocity as specified in line 97.

The flue gas velocity calculated at the minimum flue gas temperature (given in line 105) is stored in line 107. The flue gas temperature and velocity are not independent. They are calculated by using the ideal gas law. The heat conductivities of the fly ash deposit and the heat exchanger tube are stored in lines 109 and 111, respectively. The length of heat exchanger tube determines the location of the observed area on the tube. It is stored in line 113.

The deposit build-up is calculated by solving non-linear differential equations. The time step can be specified in line 115. The deposition equation is solved from time zero to a maximum time given in line 117. At this specified time, the rate of deposition is calculated. The cross section area of the convective pass can be given in line 119. The bulk density of the

deposit used to calculate the average deposit thickness and to obtain the temperature of the deposit surface is stored in line 121. The erosion factor located in line 123 is the number of dry fly ash particles from the deposit surface eroded by a colliding dry fly ash particle. In line 125, the minimal and maximal fly ash sizes are specified. Within this interval the upper value of the dividing sub-intervals is calculated by a geometric series. The number of sub-intervals is given in line 127. The $\log_{10}$ of the critical viscosity is specified in line 129. Line 131 should contain an input of "YES" if a stationary case is solved, and "NO" otherwise.

3.5 Structure of the Output Data File

A sample output data file is given in Appendix C. This file will be stored in the same directory where the main code is located. The name of the output file is specified by the second parameter of the command line. The file will contain the following information:

- the number-based cumulative distribution function of the total mineral matter this is stored between lines 6 and 104,

- the number- and volume-based cumulative size distribution functions of the fly ash are stored between lines 6 and 104; the actual number of size divisions may be different according to the specification in the IDF,

- the information for the lognormal approximation of the volume-based size distribution of the fly ash is stored in lines 106 and 107,

- the cumulative distribution functions of the MgO, Al_2O_3 , SiO_2, CaO and FeO content in the fly ash are stored between lines 110 and 638,

- the deposition rate, the rate of fly ash impaction, the impaction efficiency, the sticking efficiency and the average viscosity of the deposit are given as a function of flue gas temperature at the end of the output file.

In the course of calculation, the following additional files are created:

- MgO.prn
- Al_2O_3.prn
- SiO_2.prn
- CaO.prn
- work.dat
- raninc.dat
- "CCSEMname".dat
- work1.dat
- work2.dat
- worked.dat
- rantot.dat

3.6 Examples of the Command Line

CFT input.dat output.dat c
CFT input.dat output.dat
{in this case the calculation of chemical composition is omitted}

SECTION 4

EXPERIMENTAL RESULTS

As indicated in Section 1 above, earlier phases of the MIT research program had established a substantial data-base on fly ash formation and deposition behavior for a number of coal types. The data-base has been considerably augmented during the most recent phase, covered by this report. Five different coals or coal blends (collectively referenced in this report as the "CRF Coals") were investigated, both experimentally and by means of the CFT computer model. Analytical data on each fuel were obtained, to provide the necessary input to the CFT code. These data included the ultimate analysis of each coal, extended by the size and chemical composition distributions of mineral inclusions determined by CCSEM, and the amount and type of organically-bound minerals in the coal.

Combustion experiments were conducted in the MIT-CRF to obtain deposition data and to characterize the fly ash behavior of each of the five fuels. The analytical and experimental results are presented and discussed below.

4.1 Mapco Coal

4.1.1 Mapco Coal Characteristics

The characteristics of the Mapco coal provided by ABB-Combustion Engineering are listed in Table 1. The Mapco coal is a bituminous-type coal with low moisture and high volatile content and heating value. Its sulfur content is 0.8 wt%. The melting behavior of its ash was determined by ASTM method, and is characterized by data included in Table 1. According to these data, the temperature window within which the deformation of ash particles takes place is from 1616 K to 1724 K. The difference between the initial deformation temperature and the fluid temperature is relatively high, 108 K. The ash chemical composition indicates relatively low Fe_2O_3 and CaO content. The main chemical compounds are alumina and silica.

4.1.2 Extraneous Mineral Matter in Mapco Coal

By using a sink-float method, the extraneous mineral content of Mapco coal was determined as 0.075 wt%. By definition, the particles in coal with density larger than 2.67 g/cm^3 are considered extraneous.

4.1.3 Ion-Exchangeable Mineral Content of Mapco Coal

By using acetic acid extraction of the coal, the mass content of the ion-exchangeable mineral was determined. The result shows that less than 1% of the total ash content is ion-exchangeable.

Table 1.
Characteristics of Mapco Coal

Quantity	Mapco coal	
Moisture wt%	2.1	
Volatile Matter wt.%	33.4	
Fixed Carbon wt.%	57.7	
Ash wt.%	6.8	
Heating Value Btu/lb	13422	
Total sulfur wt.%	0.8	
IDT K	1616	
ST K	1670	
HT K	1689	
FT K	1724	
Ash SiO_2 wt.%	with Sulfur	without Sulfur
	48.2	49.7
Ash Al_2O_3 wt.%	29.2	30.1
Ash Fe_2O_3 wt.%	8.6	8.8
Ash CaO wt.%	4.3	4.4
Ash MgO wt.%	0.9	0.9
Ash Na_2O wt.%	1.2	1.2
Ash K_2O wt.%	2.4	2.5
Ash TiO_4 wt.%	2	2.1
Ash P_2O_5 wt.%	0.1	0.1
Ash SO_3 wt.%	3.0	0.0
Ash BaO wt%	0.1	0.1
Ash SrO wt%	0.2	0.2

4.1.4 Size Distribution of Mapco Coal

The volume-based size distribution of the coal can be seen in Figure 14. The frequency function represents a bimodal distribution at particle sizes of 3 μm and 10 μm, respectively. The maximal particle size is 200 μm. The volumetric mean value and standard deviation of the distribution were calculated by using the method of lognormal curve fitting. The calculated mean particle size and standard deviation are 36.6 μm and 51.9 μm, respectively.

4.1.5 Density and Ash Content as a Function of Coal Size

Due to the liberation of mineral inclusions with particle sizes of 1-10 μm from coal particles during grinding, there may be a variation of coal density and ash content as a function of coal particle size. After having sieved the Mapco coal, the mean particle density and ash content as functions of coal particle size were determined. The results are plotted in Figure 15. They show that both the mean particle density and ash content increase with decreasing coal particle size. However, the relative change is less than 15%.

4.1.6 Size Distribution of Mineral Inclusions

The volume-based size distribution of mineral inclusions is plotted in Figure 16. The volumetric mean particle size and standard deviation were approximated by using the method of lognormal curve fitting. The calculated mean particle size and standard deviation are 4.2 μm and 3.4 μm, respectively. The maximum particle size is under 20 μm. The distribution functions were determined by CCSEM method and Abelian transformation was used for the stereological correction of the raw data. In the model calculation, the same size distribution function is assumed for the mineral inclusions of different size coal particles.

4.1.7 Chemical Composition and Calculated Viscosity Distribution of Mineral Inclusions in Mapco Coal

The mean chemical compound concentrations in the mineral inclusions and the mean concentrations of mineral types are shown in Table 2. It shows that the mineral inclusions consist mainly of illite and quartz with smaller amounts of kaolinite and mixed silicates.

The viscosity of mineral inclusion particles can be calculated by using the correlation between the chemical composition of a mineral particle and the viscosity at a given temperature. The Watt-Fereday equation is used to calculate the particle viscosity. The temperature for the calculations was chosen to be the peak flame temperature (1781 K). The mass-based distribution function of mineral particle viscosity is given in Figure 17. The mean value and standard deviation of the viscosity are $10^{2.33}$ poise and $10^{1.36}$ poise, respectively. The curve shows two distinct peaks, consistent with the mineral inclusions in the Mapco coal representing a physical mixture of two major mineral types, as identified by the CCSEM.

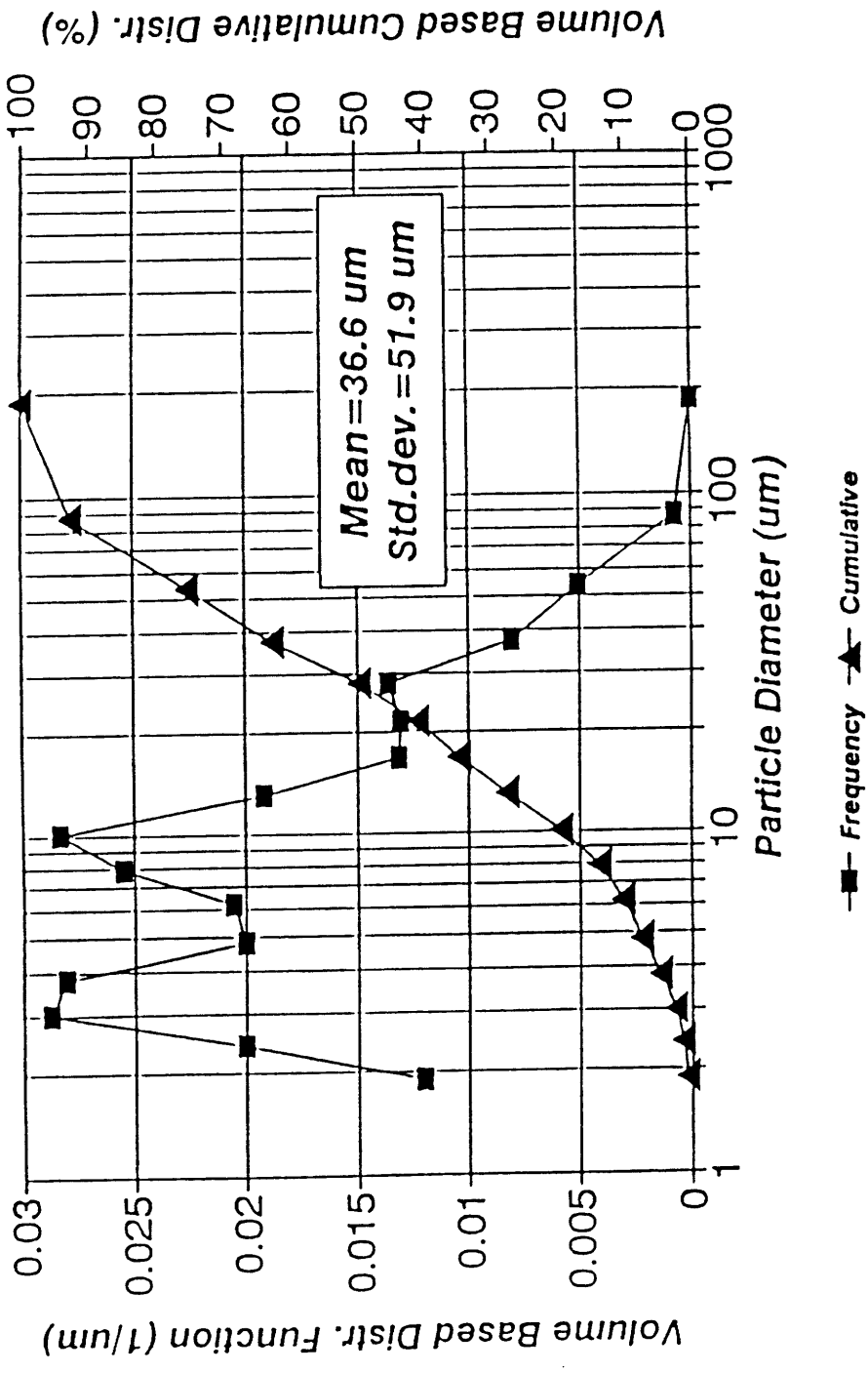

Figure 14. Size Distribution of Mapco Coal Determined by Laser Diffraction Method

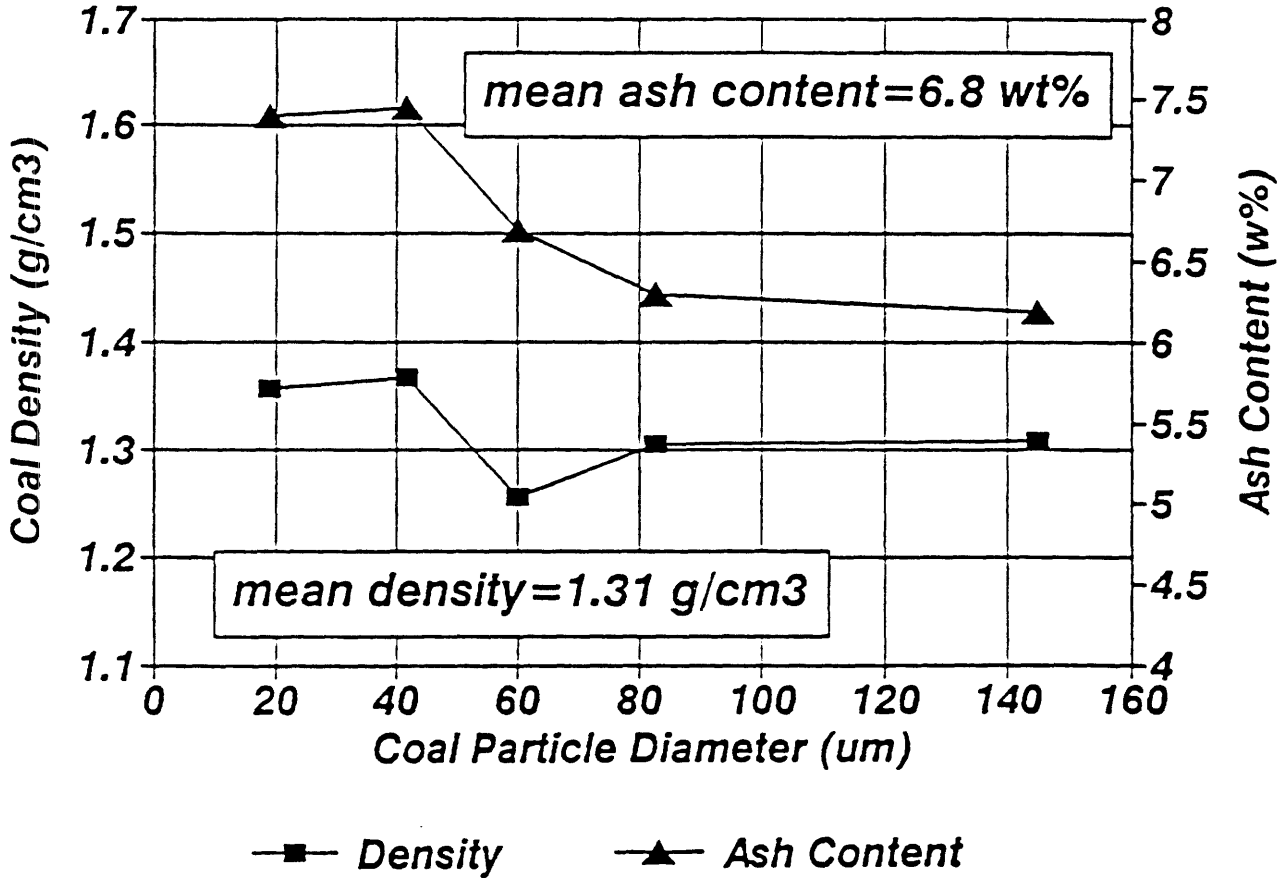

Figure 15. **Coal Density and Ash Content**
Mapco Bituminous Coal

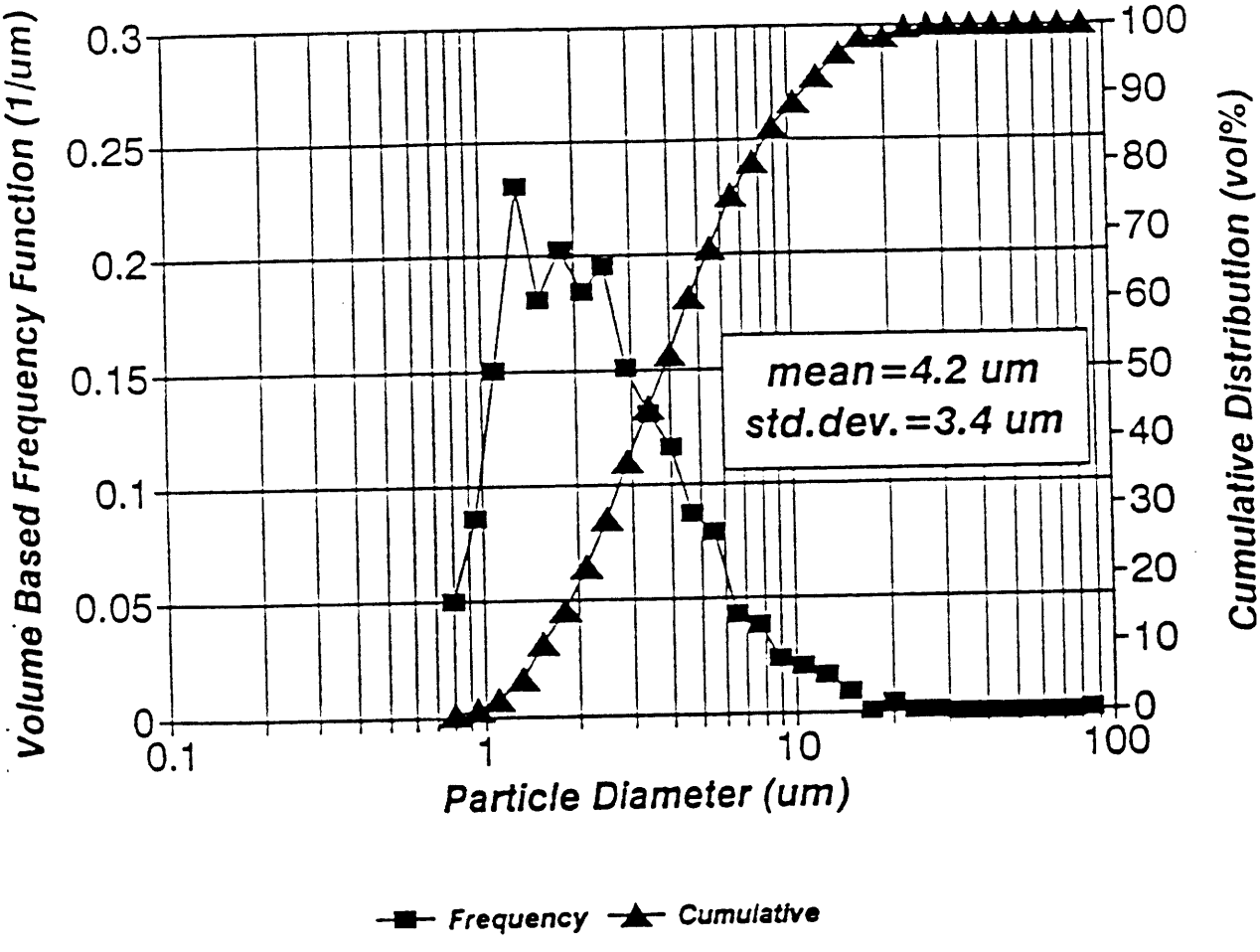

Figure 16. **Size Distribution of Mineral Inclusions**
Mapco Bituminous Coal

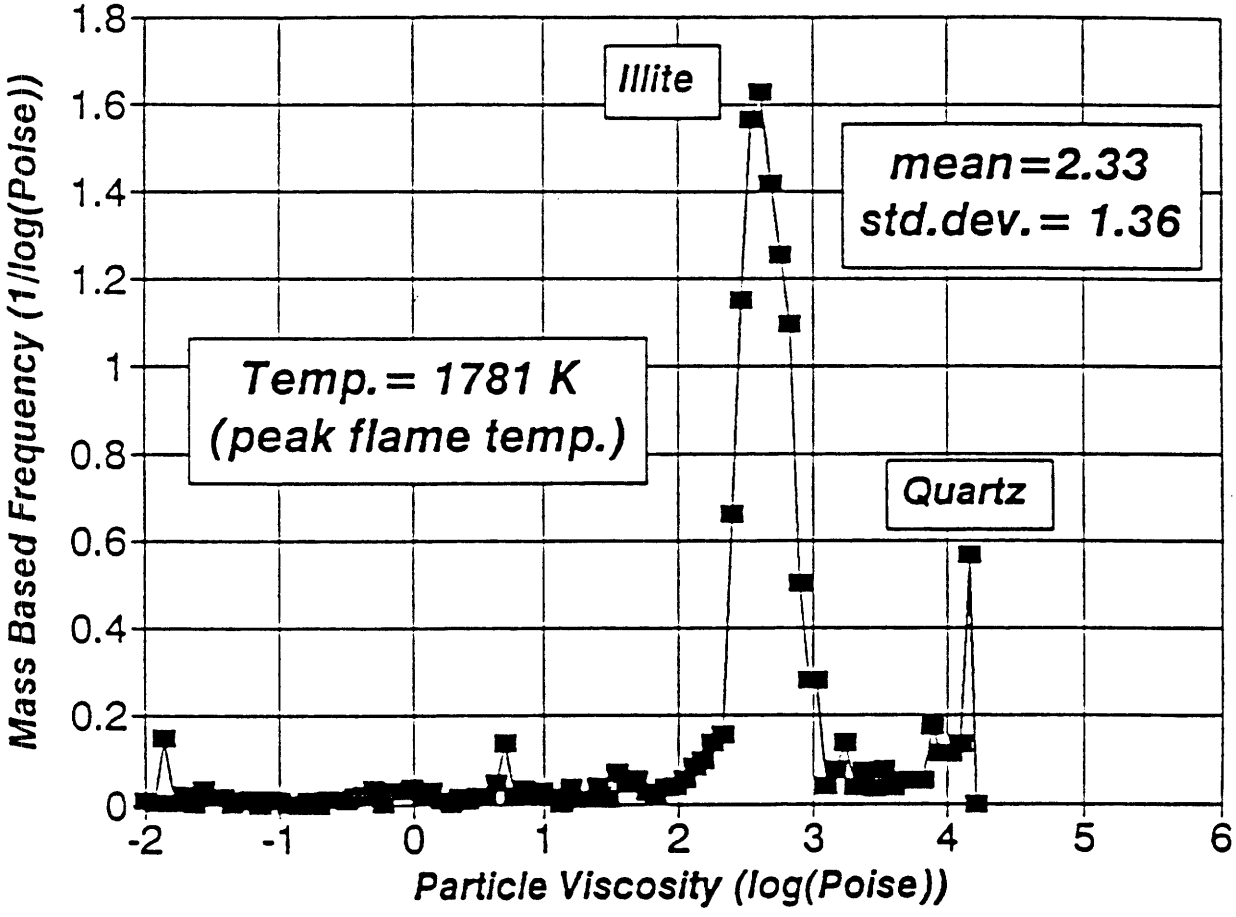

Figure 17. **Viscosity Distribution of Inclusions**
Mapco Bituminous Coal

Table 2.
Chemical Composition and Mineral Compounds of Mapco Mineral Inclusions

Oxide Formula	*Weight %*	*Mineral Type*	*Mass %*
Na_2O	0.2	Mixed Silicate	8.28
MgO	0.3	Quartz	11.75
Al_2O_3	33.2	Calcite	4.2
SiO_2	49.1	Siderite	0.94
P_2O_5	0.13	Rutile	0.46
SO_3	0.96	Illite	67.48
Cl	0.39	Pyrite/Marcasite	0.24
K_2O	3.46	Apatite/Evensite	0.01
CaO	6.07	Baryte	0.03
TiO_2	1.2	Kaolinite	6.15
FeO	4.33	Jarosite	0.45
Cr_2O_3	0.43	<u>Results by CCSEM Method</u>	
BaO	0.03		

4.1.8 Experiments in the Combustion Research Facility

The MIT-CRF was used to burn the five different coals or coal blends discussed in Section 4, including the Mapco coal of Section 4.1. A new low-NO_x burner was attached to the combustion tunnel. The setup of the combustion tunnel for the study of the deposition build-up is shown in Figure 18. The arrangement consisted of a 1.2 m × 1.2 m × 4.75 m combustion chamber, followed by a 3 m long water-cooled cylinder 0.5 m in diameter, and a 1.2 m × 1.2 m × 1.75 m water-cooled duct leading the flue gas to the stack.

The test conditions for the Mapco coal are summarized in Table 3. The coal feed rate was set to obtain 0.98 MW thermal input. The coal was carried by air from a coal silo at 1.21 air/coal mass ratio. The flow rate of air was measured by a built-in pitot tube. The flow rate of the coal was measured by a weigh belt. The primary, secondary and tertiary air flows were also monitored by pitot tubes. The air was preheated to 376 K, 522 K and 597 K, respectively. Low air flow rates were maintained for the primary and secondary air, and high rate for the tertiary air flow. A high degree of swirl was chosen for the primary and tertiary air flows, and no swirl was used for the secondary air.

The flue gas temperature profile along the axis of the combustion tunnel is plotted in Figure 19. The temperature was measured by suction pyrometer. The peak flue gas temperature (1781 K) was reached at the distance of 1.4 m from the burner.

The deposition probes were placed in the flue gas stream at two positions: 6.1 m and 5.0 m from the burner. Radial temperature profiles were taken at each of these locations. The results are plotted in Figure 20. At the position of 5.0 m from the burner, the maximum temperature was 1563 K. The maximum temperature at 6.1 m from the burner was 1423 K. The maximum temperatures were found on the axis. Due to the intensive heat extraction through the cylinder jacket, the temperature decreased as the distance from the axis increased. The flue gas temperature measured at the wall of the water-cooled cylinder on the side of the insertion of the suction pyrometer is probably low because of some penetration of outside air around the probe.

Pitot tube measurements to determine the radial flue gas velocity profile were made at the positions where the deposition probes were inserted. The results can be seen in Figure 21. At the position of 5.0 m from the burner the peak velocity was 10.6 m/s. At the distance of 6.1 m from the burner, due to the decrease of flue gas temperature, the maximum velocity of the flue gas was 9.6 m/s. Both peak velocities were measured on the axis. The flue gas velocity decreased as the radial distance from the axis increased. At the distance of 20 cm, the result may have been affected by the in-leaking air.

4.1.9 Deposition Experiment

Deposition probes were designed to simulate actual conditions in the convective section of utility boilers. The material of the tube was chosen to be 304-type stainless steel. The outer

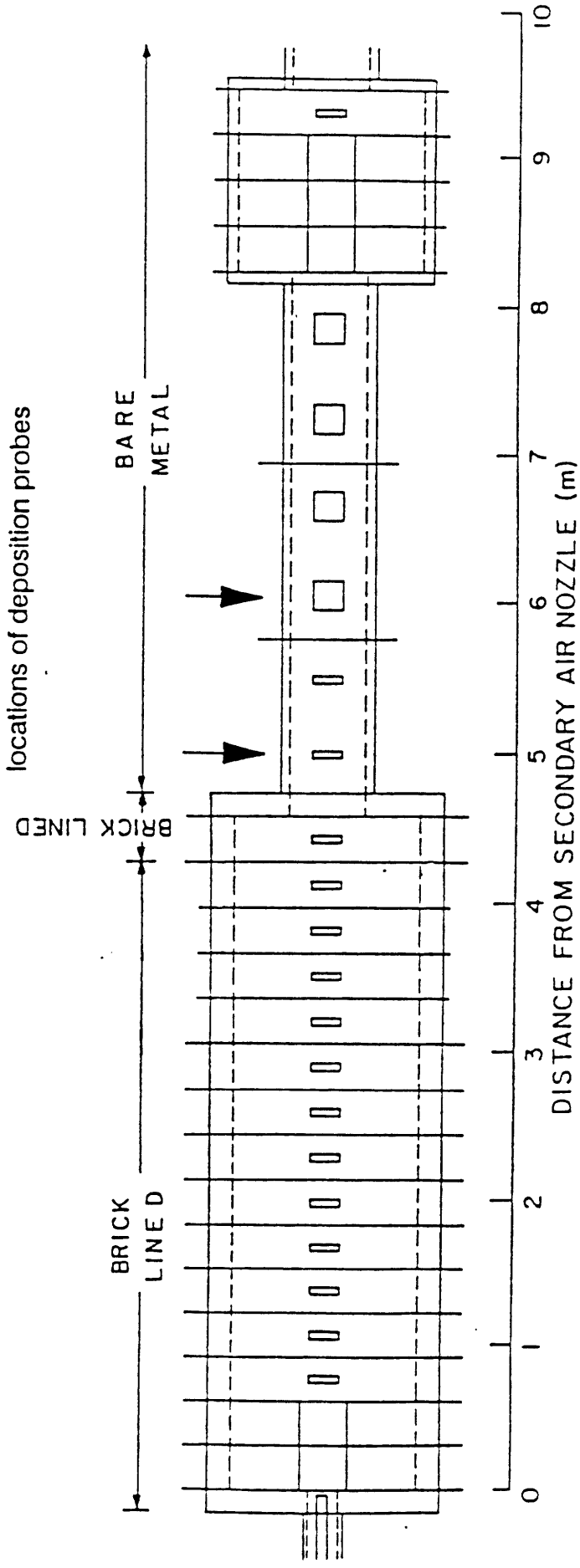

Figure 18. The Set Up of the Combustion Research Facility

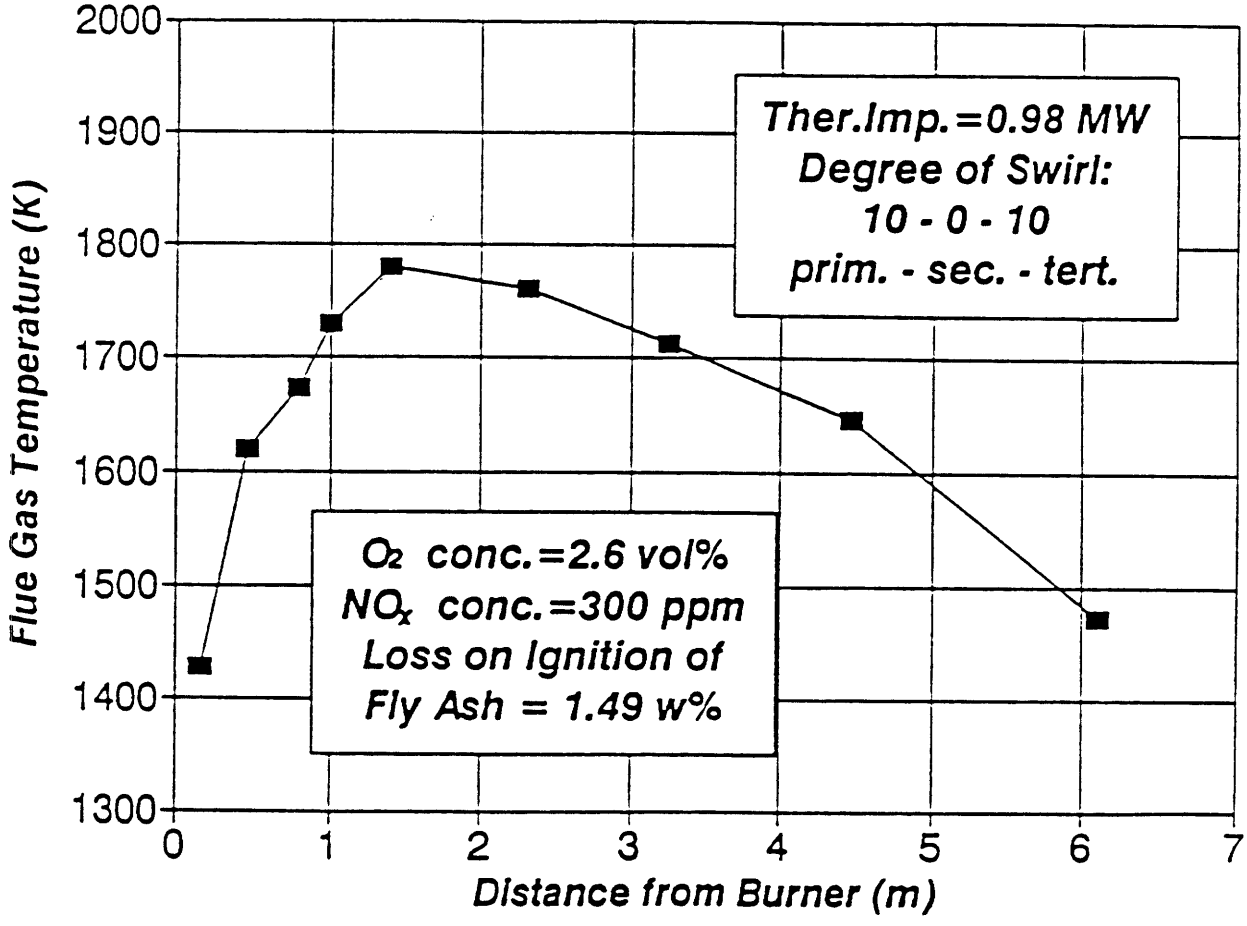

Figure 19. **Axial Flue Gas Temperature Profile**
Mapco Bituminous Coal

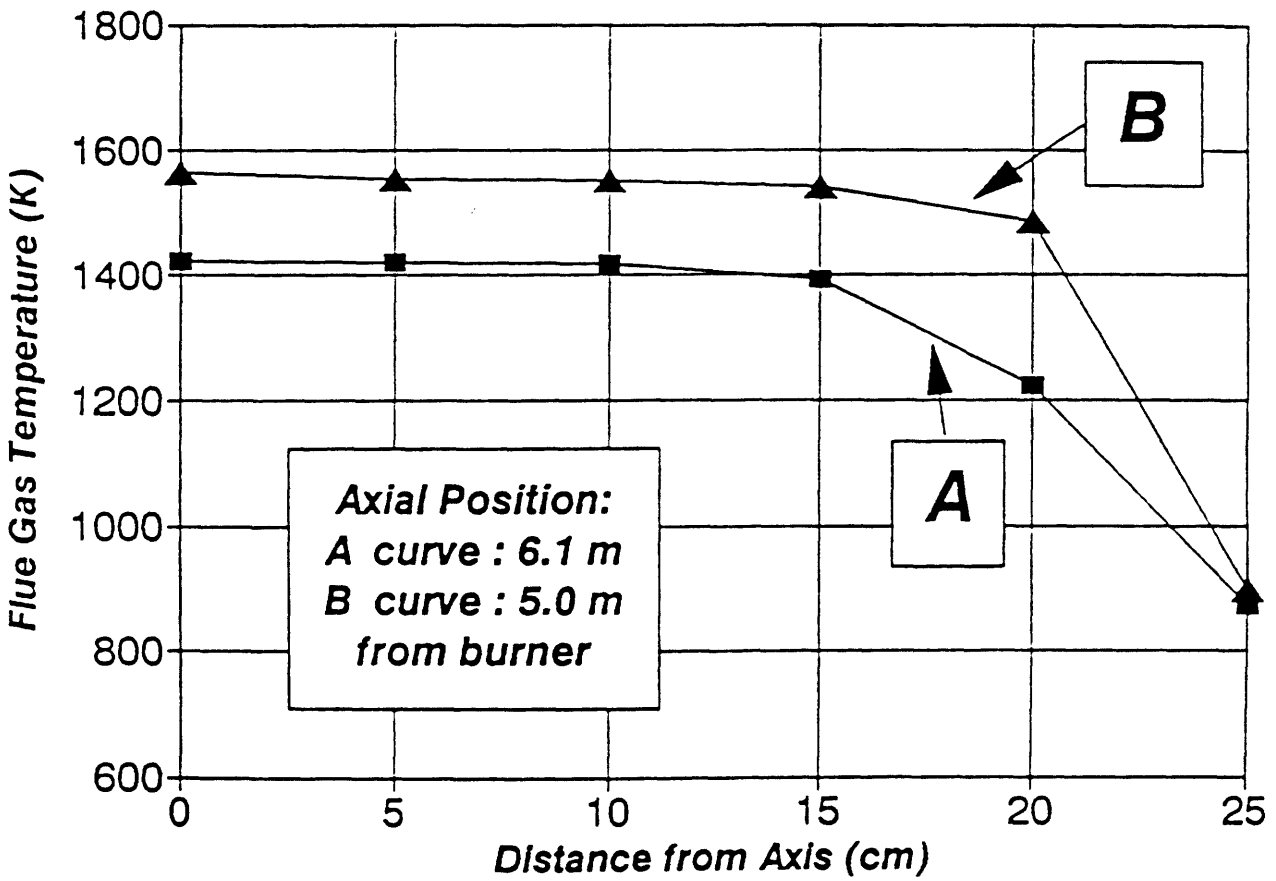

Figure 20. **Radial Flue Gas Temperature Profile**
Mapco Bituminous Coal

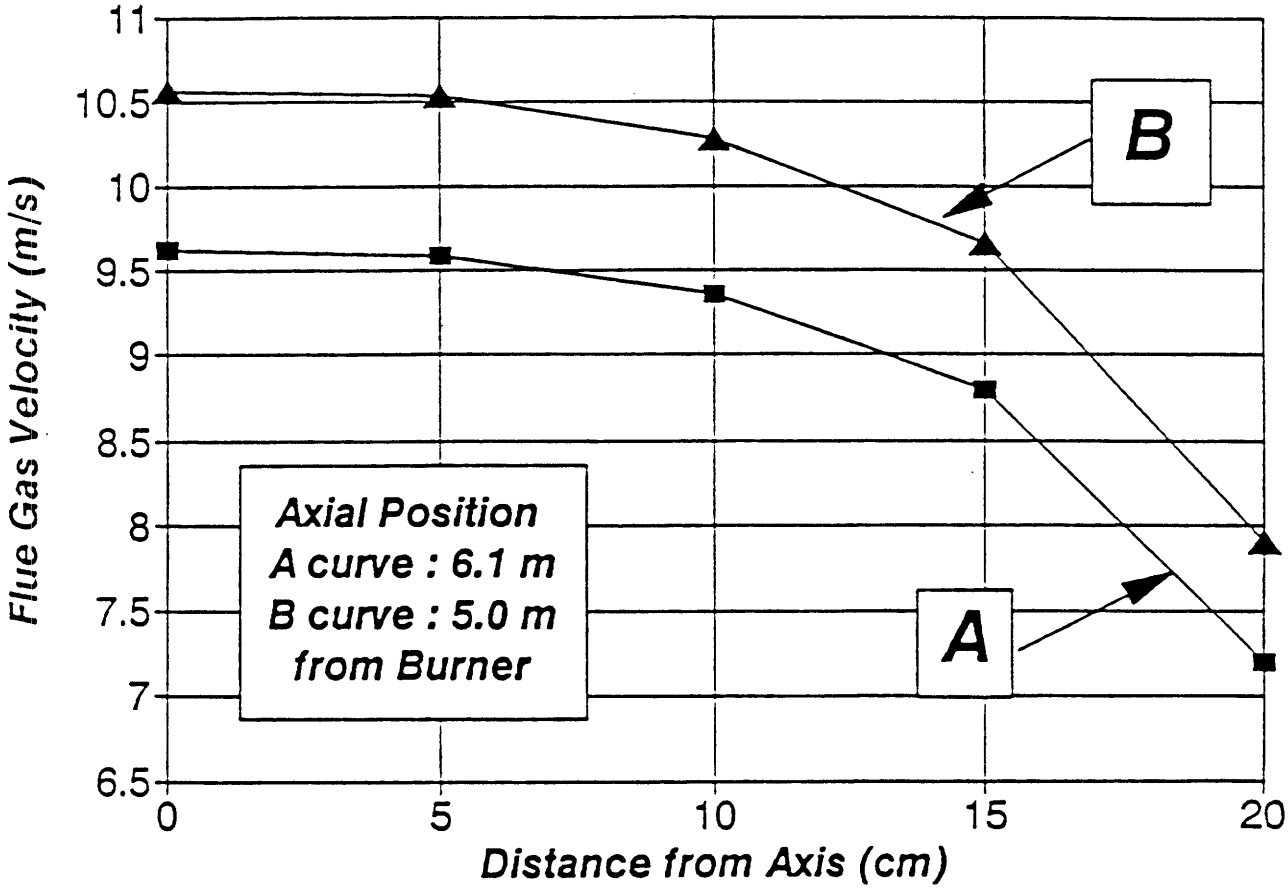

Figure 21. **Radial Flue Gas Velocity Profile**
Mapco Bituminous Coal

Table 3.
Test Parameters of Mapco Bituminous Coal in MIT-CRF

Parameters	*Data*
Thermal Input (MW)	*0.98*
Excess Air vol%	*14*
Coal Mass Flow (kg/h)	*114*
Carrying Air Mass Flow (kg/h)	*137.7*
Carrying Air/Coal Mass Ratio (1)	*1.21*
Primary Air Flow (kg/h) (high.swirl)	*78.6*
Secondary Air Flow (kg/h) (no.swirl)	*66.8*
Tertiary Air Flow (kg/h) (top+bottom) (high swirl)	*416.7 + 525*
Total Air Flow (kg/h)	*1225.0*
Prim. Air Burner Inlet Temperature (K)	*376*
Sec. Air Burner Inlet Temperature (K)	*522*
Tert. Air Burner Inlet Temperature (K)	*597*

diameter of the tube was determined by setting the Stokes number at a value of approximately 30 in the cylindrical section of the CRF, in order to achieve similar fly ash impaction efficiency in the CRF as in actual boilers. The probes were designed to be cooled by air. The inner diameter of the tube was chosen to provide an outer surface tube temperature of between 800 and 1100 K. In order to monitor the surface temperature of the probe during deposition build-up, three thermocouples were soldered along the axis of the tube. A cross section of the deposition probe is shown in Figure 22.

During the deposition sampling, a constant initial surface temperature of 1073 K was obtained by monitoring the surface temperature of the deposition probe and by adjusting the mass flow rate of the cooling air. The probes were placed in the cylindrical section of the CRF at two locations, corresponding to two different flue gas temperatures. The deposition probes were left in the flue gas for different periods of time to permit the rate of deposition to be determined.

For the flue gas temperature of 1423 K and velocity of 9.6 m/s, the deposition build-up can be seen in Figure 23. The deposition weight per unit projected probe area is plotted as a function of time. Linear regression was used to approximate the deposition flow and calculate the flow rate. The calculated specific deposition rate was 0.0069 $kg/m^2/min$. For the flue gas temperature of 1563 K and velocity of 10.6 m/s, the results are shown in Figure 24. These results indicate higher deposition flow and rate. From a linear approximation, the specific deposition rate was calculated as 0.0825 $kg/m^2/min$, which is approximately 12 times higher than that found in the previous case.

The deposit was easily removable from the deposition probe, and easily breakable in both cases, indicating low activity of sintering between deposited fly ash particles. The bulk density of the deposit was reported as a good indicator of the advance of particle sintering. The average bulk density of the deposit taken at the higher flue gas temperature and after 100 minutes was 0.64 g/cm^3.

4.1.10 Properties of Mapco Fly Ash

A fly ash sample was taken at 6.1 m from the burner by the method of isokinetic probe sampling.

By using the CCSEM technique, the fly ash size distribution and chemical composition was determined. In Figure 25, the volume-based distribution function of the fly ash is shown. The maximum fly ash particle size was 90 μm, the calculated mean particle size was 10.1 μm, and the standard deviation was 6.0 μm. By comparing the size distribution of the mineral inclusions with that of the fly ash, it can be seen that the particle size distribution of the fly ash is coarser.

The chemical composition of the fly ash given in Table 4 was used to calculate the distribution of particle viscosity at flue gas temperatures of 1423 K and 1563 K by using the

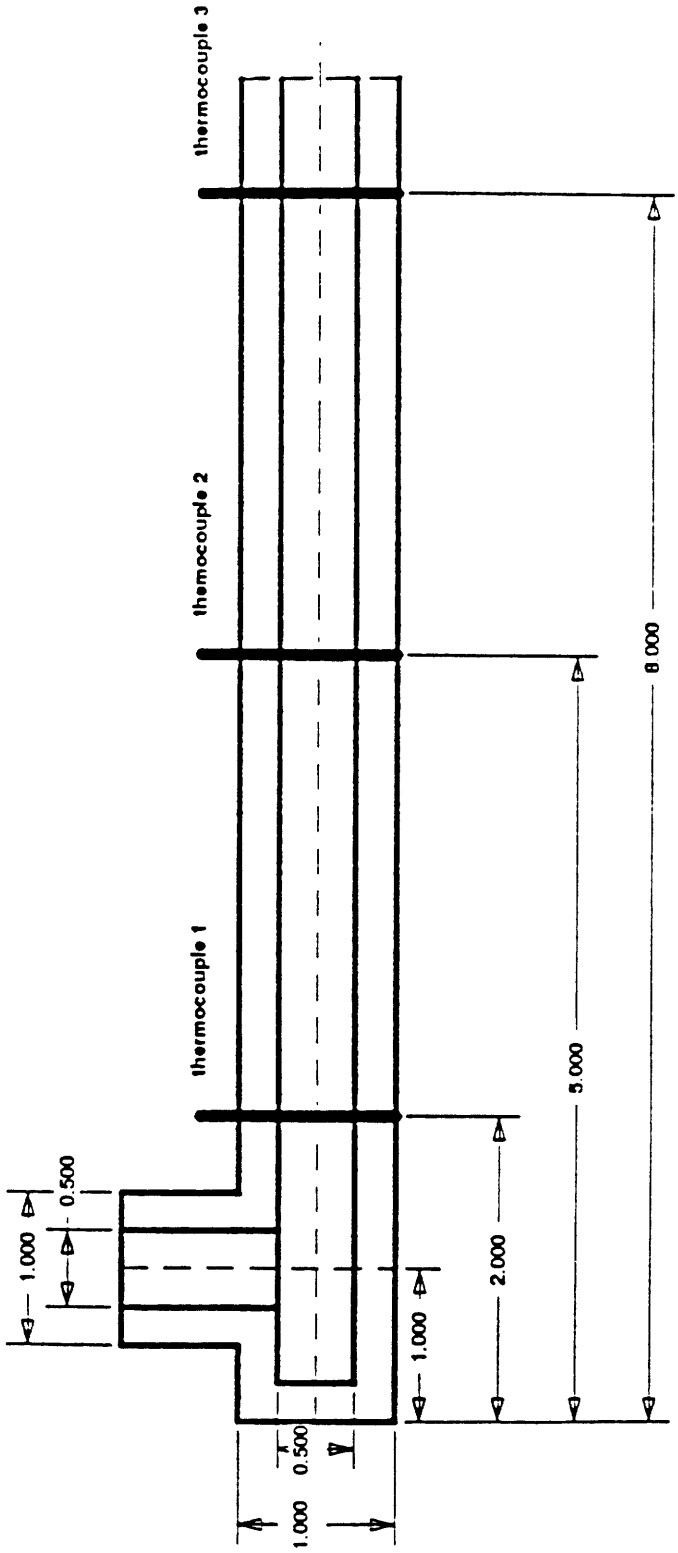

Figure 22. Geometry of the Deposition Probe
(dimensions in inches)

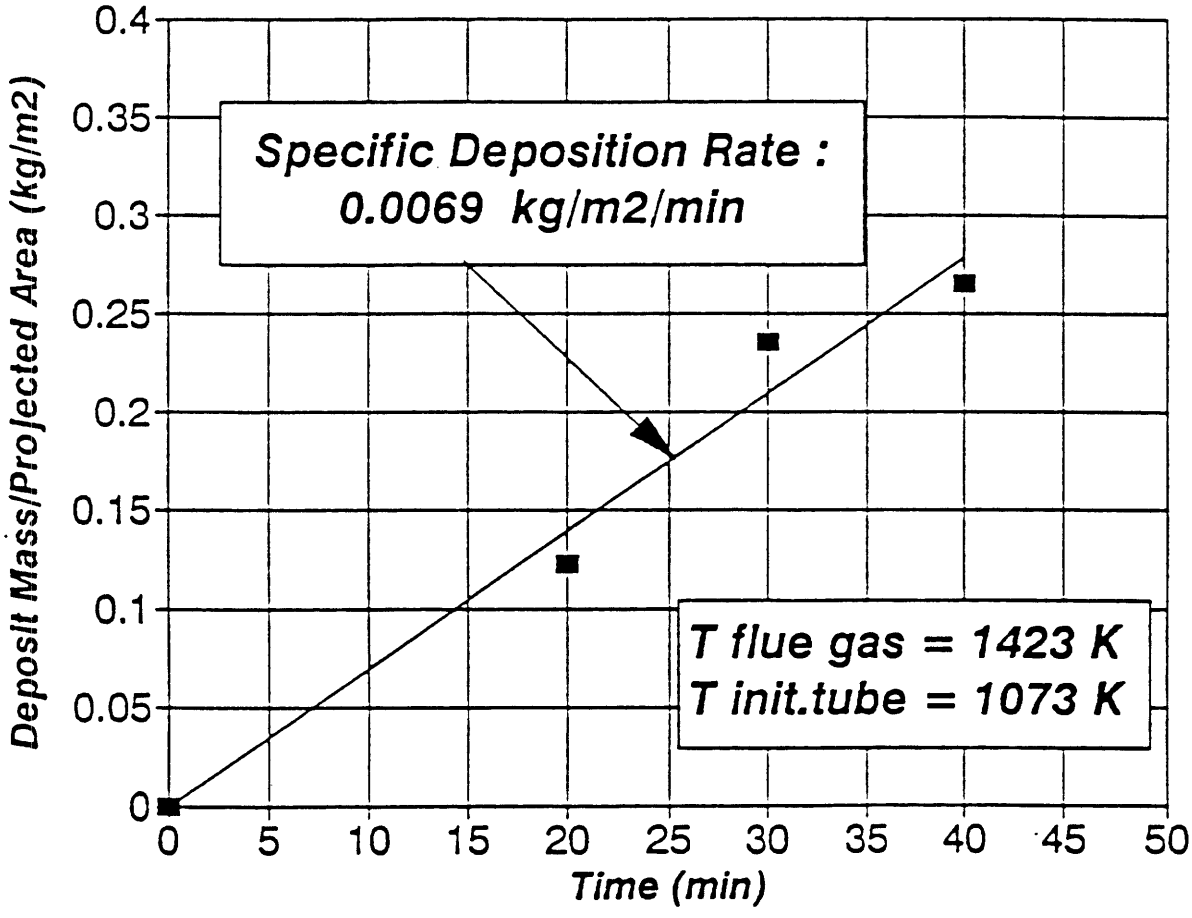

Figure 23. **Deposit Build-Up**
Mapco Bituminous Coal

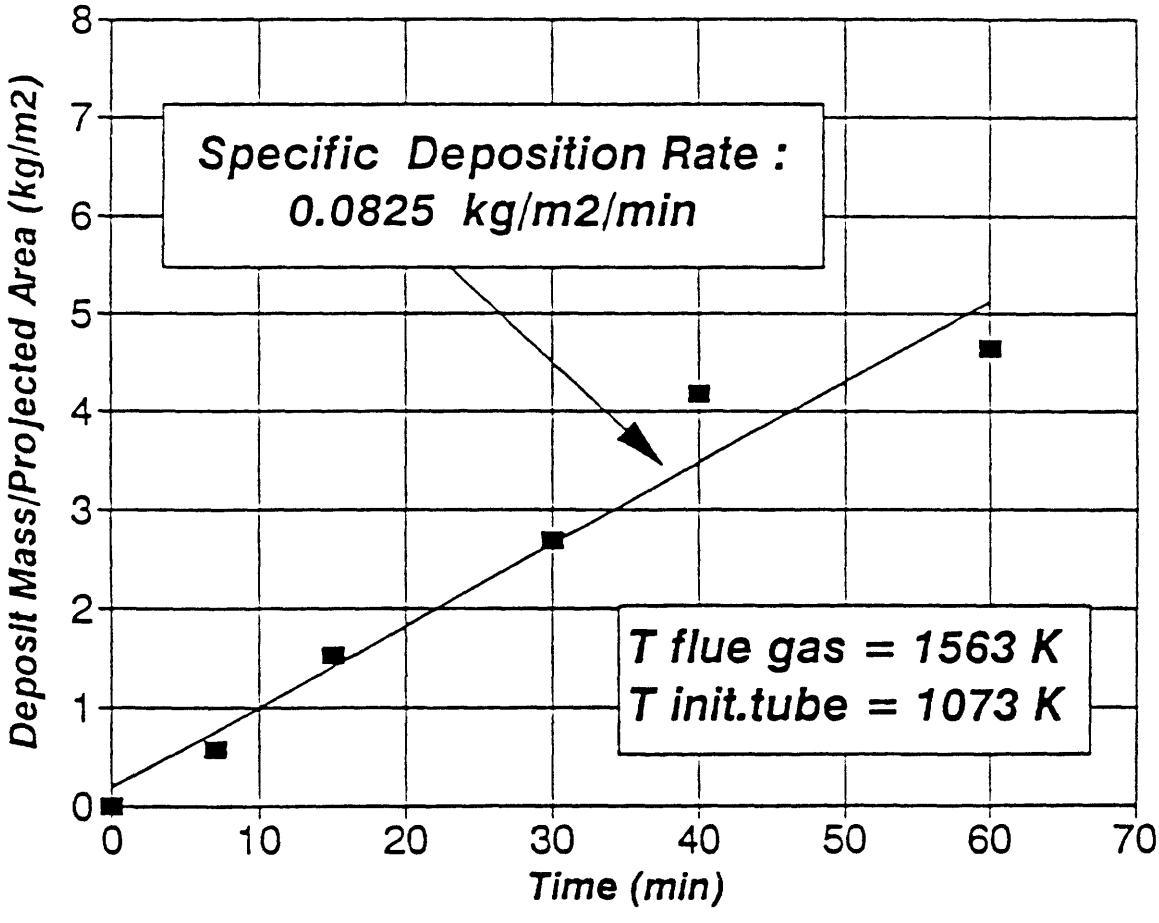

Figure 24. **Deposit Build-Up**
Mapco Bituminous Coal

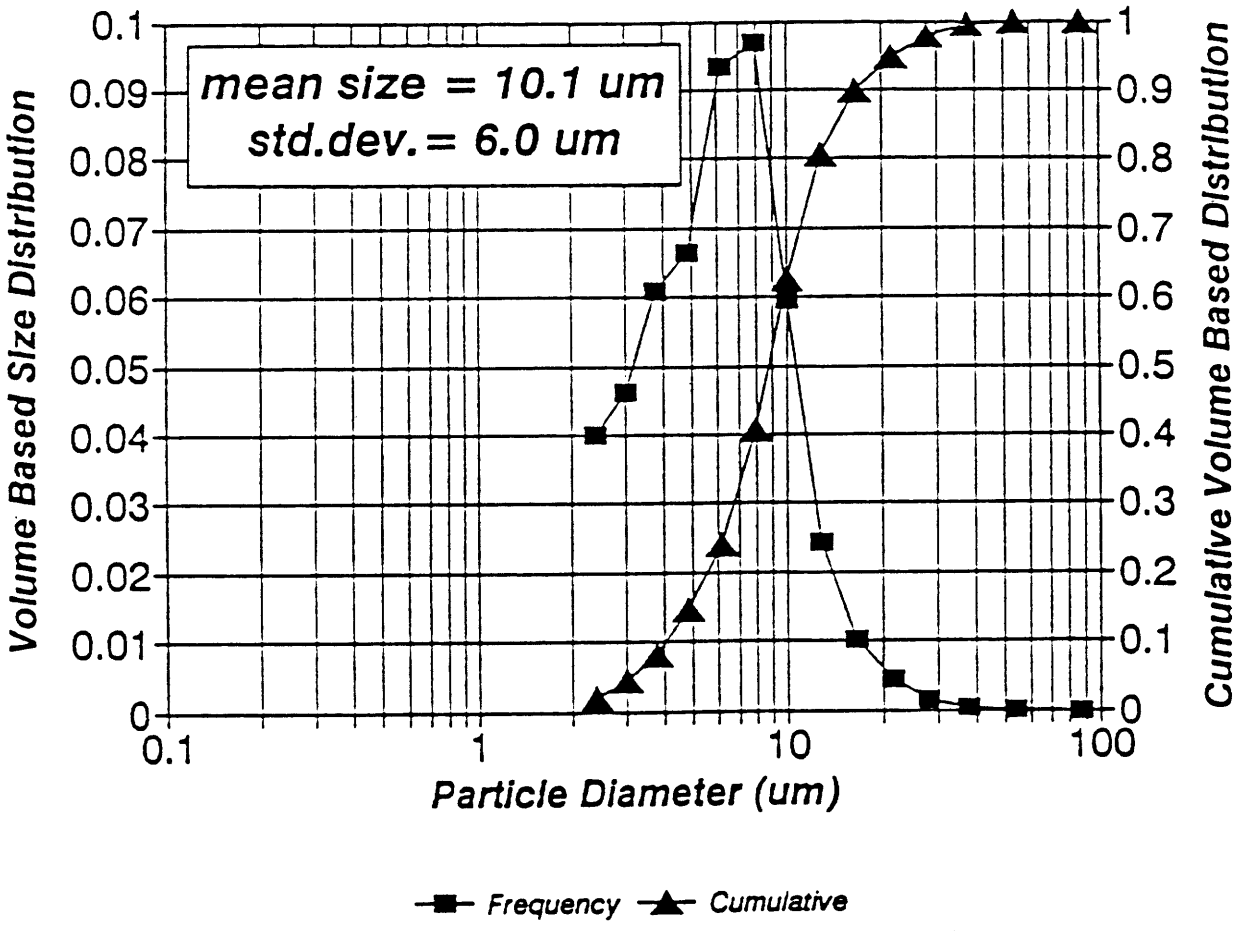

Figure 25. **Size Distribution of Fly Ash**
Mapco Bituminous Coal

Table 4.
Comparison of Chemical Composition of the MAPCO Ash and Fly Ash Determined by ASTM and CCSEM Methods, Respectively

	ASTM	*CCSEM*
Oxide Formula	*Ash*	*Fly ash*
Na_2O	1.2	0.5
MgO	0.9	0.42
Al_2O_3	29.2	27.0
SiO_2	48.2	47.5
P_2O_5	0.1	1.3
SO_3	3.0	0.5
Cl	0.0	0.2
K_2O	2.4	4.6
CaO	4.3	6.5
TiO_2	2.0	2.1
FeO	8.6	8.1
Cr_2O_3	0.0	1.3
BaO	0.1	0.0

Watt-Fereday equation. The results can be seen in Figures 26 and 27. Due to the random coalescence of included mineral matter during coal particle burnout, the viscosity distribution of the fly ash is considerably different from that of the included mineral matter. Both the mean value and standard deviation of the viscosity of the included mineral matter are smaller for the fly ash. The ratio of the mean viscosities of the included mineral matter and the fly ash, calculated for different temperatures, is plotted in Figure 28. The ratio of the respective standard deviations is also shown in Figure 28. Both ratios are independent of the temperature. The ratio of the mean viscosities and that of the standard deviations are decreased by 15% and by 28%, respectively.

The calculated sticking efficiencies of the included mineral matter and fly ash are plotted in Figure 29. The critical viscosity value was chosen to be 10^6 poise.

4.2 Wyoming Lignite

4.2.1 Wyoming Lignite Characteristics

The characteristics of the Wyoming lignite provided by ABB-Combustion Engineering are listed in Table 5. The lignite is a low rank coal with high moisture and volatile content and low heating value. Its sulfur content is low (0.15 wt%) and originates mainly from pyrite. The melting behavior of its ash was determined by ASTM method, and is characterized by data included in Table 5. According to these data, the temperature window within which the deformation of ash particles takes place is from 1426 K to 1454 K. The difference between the initial deformation temperature and the fluid temperature is very low, 28 K. The ash chemical composition indicates high CaO and SO_3 content. The high sulfur content is due to the favored conditions for the sulfation of the CaO in the coal during the ASTM coal ashing procedure.

4.2.2 Extraneous Mineral Matter in Wyoming Lignite

By using a sink-float method, the extraneous mineral content of Wyoming lignite was determined as 0.087 wt%.

4.2.3 Ion-Exchangeable Mineral Content of Wyoming Lignite

By using acetic acid extraction of the coal, the mass content of the ion-exchangeable mineral was determined. The result shows that 22% of the total ash content is ion-exchangeable. By taking the chemical composition of the ash determined by the ASTM method, and that of the included mineral matter determined by the CCSEM method, the chemical composition of the leached mineral matter can be calculated. The results show that the ion-exchangeable mineral matter consists of 82 wt% CaO, 12.5 wt% MgO and 5.5 wt% Na_2O.

4.2.4 Size Distribution of Wyoming Lignite

The volume-based size distribution of the lignite can be seen in Figure 30. The

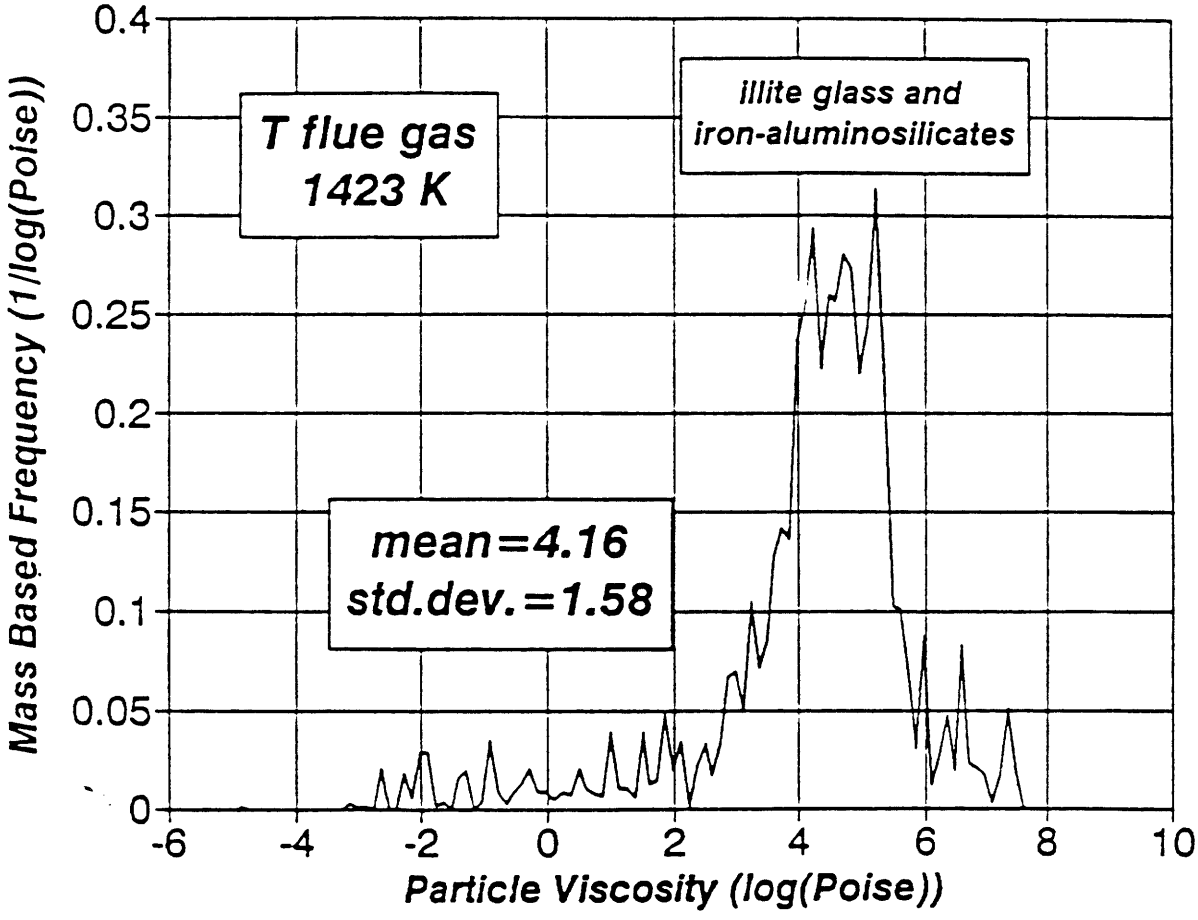

Figure 26. **Viscosity Distribution of Fly Ash**
Mapco Bituminous Coal

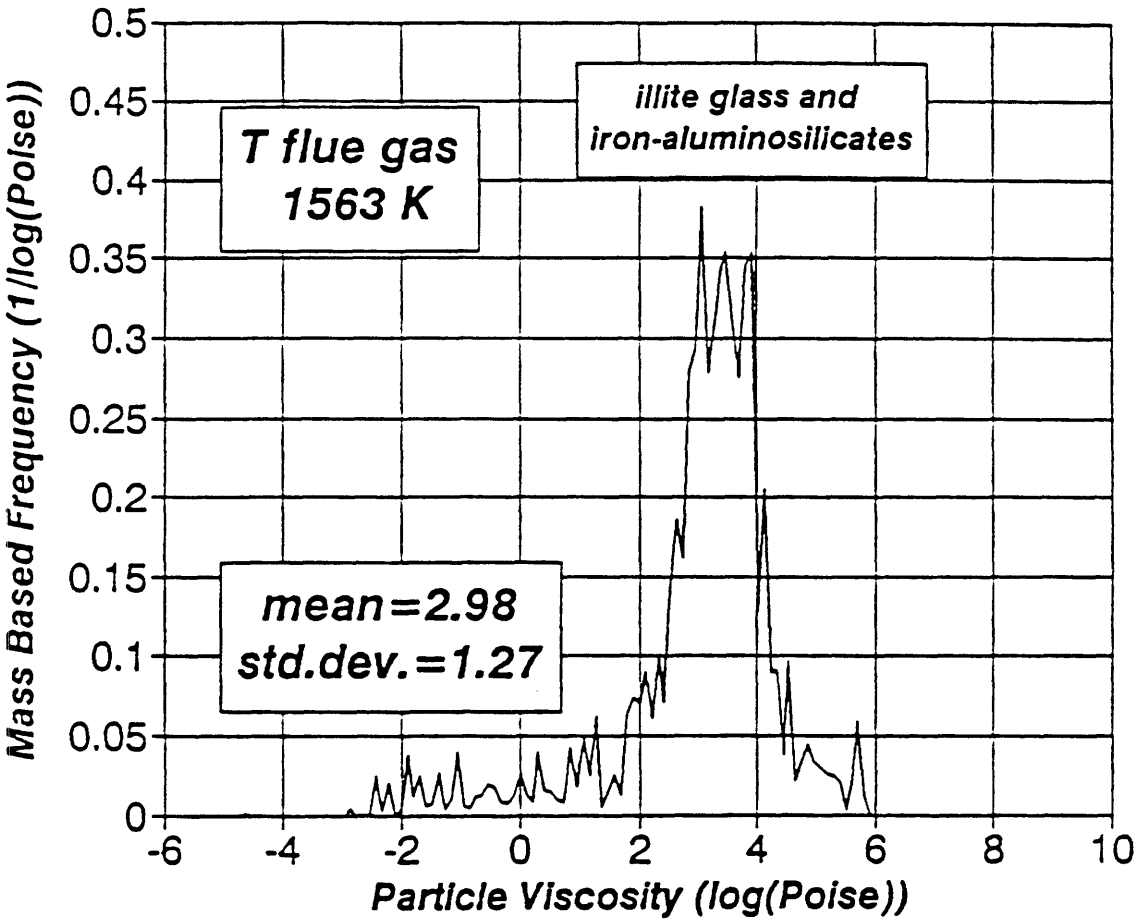

Figure 27. **Viscosity Distribution of Fly Ash**
Mapco Bituminous Coal

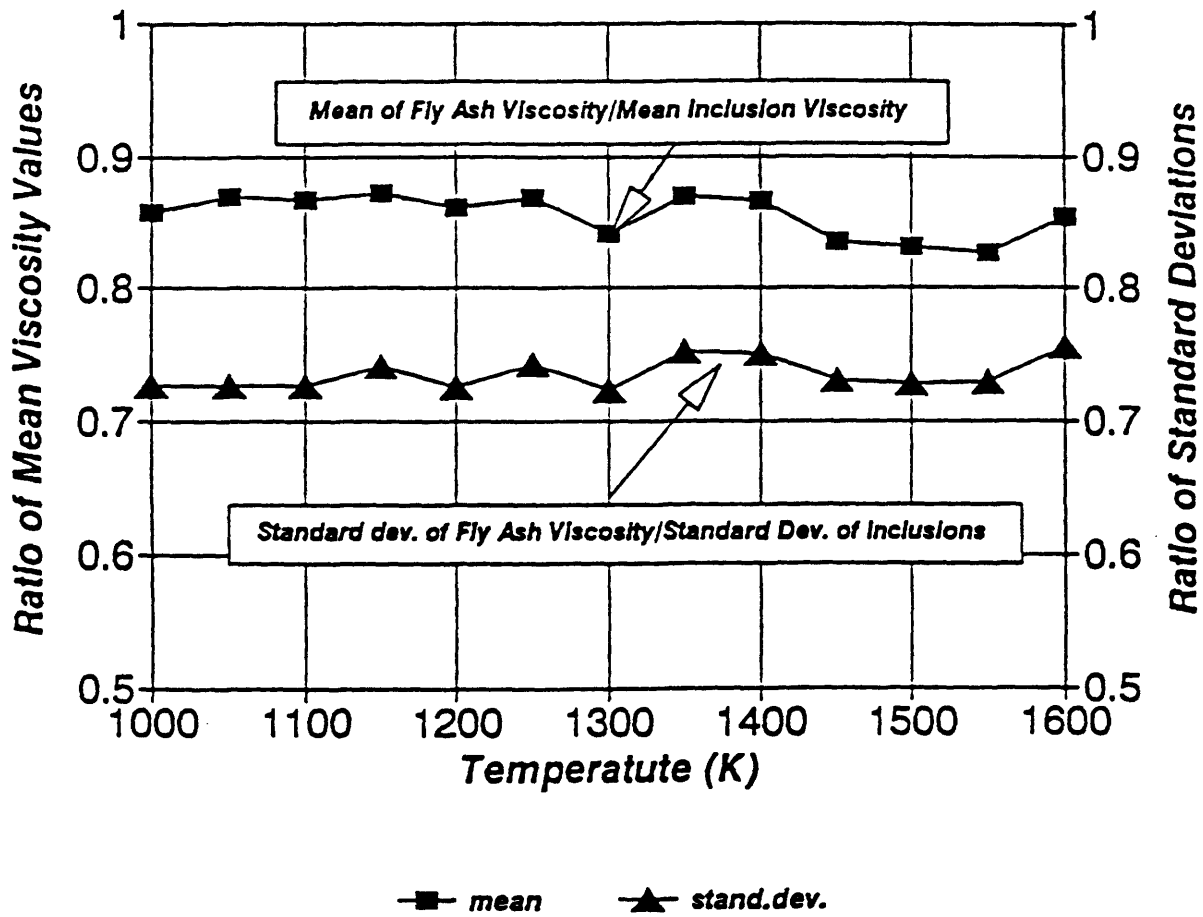

Figure 28. **Statistical Parameters of Viscosity**
Mapco Bituminous Coal

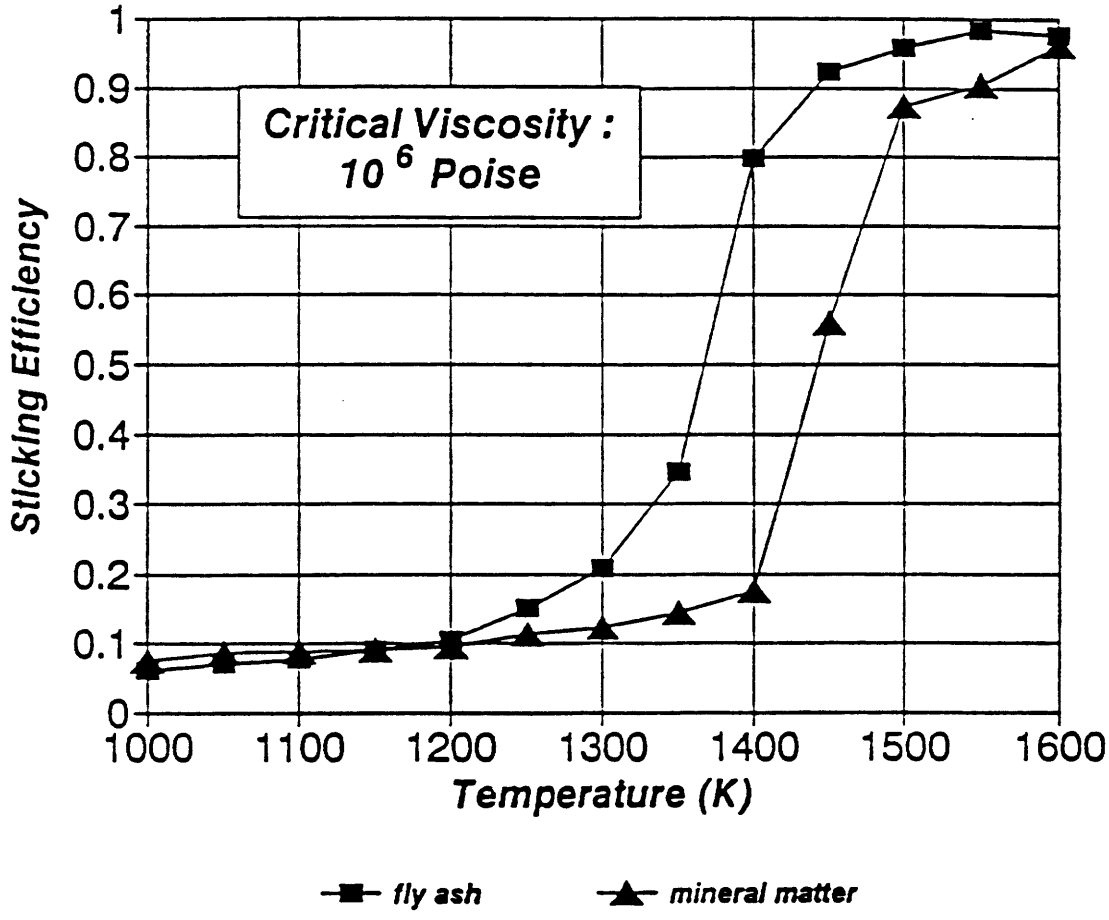

Figure 29. **Sticking Efficiency**
Mapco Coal

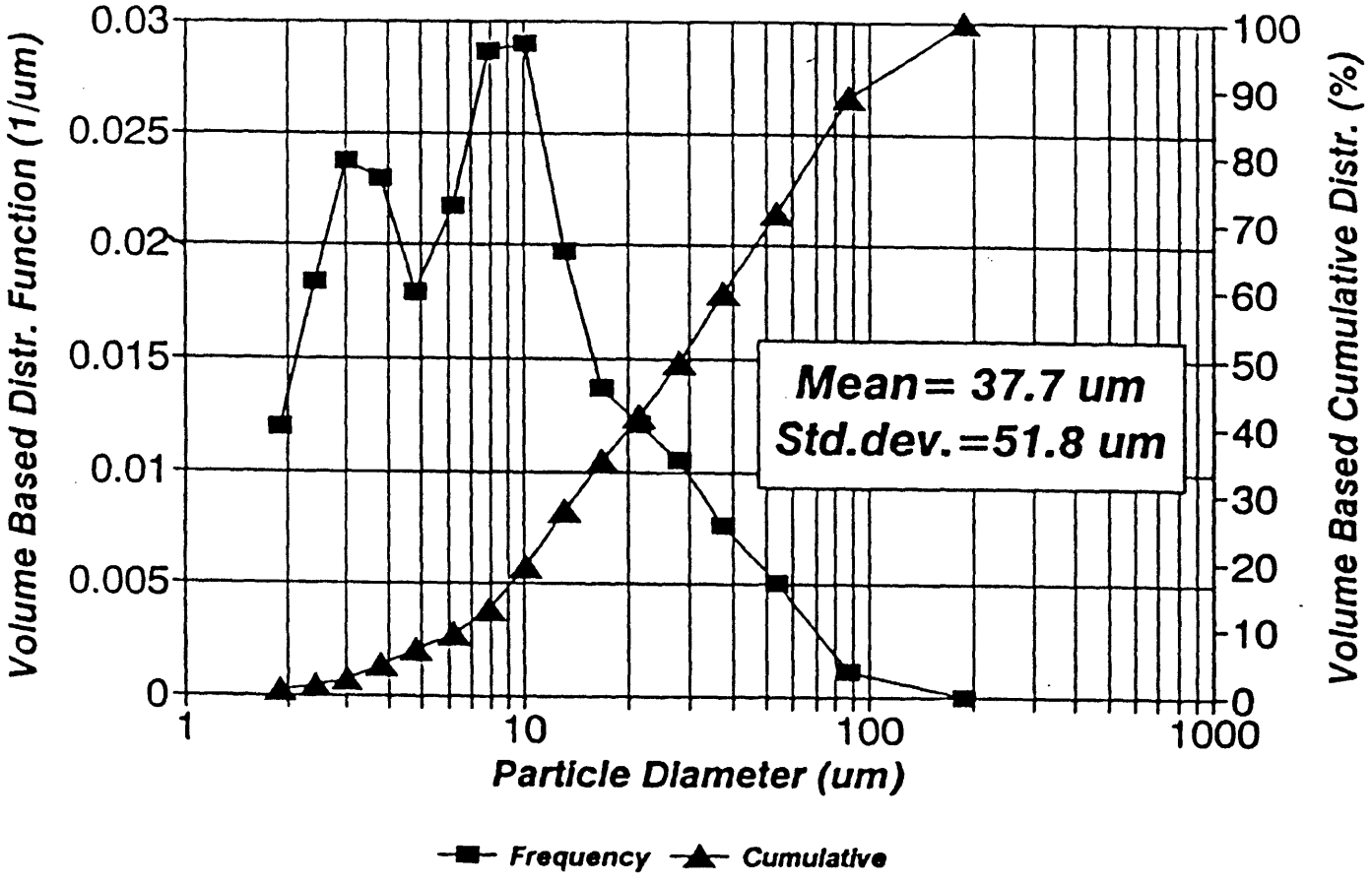

Figure 30. **Size Distribution of Wyoming Coal** Determined by Laser Diffraction Method

Table 5.
Characteristics of Wyoming Lignite

Quantity	Wyoming Lignite	
Moisture wt%	13.4	
Volatile Matter	43.8	
Fixed Carbon	35.9	
Ash wt.%	6.9	
HeatingValue	10225	
Pyritic Sulfur	0.13	
Sulfate wt.%	0.02	
Organic Sulfur	0.00	
IDT K	1426	
ST K	1439	
HT K	1444	
FT K	1454	
	with Sulfur	without Sulfur
Ash SiO_2 wt.%	31.7	39.1
Ash Al_2O_3 wt.%	15.8	19.5
Ash Fe_2O_3 wt.%	5.6	6.9
Ash CaO wt.%	19.5	24.1
Ash MgO wt.%	4.3	5.3
Ash Na_2O wt.%	0.8	1.0
Ash K_2O wt.%	0.5	0.6
Ash TiO_4 wt.%	1.2	1.5
Ash P_2O_5 wt.%	0.4	0.5
Ash SO_3 wt.%	19.0	0.0
Ash BaO wt%	0.1	0.5
Ash SrO wt%	0.3	0.3

frequency function represents a bimodal distribution at particle sizes of 3 μm and 10 μm, respectively. The maximum particle size is 200 μm. The volumetric mean value and standard deviation of the distribution were calculated by using the method of lognormal curve fitting. The calculated mean size and standard deviation are 37.7 μm and 51.8 μm, respectively.

4.2.5 Density and Ash Content as a Function of Coal Size

The results are plotted in Figure 31. They show that both the mean particle density and ash content increase with decreasing coal particle size. However, the relative change is less than 15%.

4.2.6 Size Distribution of Mineral Inclusions

The volume-based size distribution of mineral inclusions is plotted in Figure 32. The volumetric mean particle size and standard deviation were approximated by using the method of lognormal curve fitting. The calculated mean particle size and standard deviation are 4.3 μm and 3.8 μm, respectively. The maximum particle size is under 20 μm. The distribution functions were determined by CCSEM method and Abelian transformation was used for the stereological correction of the raw data.

4.2.7 Chemical Composition and Calculated Viscosity Distribution of Mineral Inclusions in Wyoming Lignite

The mean chemical compound concentrations in the mineral inclusions and the mean concentrations of mineral types are shown in Table 6. It can be seen that the mineral inclusions consist mainly of illite, evensite and quartz, with smaller amounts of kaolinite and mixed silicates. The mean chemical composition of mineral inclusions is different from that of the ash measured by the ASTM method due to the contribution of the ion-exchangeable mineral which is not detected by CCSEM. The comparison of the calculated sulfur-free chemical composition of the ash determined by ASTM and the total mineral matter is given in Table 7.

The peak flame temperature (1673 K) was chosen for the viscosity calculations. The mass-based distribution function of mineral particle viscosity is given in Figure 33. The mean value and standard deviation of the viscosity are $10^{2.25}$ poise and $10^{1.94}$ poise, respectively. The curve shows three major peaks, consistent with the mineral inclusions in the Wyoming lignite representing a physical mixture of the predominant mineral types that were identified by the CCSEM.

4.2.8 Experiments in the Combustion Research Facility

The test conditions for the Wyoming lignite are summarized in Table 8. The coal feed rate was set to obtain 0.93 MW thermal input. The coal was carried by air from a coal silo at 1.2 air/coal mass ratio. The flow rate of air was measured by a built-in pitot tube. The flow rate of the coal was measured by a weigh belt. The primary, secondary and tertiary air flows

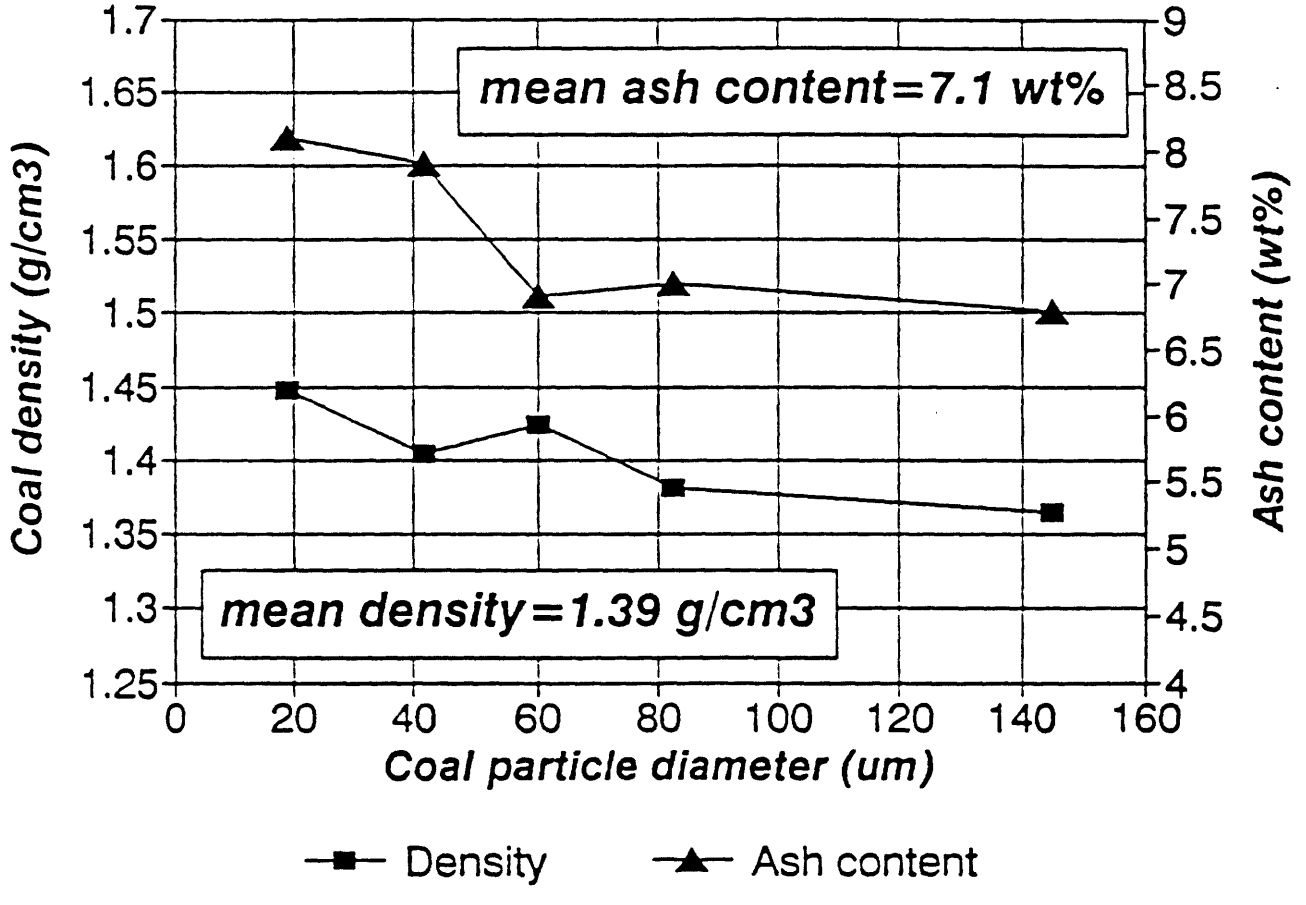

Figure 31. **Coal Density and Ash Content**
Wyoming Lignite

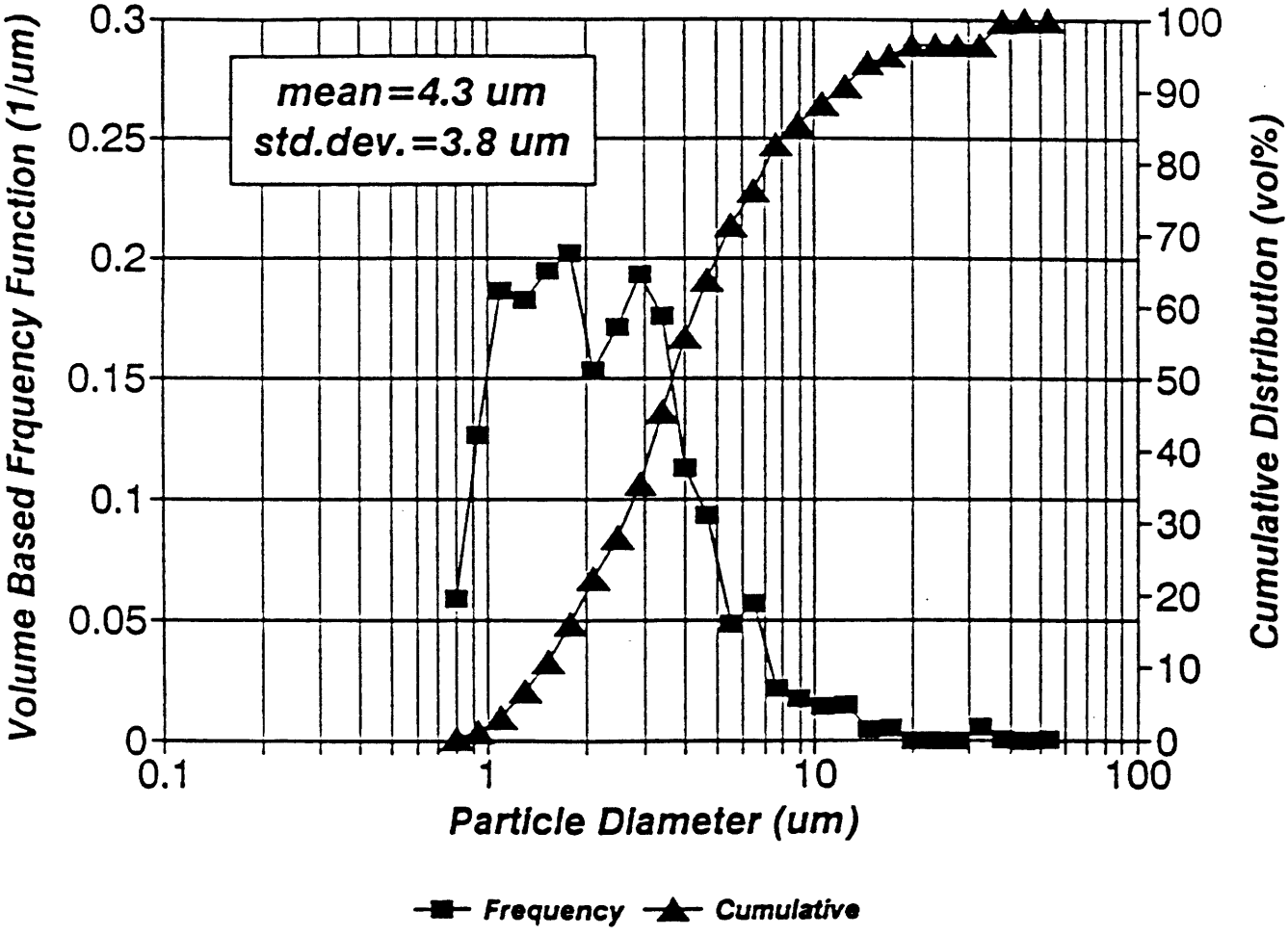

Figure 32. **Size Distribution of Mineral Inclusions**
Wyoming Lignite

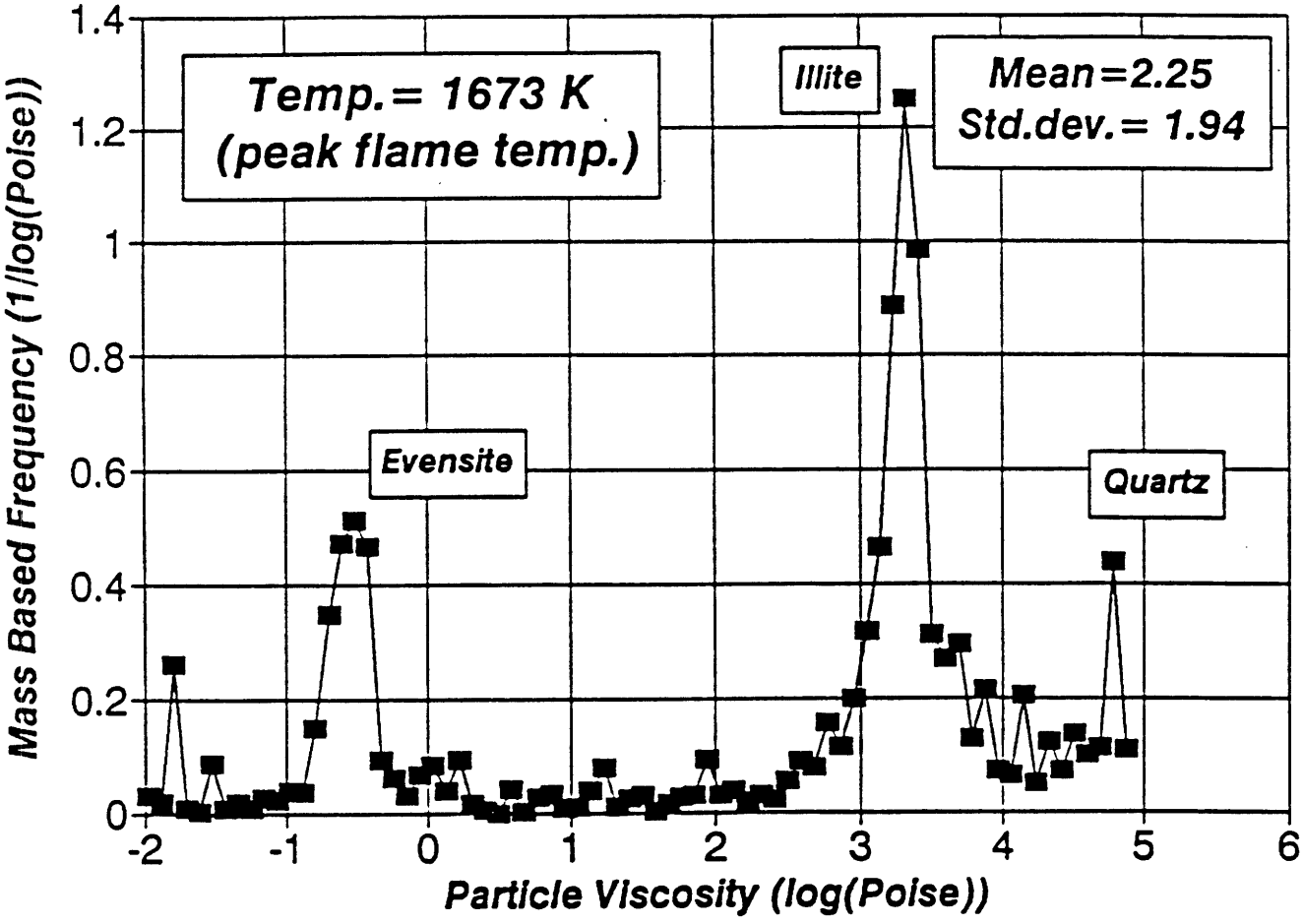

Figure 33. **Viscosity Distribution of Inclusions**
Wyoming Lignite

Table 6.
Chemical Composition and Mineral Compounds of Wyoming Lignite Mineral Inclusions

Oxide Formula	*Weight %*	*Mineral Type*	*Mass %*
Na_2O	0.2	*Mixed Silicate*	8.69
MgO	0.4	*Quartz*	22.88
Al_2O_3	26.01	*Calcite*	0.37
SiO_2	48.62	*Siderite*	0.78
P_2O_5	5.47	*Rutile*	2.16
SO_3	2.25	*Illite*	35.74
Cl	0.14	*Pyrite/Marcasite*	0.86
K_2O	1.4	*Apatite/Evensite*	18.58
CaO	7.38	*Baryte*	2.26
TiO_2	2.92	*Kaolinite*	8.37
FeO	3.89	*Jarosite*	1.3
Cr_2O_3	0.37	***Results by CCSEM Method***	
BaO	0.95		

Table 7.
Comparison of Chemical Composition of the Wyoming Lignite Ash and Mineral Matter Determined by ASTM and CCSEM Methods, Respectively

	ASTM	CCSEM
Oxide Formula	Ash	22w% ion.ex.+78w% incl.
Na_2O	1.0	1.39
MgO	5.3	3.1
Al_2O_3	19.5	20.6
SiO_2	39.1	38.6
P_2O_5	0.5	4.3
SO_3	0.0	0.0
Cl	0.0	0.11
K_2O	0.6	1.1
CaO	24.1	24.2
TiO_2	1.5	2.31
FeO	6.9	3.1
Cr_2O_3	0.0	0.29
BaO	0.5	0.75

Table 8.
Test Parameters of Wyoming Lignite in MIT-CRF

Parameters	*Data*
Thermal Input (MW)	*0.93*
Excess Air vol%	*14*
Coal Mass Flow (kg/h)	*140.6*
Carrying Air Mass Flow (kg/h)	*168.7*
Carrying Air/Coal Mass Ratio (1)	*1.2*
Primary Air Flow (kg/h) (high.swirl)	*77.5*
Secondary Air Flow (kg/h) (no.swirl)	*67.2*
Tertiary Air Flow (kg/h) (top+bottom) (high swirl)	*407.3 + 470.0*
Total Air Flow (kg/h)	*1191.0*
Prim. Air Burner Inlet Temperature (K)	*384*
Sec. Air Burner Inlet Temperature (K)	*514*
Tert. Air Burner Inlet Temperature (K)	*594*

were also monitored by pitot tubes. The air was preheated to 384 K, 514 K and 594 K, respectively. Low air flow rates were maintained for the primary and secondary air, and high rate for the tertiary air flow. A high degree of swirl was chosen for the primary and tertiary air flows, and no swirl was used for the secondary air flow.

The flue gas temperature profile along the axis of the combustion tunnel is plotted in Figure 34. The temperature was measured by suction pyrometer. The peak flue gas temperature (1674 K) was reached at the distance of 2.2 m from the burner.

The deposition probes were placed in the flue gas stream at two positions: 6.1 m and 5.5 m from the burner. Radial temperature profiles were taken at each of these locations. The results are plotted in Figure 35. At the position of 5.5 m from the burner, the maximum temperature was 1509 K. The maximum temperature at 6.1 m from the burner was 1339 K. The maximum temperatures were found on the axis. Due to the intensive heat extraction through the cylinder jacket, the temperature decreased as the distance from the axis increased.

Pitot tube measurements to determine the radial flue gas velocity profile were made at the positions where the deposition probes were inserted. The results can be seen in Figure 36. At the position of 5.5 m from the burner, the peak velocity was 8.4 m/s. At the distance of 6.1 m from the burner, due to the decrease of flue gas temperature, the maximum velocity of the flue gas was 7.5 m/s. Both peak velocities were measured on the axis. The flue gas velocity decreases as the radial distance from the axis increases. At the distance of 20 cm, the result may have been affected by the in-leaking air.

4.2.9 Deposition Experiment

During the deposition sampling, a constant initial surface temperature of 1073 K was obtained by monitoring the surface temperature of the deposition probe and by adjusting the mass flow rate of the cooling air. The probes were placed in the cylindrical section of the CRF at two locations, corresponding to two different flue gas temperatures. The deposition probes were left in the flue gas for different periods of time to permit the rate of deposition to be determined.

For the flue gas temperature of 1339 K and velocity of 7.5 m/s, the deposition build-up can be seen in Figure 37. The deposited weight per unit projected probe area is plotted as a function of time. Linear regression was used to approximate the deposition flow and calculate the flow rate. The calculated specific deposition rate was 0.048 kg/m^2/min. For the flue gas temperature of 1509 K and velocity of 8.4 m/s, the results are shown in Figure 38. These results indicate higher deposition rate. From a linear approximation, the specific deposition flow rate was calculated as 0.1 kg/m^2/min, which is approximately 2 times higher than that found in the previous case.

In both cases the deposit was easily removable from the deposition tube; however, it was bonded and not easily breakable, indicating sintering between deposited fly ash particles. The

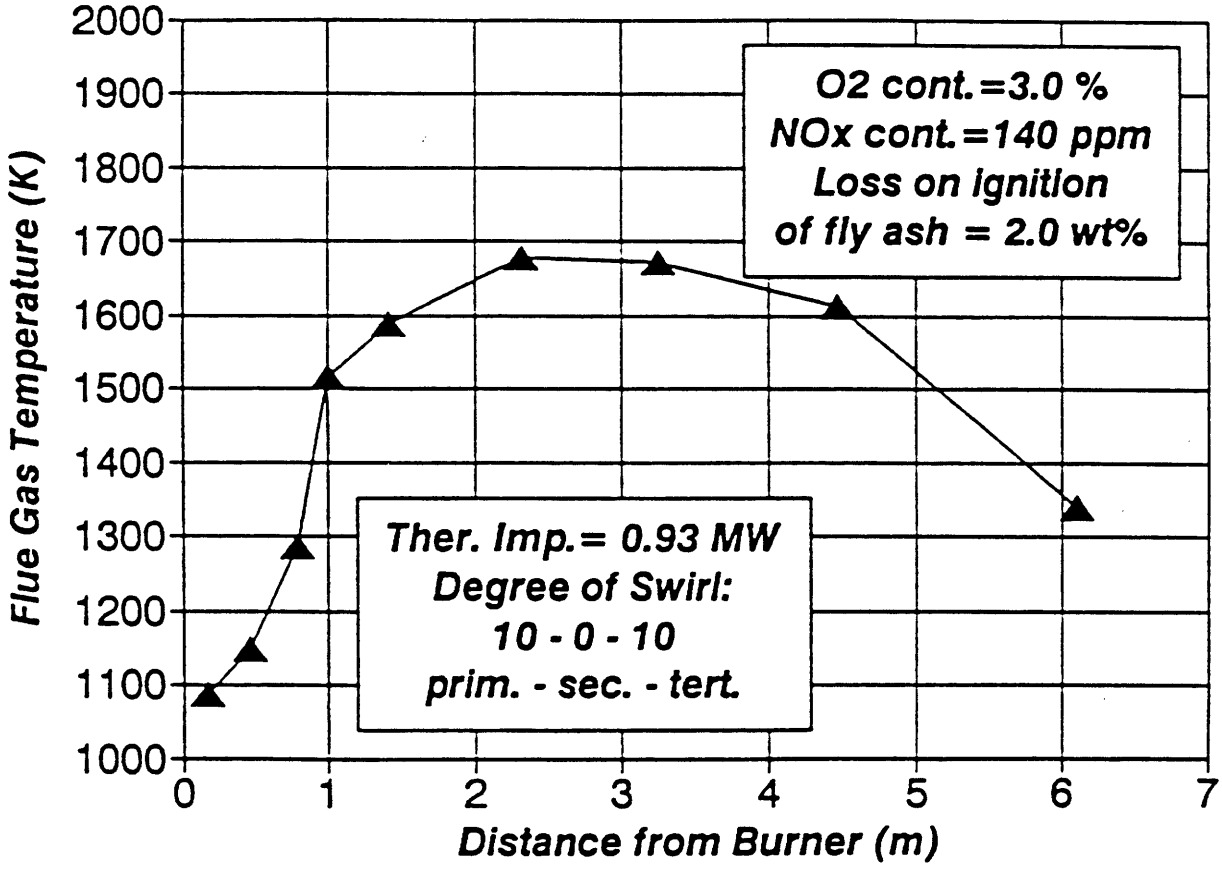

Figure 34. **Axial Flue Gas Temperature Profile**
Wyoming Lignite

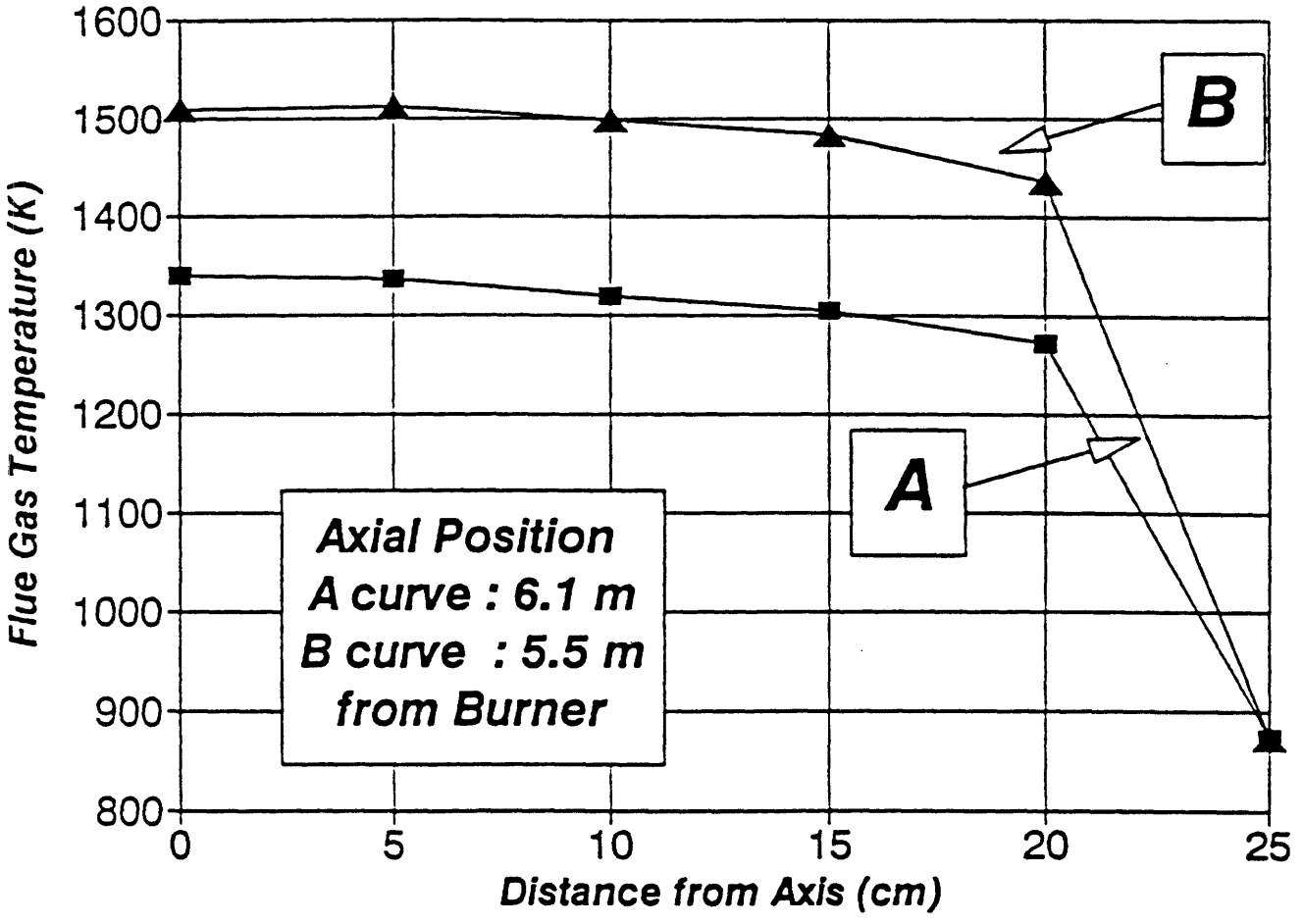

Figure 35. **Radial Flue Gas Temperature Profile** Wyoming Lignite

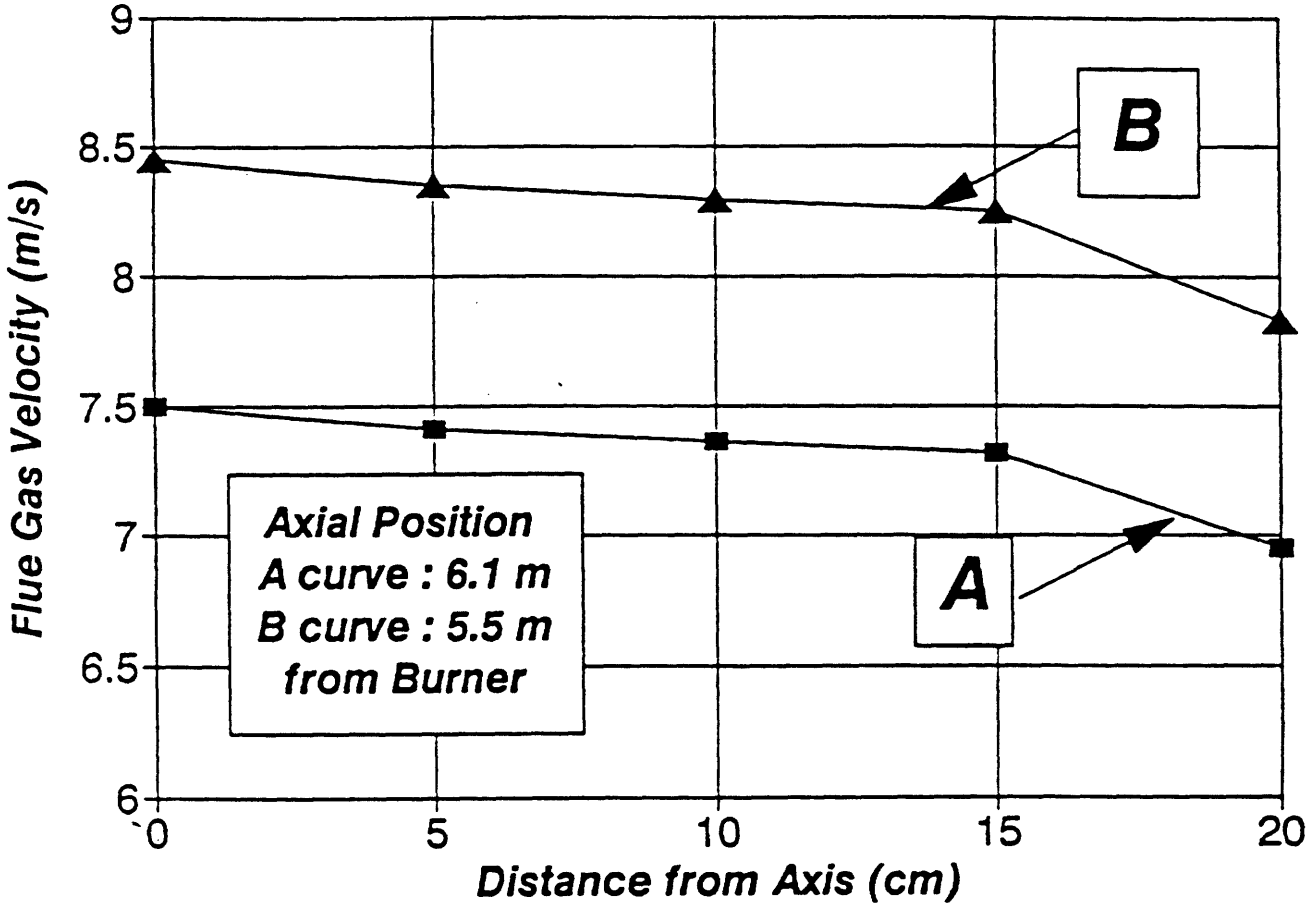

Figure 36. **Radial Flue Gas Velocity Profile**
Wyoming Lignite

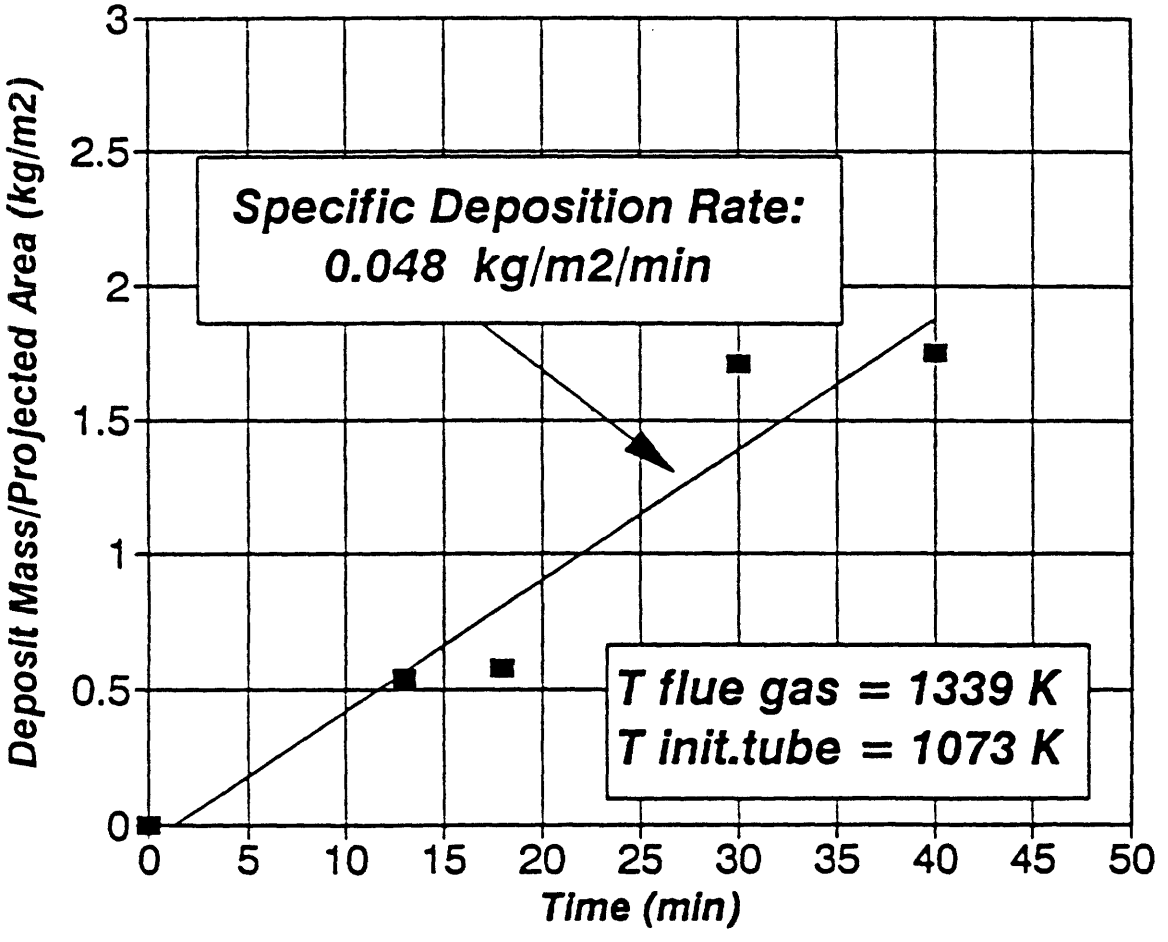

Figure 37. **Deposit Build-Up**
Wyoming Lignite

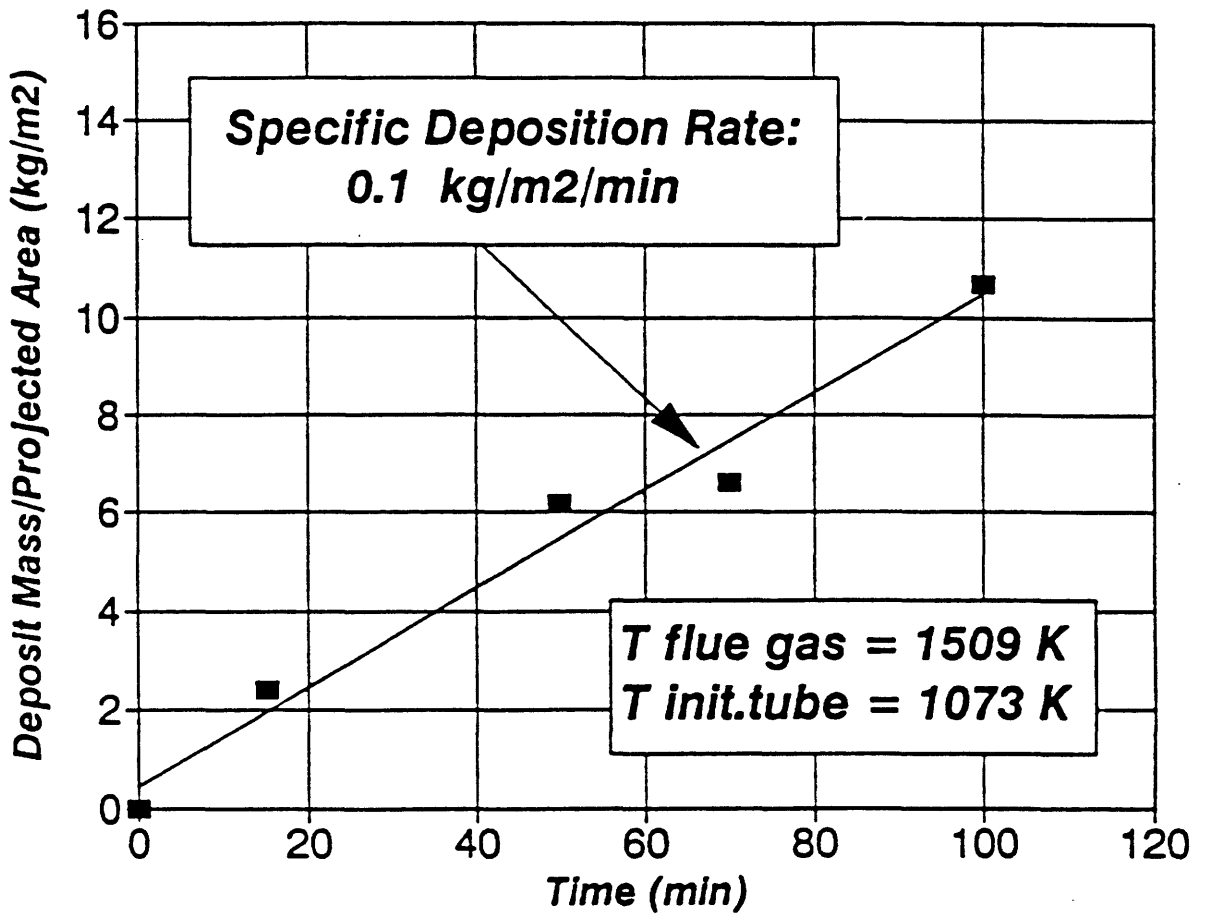

Figure 38. **Deposit Build-Up**
Wyoming Lignite

average bulk density of the deposit taken at the higher flue gas temperature and after 100 minutes was 0.99 g/cm^3.

4.2.10 Properties of Wyoming Fly Ash

A fly ash sample was taken at 6.1 m from the burner by the method of isokinetic probe sampling.

By using the CCSEM technique, the fly ash size distribution and chemical composition was determined. In Figure 39, the volume-based distribution function of the fly ash is shown. The maximum fly ash particle size was 90 μm, the calculated mean particle size was 12.6 μm, and the standard deviation was 7.0 μm. By comparing the size distribution of the mineral inclusions with that of the fly ash, it can be seen that the particle size distribution of the fly ash is coarser.

The chemical composition of fly ash was also determined by CCSEM. The results are shown in Table 9. In the same table, the chemical composition of the ash determined by the ASTM method is also given.

The chemical composition of the fly ash was used to calculate the distribution of particle viscosity at flue gas temperatures of 1509 K and 1339 K by using the Watt-Fereday equation. The results can be seen in Figures 40 and 41. Due to the random coalescence of included and ion-exchangeable mineral matter during coal particle burnout, the viscosity distribution of the fly ash is considerably different from that of the included mineral matter. Both the mean value and standard deviation of the viscosity of the included mineral matter are smaller for the fly ash. The ratio of the mean viscosities of the included mineral matter and the fly ash, calculated for different temperatures, is plotted in Figure 42. This ratio depends on the temperature, and decreases from 0.6 to 0.4 as the temperature increases from 1000 K to 1600 K. The ratio of the respective standard deviations is also shown in Figure 42. This ratio is independent of the temperature and is equal to 0.75.

The calculated sticking efficiencies of the included mineral matter and fly ash are plotted in Figure 43. The critical viscosity value was chosen as 10^6 poise.

4.3 Blend Coal

4.3.1 Blend Coal Characteristics

The characteristics of the Blend coal provided by ABB-Combustion Engineering are listed in Table 10. The Blend coal is a mixture of a low rank lignite (Wyoming lignite 70%) and a bituminous coal (Oklahoma 30%). It also has high moisture and volatile content and low heating value. Its sulfur content is fairly low (0.5 wt%), and originates mainly from pyrite. The melting behavior of its ash was determined by ASTM method, and is characterized by data included in Table 10. According to these data, the temperature window within which the

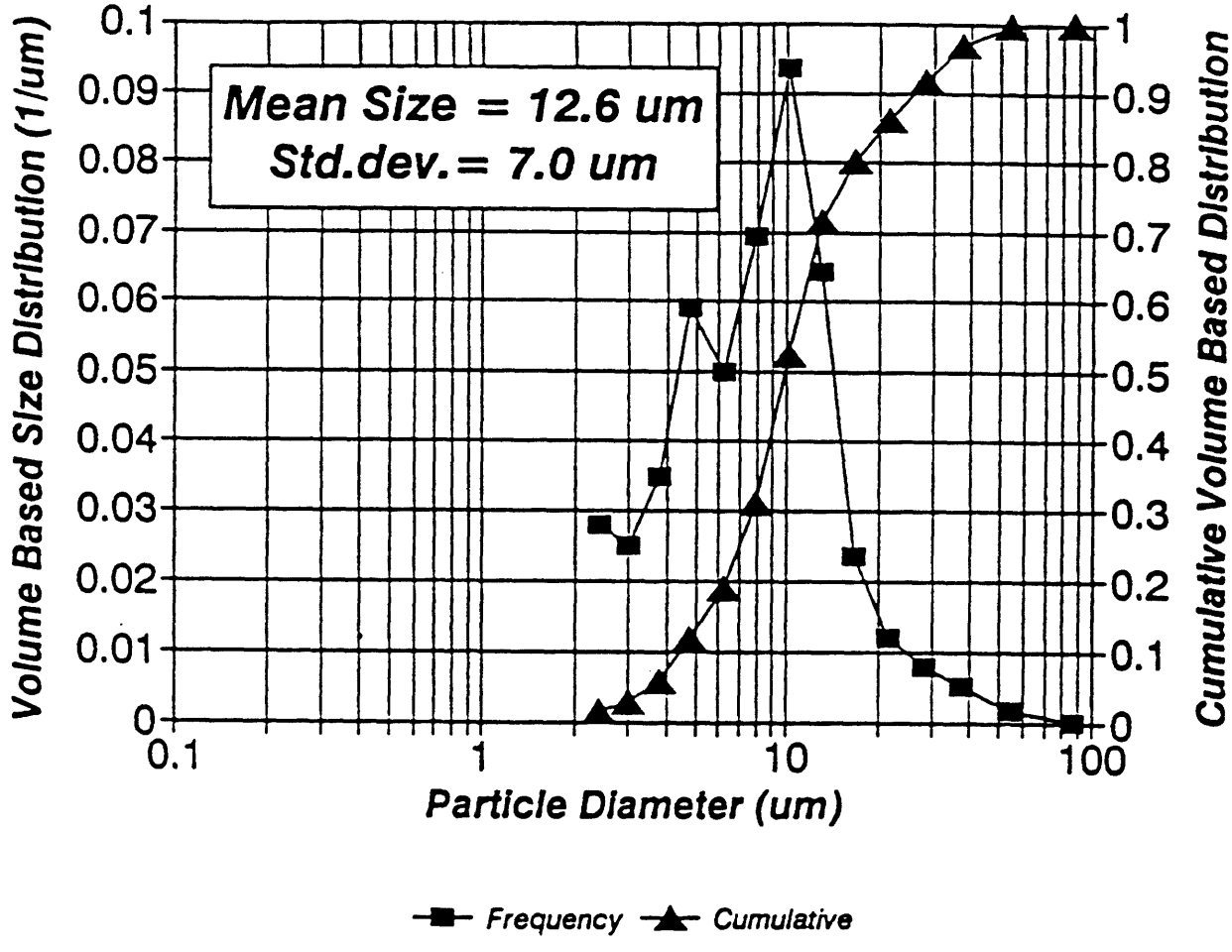

Figure 39. **Size Distribution of Fly Ash**
Wyoming Lignite

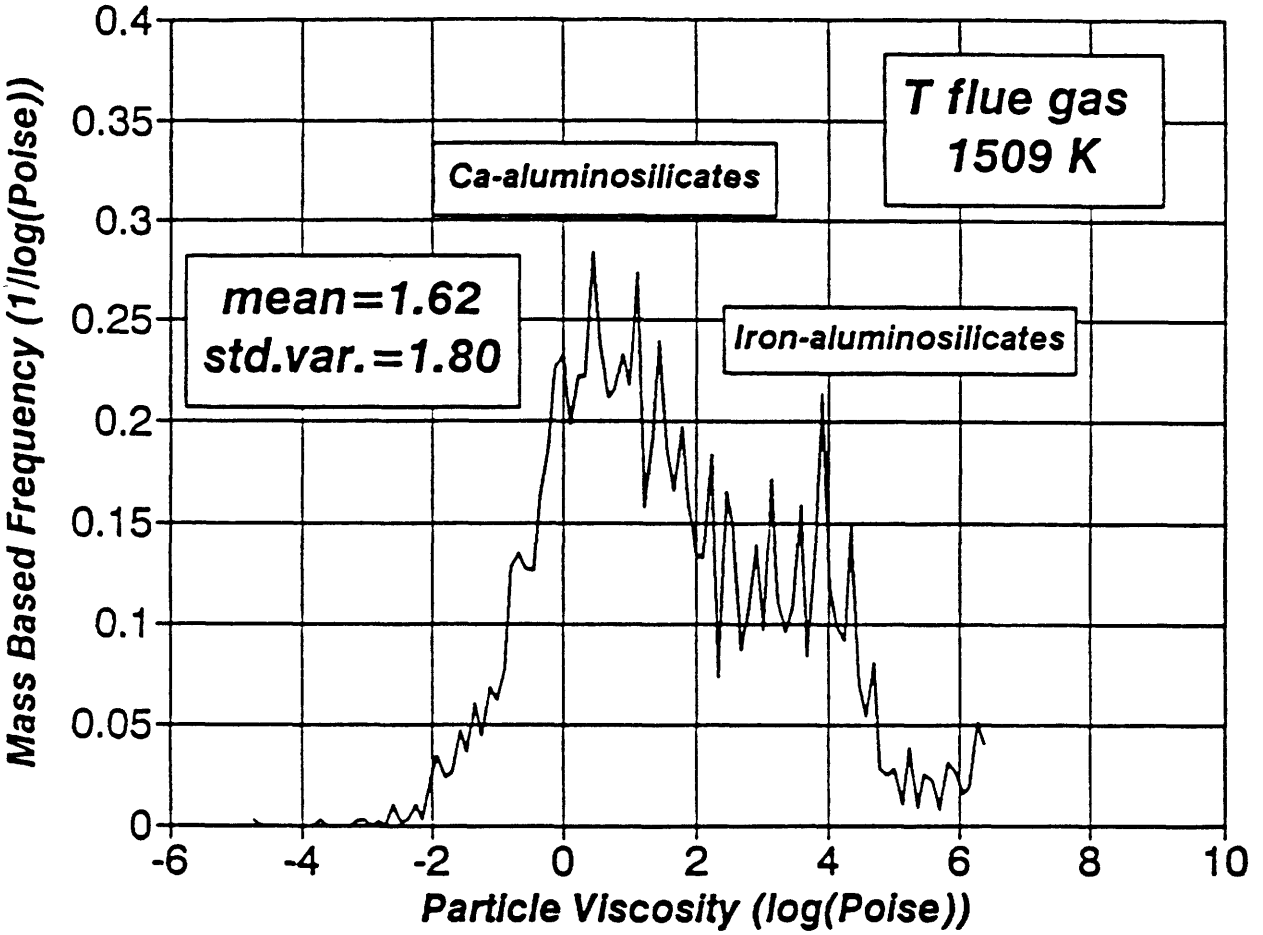

Figure 40. **Viscosity Distribution of Fly Ash**
Wyoming Lignite

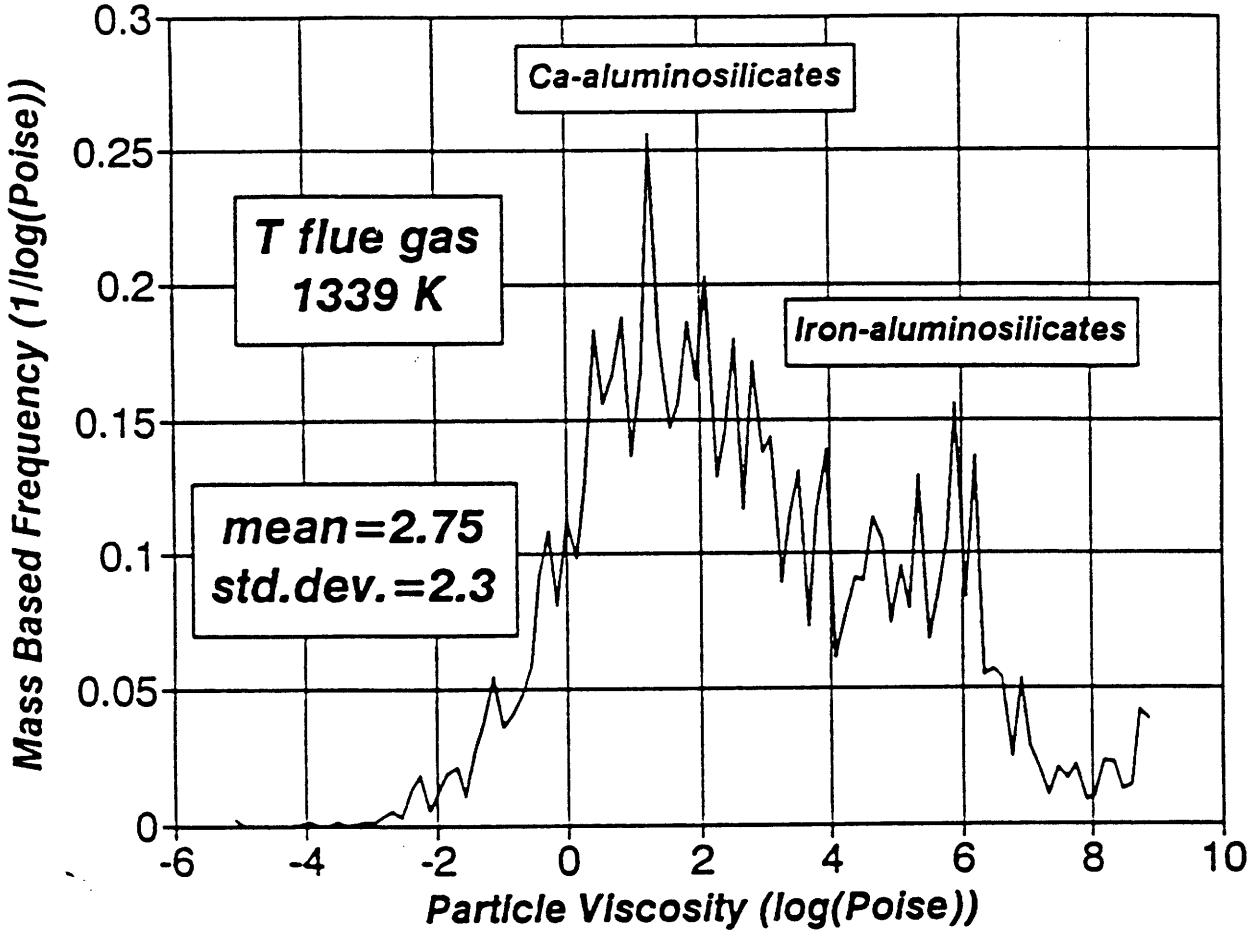

Figure 41. **Viscosity Distribution of Fly Ash** Wyoming Lignite

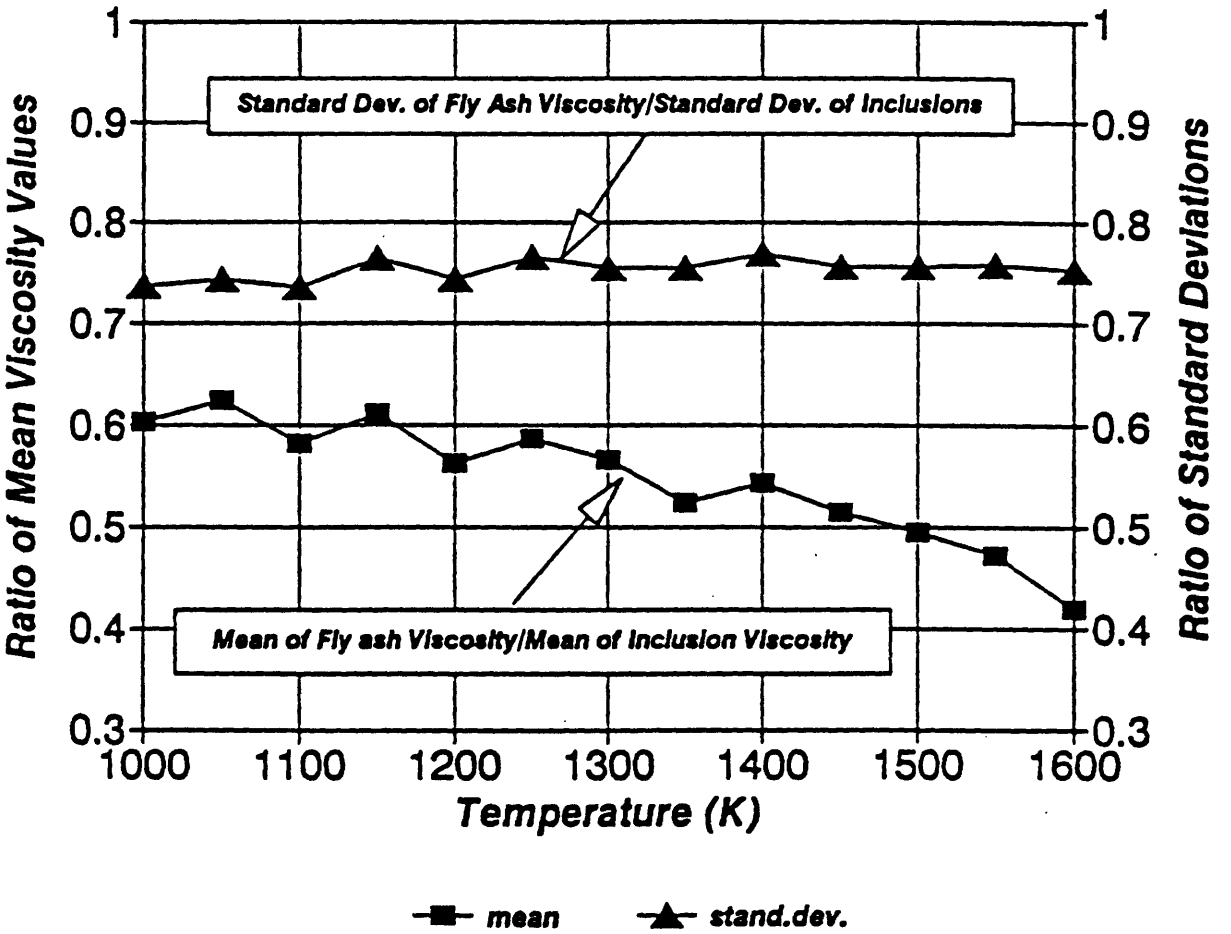

Figure 42. **Statistical Parameters of Viscosity** Wyoming Lignite

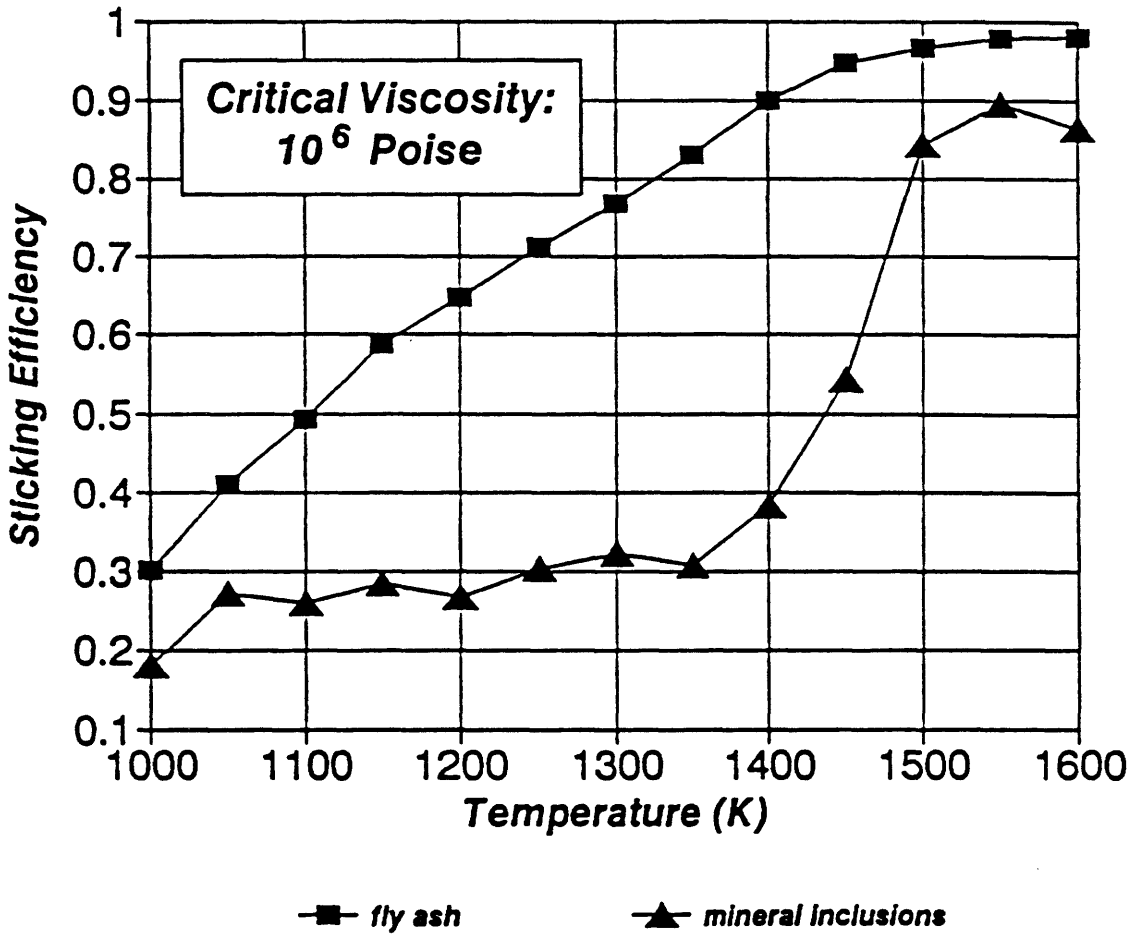

Figure 43. **Sticking Efficiency**
Wyoming Lignite

Table 9.
Comparison of Chemical Composition of the Wyoming Lignite Ash and Fly Ash Determined by ASTM and CCSEM Methods, Respectively

	ASTM	CCSEM
Oxide Formula	Ash	Fly ash
Na_2O	1.0	0.4
MgO	5.3	3.6
Al_2O_3	19.5	20.7
SiO_2	39.1	38.2
P_2O_5	0.5	0.9
SO_3	0.0	0.0
Cl	0.0	0.1
K_2O	0.6	0.9
CaO	24.1	23.8
TiO_2	1.5	2.2
FeO	6.9	8.5
Cr_2O_3	0.0	0.5
BaO	0.5	0.0

Table 10.
Characteristics of Wyoming/Oklahoma Blend Coal

Quantity	Blend Coal	
Moisture wt%	23.4	
Volatile Matter wt.%	36.1	
Fixed Carbon wt.%	34.6	
Ash wt.%	5.9	
Heating Value Btu/lb	9323	
Total Sulfur wt.%	0.5	
IDT K (ox.atm.)	1,427	
ST K (ox.atm.)	1,433	
HT K (ox.atm.)	1,440	
FT K (ox.atm.)	1,444	
Ash SiO_2 wt.%	with Sulfur	without Sulfur
	32.7	38.89
Ash Al_2O_3 wt.%	16.1	19.15
Ash Fe_2O_3 wt.%	6.7	7.97
Ash CaO wt.%	22.5	26.76
Ash MgO wt.%	3.8	4.52
Ash Na_2O wt.%	0.8	0.95
Ash K_2O wt.%	0.9	1.07
Ash TiO_4 wt.%	1.2	1.43
Ash P_2O_5 wt.%	n.d	n.d.
Ash SO_3 wt.%	15.9	0.0
Ash BaO wt.%	n.d	n.d.
Ash SrO wt%	n.d	n.d.

n.d. = non determined

deformation of ash particles takes place is from 1427 K to 1444 K. The difference between the initial deformation temperature and the fluid temperature is very low, 17 K. The ash chemical composition indicates high CaO and SO_3 content.

4.3.2 Extraneous Mineral Matter in Blend Coal

By using a sink-float method, the extraneous mineral content of Blend coal was determined to be 0.015 wt% (dry basis, 95.2 wt% ash).

4.3.3 Ion-Exchangeable Mineral Content of Blend Coal

The mass fraction of the ion-exchangeable mineral was determined by using acetic acid extraction of the coal. The result shows that 27.8 wt% of the total ash content is ion-exchangeable. By taking the chemical composition of the ash determined by the CCSEM method, the chemical composition of the leached mineral matter can be calculated. The results show that the ion-exchangeable mineral matter consists of 80 wt% CaO, 15 wt% MgO and 5 wt% Na_2O.

4.3.4 Size Distribution of Blend Coal

The volume-based size distribution of the lignite can be seen in Figure 44. The frequency function represents a bimodal distribution at particle sizes of 3 μm and 9 μm, respectively. The maximal particle size is 200 μm. The volumetric mean value and standard deviation of the distribution were calculated by using the method of lognormal curve fitting. The calculated mean particle size and standard deviation are 45.6 μm and 85.8 μm, respectively.

4.3.5 Density and Ash Content as a Function of Coal Size

The results are plotted in Figure 45. It can be seen that the mean particle density increases with decreasing coal particle size; however, the ash content has a minimal value at the coal particle size 60 μm.

4.3.6 Size Distribution of Mineral Inclusions

The volume-based size distribution of mineral inclusions is plotted in Figure 46. The volumetric mean particle size and standard deviation were approximated by using the method of lognormal curve fitting. The calculated mean particle size and standard deviation are 4.4 μm and 3.7 μm, respectively. The maximum particle size is under 40 μm. The distribution functions were determined by CCSEM method and Abelian transformation was used for the stereological correction of the raw data.

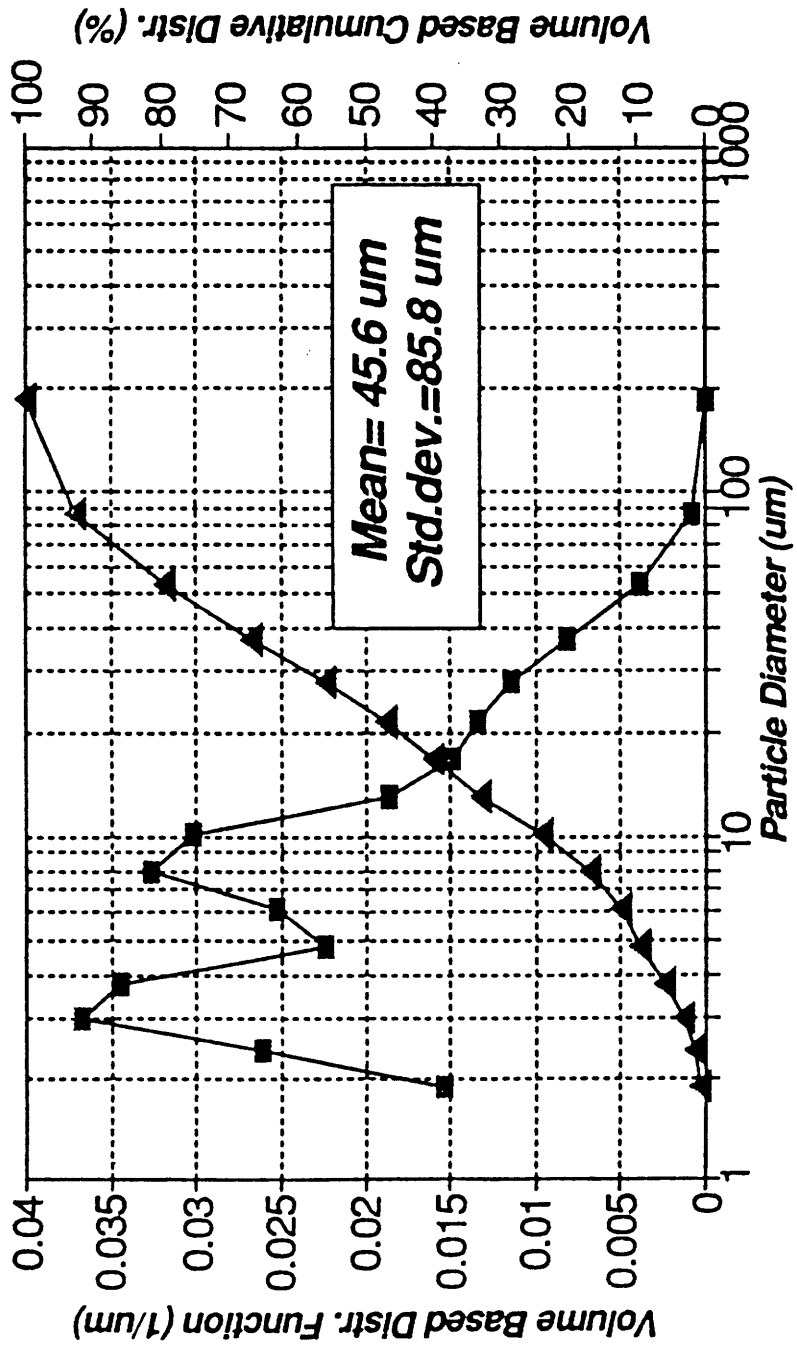

Figure 44. **Size Distribution of Blend Coal**
Determined by Laser Diffraction Method

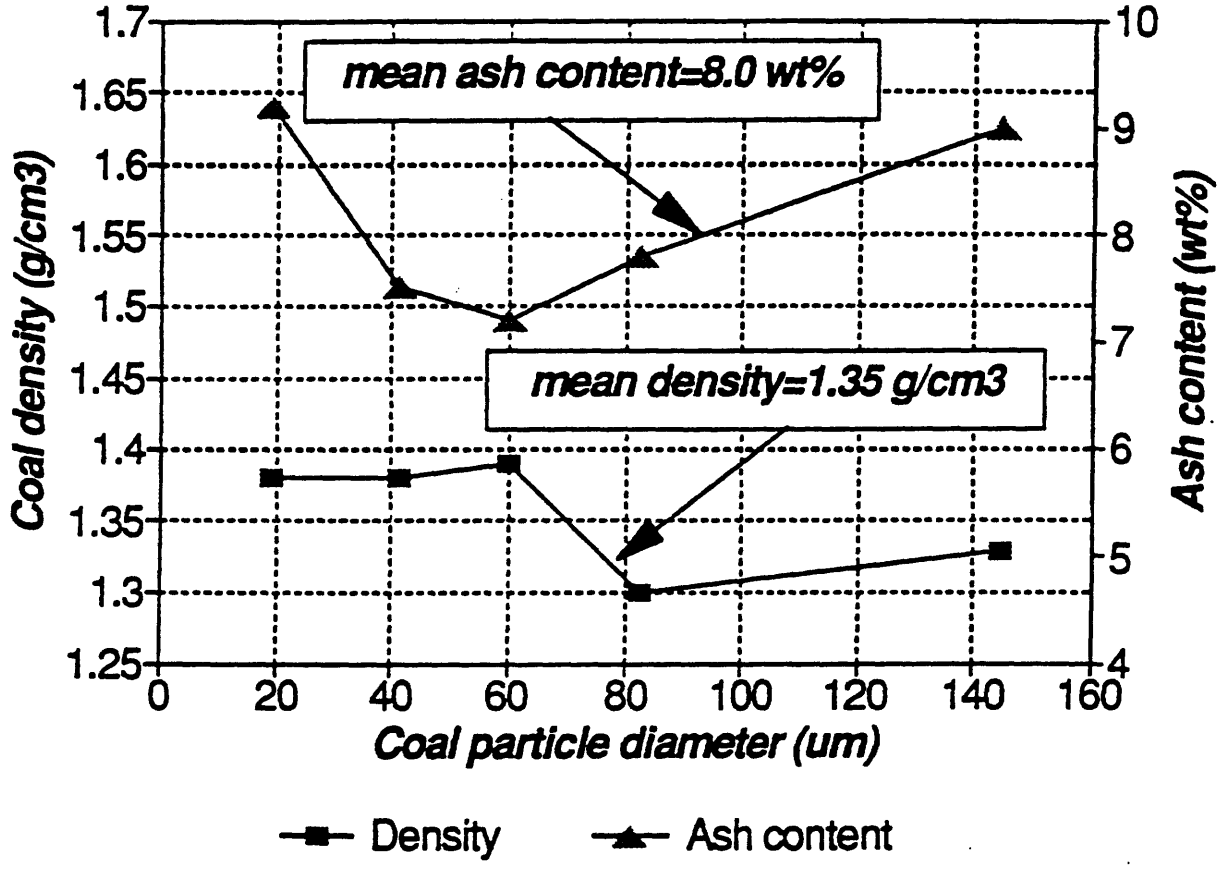

Figure 45. **Coal Density and Ash Content**
Blend Coal of Wyoming and Oklahoma

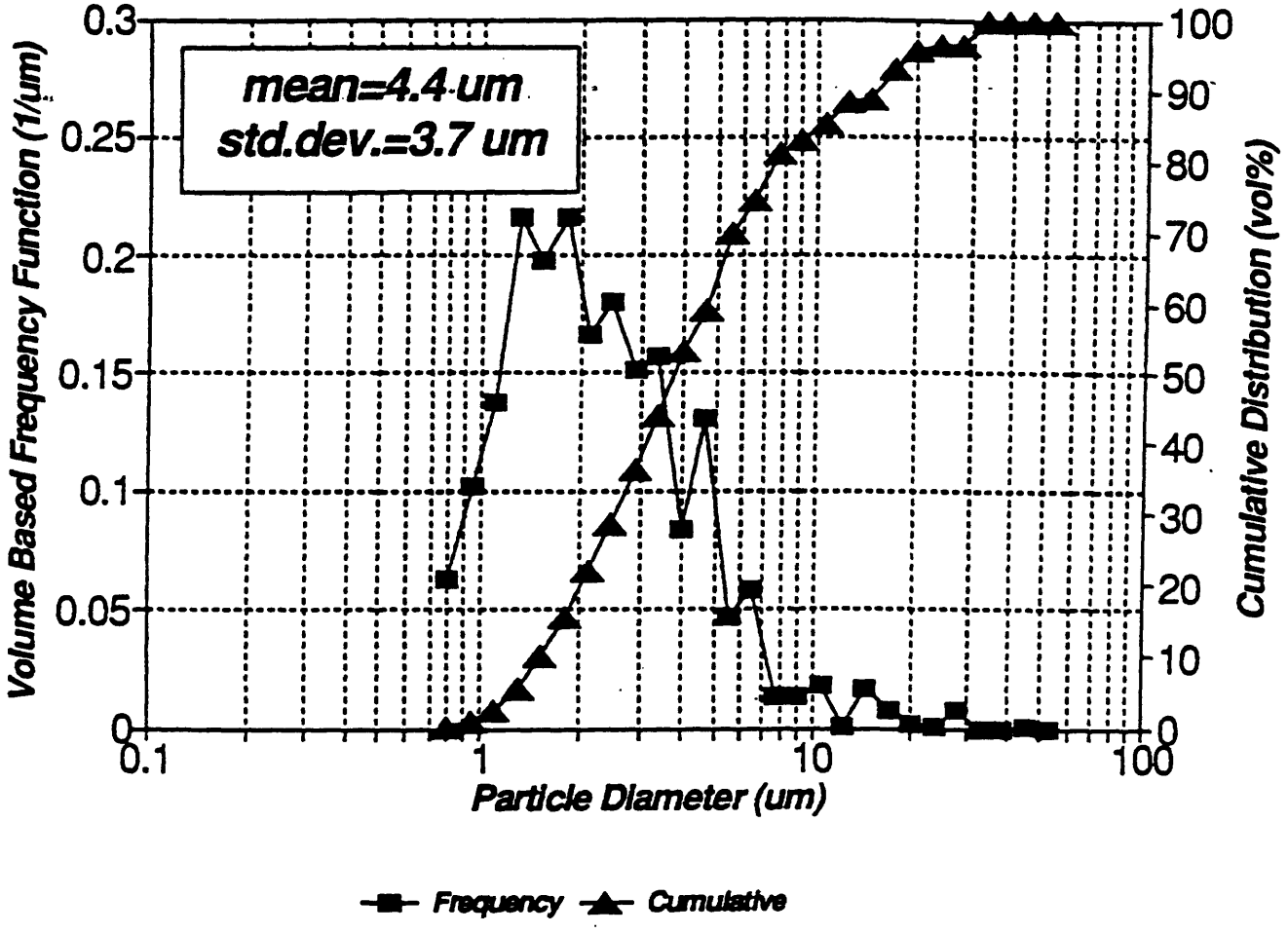

Figure 46. **Size Distribution of Mineral Inclusions** Blend Coal

4.3.7 Chemical Composition and Calculated Viscosity Distribution of Mineral Inclusions in Blend Coal

The mean chemical compound concentrations in the mineral inclusions and the mean concentrations of mineral types are listed in Table 11. It shows that the mineral inclusions consist mainly of illite, quartz and mixed silicates with smaller amounts of kaolinite. The mean chemical composition of mineral inclusions is different from that of the ash measured by the ASTM method due to the contribution of the ion-exchangeable mineral which is not detected by CCSEM. The comparison of the calculated sulfur-free chemical composition of the ash determined by ASTM and the total mineral matter is given in Table 12.

The Watt-Fereday equation was used to calculate the particle viscosity. The peak flame temperature (1675 K) was chosen for the calculations. The mass-based distribution function of mineral particle viscosity is given in Figure 47. The mean value and standard deviation of the viscosity are $10^{2.9}$ poise and $10^{1.7}$ poise, respectively. The curve shows four distinct peaks. Three of these correspond to the contributions of the predominant illite, quartz and mixed silicates, as identified by the CCSEM. The fourth peak, at the extreme left in Figure 47, is due to the pyrite component of the mineral inclusions in the Blend coal.

4.3.8 Experiments in the Combustion Research Facility

The test conditions for the Blend coal are summarized in Table 13. The coal feed rate was set to obtain 0.99 MW thermal input. The coal was carried by air from a coal silo at 1.21 air/coal mass ratio. The flow rate of air was measured by a built-in pitot tube. The flow rate of the coal was measured by a weigh belt. The primary, secondary and tertiary air flows were also monitored by pitot tubes. The air was preheated to 488 K, 527 K and 554 K, respectively. Low air flow rate were maintained for the primary and secondary air, and high rate for the tertiary air flow. A high degree of swirl was chosen for the primary and tertiary air flows, and no swirl was used for the secondary air.

The flue gas temperature profile along the axis of the combustion tunnel is plotted in Figure 48. The temperature was measured by suction pyrometer. The peak flue gas temperature (1675 K) was reached at the distance of 2.2 m from the burner. At a distance of 0.5 m from the nozzle, a sharp increase of temperature was observed due to the early ignition of the bituminous coal fraction in the blend.

The deposition probes were placed in the flue gas stream at two positions: 6.1 m and 5.0 m from the burner. Radial temperature profiles were taken at each of these locations. The results are plotted in Figure 49. At the position of 5.0 m from the burner, the maximum temperature was 1573 K. The maximum temperature at 6.1 m from the burner was 1458 K. The maximum temperatures were found on the axis. Due to the intensive heat extraction through the cylinder jacket, the temperature decreased as the distance from the axis increased.

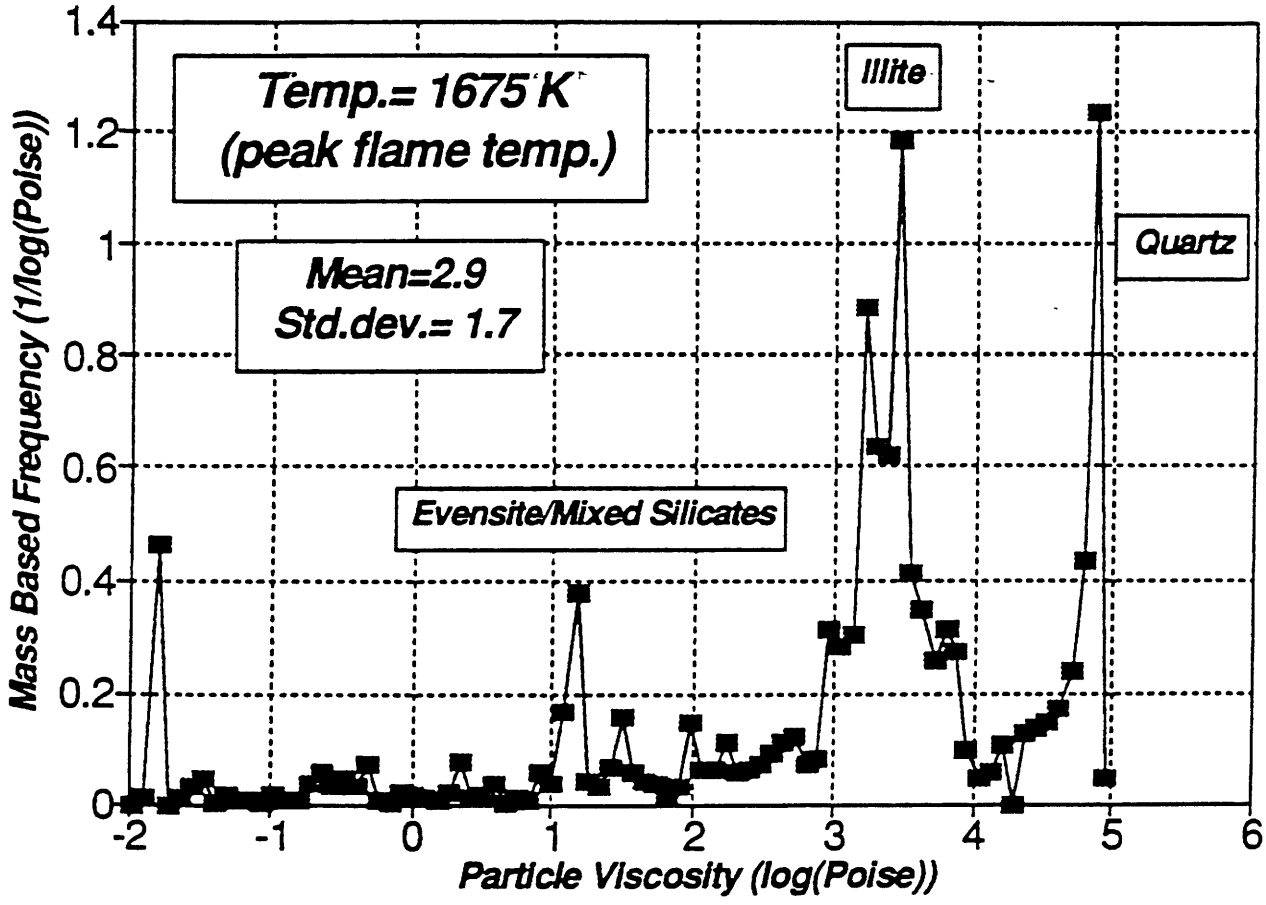

Figure 47. **Viscosity Distribution of Inclusions**
Blend Coal

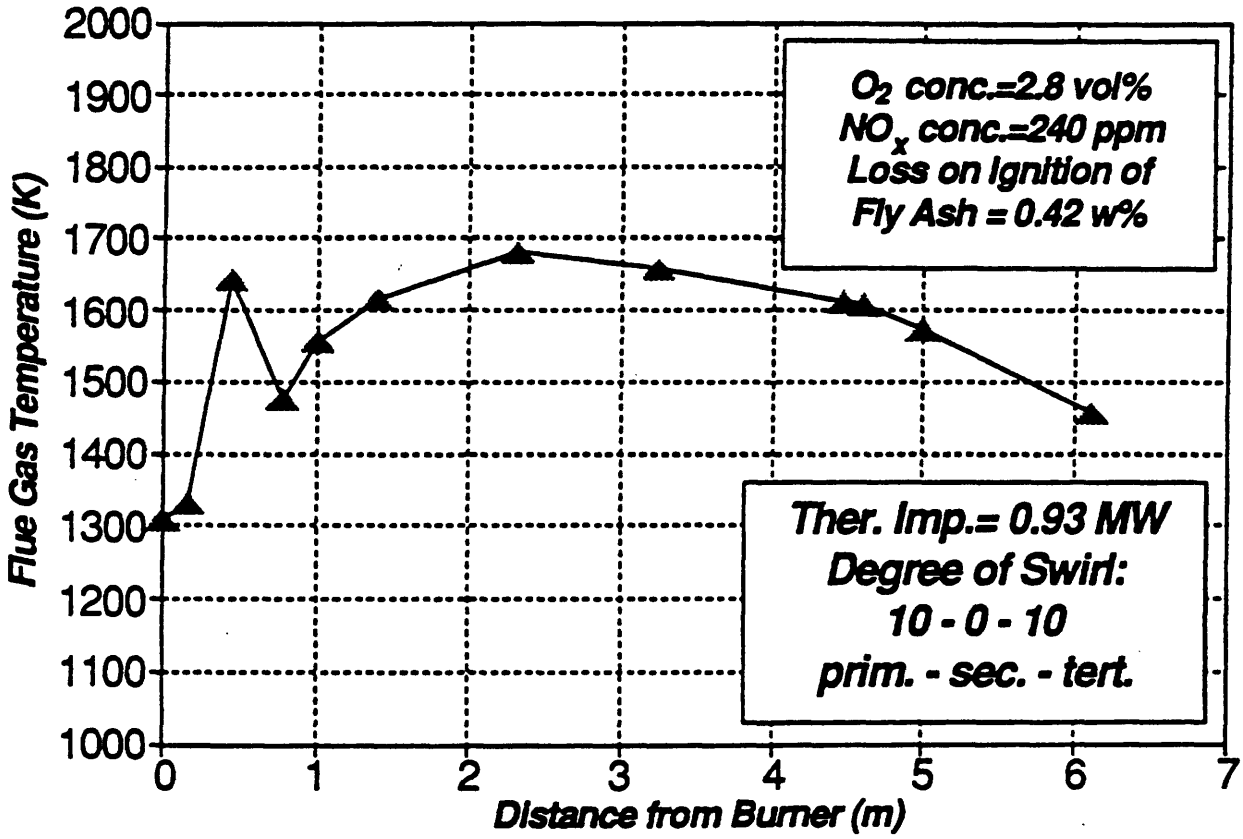

Figure 48. **Axial Flue Gas Temperature Profile**
Blend Coal

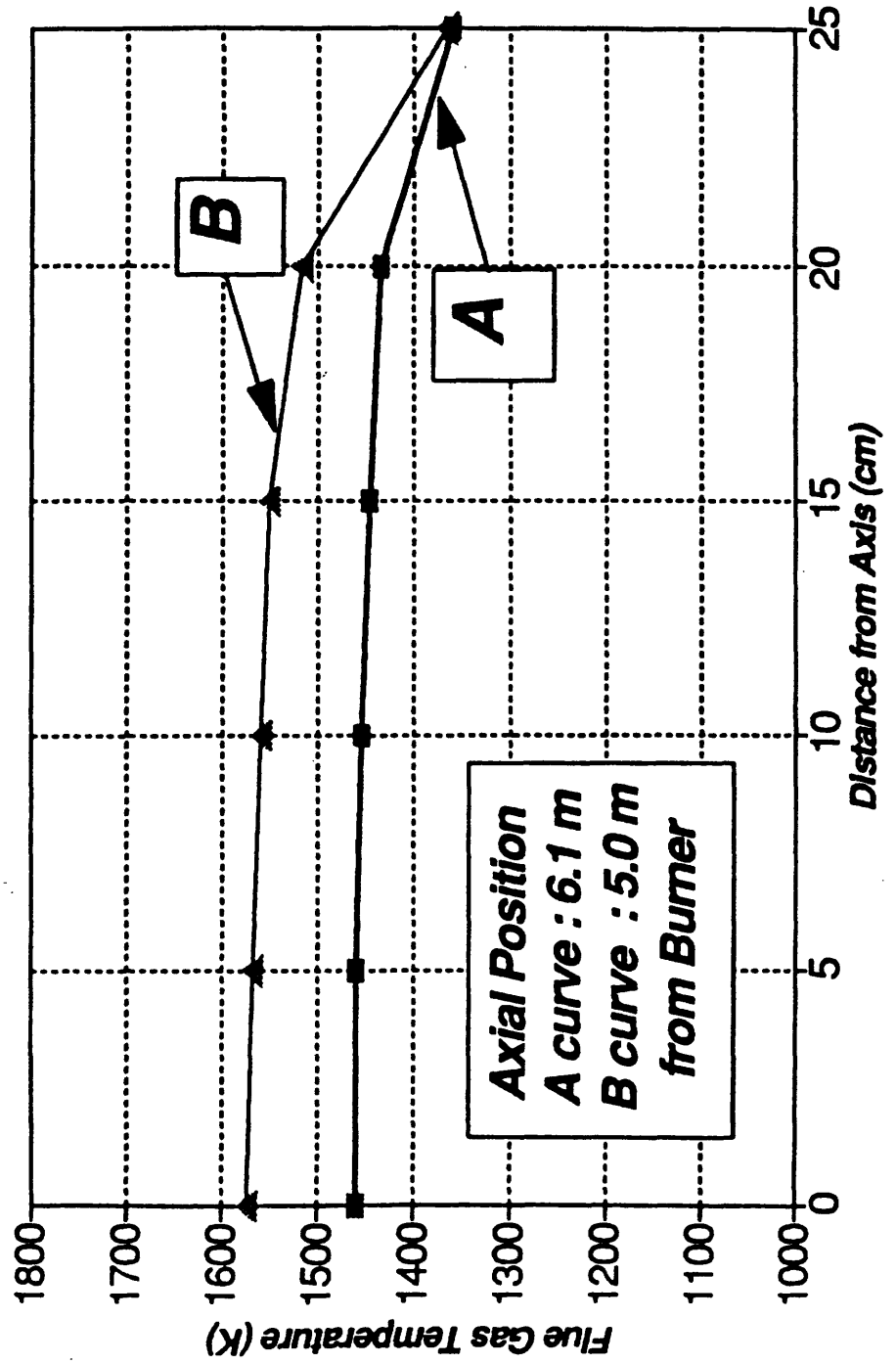

Figure 49. Radial Flue Gas Temperature Profile
Blend Coal

Table 11.
Chemical Composition and Mineral Compounds of Blend Coal Mineral Inclusions

Oxide Formula	Weight %	Mineral Type	Mass %
Na_2O	0.58	Mixed Silicate	17.86
MgO	0.56	Quartz	24.56
Al_2O_3	24.63	Calcite	0.98
SiO_2	54.03	Siderite	0.38
P_2O_5	1.02	Rutile	0.26
SO_3	3.64	Illite	43.2
Cl	0.56	Pyrite/Marcasite	1.84
K_2O	3.62	Apatite/Evensite	2.06
CaO	3.46	Baryte	0.79
TiO_2	0.98	Kaolinite	5.65
FeO	6.13	Jarosite	2.28
Cr_2O_3	0.53	Results by CCSEM Method	
BaO	0.26		

Table 12.
Comparison of Chemical Composition of the Blend Coal Ash and Mineral Matter Determined by ASTM and CCSEM Methods, Respectively

	ASTM	CCSEM
Oxide Formula	Ash	28w% ion.ex.+72w% incl.
Na_2O	0.95	2.0
MgO	4.52	4.0
Al_2O_3	19.15	18.2
SiO_2	38.89	39.9
P_2O_5	n.d.	0.75
SO_3	0.0	0.0
Cl	0.0	0.41
K_2O	1.07	2.67
CaO	26.76	26.13
TiO_2	1.43	0.72
FeO	7.97	4.53
Cr_2O_3	0.0	0.4
BaO	n.d.	0.19

Table 13.
Test Parameters of Blend Coal in MIT-CRF

Parameters	Data
Thermal Input (MW)	0.99
Excess Air vol%	14
Coal Mass Flow (kg/h)	130.5
Carrying Air Mass Flow (kg/h)	158.2
Carrying Air/Coal Mass Ratio (1)	1.212
Primary Air Flow (kg/h) (high.swirl)	124.6
Secondary Air Flow (kg/h) (no.swirl)	55.6
Tertiary Air Flow (kg/h) (top+bottom) (high swirl)	779.5
Total Air Flow (kg/h)	1,117.9
Prim. Air Burner Inlet Temperature (K)	488
Sec. Air Burner Inlet Temperature (K)	527
Tert. Air Burner Inlet Temperature (K)	554

Pitot tube measurements to determine the radial flue gas velocity profile were made at the positions where the deposition probes were inserted. The results can be seen in Figure 50. At the position of 5.0 m from the burner the peak velocity was 11.7 m/s. At the distance of 6.1 m from the burner, due to the decrease of flue gas temperature, the maximum velocity of the flue gas was 9.8 m/s. Both peak velocities were measured on the axis. The flue gas velocity decreased as the radial distance from the axis increased.

4.3.9 Deposition Experiment

During the deposition sampling, a constant initial surface temperature of 1073 K was obtained by monitoring the surface temperature of the deposition probe and by adjusting the mass flow rate of the cooling air. The probes were placed in the cylindrical section of the CRF at two locations, corresponding to two different flue gas temperatures. The deposition probes were left in the flue gas for different periods of time to permit the rate of deposition to be determined.

For the flue gas temperature of 1458 K and velocity of 9.8 m/s, the deposition build-up can be seen in Figure 51. The deposition weight per unit projected probe area is plotted as a function of time. Linear regression was used to approximate the deposition flow and calculate the flow rate. The calculated specific deposition rate was 0.042 $kg/m^2/min$. For the flue gas temperature of 1573 K and velocity of 11.7 m/s, the results are shown in Figure 52. The results indicate higher deposition flow and rate. From a linear approximation, the specific deposition rate was calculated as 0.152 $kg/m^2/min$, which is approximately 3.7 times higher than that found in the previous case.

The deposit was easily removable from the deposition probe, and easily breakable in both cases, indicating low activity of sintering between deposited fly ash particles. The average bulk density of the deposit taken at the higher flue gas temperature and after 90 minutes was 1.22 g/cm^3.

4.3.10 Properties of Blend Fly Ash

A fly ash sample was taken at 6.1 m from the burner by the method of isokinetic probe sampling.

By using the CCSEM technique, the fly ash size distribution and chemical composition was determined. In Figure 53, the volume-based distribution function of the fly ash is shown. The maximum fly ash particle size was 90 μm and the calculated mean particle size was 16.1 μm, and the standard deviation was 14.1 μm. By comparing the size distribution of the mineral inclusions with that of the fly ash, it can be seen that the particle size distribution of the fly ash is coarser.

The chemical composition of the fly ash given in Table 14 was used to calculate the distribution of particle viscosity at flue gas temperatures of 1573 K and 1458 K by using the

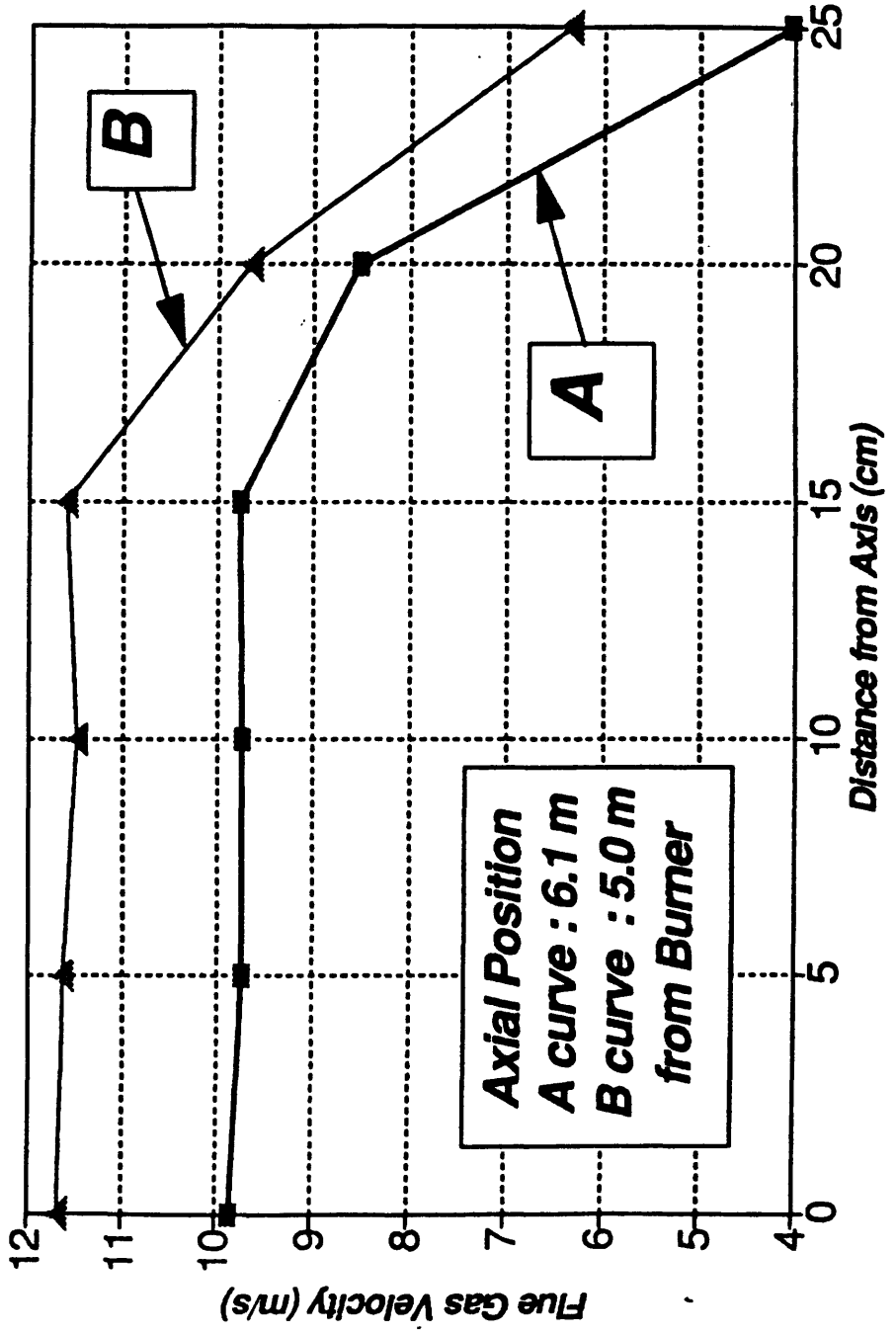

Figure 50. Radial Flue Gas Velocity Profile
Wyoming/Oklahoma Blend

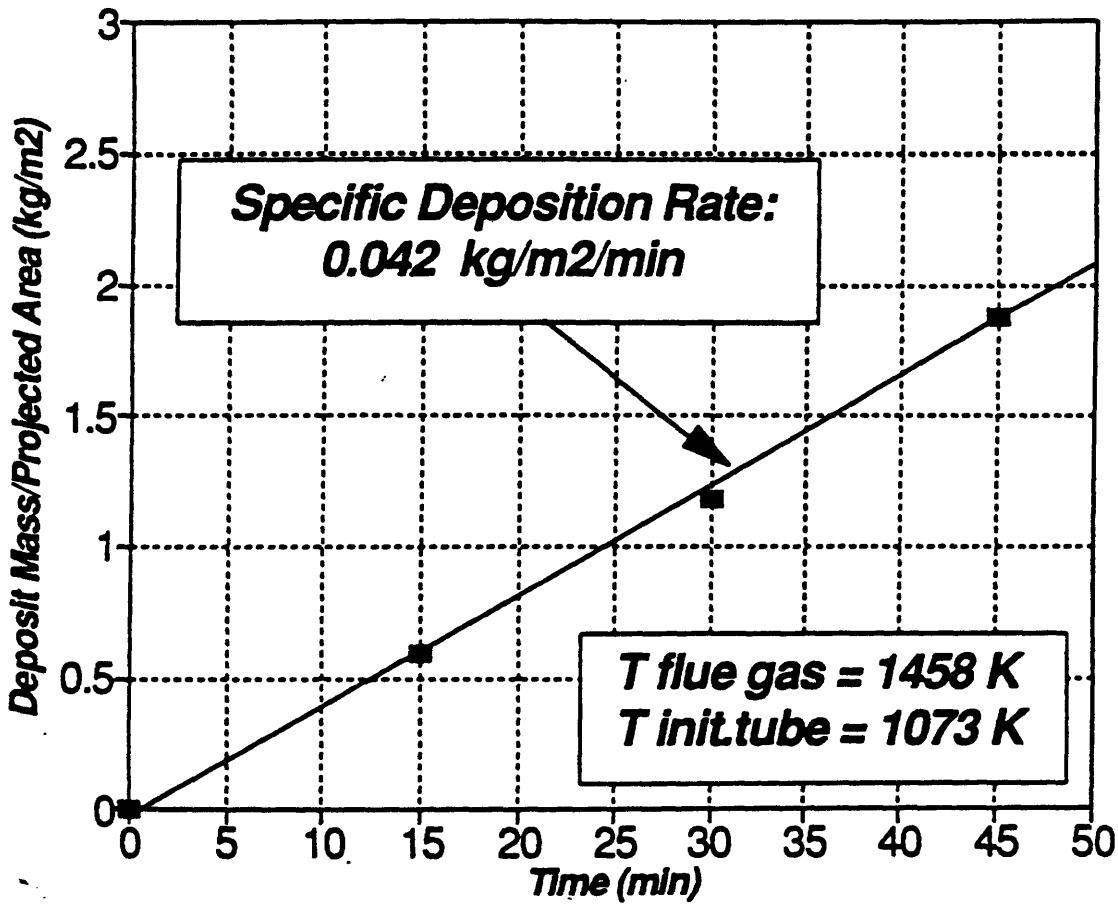

Figure 51. **Deposit Build-Up**
Wyoming/Oklahoma Blend

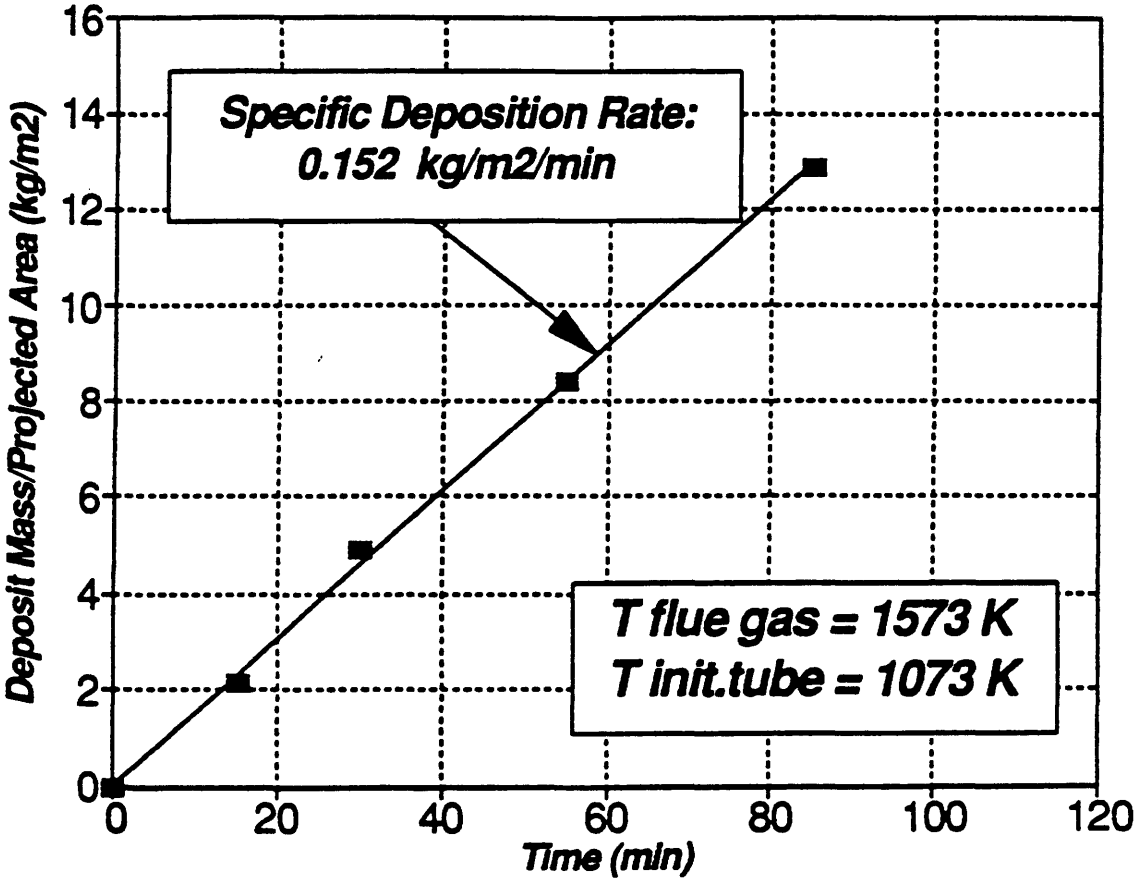

Figure 52. **Deposit Build-Up**
Wyoming/Oklahoma Blend

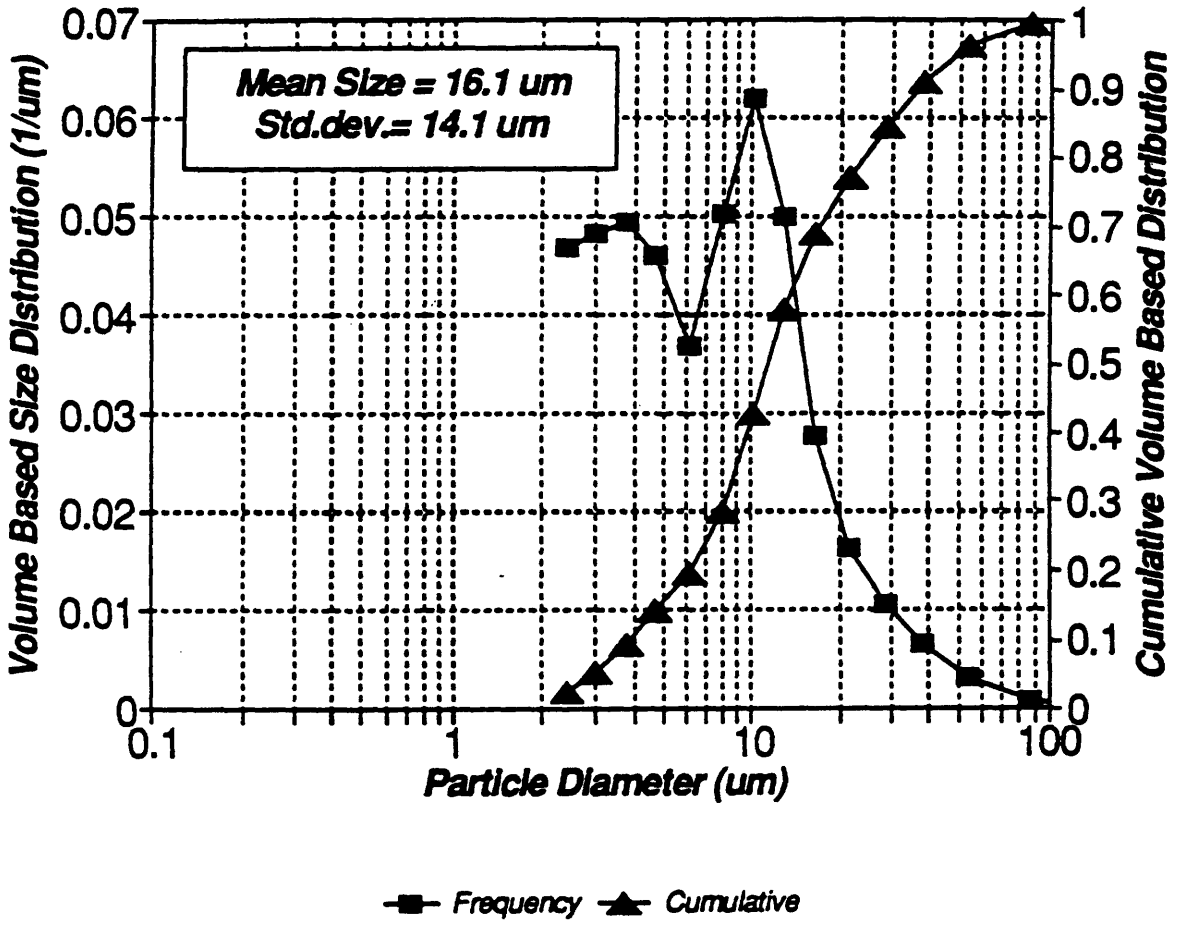

Figure 53. **Size Distribution of Fly Ash Blend Coal**

Table 14.
Comparison of Chemical Composition of the Blend Coal Ash and Fly Ash Determined by ASTM and CCSEM Methods, Respectively

	ASTM	CCSEM
Oxide Formula	Ash	Fly ash
Na_2O	1.0	0.1
MgO	4.5	1.7
Al_2O_3	19.2	20.1
SiO_2	38.9	44.0
P_2O_5	0.0	0.4
SO_3	0.0	0.0
Cl	n.d.	0.0
K_2O	1.1	2.3
CaO	26.7	22.2
TiO_2	1.4	0.9
FeO	7.9	8.2
Cr_2O_3	n.d.	0.1
BaO	n.d.	0.0

Watt-Fereday equation. The results can be seen in Figures 54 and 55. Due to the random coalescence of included mineral matter during coal particle burnout, the viscosity distribution of the fly ash is considerably different from that of the included mineral matter. Both the mean value and standard deviation of the viscosity of the included mineral matter are smaller for the fly ash. The ratio of the mean viscosities of the included mineral matter and the fly ash, calculated for different temperatures, is plotted in Figure 56. This ratio decreased from 0.75 to 0.58 as the temperature increased from 1000 K to 1600 K. The ratio of the respective standard deviations is also shown in Figure 56. This ratio is independent of the temperature and is equal to 0.9.

The calculated sticking efficiencies of the included mineral matter and fly ash are plotted in Figure 57. The critical viscosity value was chosen to be 10^6 poise.

4.4 Jader Coal

4.4.1 Jader Coal Characteristics

The characteristics of the Jader coal provided by ABB-Combustion Engineering are listed in Table 15. The Jader coal is of the bituminous type with 1.4 wt% moisture, 32.6 wt% volatile content and 13335 Btu/lb heating value. Its sulfur content is high, 2.86 wt%. The melting behavior of its ash was determined by ASTM method, and is characterized by data included in Table 15. According to these data, the temperature window within which the deformation of ash particles takes place is from 1632 K to 1676 K. The difference between the initial deformation temperature and the fluid temperature is relatively low, 44 K. The ash chemical composition indicates high Fe_2O_3 and low CaO content. The main chemical compounds are alumina and silica.

4.4.2 Extraneous Mineral Matter in Jader Coal

By using a sink-float method, the extraneous mineral content of Jader coal was determined to be 0.83 wt%.

4.4.3 Ion-Exchangeable Mineral Content of Jader Coal

The mass fraction of the ion-exchangeable mineral was determined by using acetic acid extraction of the coal. The result shows that less than 0.1 wt% of the total ash content is ion-exchangeable.

4.4.4 Size Distribution of Jader Coal

The volume-based size distribution of the coal can be seen in Figure 58. The frequency function represents a bimodal distribution at particle sizes of 4 μm and 9 μm, respectively. The maximum particle size is 200 μm. The volumetric mean value and standard deviation of the distribution were calculated by using the method of lognormal curve fitting. The calculated mean size and standard deviation are 36.6 μm and 51.9 μm, respectively.

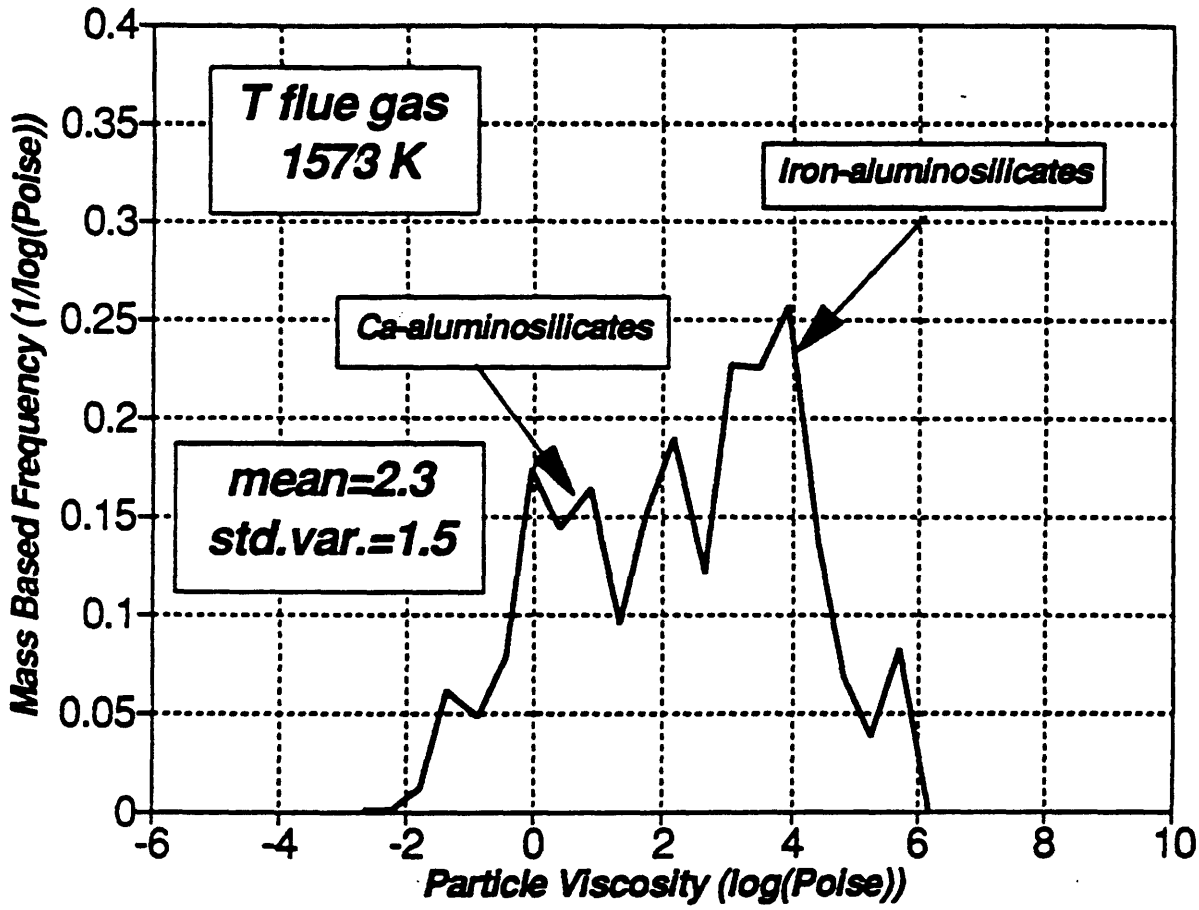

Figure 54. **Viscosity Distribution of Fly Ash** Blend Coal

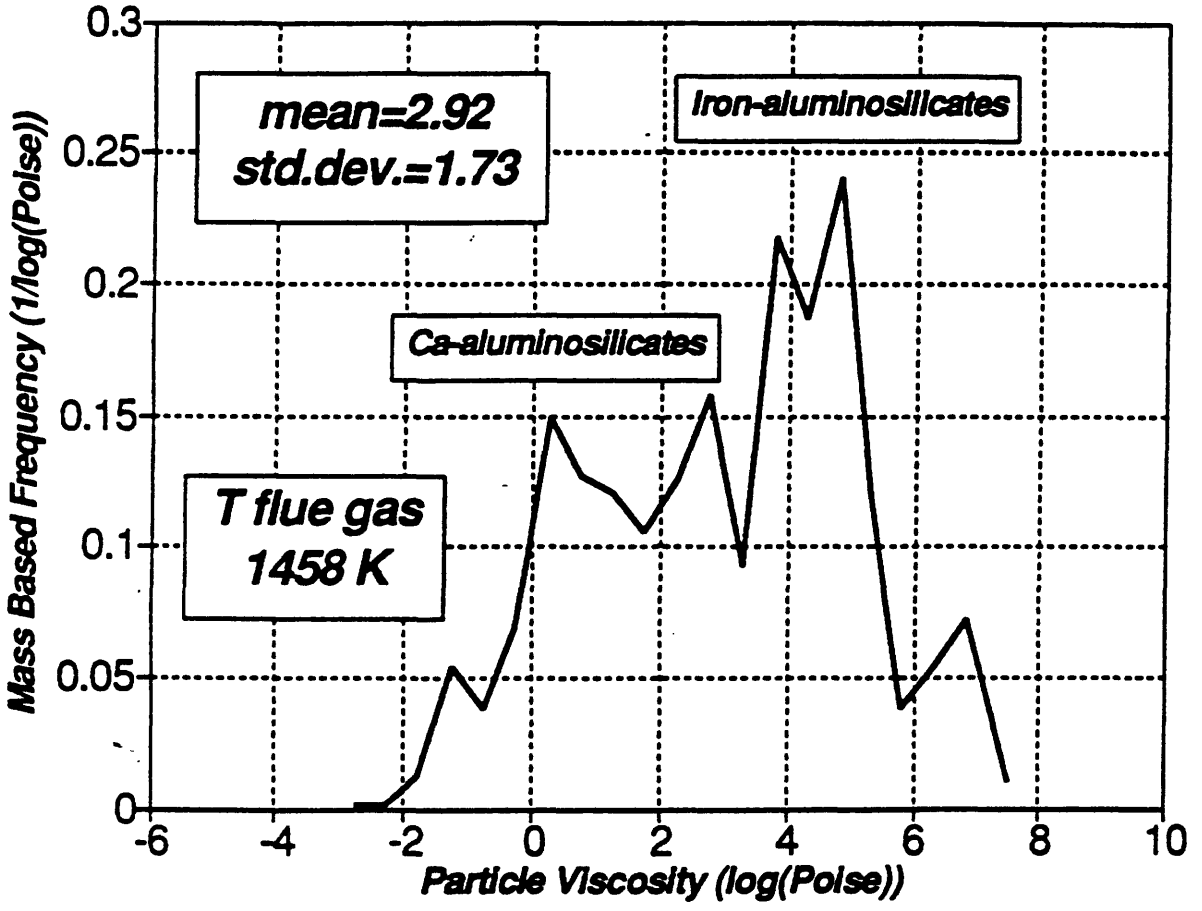

Figure 55. **Viscosity Distribution of Fly Ash** Blend Coal

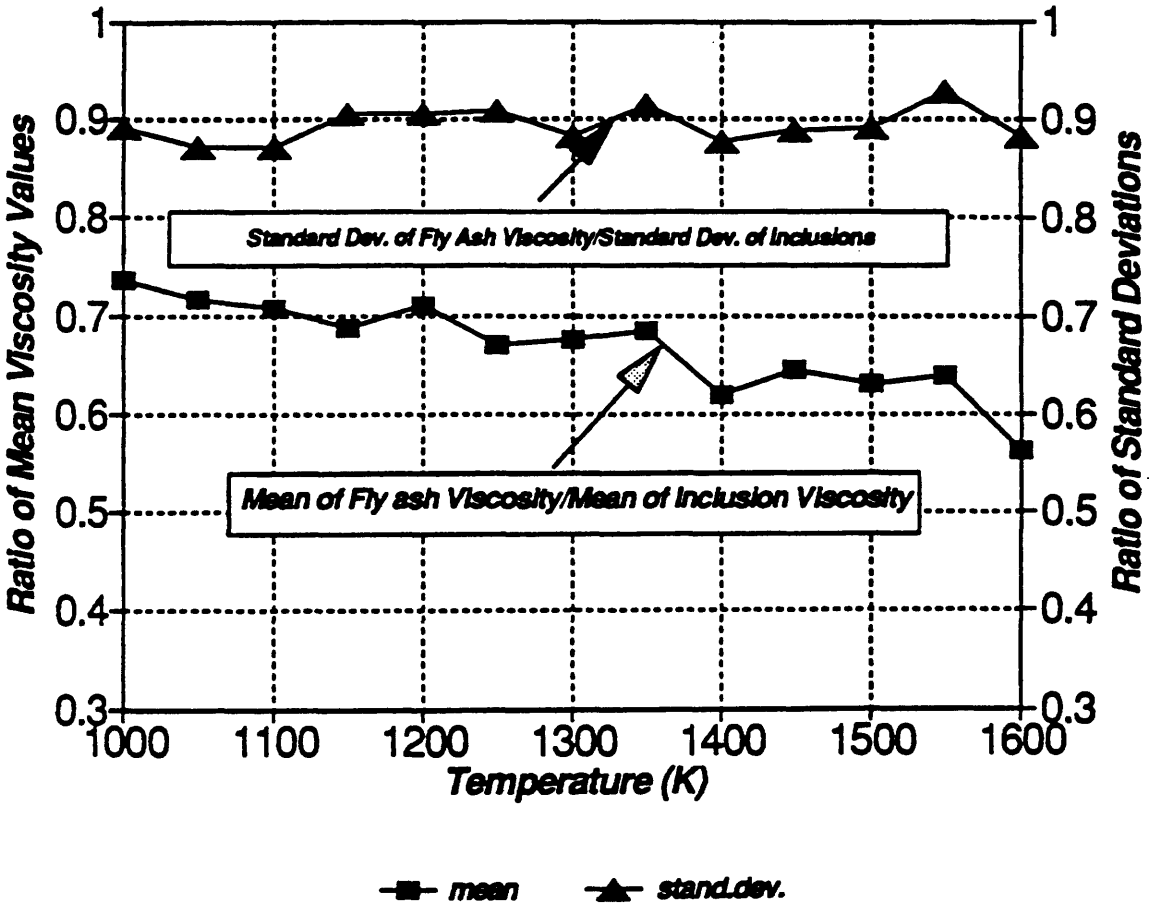

Figure 56. **Statistical Parameters of Viscosity** Blend Coal

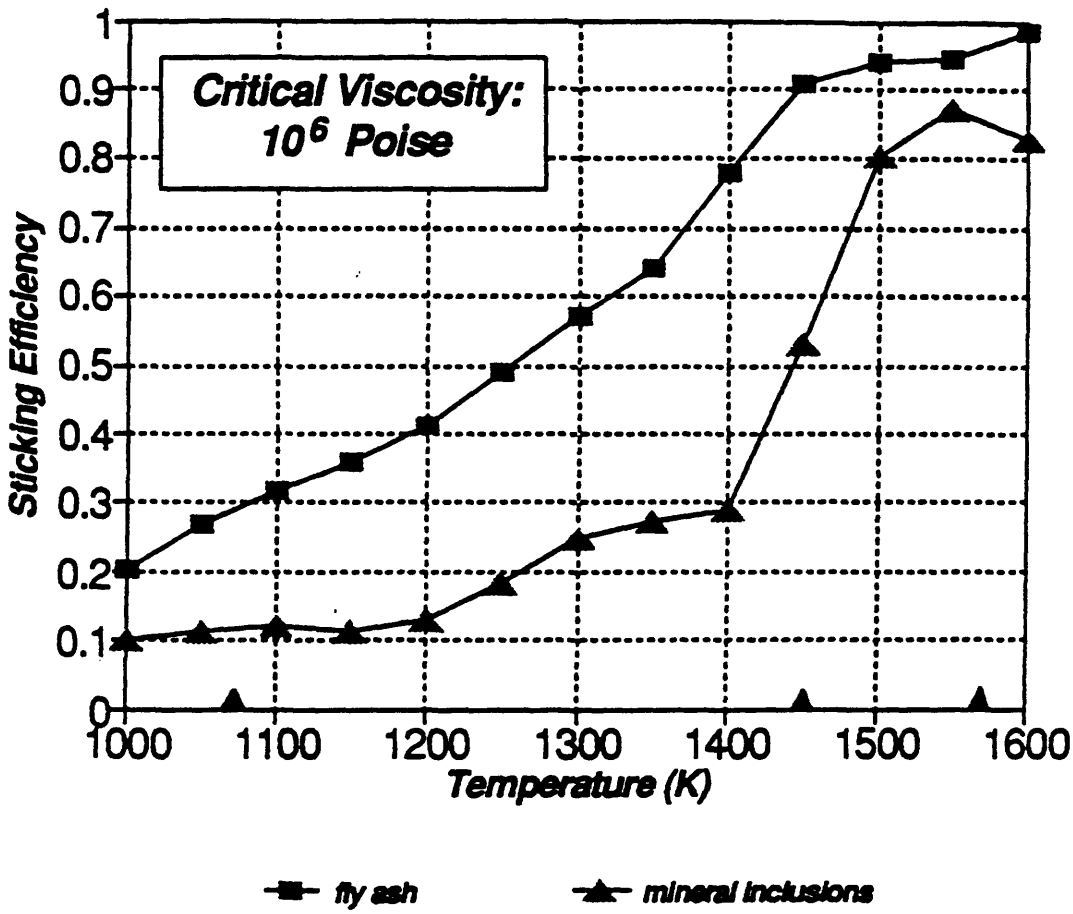

Figure 57. **Sticking Efficiency**
Blend Coal

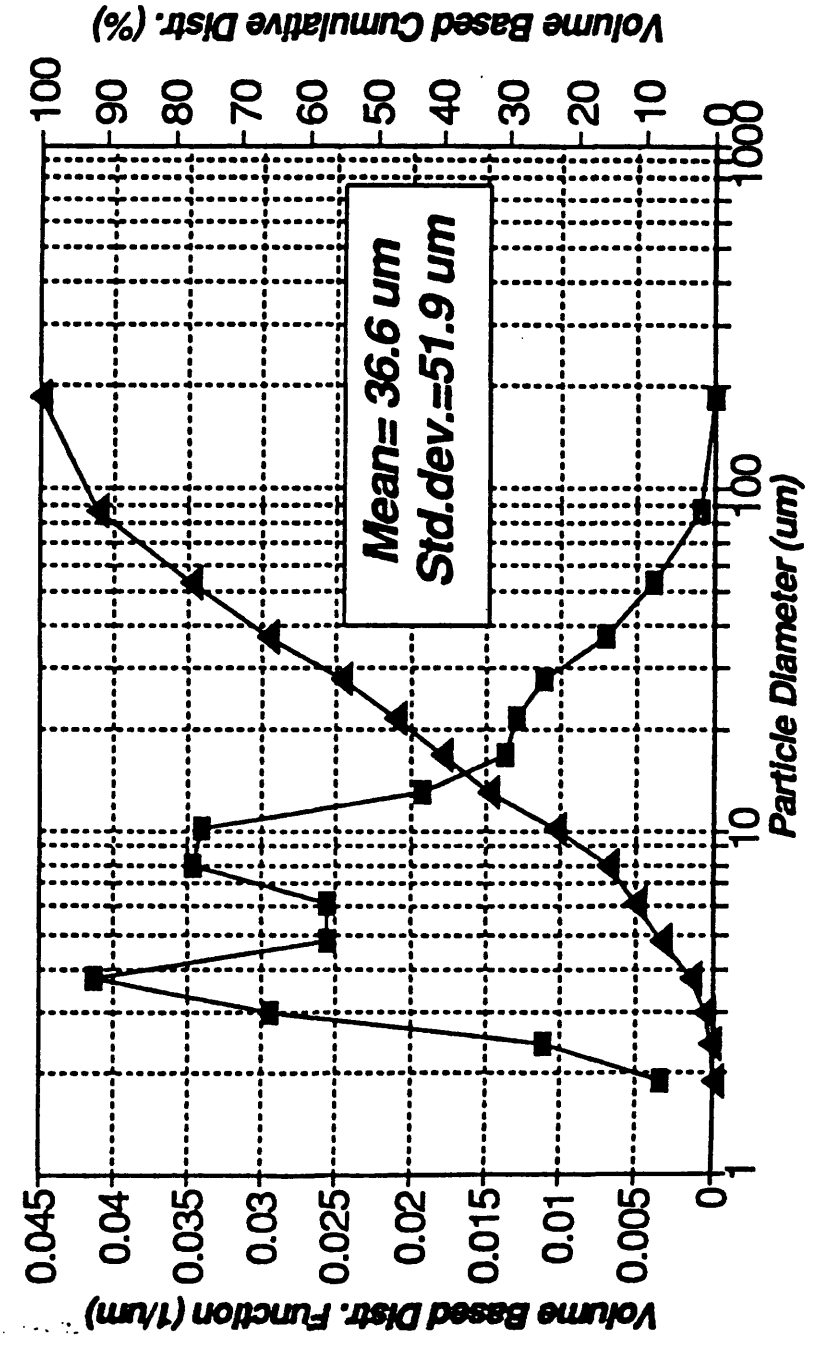

Figure 58. Size Distribution of Jader Coal
Determined by Laser Diffraction Method

Table 15.
Characteristics of Jader Coal

Quantity	Jader Coal	
Moisture wt%	1.4	
Volatile Matter wt.%	32.6	
Fixed Carbon wt.%	52.5	
Ash wt.%	8.3	
Heating Value Btu/lb	13335	
Total Sulfur wt.%	2.86	
IDT K	1632	
ST K	1646	
HT K	1656	
FT K	1676	
Ash SiO_2 wt.%	with Sulfur	without Sulfur
	50.6	51.7
Ash Al_2O_3 wt.%	19.9	20.3
Ash Fe_2O_3 wt.%	20.2	20.7
Ash CaO wt.%	1.9	1.9
Ash MgO wt.%	0.9	0.9
Ash Na_2O	0.3	0.3
Ash K_2O wt.%	2.4	2.5
Ash TiO_4 wt.%	1.0	1.02
Ash P_2O_5 wt.%	0.2	0.2
Ash So_3 wt.%	2.2	0.0
Ash BaO wt.%	0.1	0.1
Ash SrO wt.%	0.1	0.2

4.4.5 Density and Ash Content as a Function of Coal Size

The results are plotted in Figure 59. They show that neither the mean particle density nor the ash content changes significantly with coal particle size.

4.4.6 Size Distribution of Mineral Matter

The volume-based size distribution of mineral inclusions is plotted in Figure 60. The volumetric mean particle size and standard deviation were approximated by using the method of lognormal curve fitting. The calculated mean particle size and standard deviation are 5.3 μm and 4.69 μm, respectively. The maximum particle size is under 50 μm. The distribution functions were determined by CCSEM method and Abelian transformation was used for the stereological correction of the raw data.

The volume-based size distribution of the extraneous mineral matter is plotted in Figure 61. The volumetric mean particle size and standard deviation were approximated by using the method of lognormal curve fitting. The calculated mean particle size and standard deviation were 53.9 μm and 42.1 μm, respectively. The maximum particle size was under 200 μm.

4.4.7 Chemical Composition and Calculated Viscosity Distribution of Mineral Inclusions in Jader Coal

The mean chemical compound concentrations in the mineral inclusions and the mean concentrations of mineral types are shown in Table 16. It can be seen that the mineral inclusions consist mainly of illite and quartz with smaller amounts of kaolinite, pyrite and mixed silicates.

The Watt-Fereday equation was used to calculate the particle viscosity. The peak flame temperature (1750 K) was chosen for the calculations. The mass-based distribution function of mineral particle viscosity is given in Figure 62. The mean value and standard deviation of the viscosity are $10^{2.58}$ poise and $10^{1.81}$ poise, respectively. The curve shows three distinct peaks, corresponding to the contributions of the pyrite, illite and quartz, which were among the mineral types identified by the CCSEM as components of the mineral inclusions in the Jader coal.

The mean chemical compound concentrations in the extraneous mineral matter and the mean concentrations of mineral types are shown in Table 17. It shows that the mineral inclusions consist mainly of pyrite with smaller amounts of jarosite. The chemical composition of the total mineral matter (included and extraneous mineral matter) and the coal ash can be seen in Table 18.

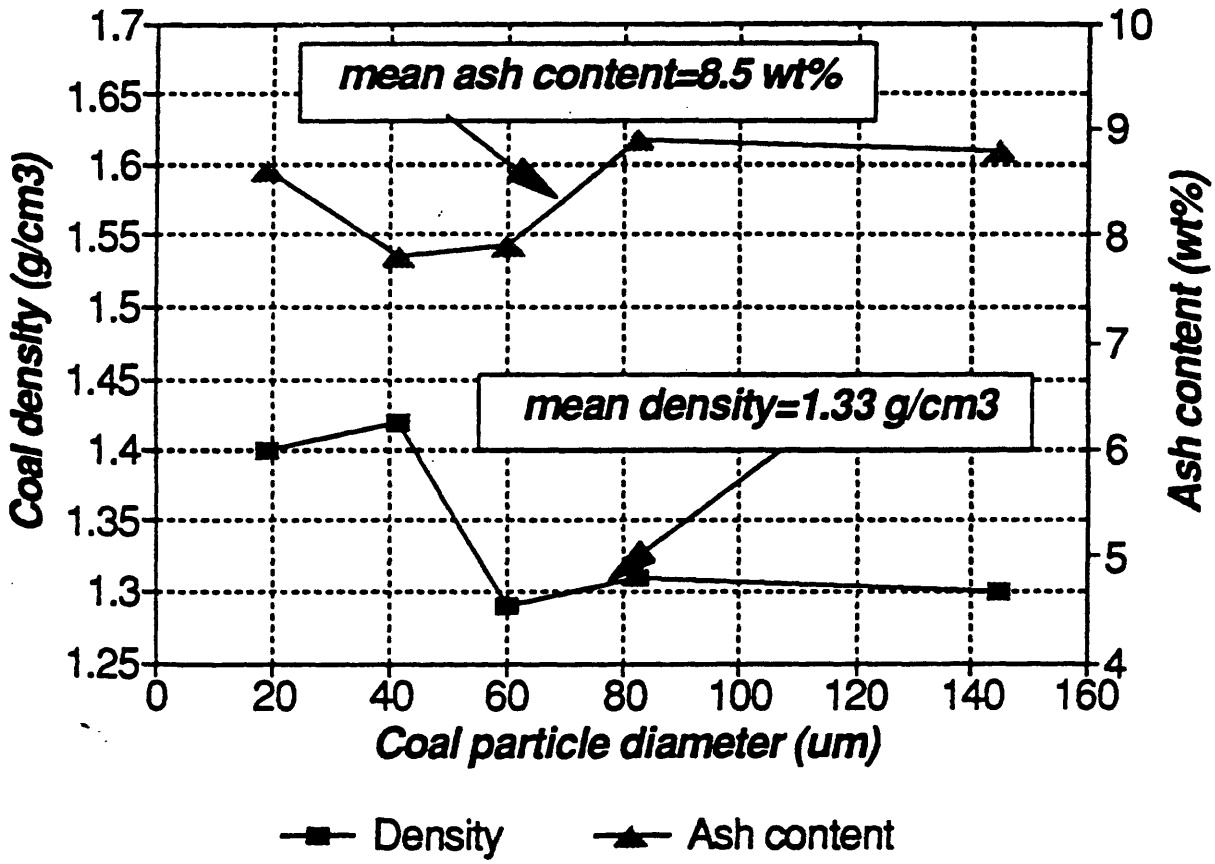

Figure 59. **Coal Density and Ash Content**
Jader Coal

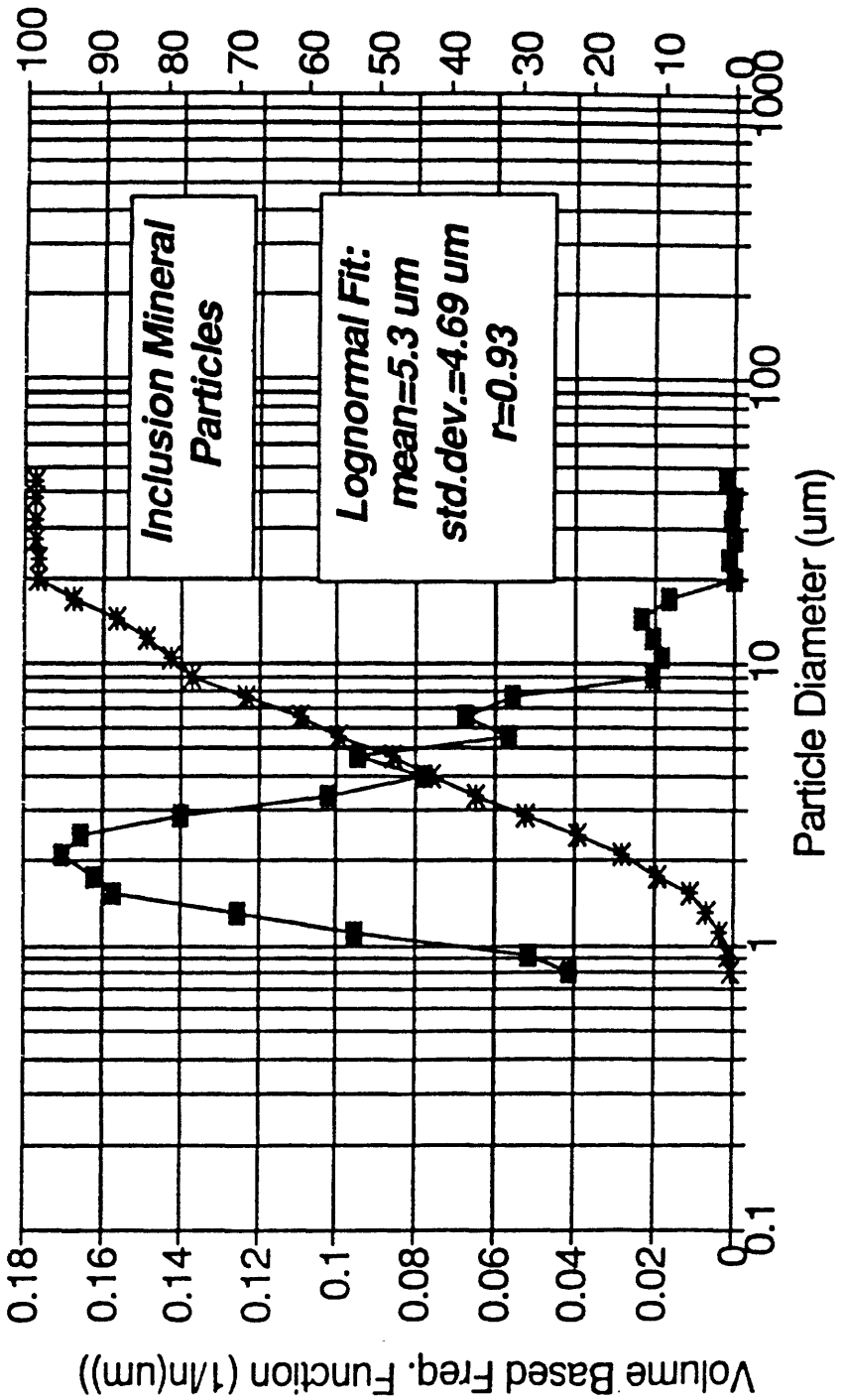

Figure 60. **Size Distribution of Mineral Inclusions**
Jader Coal

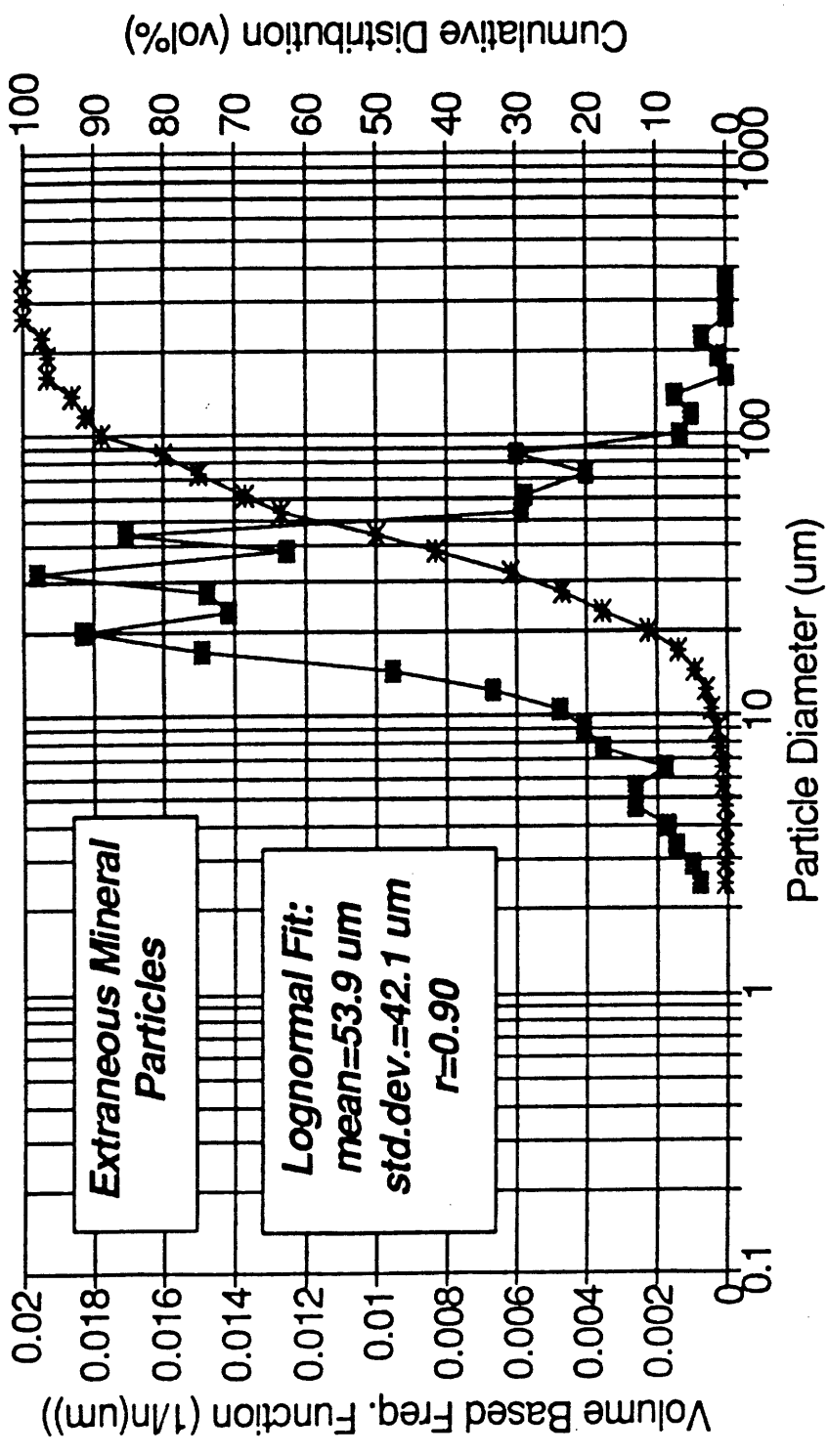

Figure 61. **Size Distribution of Extraneous Mineral Particles;** Jader Coal

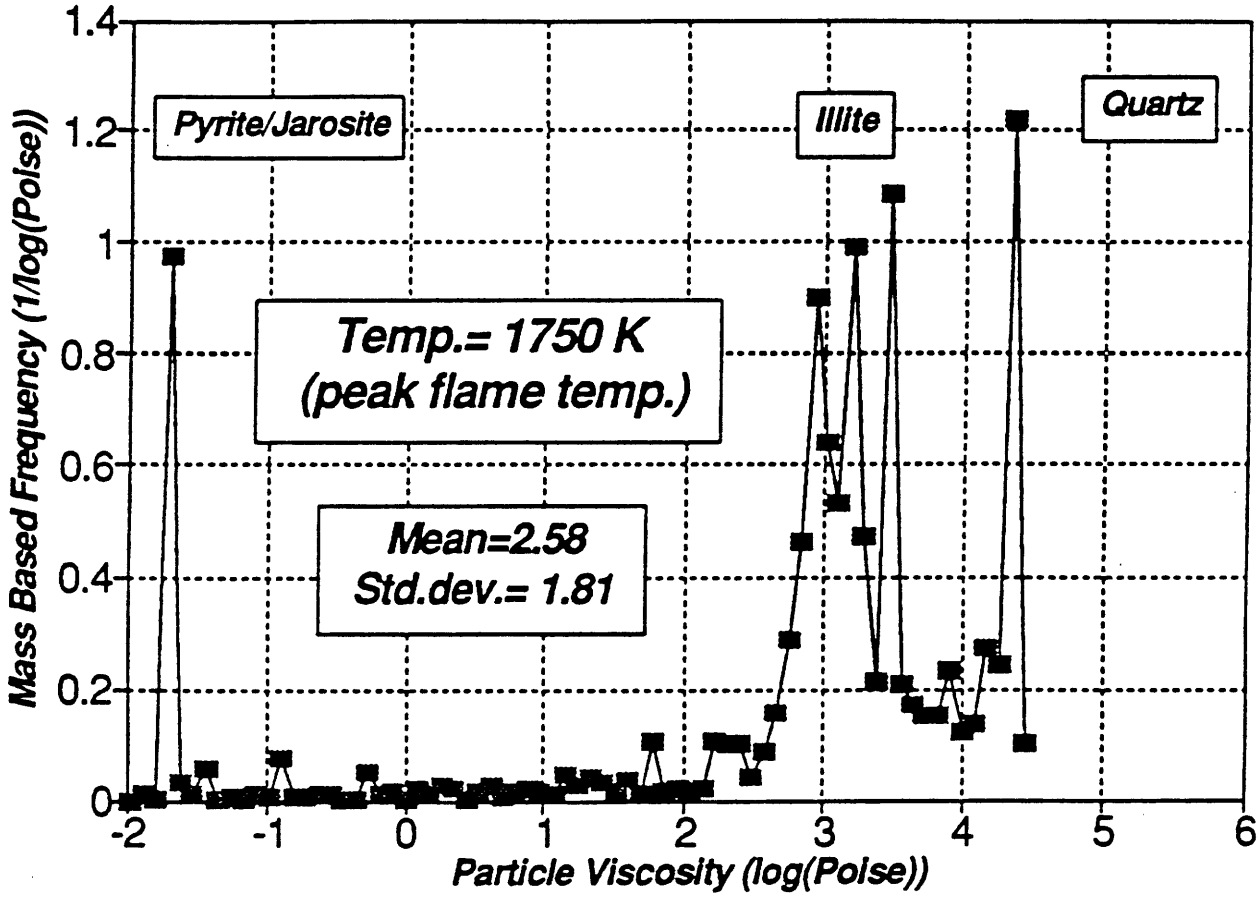

Figure 62. **Viscosity Distribution of Inclusions**
Jader Coal

Table 16.
Chemical Composition and Mineral Compounds of Jader Coal Mineral Inclusions

Oxide Formula	Weight %	Mineral Type	Mass %
Na_2O	0.2	Mixed Silicate	13.2
MgO	0.53	Quartz	34.3
Al_2O_3	19.5	Calcite	0.00
SiO_2	57.3	Siderite	0.77
P_2O_5	0.3	Rutile	0.03
SO_3	7.8	Illite	36.23
Cl	0.3	Pyrite/Marcasite	7.57
K_2O	3.1	Apatite/Evensite	0.48
CaO	1.8	Baryte	0.1
TiO_2	0.2	Kaolinite	4.91
FeO	8.7	Jarosite	2.05
Cr_2O_3	0.2	**Results by CCSEM Method**	
BaO	0.04		

Table 17.
Chemical Composition and Mineral Compounds of Jader Coal Extraneous Mineral Matter

Oxide Formula	Weight %	Mineral Type	Mass %
Na_2O	0.08	Mixed Silicate	1.1
MgO	0.1	Quartz	1.7
Al_2O_3	0.41	Calcite	0.34
SiO_2	2.22	Siderite	7.8
P_2O_5	0.16	Rutile	0.0
SO_3	57.58	Illite	0.14
Cl	0.02	Pyrite/Marcasite	76.7
K_2O	0.15	Apatite/Evensite	0.06
CaO	1.14	Baryte	0.0
TiO_2	0.82	Kaolinite	0.01
FeO	35.91	Jarosite	12.02
Cr_2O_3	1.42	**Results by CCSEM**	
BaO	0.0		

Table 18.
Comparison of Chemical Composition of the Ash and the Total Mineral Matter of the Jader Coal Determined by ASTM and CCSEM Method, Respectively

	ASTM	CCSEM *
Oxide Formula	Ash	Mineral matter
Na_2O	0.3	0.2
MgO	0.9	0.5
Al_2O_3	20.3	18.1
SiO_2	51.7	53.5
P_2O_5	0.2	0.3
SO_3	0.0	0.0
Cl	0.0	0.2
K_2O	2.5	2.9
CaO	1.9	2.0
TiO_2	1.0	0.5
FeO	20.7	20.8
Cr_2O_3	0.0	0.7
BaO	0.1	0.04

* : Calculated by taking the inclusion/extraneous mineral matter ratio of 90%/10%

4.4.8 Experiments in the Combustion Research Facility

The test conditions for the Jader coal are summarized in Table 19. The coal feed rate was set to obtain 0.98 MW thermal input. The coal was carried by air from a coal silo at 1.2 air/coal mass ratio. The flow rate of air was measured by a built-in pitot tube. The flow rate of the coal was measured by a weigh belt. The primary, secondary and tertiary air flows were also monitored by pitot tubes. The air was preheated to 491 K, 524 K and 553 K, respectively. Low air flow rates were maintained for the primary and secondary air, and a high rate for the tertiary air flow. A high degree of swirl was chosen for the primary and tertiary air flows, and no swirl was used for the secondary air flow.

The flue gas temperature profile along the axis of the combustion tunnel is plotted in Figure 63. The temperature was measured by suction pyrometer. The peak flue gas temperature (1750 K) was reached at the distance of 1.4 m from the burner.

The deposition probes were placed in the flue gas stream at two positions: 5.5 m and 5.0 m from the burner. Radial temperature profiles were taken at each of these locations. The results are plotted in Figure 64. At the position of 5.0 m from the burner, the maximum temperature was 1508 K. The maximum temperature at 5.5 m from the burner was 1450 K. The maximum temperatures were found on the axis. Due to the intensive heat extraction through the cylinder jacket, the temperature decreased as the distance from the axis increased.

Pitot tube measurements to determine the radial flue gas velocity profile were made at the positions where the deposition probes were inserted. The results can be seen in Figure 65. At the position of 5.0 m from the burner the peak velocity was 12.3 m/s. At the distance of 5.5 m from the burner, due to the decrease of flue gas temperature, the maximum velocity of the flue gas was 10.5 m/s. Both peak velocities were measured at a radius of 10 cm from the axis. The flue gas velocity first increased and then decreased as the radial distance from the axis increased.

4.4.9 Deposition Experiment

During the deposition sampling, a constant initial surface temperature of 1073 K was obtained by monitoring the surface temperature of the deposition probe and by adjusting the mass flow rate of the cooling air. The probes were placed in the cylindrical section of the CRF at two locations, corresponding to two different flue gas temperatures. The deposition probes were left in the flue gas for different periods of time to permit the rate of deposition to be determined.

For the flue gas temperature of 1450 K and mean velocity of 10.2 m/s, the deposition build-up can be seen in Figure 66. The deposited weight per unit projected probe area is plotted as a function of time. Linear regression was used to approximate the deposition flow and calculate the flow rate. The calculated specific deposition rate was 0.029 kg/m^2/min. For the flue gas temperature of 1508 K and mean velocity of 11.8 m/s, the results are shown in

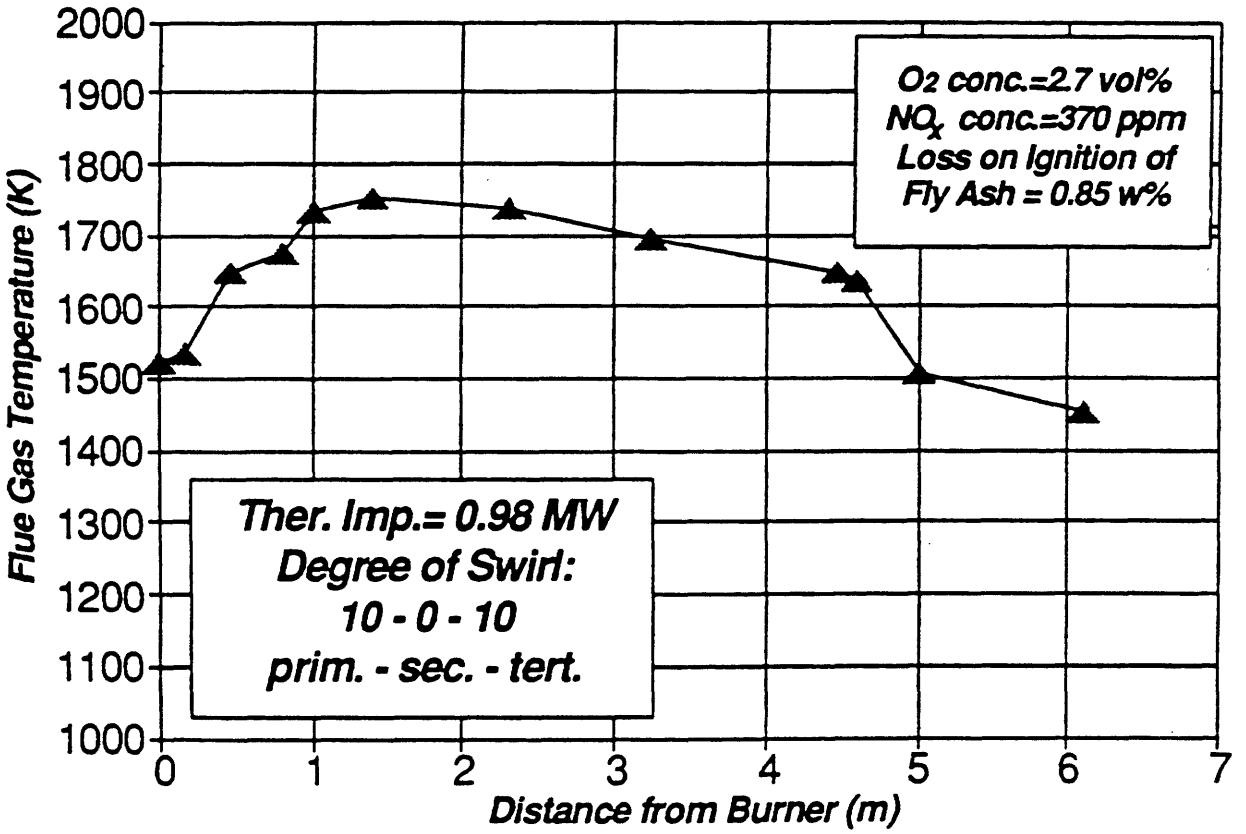

Figure 63. **Axial Flue Gas Temperature Profile**
Jader Coal

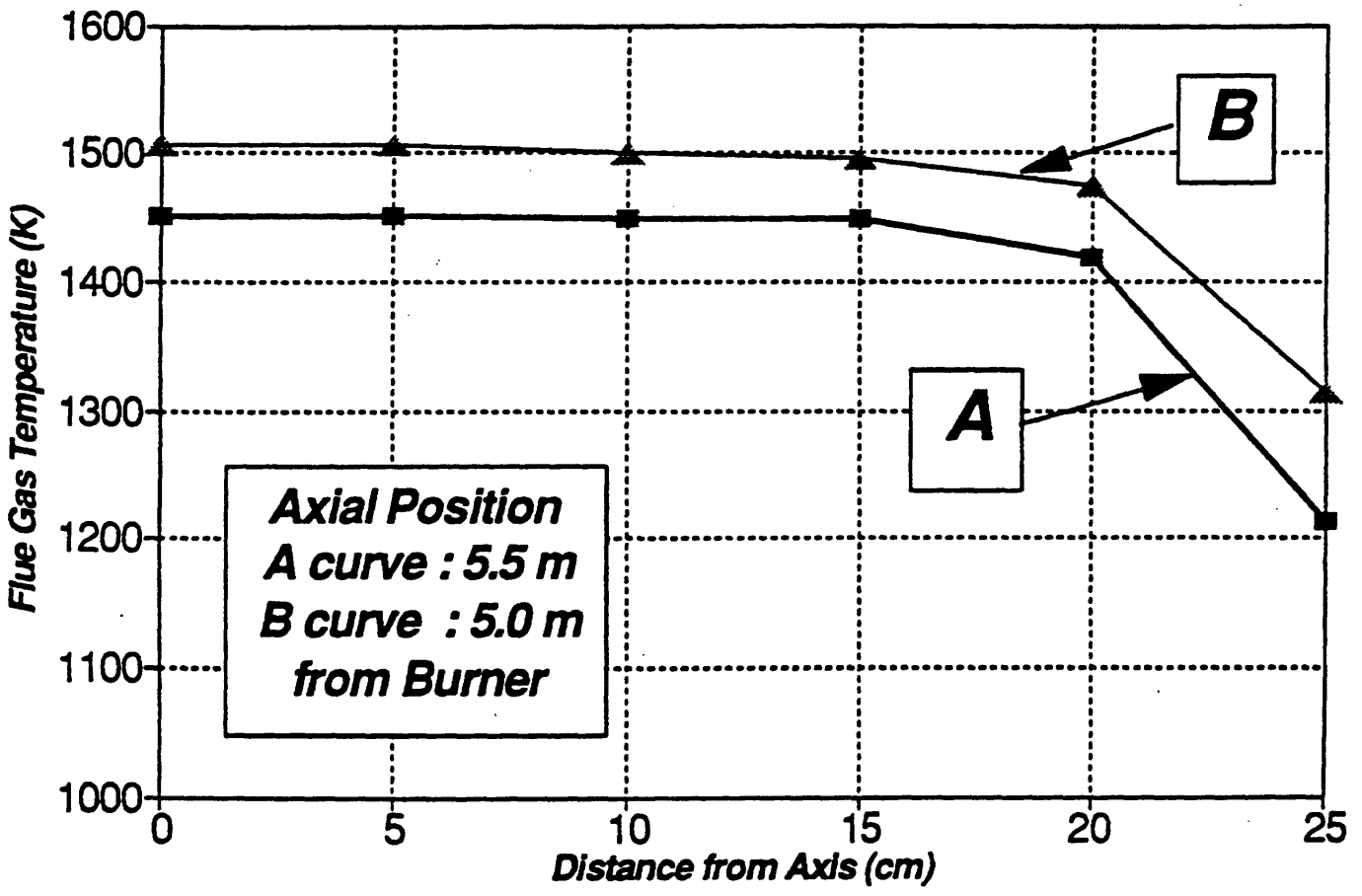

Figure 64. **Radial Temperature Profile**
Jader Coal

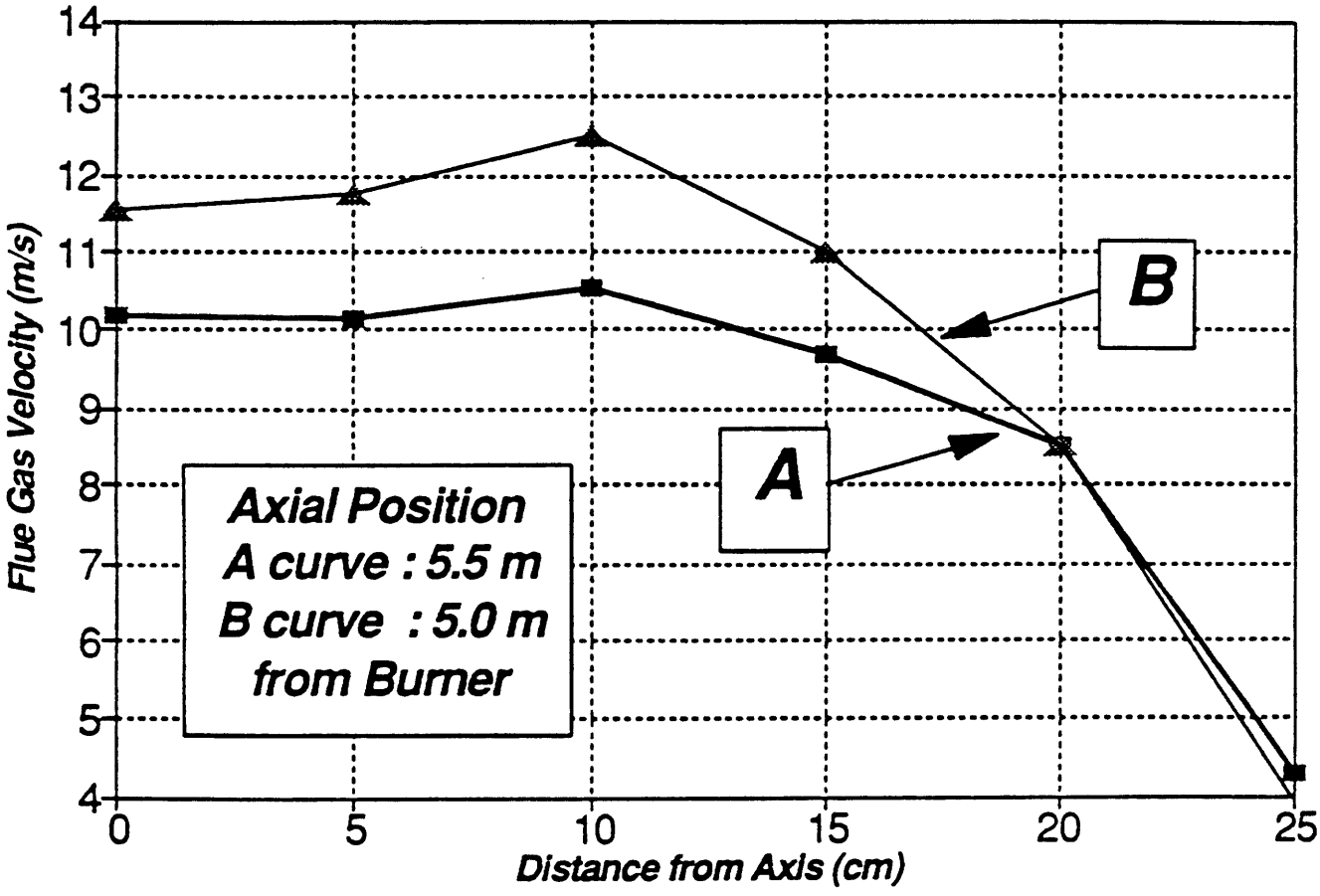

Figure 65. **Radial Flue Gas Velocity Profile**
Jader Coal

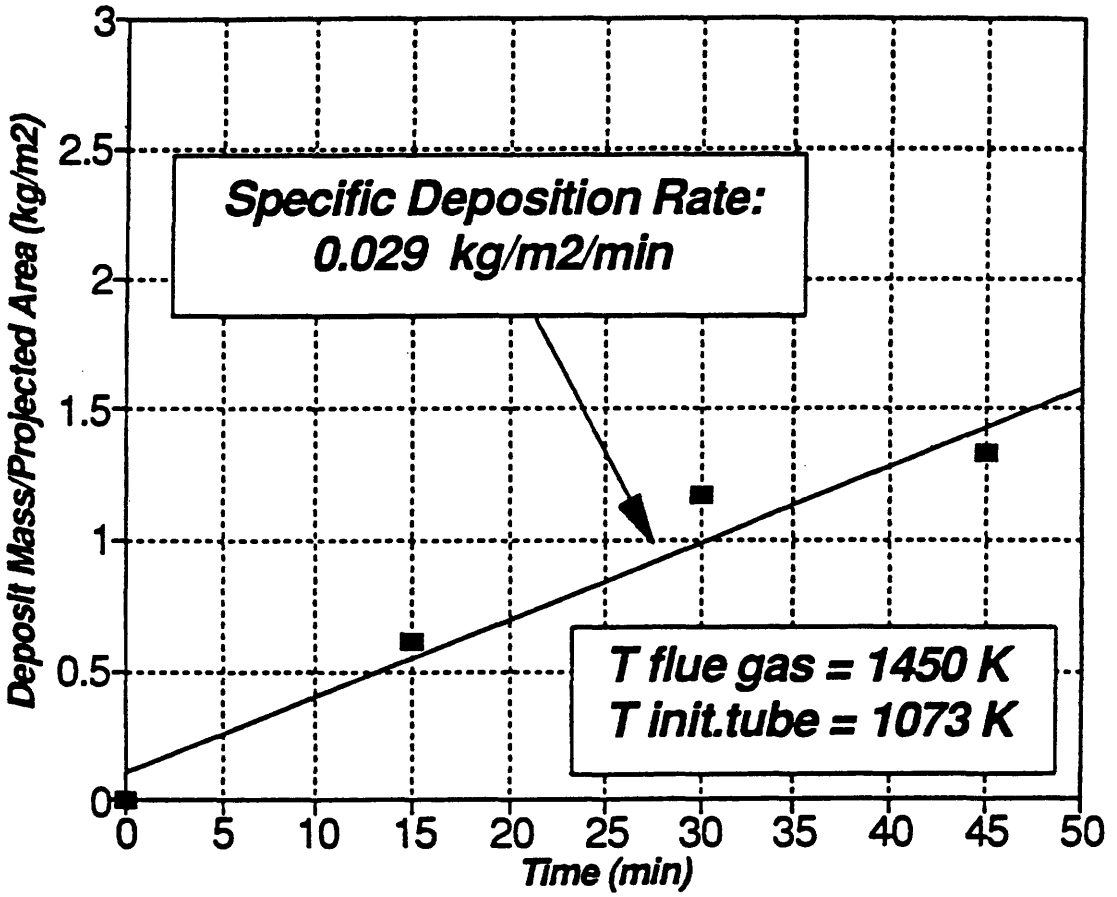

Figure 66. **Deposit Build-Up**
Jader Coal

Table 19.
Test parameters of Jader Bituminous Coal in MIT-CRF

Parameters	Data
Thermal Input (MW)	0.98
Excess Air vol%	14
Coal Mass Flow (kg/h)	114
Carrying Air Mass Flow (kg/h)	137.4
Carrying Air/Coal Mass Ratio (1)	1.212
Primary Air Flow (kg/h) (high.swirl)	142.5
Secondary Air Flow (kg/h) (no.swirl)	63.5
Tertiary Air Flow (kg/h) (top+bottom) (high swirl)	891.1
Total Air Flow (kg/h)	1239
Prim. Air Burner Inlet Temperature (K)	491
Sec. Air Burner Inlet Temperature (K)	524
Tert. Air Burner Inlet Temperature (K)	553

Figure 67. These results indicate a higher deposition rate. From a linear approximation, the specific deposition flow rate was calculated as 0.179 kg/m^2/min, which is approximately 6 times higher than that found in the previous case.

The deposit was easily removable from the deposition tube, and easily breakable in both cases, indicating low activity of sintering between deposited fly ash particles. The average bulk density of the deposit taken at the higher flue gas temperature and after 20 minutes was 1.5 g/cm^3.

4.4.10 Properties of Jader Fly Ash

A fly ash sample was taken at 6.1 m from the burner by the method of isokinetic probe sampling.

By using the CCSEM technique, the fly ash size distribution and chemical composition were determined. In Figure 68, the volume-based distribution function of the fly ash is shown. The maximum fly ash particle size was 90 μm, the calculated mean particle size was 15.4 μm, and the standard deviation was 15.1 μm. By comparing the size distribution of the mineral inclusions with that of the fly ash, it can be seen that the particle size distribution of the fly ash is coarser.

The chemical composition of the fly ash shown in Table 20 was used to calculate the distribution of particle viscosity at flue gas temperatures of 1508 K and 1450 K by using the Watt-Fereday equation. The results can be seen in Figures 69 and 70. Due to the random coalescence of included and ion-exchangeable mineral matter during coal particle burnout, the viscosity distribution of the fly ash is considerably different from that of the included mineral matter. Both the mean value and standard deviation of the viscosity of the included mineral matter are smaller for the fly ash. The ratio of the mean viscosities of the included mineral matter and of the fly ash, calculated for different temperatures, is plotted in Figure 71. The ratio of the respective standard deviations is also shown in Figure 71. Both ratios are independent of the temperature. The ratio of mean viscosities and that of the standard deviations are decreased by 15% and 40%, respectively.

The calculated sticking efficiencies of the included mineral matter and fly ash are plotted in Figure 72. The critical viscosity value was chosen to be 10^6 poise.

4.5 Island Creek Coal

4.5.1 Island Creek Coal Characteristics

The characteristics of the Island Creek coal provided by ABB-Combustion Engineering are listed in Table 21. The coal is of the bituminous type, with 11.9 wt% moisture, 35.2 wt% volatile content and 11794 Btu/lb heating value. Its sulfur content is 2.7 wt%. The melting behavior of its ash was determined by ASTM method, and is characterized by data included in

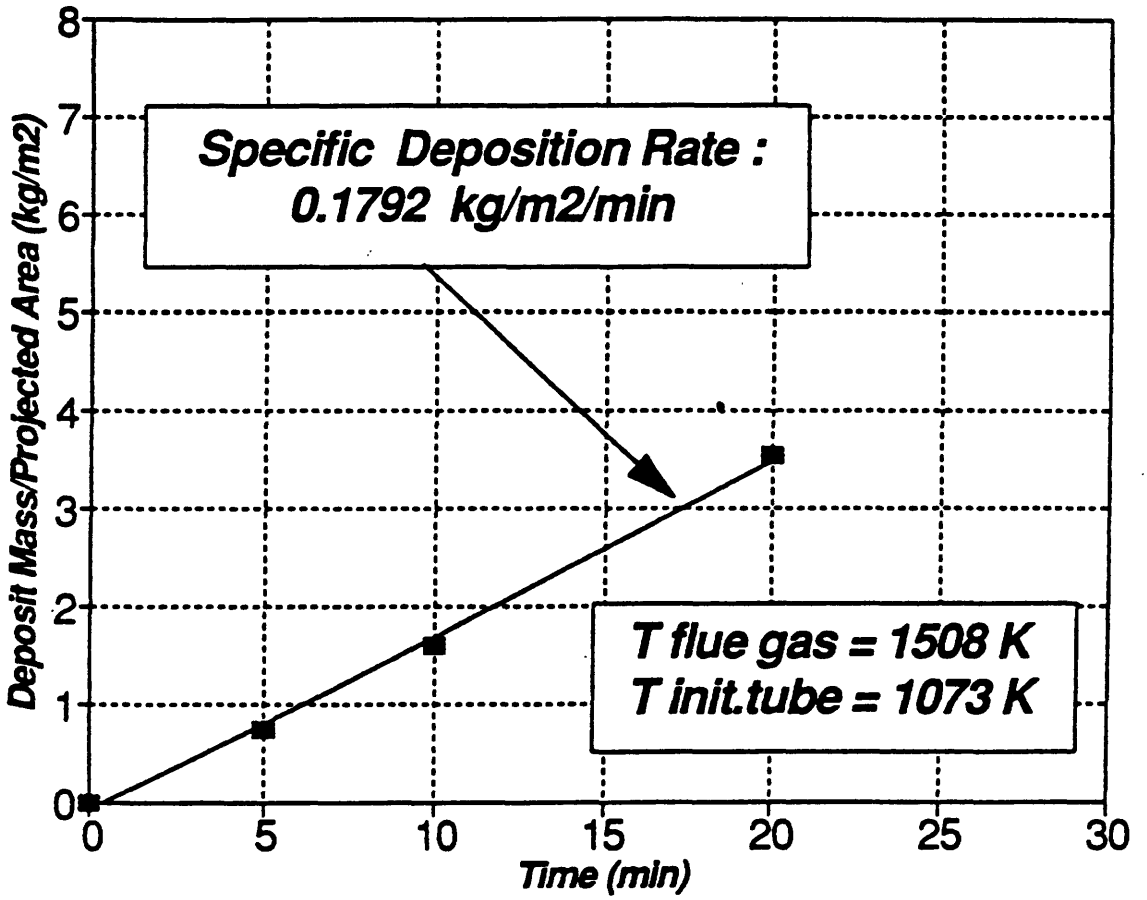

Figure 67. **Deposit Build-Up**
Jader Coal

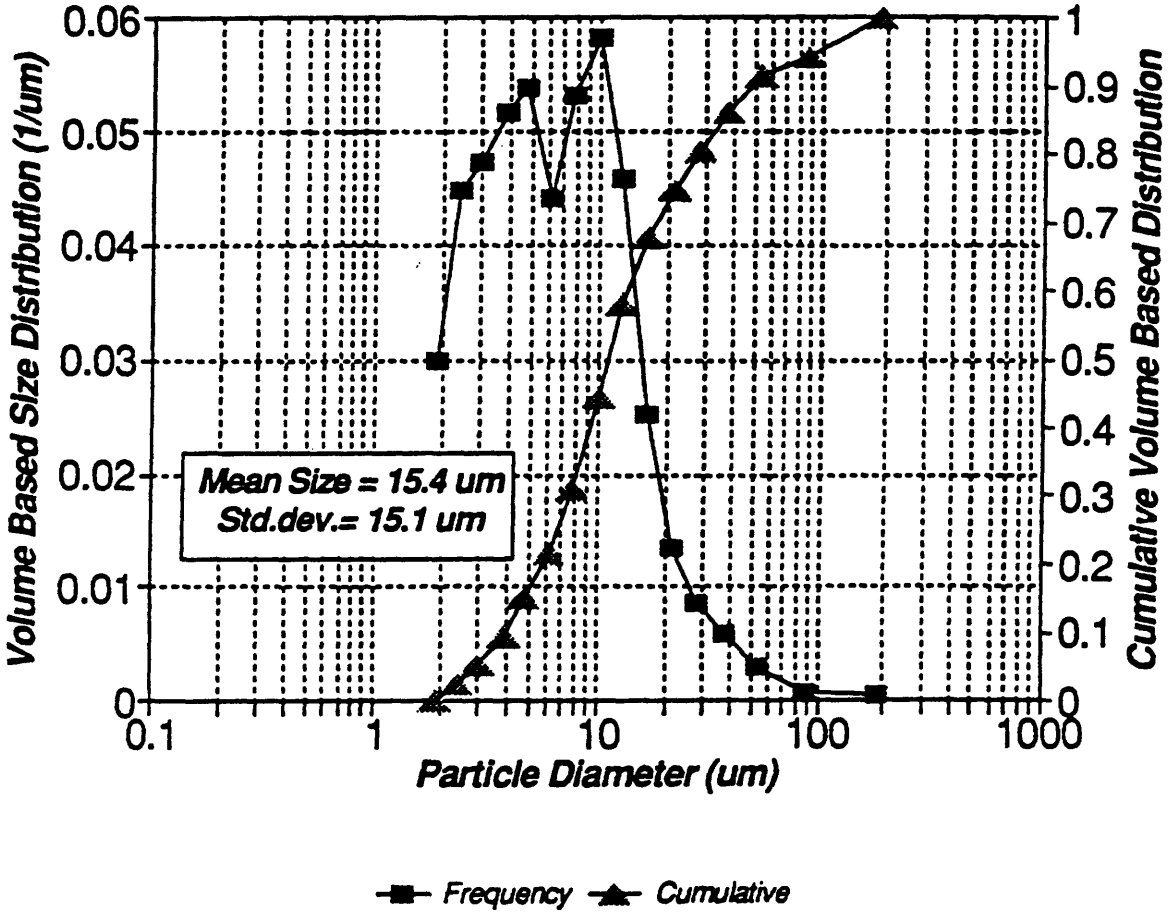

Figure 68. **Size Distribution of Fly Ash**
Jader Coal

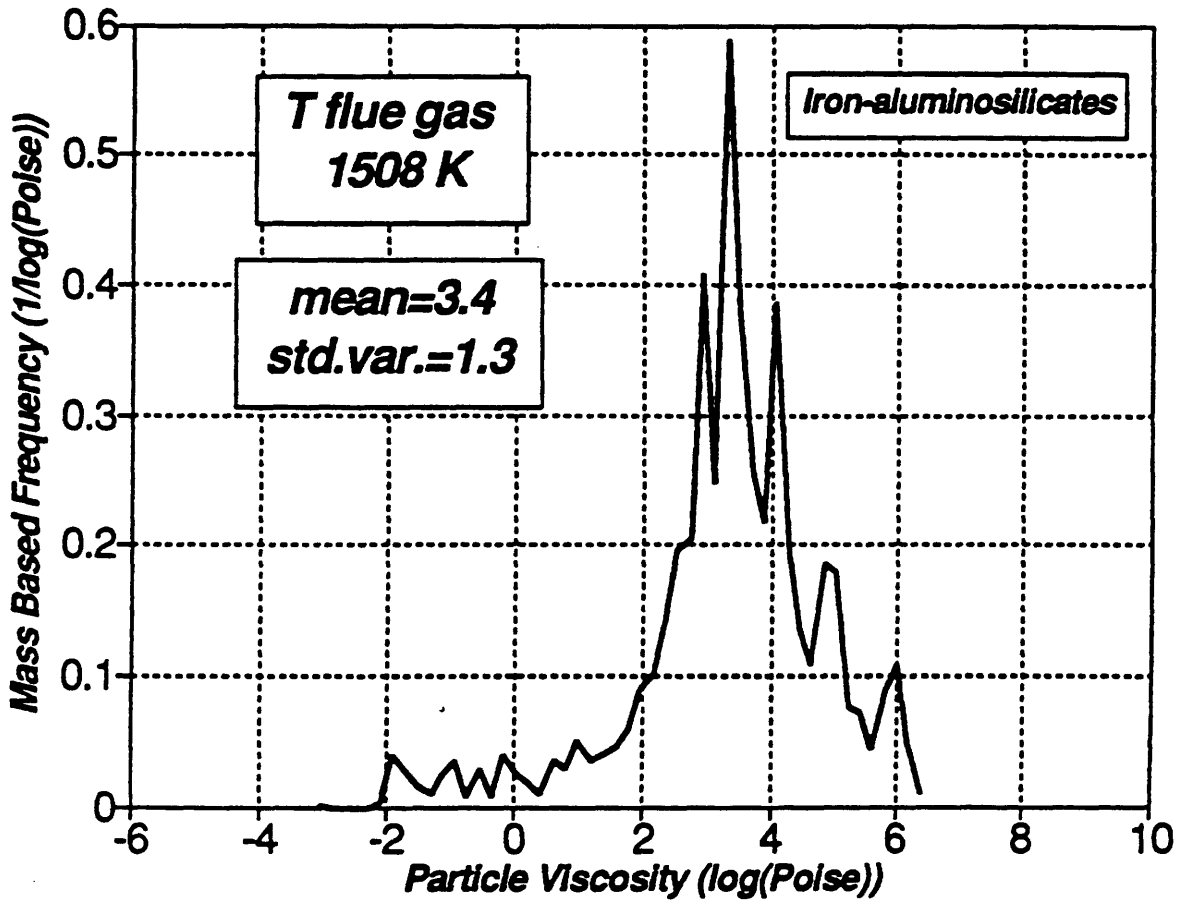

Figure 69. **Viscosity Distribution of Fly Ash Jader Coal**

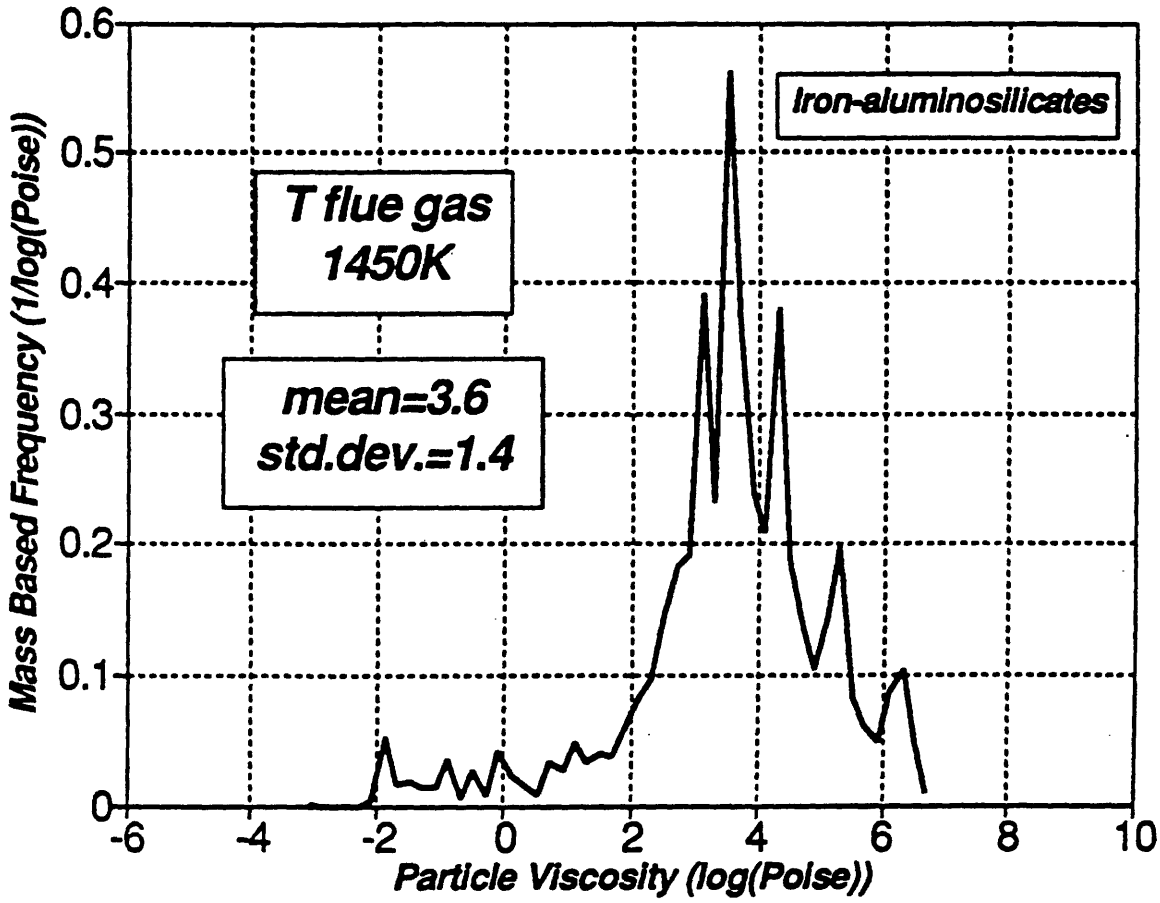

Figure 70. **Viscosity Distribution of Fly Ash** Jader Coal

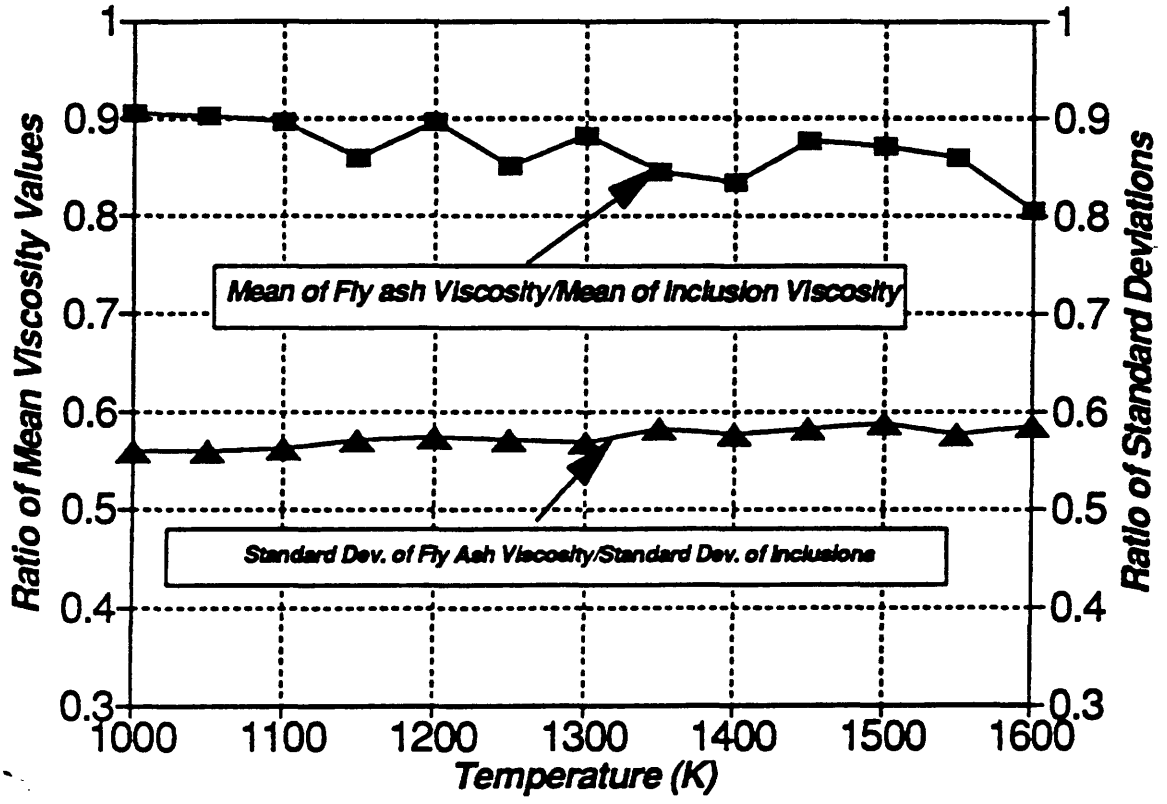

Figure 71. **Statistical Parameters of Viscosity**
Jader Coal

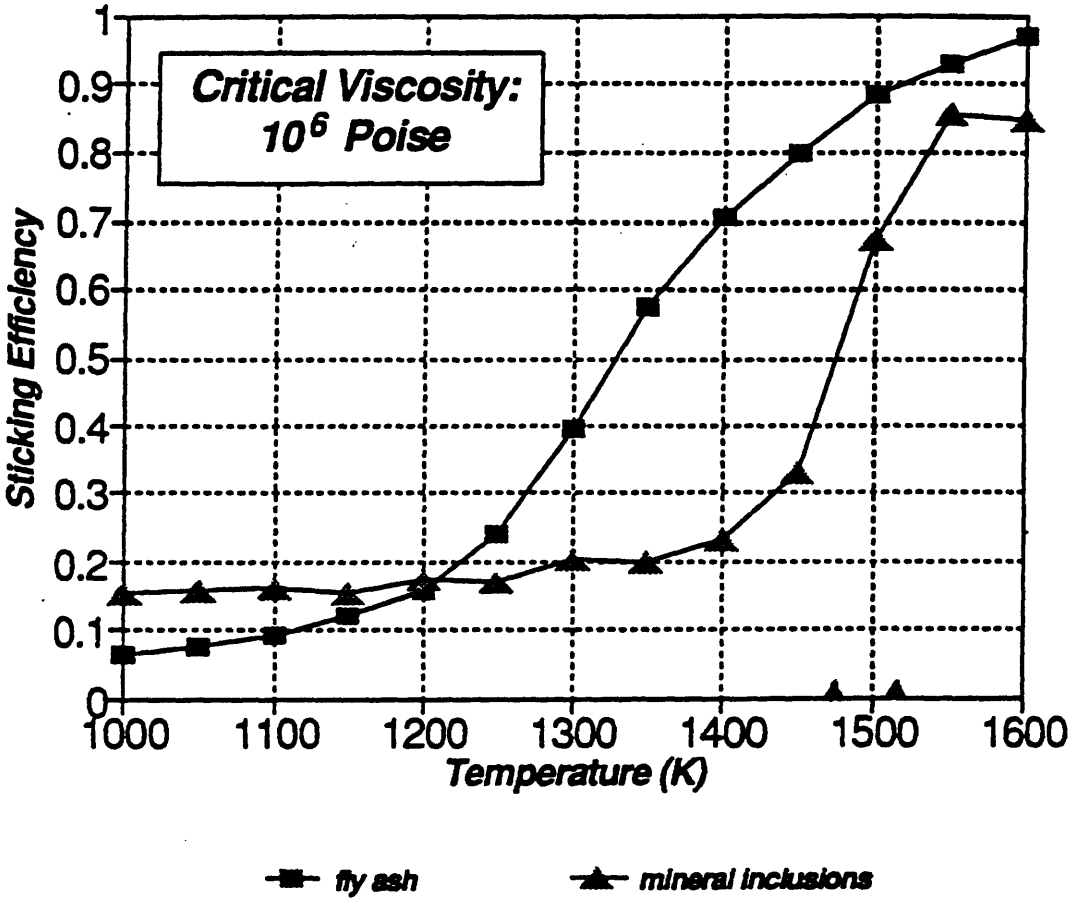

Figure 72. **Sticking Efficiency**
Jader Coal

Table 20.
Comparison of Chemical Composition of the Jader Coal Ash and Fly Ash Determined by ASTM and CCSEM Methods, Respectively

	ASTM	CCSEM
Oxide Formula	Ash	Fly Ash
Na_2O	0.3	0.0
MgO	0.9	0.5
Al_2O_3	20.3	22.1
SiO_2	51.7	49.4
P_2O_5	0.2	1.3
SO_3	0.0	0.0
Cl	0.0	0.2
K_2O	2.5	2.0
CaO	1.9	4.1
TiO_2	1.0	0.2
FeO	20.7	19.2
Cr_2O_3	0.0	0.2
BaO	0.1	0.0

Table 21.
Characteristics of Island Creek Coal

Quantity	Island Coal	
Moisture wt%	11.9	
Volatile Matter wt.%	35.2	
Fixed Carbon wt.%	46.7	
Ash wt.%	6.2	
Heating Value Btu/lb	11794	
Total Sulfur wt.%	2.7	
IDT K (ox.atm.)	1541	
ST K (ox.atm.)	1598	
HT K (ox.atm.)	1629	
FT K (ox.atm.)	1648	
Ash SiO_2 wt.%	with Sulfur	without Sulfur
	42.2	44.76
Ash Al_2O_3 wt.%	18.2	19.30
Ash Fe_2O_3 wt.%	22.0	23.33
Ash CaO wt.%	4.4	4.67
Ash MgO wt.%	0.7	0.74
Ash Na_2O wt.%	0.8	0.85
Ash K_2O wt.%	2.2	2.33
Ash TiO_4 wt.%	1.0	1.06
Ash P_2O_5 wt.%	0.2	0.21
Ash SO_3 wt.%	5.7	0.0
Ash BaO wt.%	0.2	0.21
Ash SrO wt.%	0.1	0.11

Table 21. According to these data, the temperature window within which the deformation of ash particles takes place is from 1541 K to 1648 K. The difference between the initial deformation and fluid temperatures is relatively high, 107 K. The ash chemical composition indicates high Fe_2O_3 and low CaO content. The main chemical compounds are alumina and silica.

4.5.2 Extraneous Mineral Matter in Island Creek Coal

By using a sink-float method the extraneous mineral content of Island Creek coal was determined as 0.025 wt%.

4.5.3 Ion-Exchangeable Mineral Content of Island Creek Coal

The mass fraction of the ion-exchangeable mineral was determined by using acetic acid extraction of the coal, The result shows that less than 1 wt% of the total ash content is ion-exchangeable.

4.5.4 Size Distribution of Island Creek Coal

The volume-based size distribution of the coal can be seen in Figure 73. The frequency function represents a unimodal distribution at particle size of 10 μm. The maximum particle size is 200 μm. The volumetric mean value and standard deviation of the distribution were calculated by using the method of lognormal curve fitting. The calculated mean size and standard deviation are 60.3 μm and 127.8 μm, respectively.

4.5.5 Density and Ash Content as a Function of Coal Size

The results are plotted in Figure 74. They show that both the mean particle density and ash content increase with decreasing coal particle size. However, their variation relative to the mean value is less than 15%.

4.5.6 Size Distribution of Mineral Inclusions

The volume-based size distribution of mineral inclusions is plotted in Figure 75. The volumetric mean particle size and standard deviation were approximated by using the method of lognormal curve fitting. The calculated mean particle size and standard deviation are 3.86 μm and 2.8 μm, respectively. The maximum particle size is under 20 μm. The distribution functions were determined by CCSEM method and Abelian transformation was used for the stereological correction of the raw data.

4.5.7 Chemical Composition and Calculated Viscosity Distribution of Mineral Inclusions in Island Creek Coal

The mean chemical compound concentrations in the mineral inclusions and the mean

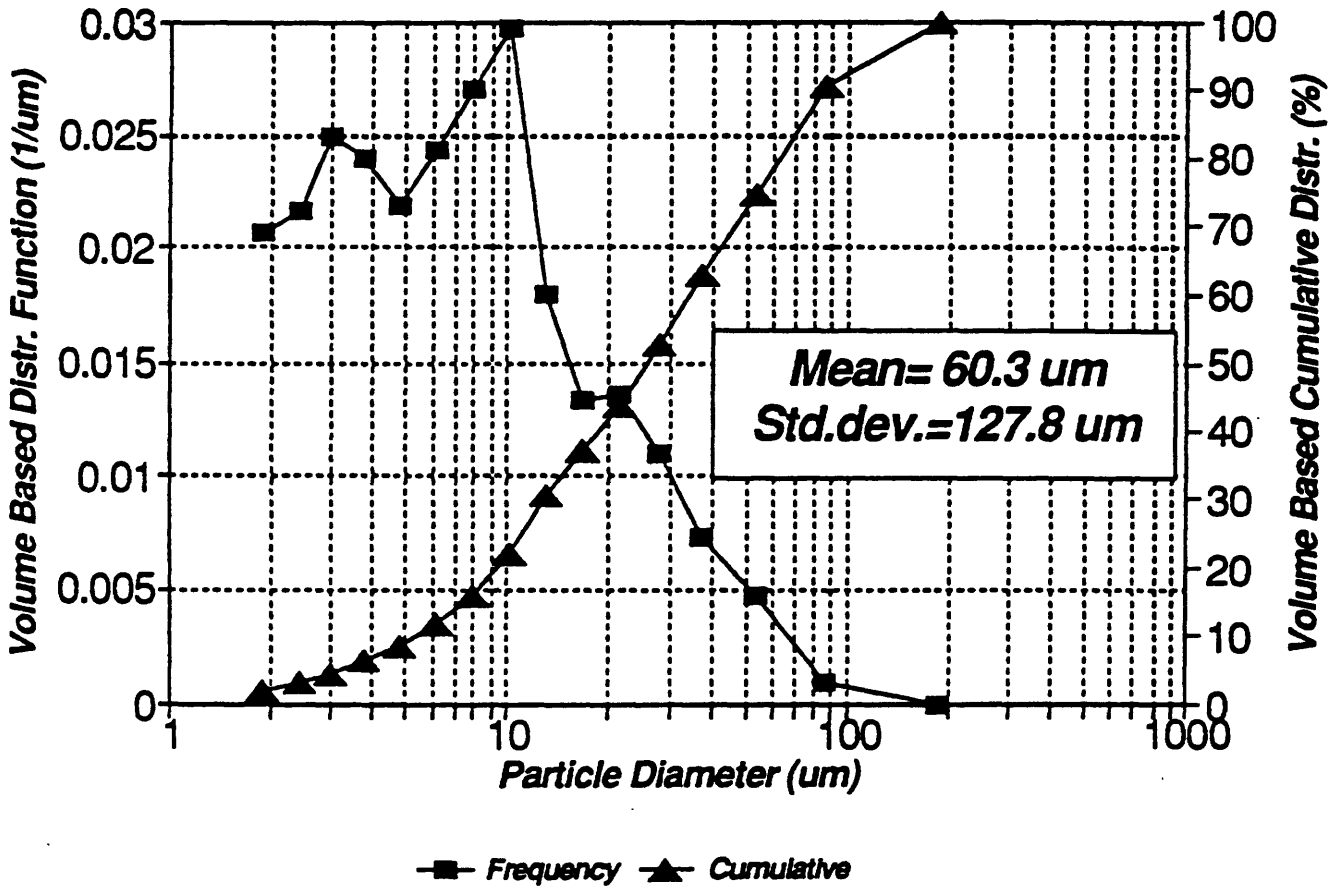

Figure 73. **Size Distribution of Island Creek Coal** Determined by Laser Diffraction Method

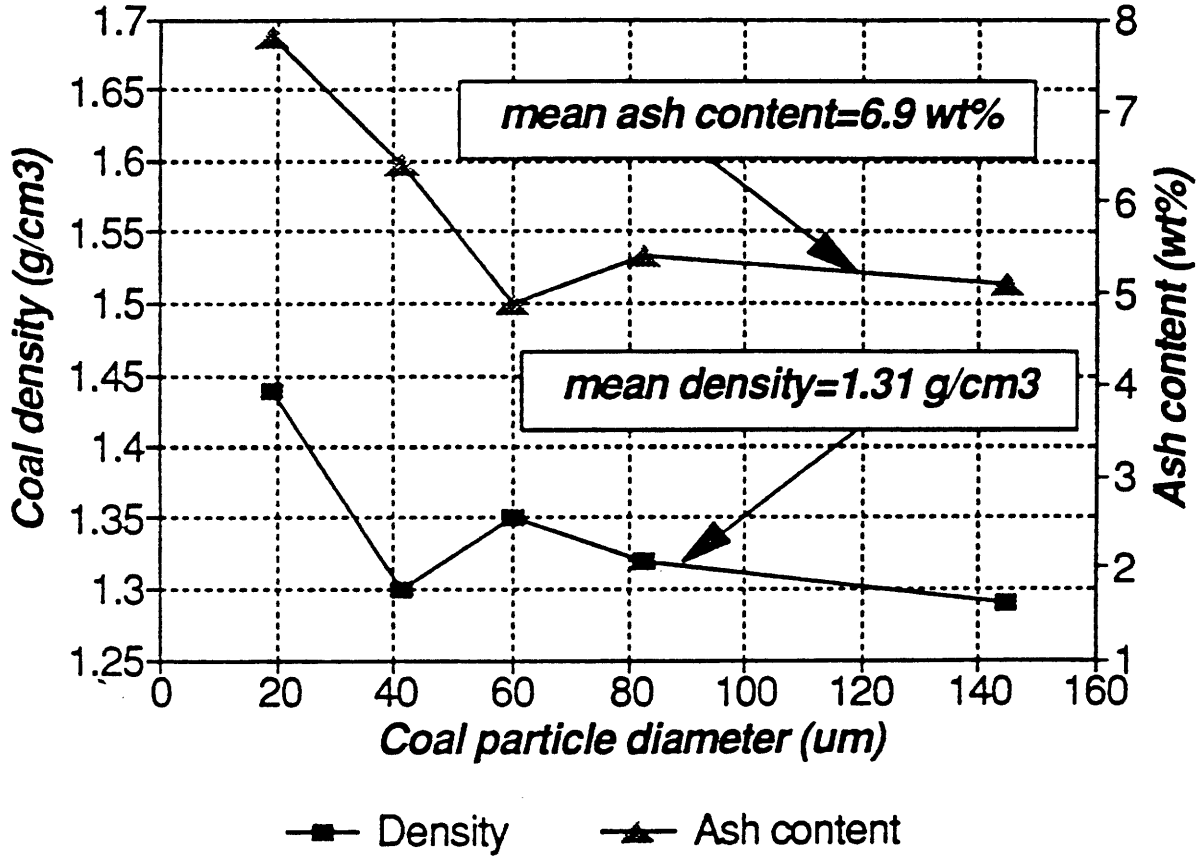

Figure 74. **Coal Density and Ash Content**
Island Creek Coal

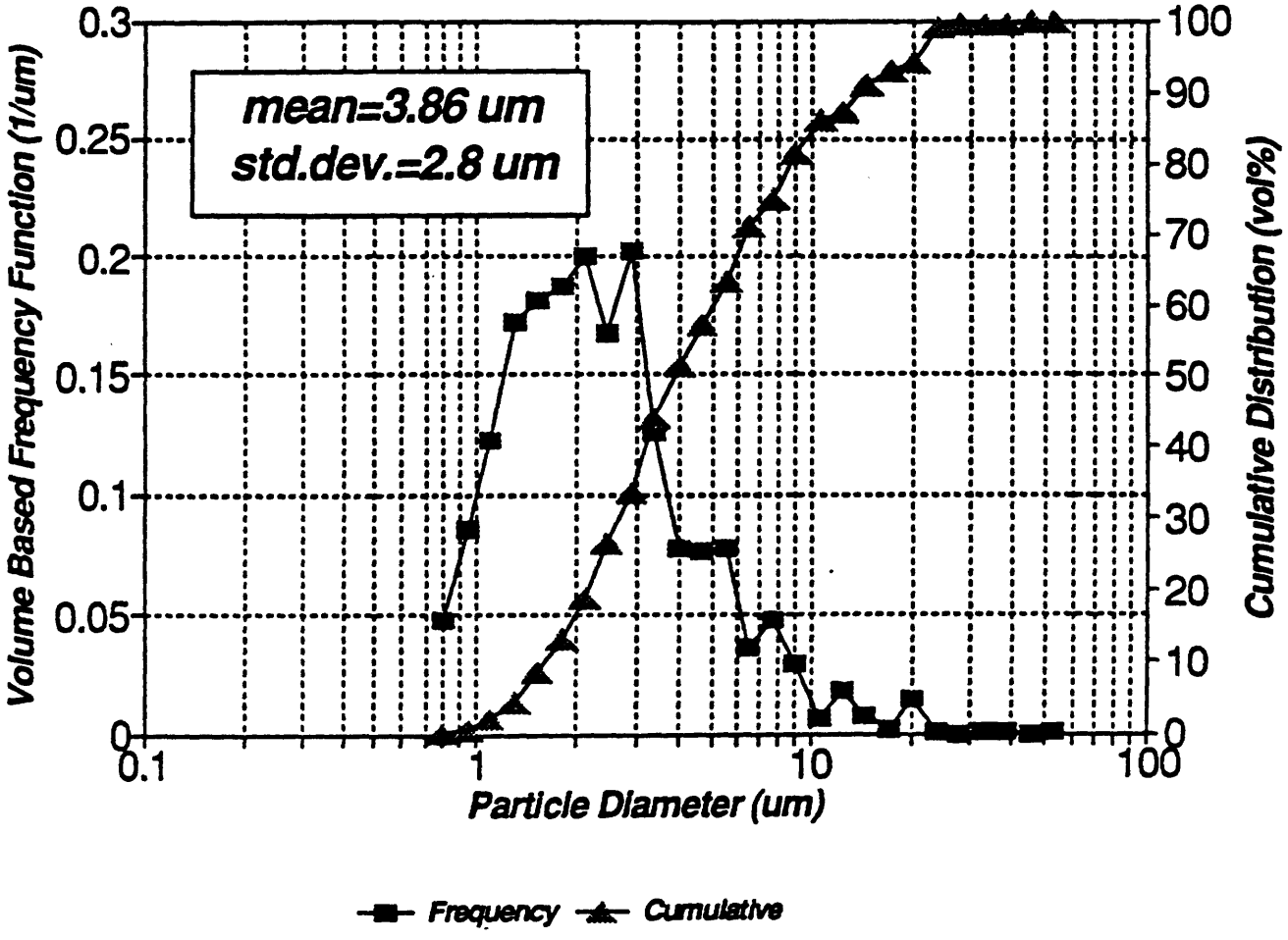

Figure 75. **Size Distribution of Mineral Inclusions** Island Creek Coal

concentrations of mineral types are shown in the Table 22. It can be seen that the mineral inclusions consist mainly of illite, quartz, pyrite and jarosite with smaller amounts of kaolinite, siderite and mixed silicates.

The Watt-Fereday equation was used to calculate the particle viscosity. The peak flame temperature (1750 K) was chosen for the calculations. The mass-based distribution function of mineral particle viscosity is given in Figure 76. The mean value and standard deviation of the viscosity are $10^{1.26}$ poise and $10^{2.29}$ poise, respectively. The curve shows three distinct peaks, corresponding to the contributions of the jarosite/pyrite, illite and quartz, which were identified by the CCSEM as the dominant mineral types in the mineral inclusions in the Island Creek coal.

4.5.8 Experiments in the Combustion Research Facility

The test conditions for the Island Creek coal are summarized in Table 23. The coal feed rate was set to obtain 0.98 MW thermal input. The coal was carried by air from a coal silo at 1.2 air/coal mass ratio. The flow rate of air was measured by a built-in pitot tube. The flow rate of the coal was measured by a weigh belt. The primary, secondary and tertiary air flows were also monitored by pitot tubes. The air was preheated to 488 K, 527 K and 554 K, respectively. Low air flow rates were maintained for the primary and secondary air, and a high rate for the tertiary air flow. A high degree of swirl was chosen for the primary and tertiary air flows, and no swirl was used for the secondary air flow.

The flue gas temperature profile along the axis of the combustion tunnel is plotted in Figure 77. The temperature was measured by suction pyrometer. The peak flue gas temperature (1750 K) was reached at the distance of 2.2 m from the burner.

The deposition probes were placed in the flue gas stream at two positions: 6.1 m and 5.0 m from the burner. Radial temperature profiles were taken at each of these locations. The results are plotted in Figure 78. At the position of 5.0 m from the burner, the maximum temperature was 1500 K. The maximum temperature at 6.1 m from the burner was 1369 K. The maximum temperatures were found on the axis. Due to the intensive heat extraction through the cylinder jacket, the temperature decreased as the distance from the axis increased.

Pitot tube measurements to determine the radial flue gas velocity profile were made at the positions where the deposition probes were inserted. The results can be seen in Figure 79. At the position of 5.0 m from the burner the peak velocity was 11.0 m/s. At the distance of 6.1 m from the burner, due to the decrease of flue gas temperature, the maximum velocity of the flue gas was 9.6 m/s. Both peak velocities were measured at a radius of 15 cm from the axis. The flue gas velocity first increased and then decreased as the radial distance from the axis increased.

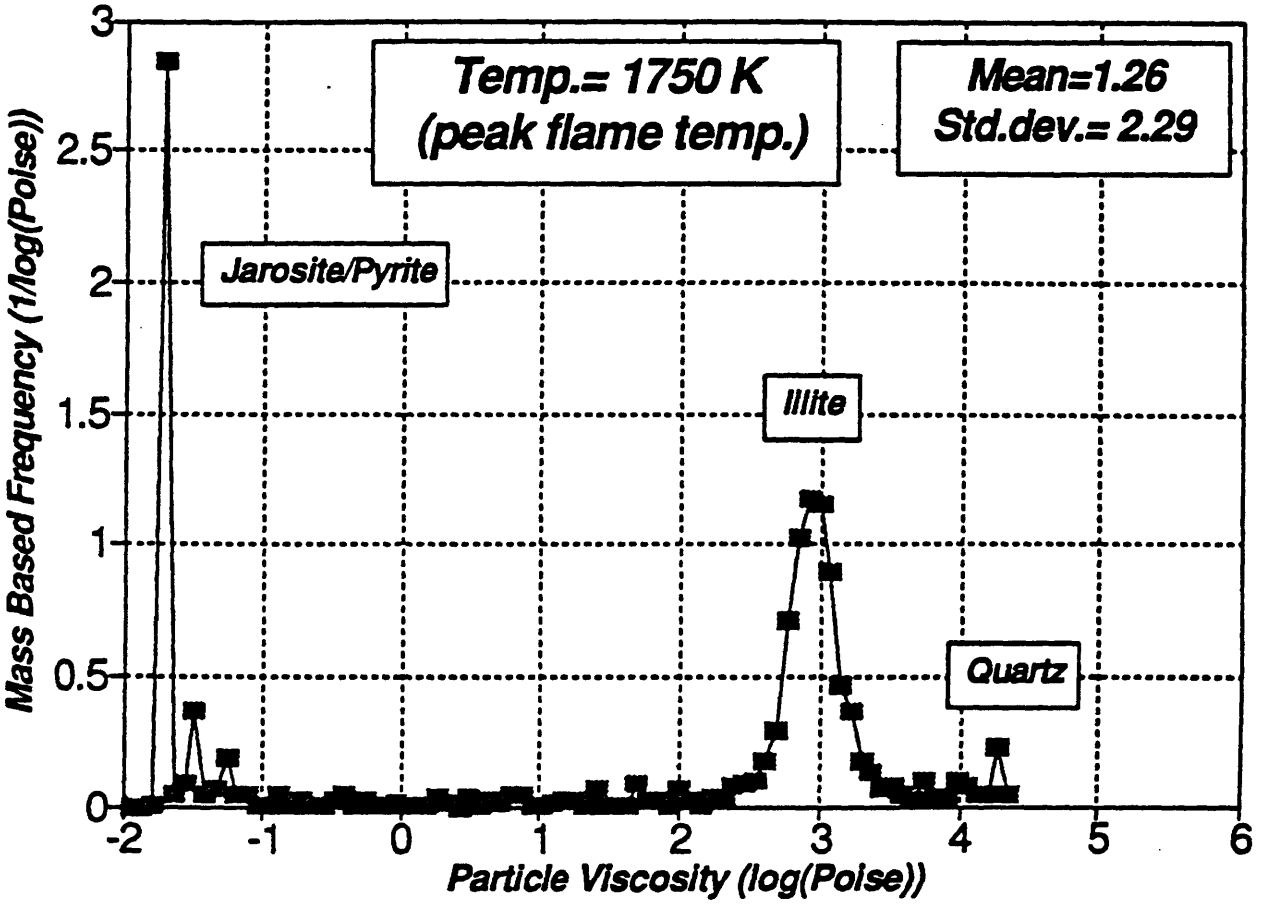

Figure 76. **Viscosity Distribution of Inclusions**
Island Creek Coal

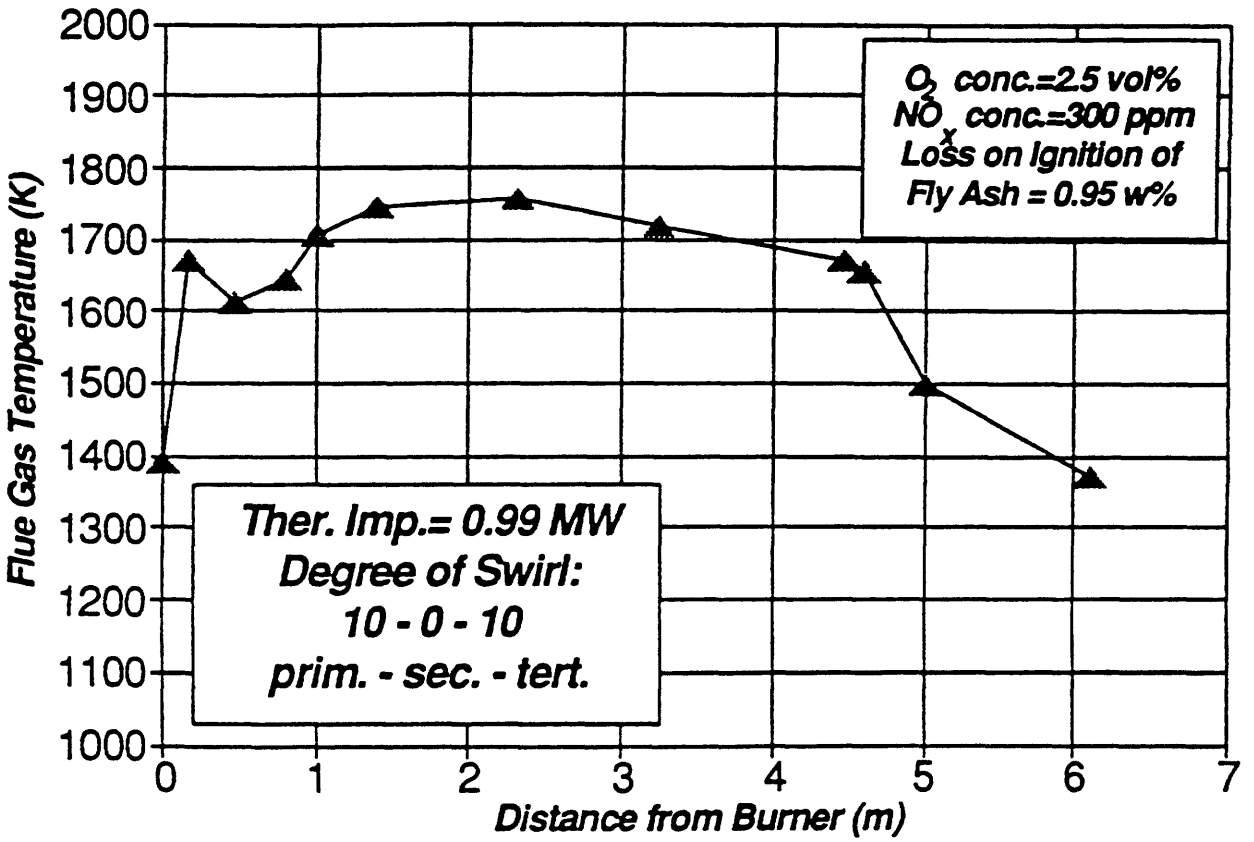

Figure 77. **Axial Flue Gas Temperature Profile**
Island Creek Coal

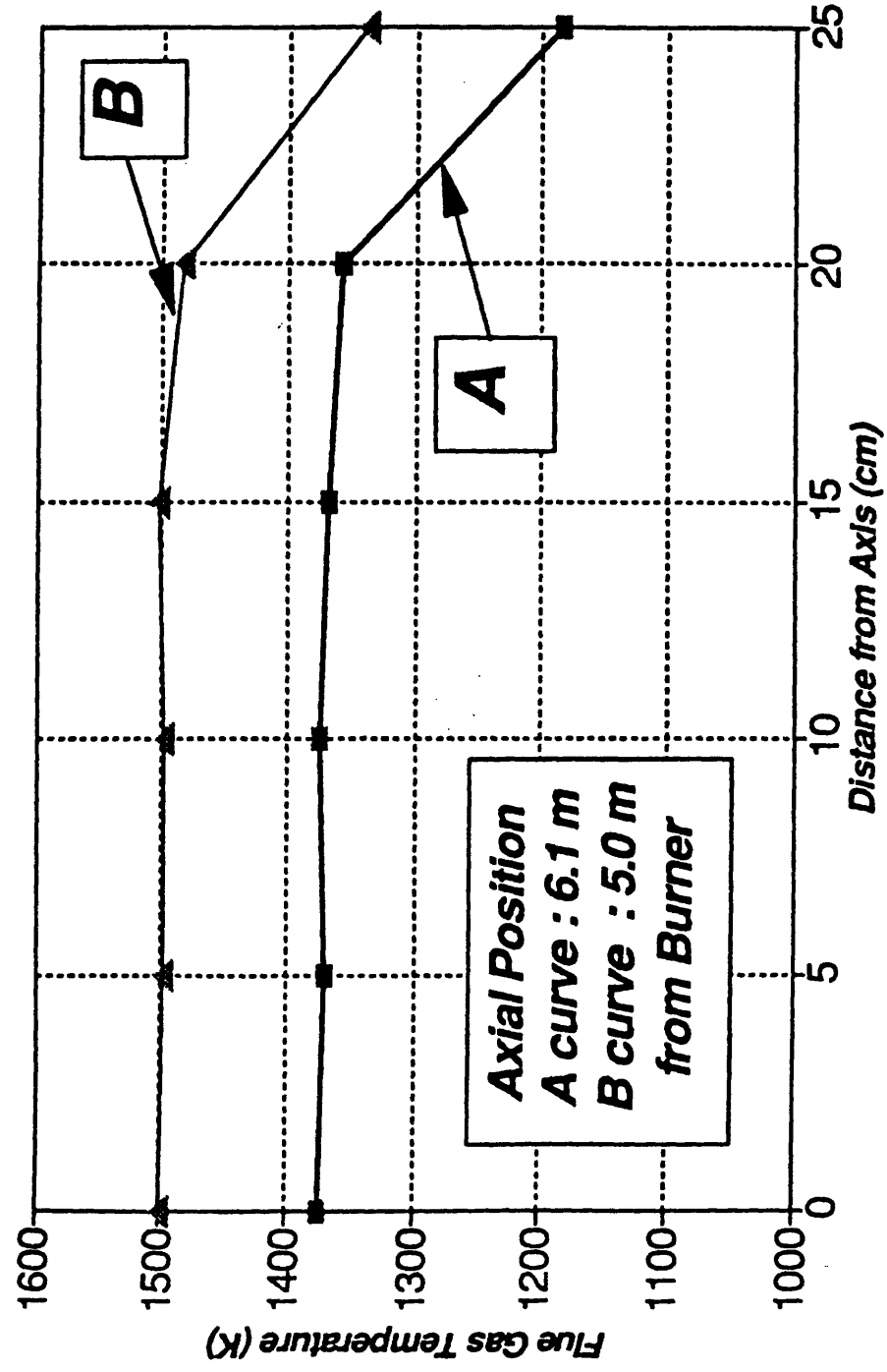

Figure 78. Radial Flue Gas Temperature Profile
Island Creek Coal

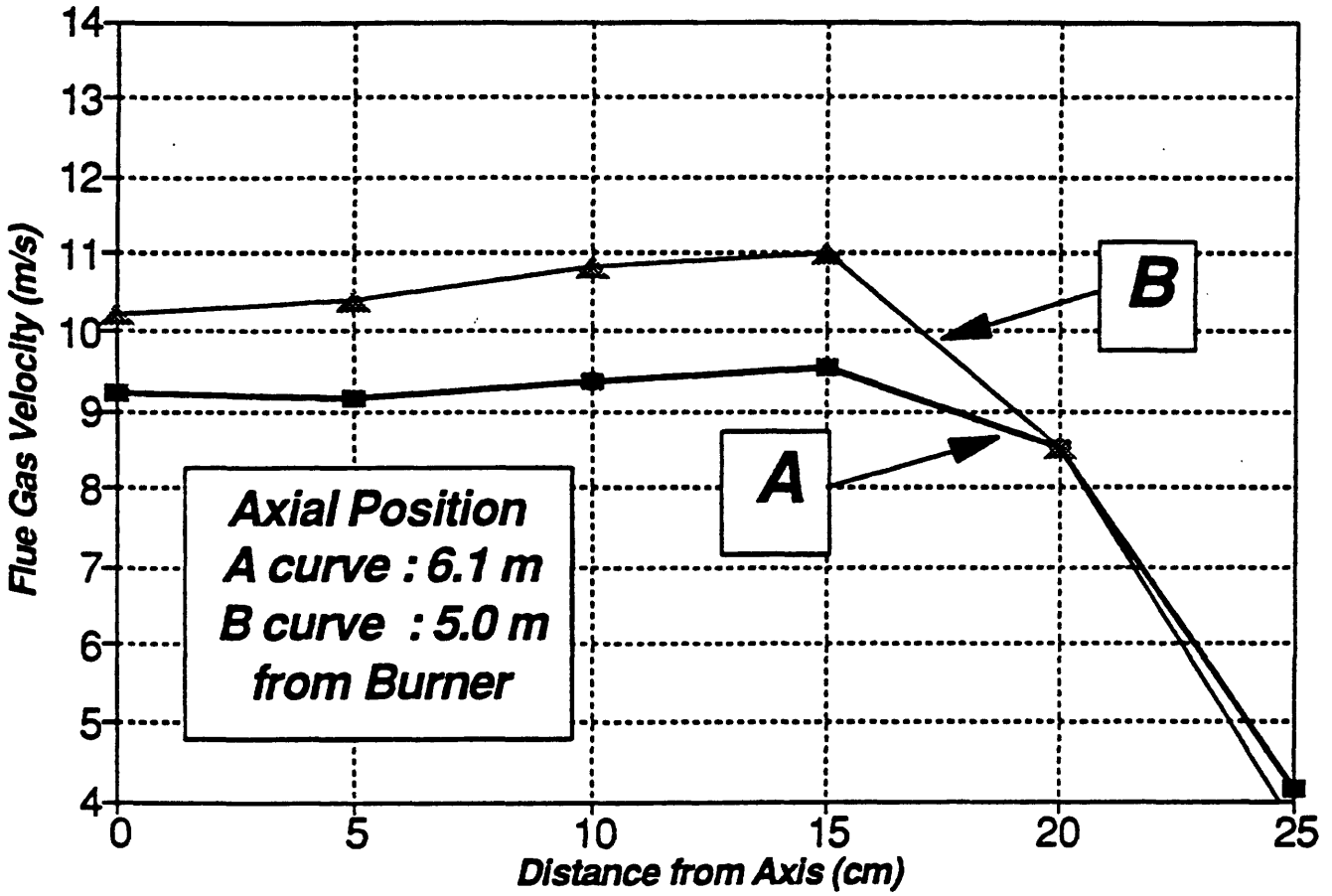

Figure 79. **Radial Flue Gas Velocity Profile**
Island Creek Coal

Table 22.
Chemical Composition and Mineral Compounds of Island Creek Coal Mineral Inclusions

Oxide Formula	Weight %	Mineral Type	Mass %
Na_2O	0.3	Mixed Silicate	7.4
MgO	1.0	Quartz	14.6
Al_2O_3	20.5	Calcite	3.7
SiO_2	49.7	Siderite	5.8
P_2O_5	0.25	Rutile	0.0
SO_3	0.0	Illite	41.6
Cl	0.2	Pyrite/Marcasite	9.3
K_2O	2.7	Apatite/Evensite	0.3
CaO	4.2	Baryte	0.3
TiO_2	0.32	Kaolinite	5.4
FeO	20.1	Jarosite	10.0
Cr_2O_3	0.35	**Results by CCSEM**	
BaO	0.2		

Table 23.
Test Parameters of Island Creek Coal in MIT-CRF

Parameters	Data
Thermal Input (MW)	0.98
Excess Air vol%	14
Coal Mass Flow (kg/h)	113
Carrying Air Mass Flow (kg/h)	138
Carrying Air/Coal Mass Ratio (1)	1.21
Primary Air Flow (kg/h) (high.swirl)	143
Secondary Air Flow (kg/h) (no.swirl)	64
Tertiary Air Flow (kg/h) (top+bottom) (high swirl)	898
Total Air Flow (kg/h)	1,243
Prim. Air Burner Inlet Temperature (K)	488
Sec. Air Burner Inlet Temperature (K)	527
Tert. Air Burner Inlet Temperature (K)	554

4.5.9 Deposition Experiment

During the deposition sampling, a constant initial surface temperature of 1073 K was obtained by monitoring the surface temperature of the deposition probe and by adjusting the mass flow rate of the cooling air. The probes were placed in the cylindrical section of the CRF at two locations, corresponding to two different flue gas temperatures. The deposition probes were left in the flue gas for different periods of time to permit the rate of deposition to be determined.

For the flue gas temperature of 1369 K and mean velocity of 9.4 m/s, the deposition build-up can be seen in Figure 80. The deposited weight per unit projected probe area is plotted as a function of time. Linear regression was used to approximate the deposition flow and calculate the flow rate. The calculated specific deposition rate was 0.011 $kg/m^2/min$. For the flue gas temperature of 1500 K and mean velocity of 10.5 m/s, the results are shown in Figure 81. These results indicate higher deposition rate. From a linear approximation, the specific deposition flow rate was calculated as 0.129 $kg/m^2/min$, which is approximately 11 times higher than that found in the previous case.

The deposit was easily removable from the deposition tube, and easily breakable in both cases, indicating low activity of sintering between deposited fly ash particles. The average bulk density of the deposit taken at the higher flue gas temperature and after 60 minutes was 1.3 g/cm^3.

4.5.10 Properties of Island Creek Fly Ash

A fly ash sample was taken at 6.1 m from the burner by the method of isokinetic probe sampling.

By using the CCSEM technique, the fly ash size distribution and chemical composition was determined. In Figure 82, the volume-based distribution function of the fly ash is shown. The maximum fly ash particle size was 90 μm, the calculated mean particle size was 12.8 μm, and the standard deviation was 15.5 μm. By comparing the size distribution of the mineral inclusions with that of the fly ash, it can be seen that the particle size distribution of the fly ash is coarser.

The chemical composition of the fly ash shown in Table 24 was used to calculate the distribution of particle viscosity at flue gas temperatures of 1500 K and 1369 K by using the Watt-Fereday equation. The results can be seen in Figures 83 and 84. Due to the random coalescence of included and ion-exchangeable mineral matter during coal particle burnout the viscosity distribution of the fly ash is considerably different from that of the included mineral matter. Both the mean value and standard deviation of the viscosity of the included mineral matter are smaller for the fly ash. The ratio of the mean viscosities of the included mineral matter and the fly ash, calculated for different temperatures, is plotted in Figure 85. The ratio of the respective standard deviations is also shown in Figure 85. Both ratios are independent

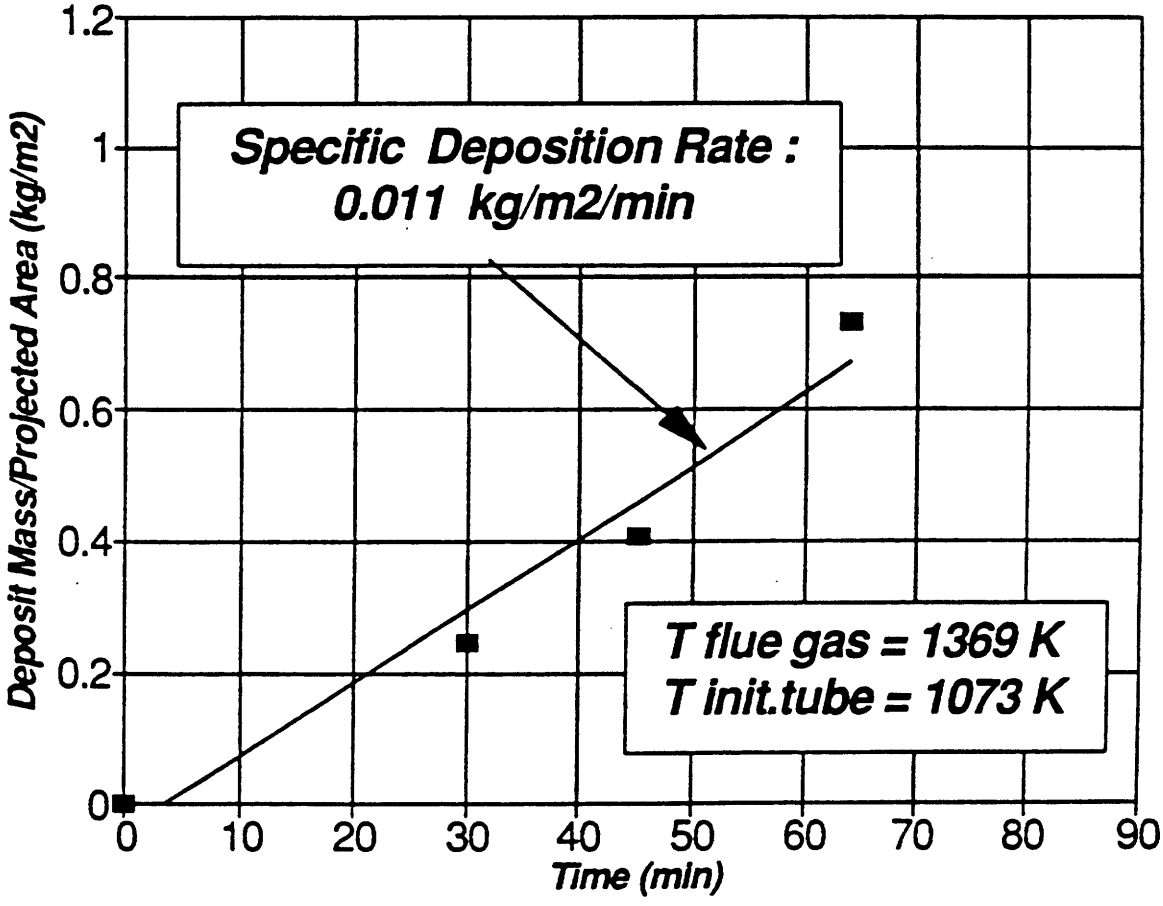

Figure 80. **Deposit Build-Up**
Island Creek Coal

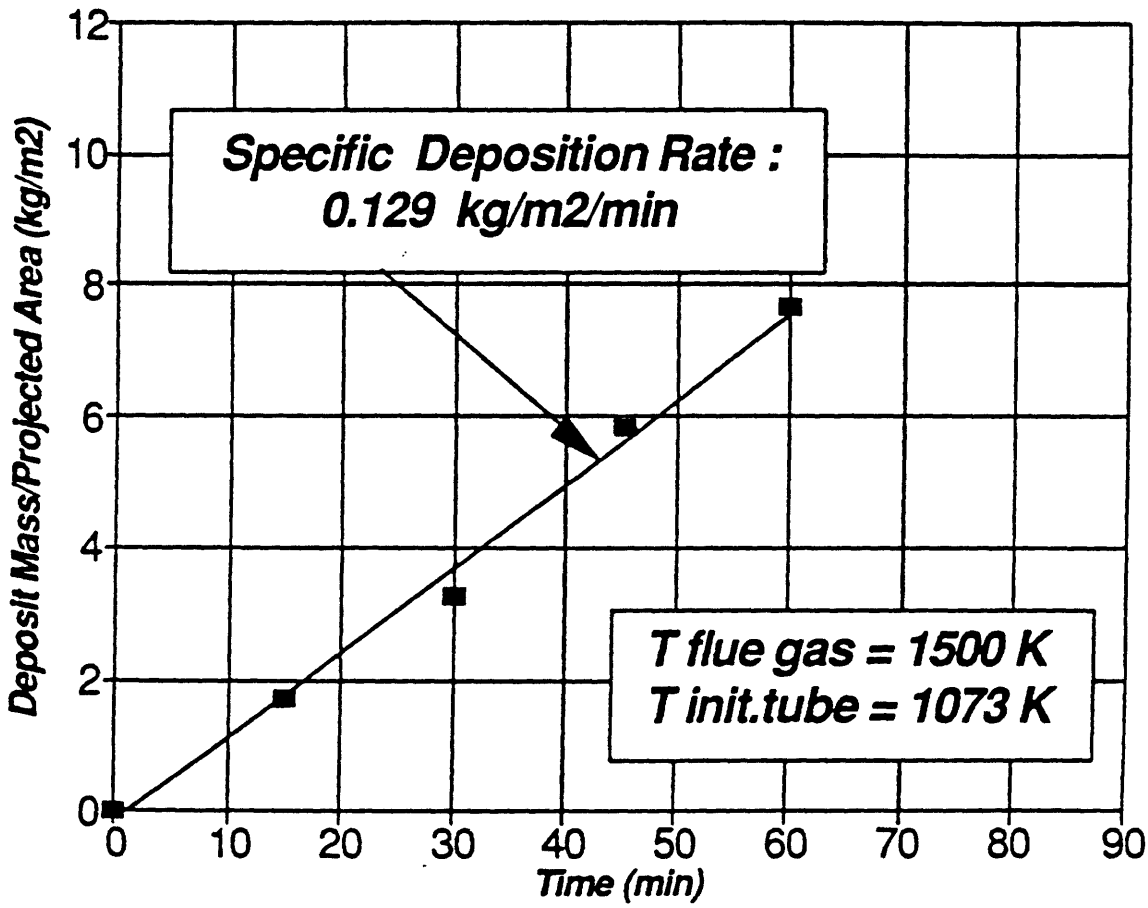

Figure 81. **Deposit Build-Up**
Island Creek Coal

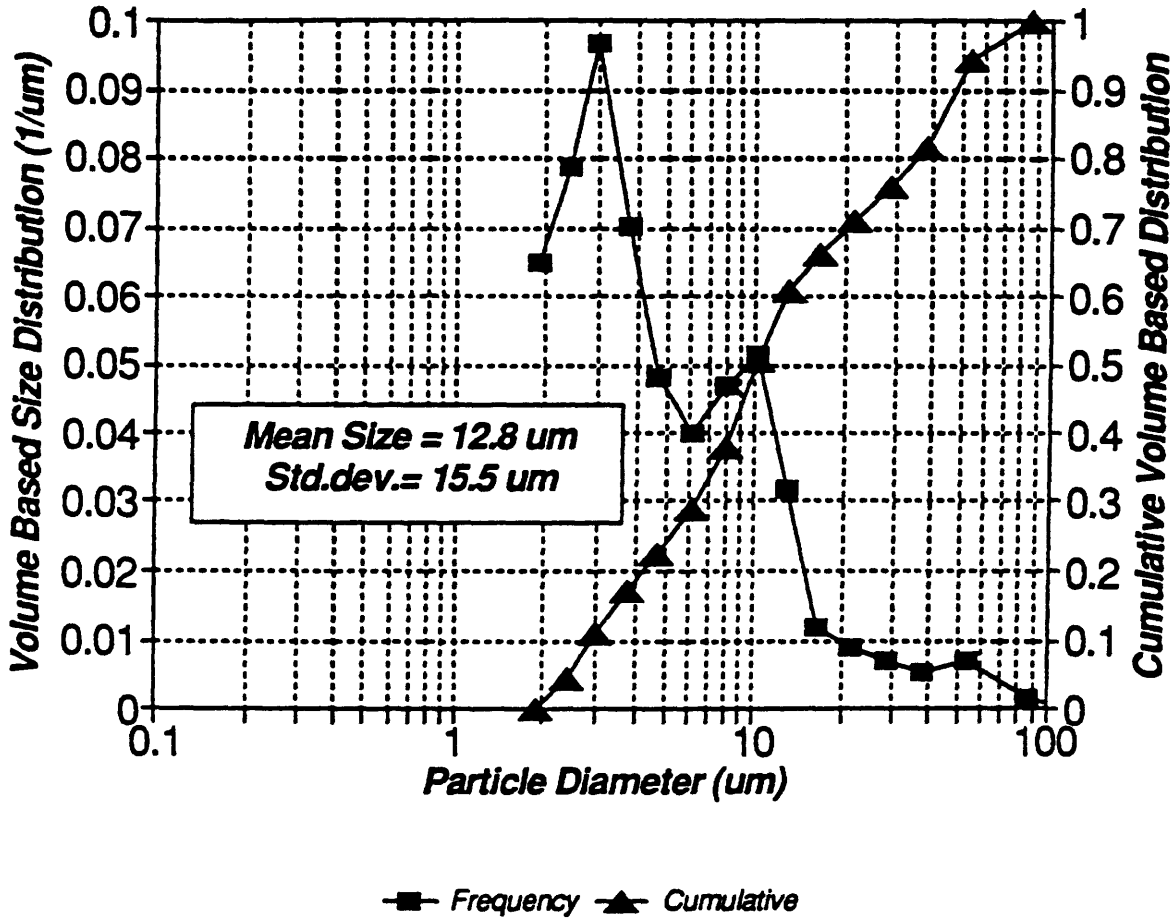

Figure 82. **Size Distribution of Fly Ash**
Island Creek Coal

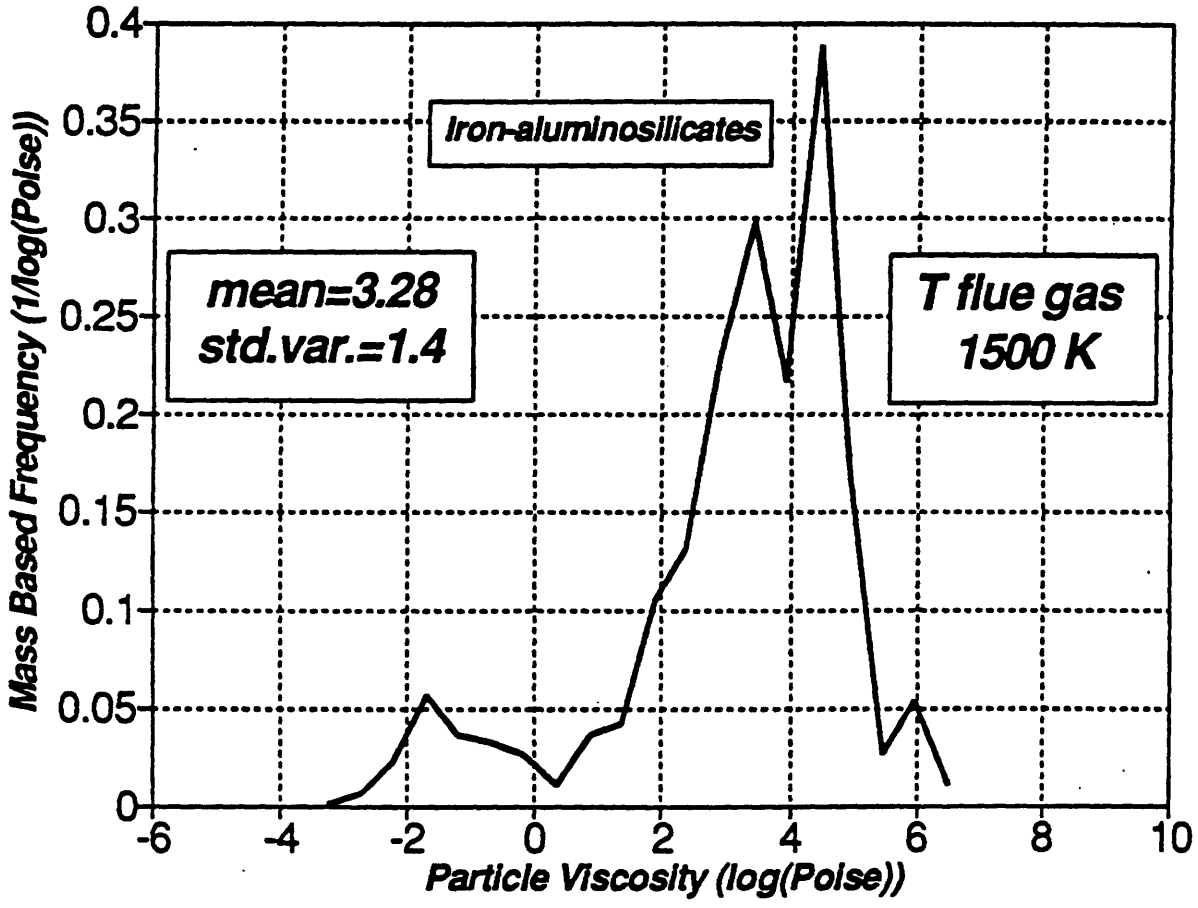

Figure 83. **Viscosity Distribution of Fly Ash** Island Creek Coal

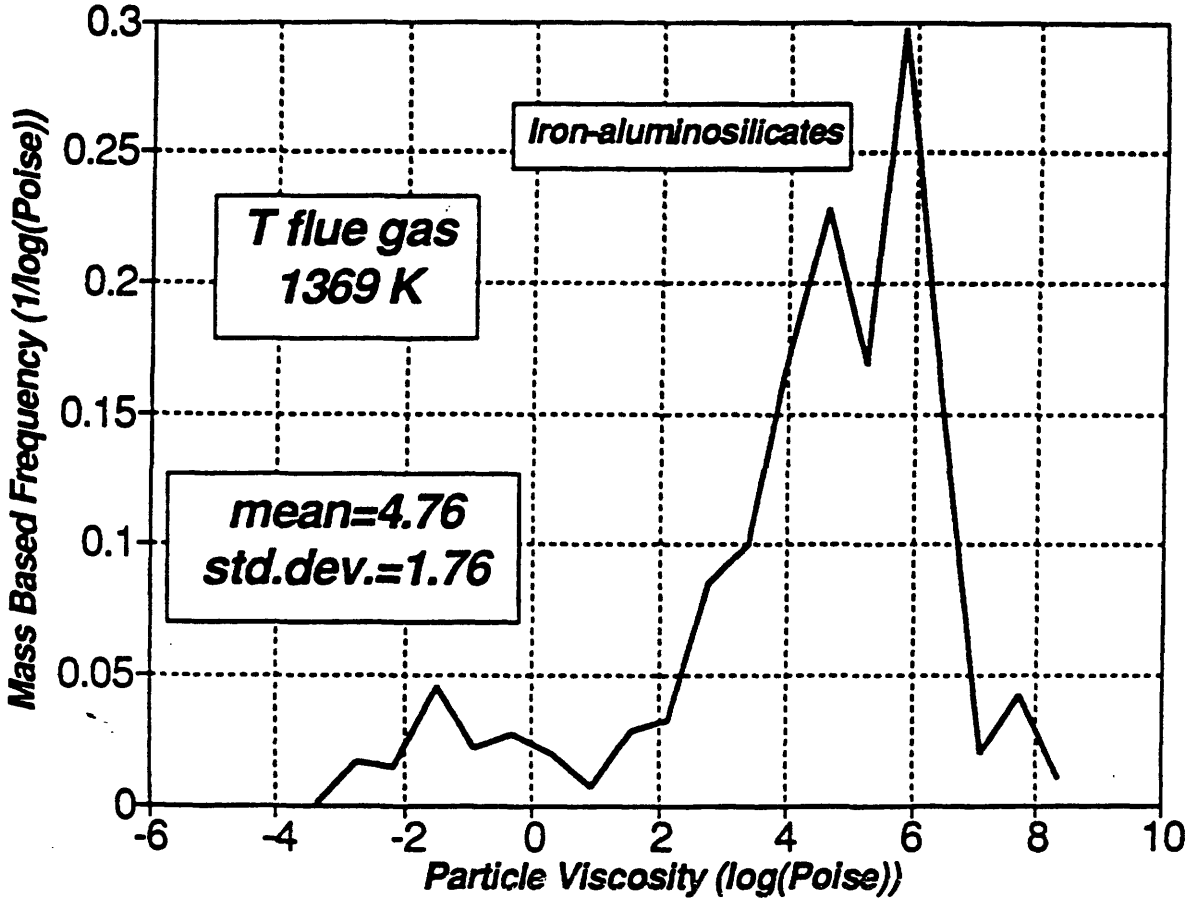

Figure 84. **Viscosity Distribution of Fly Ash** Island Creek Coal

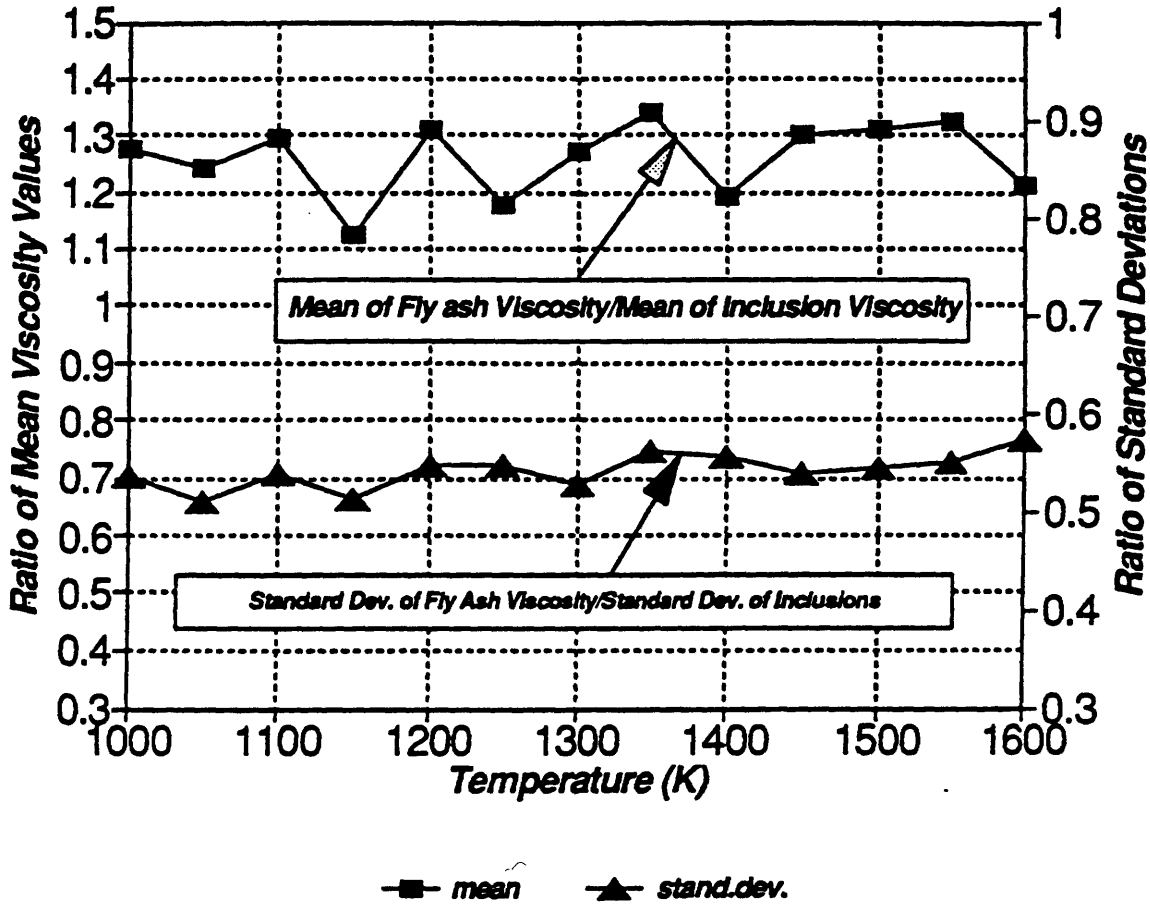

Figure 85. **Statistical Parameters of Viscosity**
Island Creek Coal

Table 24.
Comparison of Chemical Composition of the Island Creek Coal Ash and Fly Ash Determined by ASTM and CCSEM Methods, Respectively

	ASTM	CCSEM
Oxide Formula	Ash	Fly ash
Na_2O	0.9	0.42
MgO	0.7	0.37
Al_2O_3	19.3	21.1
SiO_2	44.8	48.0
P_2O_5	0.2	0.44
SO_3	0.0	0.0
Cl	0.0	0.2
K_2O	2.3	3.2
CaO	4.7	5.0
TiO_2	1.1	0.45
FeO	23.3	20.2
Cr_2O_3	n.d.	0.6
BaO	0.2	0.1

of the temperature. The mean viscosity increased by 20-30%, whereas the standard deviation is decreased by 45%.

The calculated sticking efficiencies of the included mineral matter and fly ash are plotted in Figure 86. The critical viscosity value was chosen to be 10^6 poise.

4.6 Summary of the Experimental Results

The characteristics of the five experimental coals can be seen in Table 25. The Wyoming lignite had the highest moisture and volatile content; however, its sulfur content was the lowest. The Blend coal consisted of 30% Oklahoma bituminous coal and of 70% Wyoming lignite. The objective of blending of these two coals was to increase the calorific value of the lignite and to lower the sulfur content of the Oklahoma coal. Thus the Blend coal became a coal of lower ratio of sulfur content per heating value. One of the objectives of this study was to determine the effect of blending on the relative fouling tendency of the coal.

The temperature at which the lignite ash began its deformation was 1426 K, and with a temperature increase of 28 K the ash became completely fluid. The blend coal ash had the same initial deformation temperature, although after a temperature increase of 17 K it became fluid.

Although both the Jader and the Island Creek coals had high iron contents (20% and 23%, respectively), their initial deformation temperatures were higher (1632 K and 1541 K respectively) than that of either the Wyoming or the Blend coal. These two coals, however, had wider temperature ranges, 107 K and 44 K, respectively, within which their deformation occurred.

The Mapco was also bituminous coal with 58% fixed carbon and 33% volatile, however its sulfur content (0.8%) was lower than that of either the Jader (2.9%) or the Island Creek coal (2.7%). The temperature range for reaching complete deformation from its initial deformation state was wide, 108 K.

A viscosity value calculated at 1500 K by using the mean ash chemical composition was assigned for each coal. These values (Table 25) showed similar trends of deformation behavior for the ashes to what had been predicted by the deformation temperatures. The deformation temperatures or the calculated viscosities supplied valuable *qualitative* information on coal fouling tendencies, but they were insufficient for *quantitative* description of the fly ash deposition rates, especially for low temperature ranges.

Combustion experiments were carried out at the MIT-CRF to determine fly ash deposition rates as a function of flue gas temperature. A summary of the measured parameters can be seen in Table 26. The coal feed rates were set to obtain approximately 1 MW thermal input for each coal. Coal size distributions were determined by laser diffraction method. The results showed that the blending of the Wyoming lignite and the Oklahoma coal resulted in a coarser coal size distribution. Both the mean value and the standard deviation increased by 20%

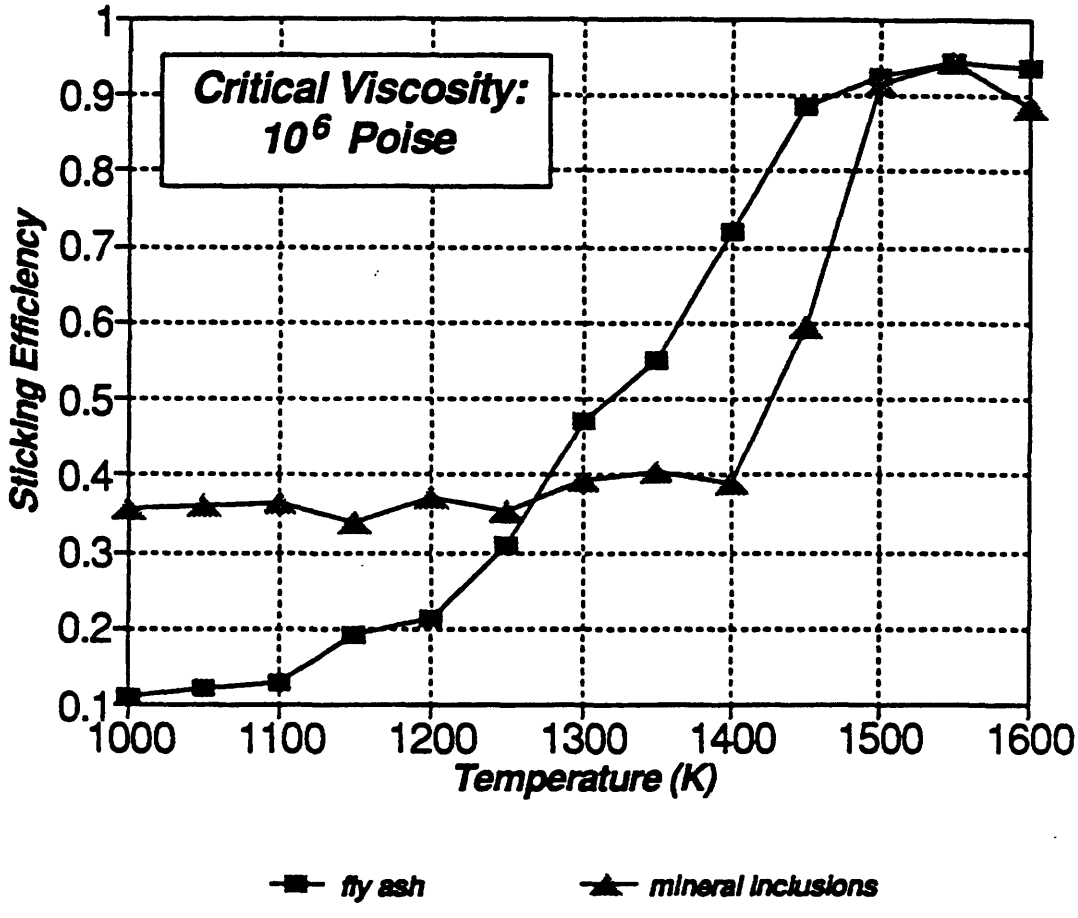

Figure 86. **Sticking Efficiency**
Island Creek Coal

Table 25.
Summary: Characteristics of Coals Burned in CRF

Quantity	Mapco Coal	Island Creek Coal	Blend Coal	Wyoming Lignite	Jader Coal
Moisture wt%	2.1/1.1*	11.9/3.17*	23.4/7.06*	13.4/7.2*	1.4/1.4*
Volatile Matter wt.%	33.4	35.2	36.1	43.8	32.6
Fixed Carbon wt.%	57.7	46.7	34.6	35.9	52.5
Ash wt.%	6.8	6.2	5.9	6.9	8.3
Heating Value Btu/lb	13422	11794	9323	10225	13335
Total Sulfur wt.%	0.8	2.7	0.5	0.15	2.86
IDT K^+	1616	1541	1427	1426	1632
ST K^+	1670	1598	1433	1439	1646
HT K^+	1689	1629	1439	1444	1656
FT K^+	1724	1648	1444	1454	1676
Ash SiO_2 wt.%	49.7	44.76	38.89	39.1	51.7
Ash Al_2O_3 wt.%	30.1	19.30	19.15	19.5	20.3
Ash Fe_2O_3 wt.%	8.8	23.33	7.97	6.9	20.7
Ash CaO wt.%	4.4	4.67	26.76	24.1	1.9
Other Flux Comp. wt.%	7.10	5.51	7.97	9.80	5.22
Viscosity $\log_{10}$ Poise, 1500K	3.76	2.87	1.74	1.88	3.42

* As received at MIT ; + oxidative atmosphere

Table 26.
Coal Characteristics

Quantity	Mapco Coal		Island Creek Coal		Blend Coal		Wyoming Lignite		Jader Coal	
Thermal Input (MW)	0.98		0.98		0.99		0.93		0.98	
Coal Mass Flow (Kg/h)	114		113		131		141		114	
Mean Coal Size (μm)	36.6		60.3		45.6		37.7		36.6	
Std. Dev. (μm)	51.9		127.8		85.8		51.8		51.9	
Mean Inclusion size(μm)	4.2		3.86		4.4		4.4		5.3/53.9*	
Std.Dev. of Inc.Size(μm)	3.4		2.8		3.7		3.7		4.7/42.1*	
Peak Flame Temp (K)	1781		1750		1675		1673		1750	
Loc. of Peak Temp (m)	1.4		2.2		2.2		2.2		1.4	
O_2 in Flue Gas v%	2.6		2.5		2.8		3.0		2.7	
NO_x in Flue Gas ppm	300		300		240		140		370	
C in Fly Ash wt %	1.49		0.95		0.42		2.0		0.85	
Mean Fly Ash Size (μm)	10.1		12.8		16.1		12.6		15.4	
Std. Dev. (μm)	6.0		15.5		14.1		7.0		15.1	
Fly Ash Mass Flux Kg/m^2/min	0.658		0.662		0.779		0.872		0.849	
Temperature (K)	1423	1563	1369	1500	1458	1573	1339	1509	1450	1508
Velocity (m/sec)	9.6	10.6	9.4	10.5	9.8	11.7	7.5	8.4	10.2	11.8
$^+\Delta R_d/\Delta T*10^4$	5.04		9.0		9.56		3.06		25.8	
Dep. Rate Kg/m^2/min	0.0069	0.083	0.011	0.129	0.042	0.152	0.048	0.10	0.029	0.179

* extraneous mineral matter ; + derivative of deposition rate by temperature (kg/m^2/min/K)

and 40%, respectively. No significant change was observed for their inclusion size distributions. The Island Creek coal had the coarsest size distribution among the bituminous coals with a mean size of 60.3 μm and a standard deviation of 128 μm. The Mapco and Jader coals had very similar size distributions.

The combustion behavior of the Wyoming lignite and the Blend coal was also similar; in both cases, the maximum flame temperature was the same, although there was a sharp increase of the flue gas temperature close to the burner for the Blend coal, possibly indicating earlier ignition and burnout of the Oklahoma coal. The locations for the peak flame temperatures were the same (2.2 m from the burner nozzle) in both cases. The carbon content of the fly ash decreased as a result of better carbon burnout for the Blend coal case.

The locations of maximum flame temperatures for the bituminous coals were found closer to the burner nozzle (1.5 m) than that for the lignite. The highest flame temperature was observed for the Mapco coal (1781 K). At the exit of the combustion tunnel, the oxygen and NO_x concentrations were also measured. The least NO_x concentration was observed with the lignite (140 ppm), and the highest was measured with the Jader coal (370 ppm). As a consequence of higher N content in the Oklahoma coal, the NO_x concentration was higher for the Blend coal than for the Wyoming lignite.

The size distribution of the Blend fly ash became coarser as a result of coarser coal size distribution. This effect increased the impaction efficiency for the Blend fly ash, which diminished the advantage of lower fly ash mass flux due to the higher calorific value of the Blend coal. The deposit mass per unit tube surface area is plotted for the lignite and Blend coal in Figures 87 and 88, respectively. In both cases, the deposit mass per unit tube surface increased linearly as a function of time. The effect of flue gas temperature on the deposit mass is also shown -- the higher the flue gas temperature, the higher the rate of deposit accumulation on the target tube. The effect of temperature on the deposition rate was larger for the Blend coal. It could be evaluated by the temperature derivative of the deposition rate, which was found 3 times higher for the Blend coal than for the Wyoming lignite. The sensitivity of the deposition rate to flue gas temperature can be explained by using the derivative function of the sticking efficiency vs. temperature. These functions are shown in Figure 89 for the lignite and for the Blend coal. The function of sticking efficiency vs. temperature determines the mass ratio of sticky fly ash particles at a given temperature. It can be seen that the Blend fly ash has a narrower sticking efficiency distribution in comparison with that of the lignite fly ash, indicating higher deposition sensitivity to the temperature within the temperature range of 1300-1500 K.

The size distribution of the Jader fly ash was found to be the coarsest with a mean value of 15.4 μm and standard deviation of 15.1 μm. Also, the Jader coal had the coarsest inclusion size distribution. It was the only coal among the five for which extraneous mineral content was not negligible. The size distribution of the extraneous mineral matter had a mean value of 10 times higher than that of the inclusion minerals, and also the standard deviation was higher by about 9 times. The Island Creek coal fly ash also had a coarse size distribution; however, in this case it was the consequence of the coarse size distribution of the coal, which resulted in a

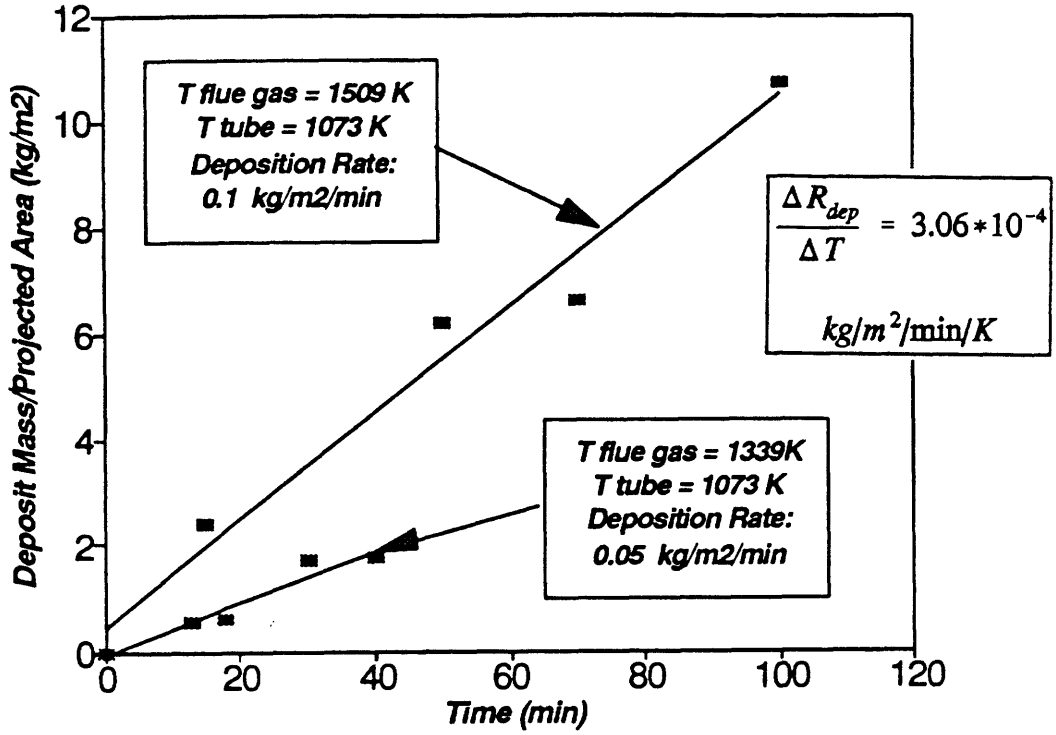

Figure 87. **Deposit Build-Up**
Wyoming Lignite

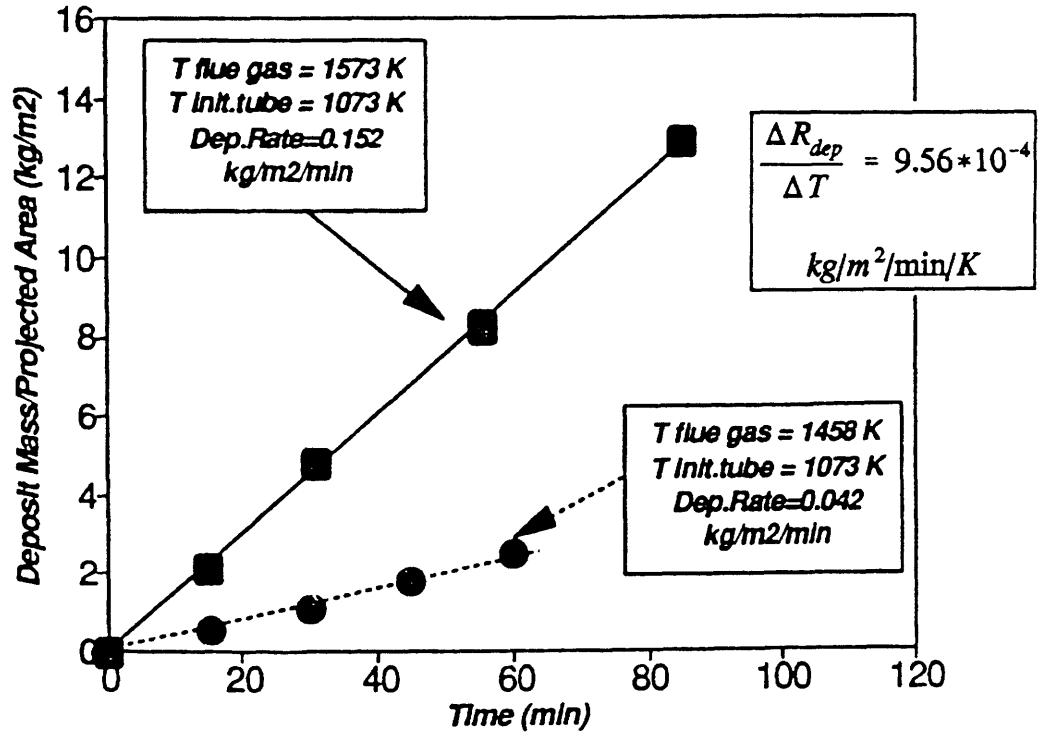

Figure 88. **Deposit Build-up**
Blend Coal

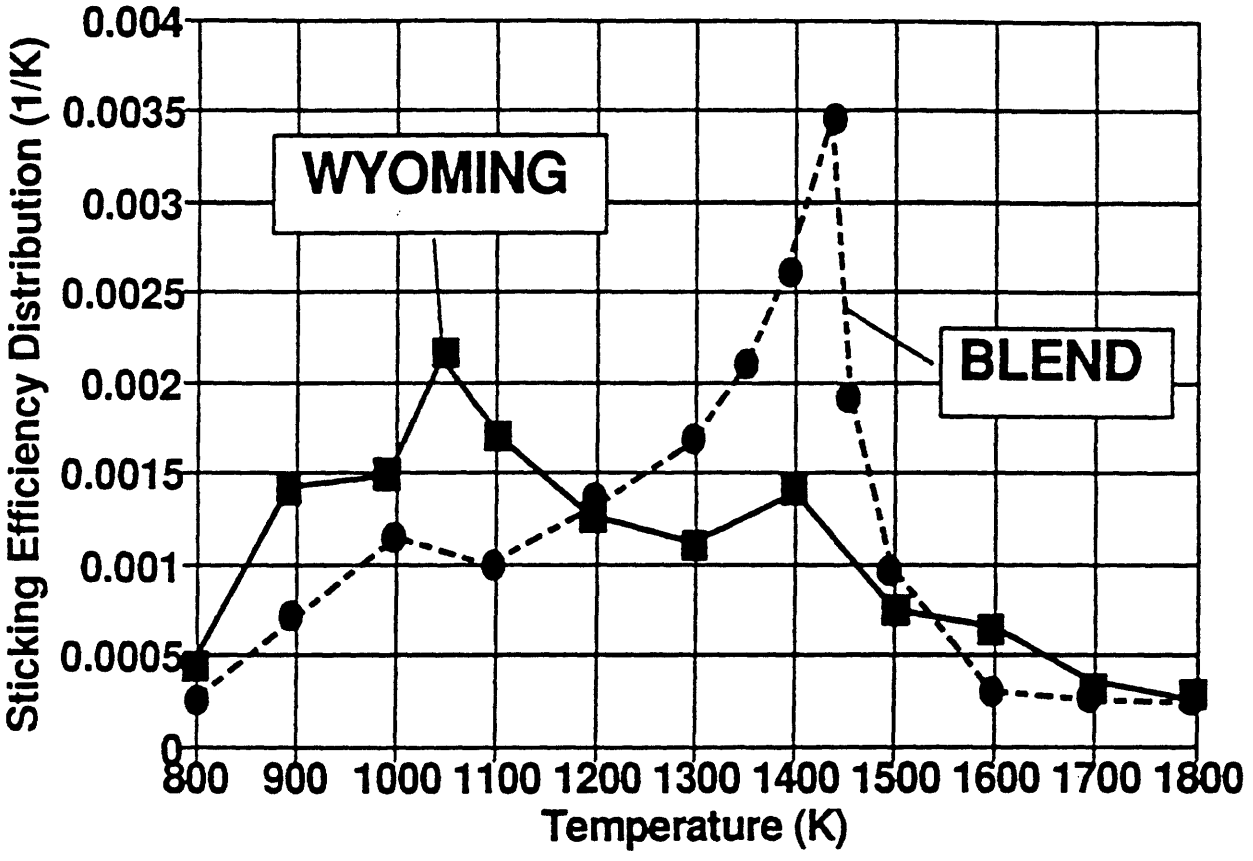

Figure 89. **Sticking Efficiency Distribution**
Wyoming Lignite and Blend Coal

higher rate of inclusion coalescence during combustion. The impaction efficiencies for these two coals were the highest. The increase of deposit mass as a function time was linear for all the bituminous coals. The results for the Mapco, Jader and Island Creek coal are shown in Figures 90 - 92. In each case, higher flue gas temperature resulted in higher deposition rate. Very high sensitivity was recorded for the Jader coal, which may be partially due to the change of stickiness of the fly ash deposit surface formed by the extraneous mineral matter.

It can be of interest to note that no correlation was found between the actual deposition rates and the ASTM predictions, e.g., no different deposition behavior was predicted by the ASTM method for the lignite and the Blend; however, major differences were detected by the experiments between these two coals.

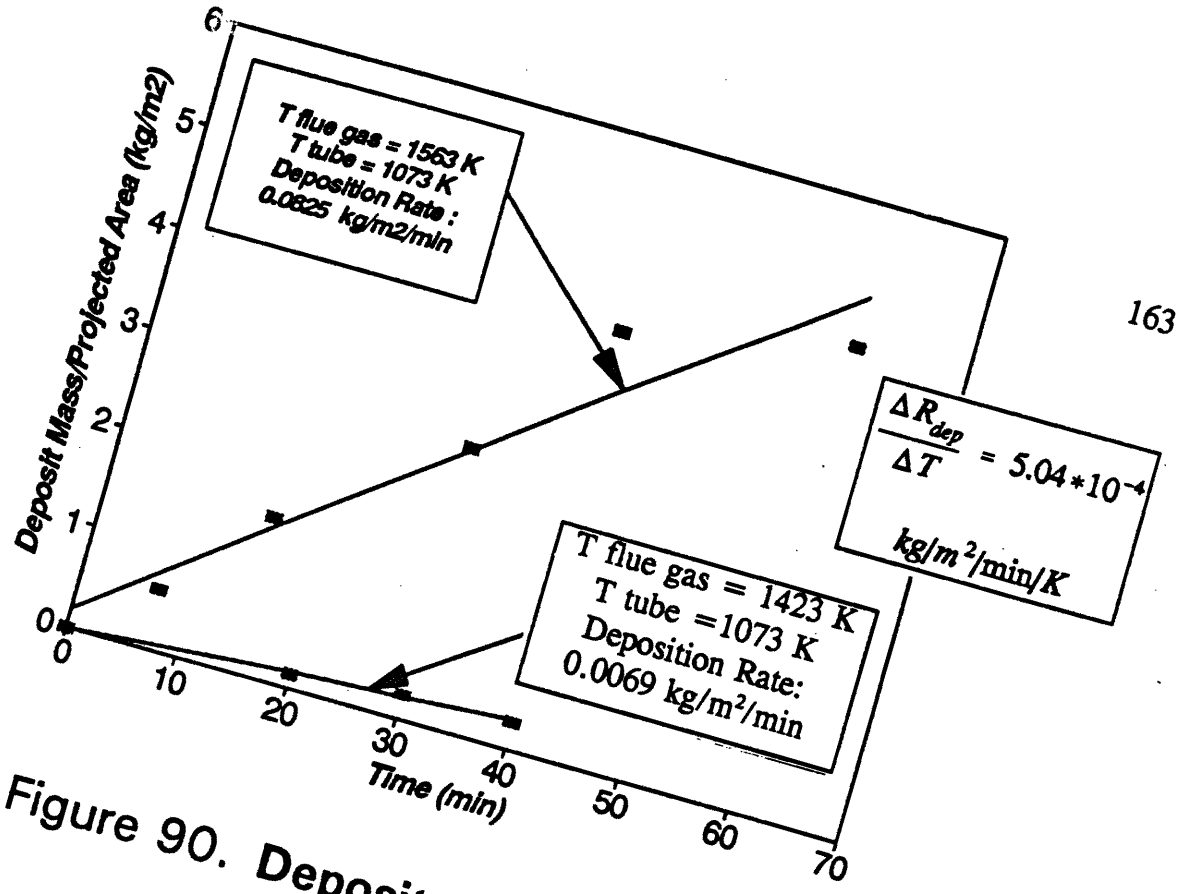

Figure 90. **Deposit Build-Up**
Mapco Bituminous Coal

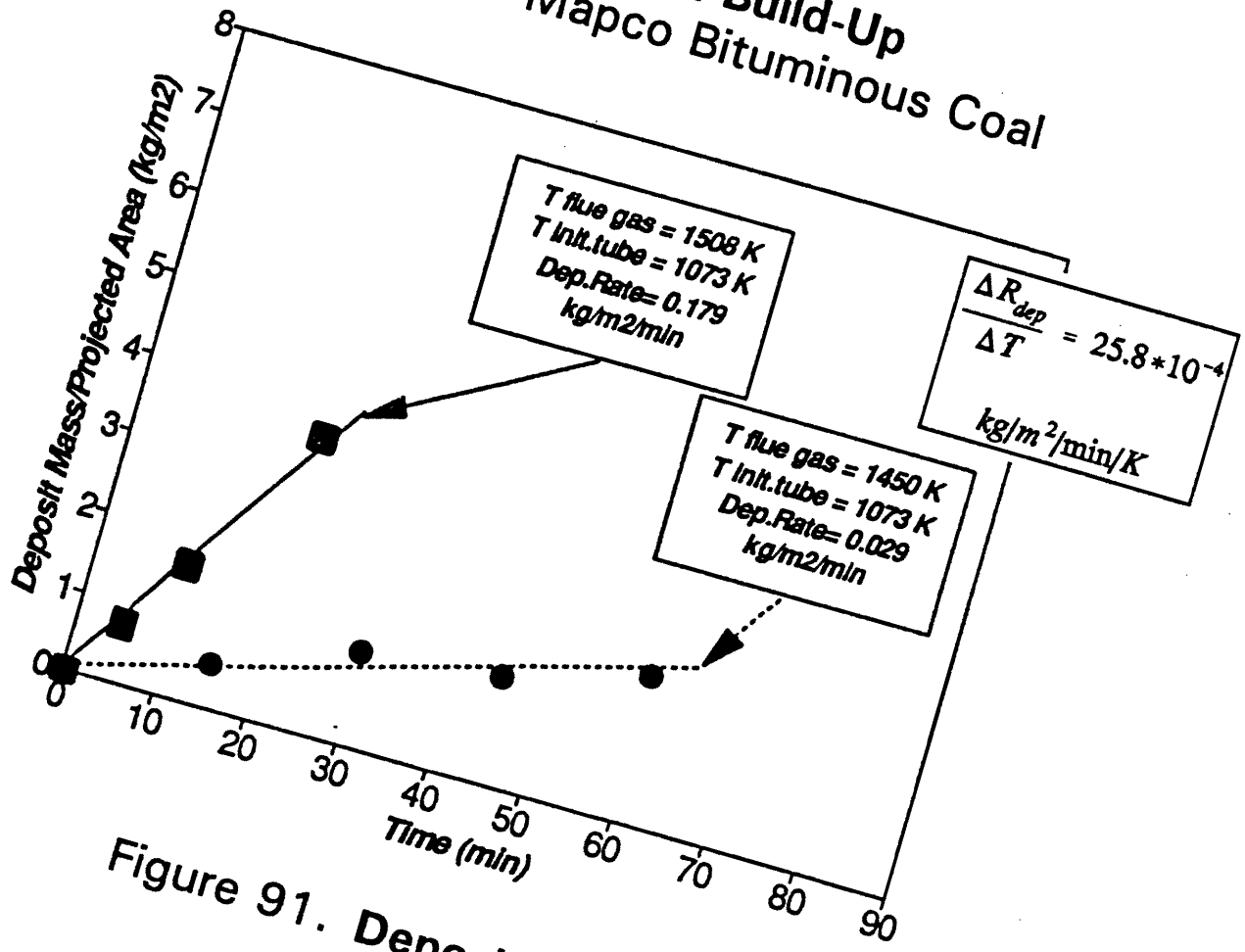

Figure 91. **Deposit Build-Up**
Jader Coal

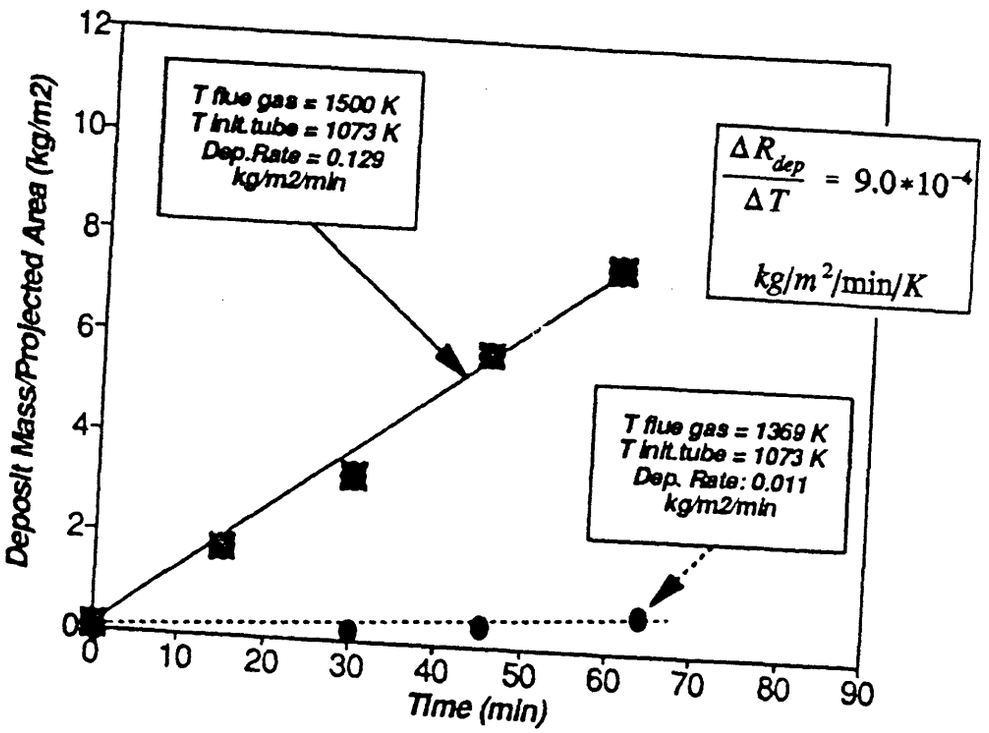

Figure 92. **Deposit Build-Up**
Island Creek Coal

SECTION 5

COMPARISON OF THE CFT MODEL PREDICTIONS WITH EXPERIMENTAL RESULTS

The input data of model calculations are listed in Table 27. A series of model sensitivity analyses indicated that there are three input parameters which had the strongest impact on the CFT predictions. These are

- particle size of coal,
- the transition ratio of the coal particle radius, and
- critical viscosity.

The coal particle size distribution can be determined to high degree of accuracy by various methods (e.g., by laser diffraction method), but no direct method is known to determine the transition radius and the critical viscosity. However, the comparison of mineral matter and fly ash size distributions can provide us with an indirect method for predicting the transition radius. Also, the fly ash deposition rate as a function of temperature can supply information to approximate the critical viscosity. The best fit between predicted and experimentally determined distribution functions, such as fly ash size and SiO_2 content distributions, were obtained by setting the transition radius ratio between 0.26 and 0.27 and the critical viscosity value between $10^{5.1}$ and $10^{5.2}$ poise, respectively. Erosion plays an important role in the deposit formation when the fly ash sticking efficiency is low. In all cases studied in this report, the fly ash sticking efficiencies were high. Thus, the effect of erosion on the deposit build-up was negligible. Consequently, the model calculations were made by setting the value of the erosion factor (k) to zero. Results of calculations and experimental data for the distribution functions of fly ash size and SiO_2 content and fly ash deposition rates as a function of time are shown in Figures 93 - 107.

The predictions for the Wyoming lignite fly ash size distribution show excellent agreement with the measured data (Figure 93). The Wyoming lignite contains ion-exchangeable mineral matter. The inclusions within a coal particle receive a fraction of the ion-exchangeable mineral matter during the coal particle burning, increasing their sizes and changing their chemical composition. Further, random coalescence occurs between inclusion particles which contributes to additional changes in size and chemical composition. The increase of mineral size is a good indicator of coalescence. In Figure 94, the distribution of SiO_2 content in fly ash particles is plotted. The agreement between the predicted and measured distribution functions is good. In Figure 95, the deposition rate, the total and impacted mass rate of fly ash are shown. The results indicate a fly ash impaction efficiency of between 12.3% and 13.0%. It is also shown that the impacted mass rate does not vary significantly with the flue gas temperature, which is a consequence of the constant Reynolds and Stokes numbers. However, the effect of flue gas temperature for the sticking efficiency is considerable. The sticking fraction of fly ash is doubled by increasing the flue gas temperature from 1339 K to 1509 K.

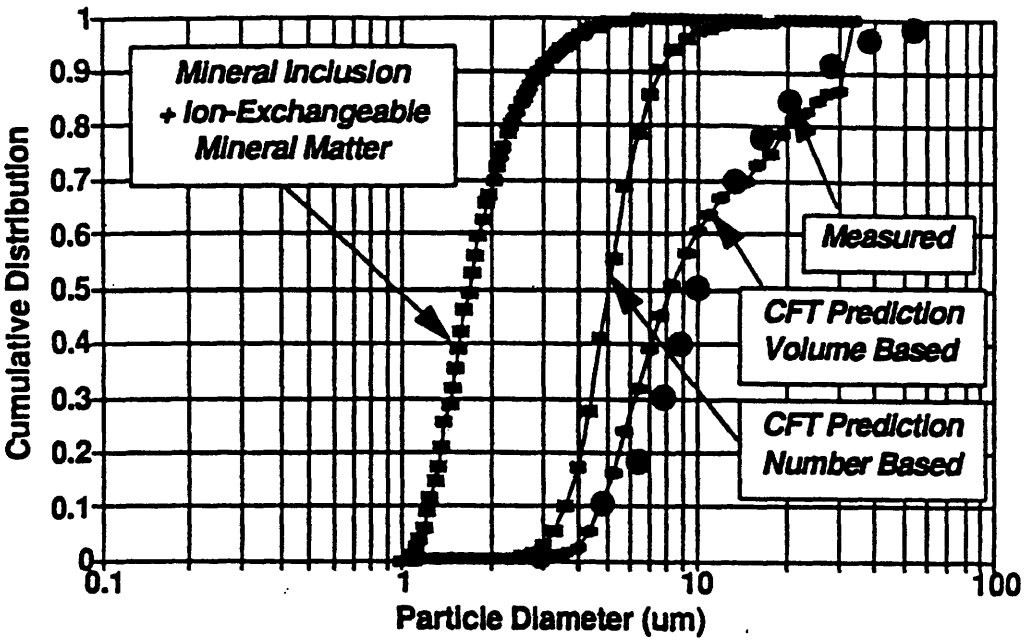

Figure 93. **Fly Ash Size Distribution Predictions and Correlation with Measurements:** Wyoming Lignite

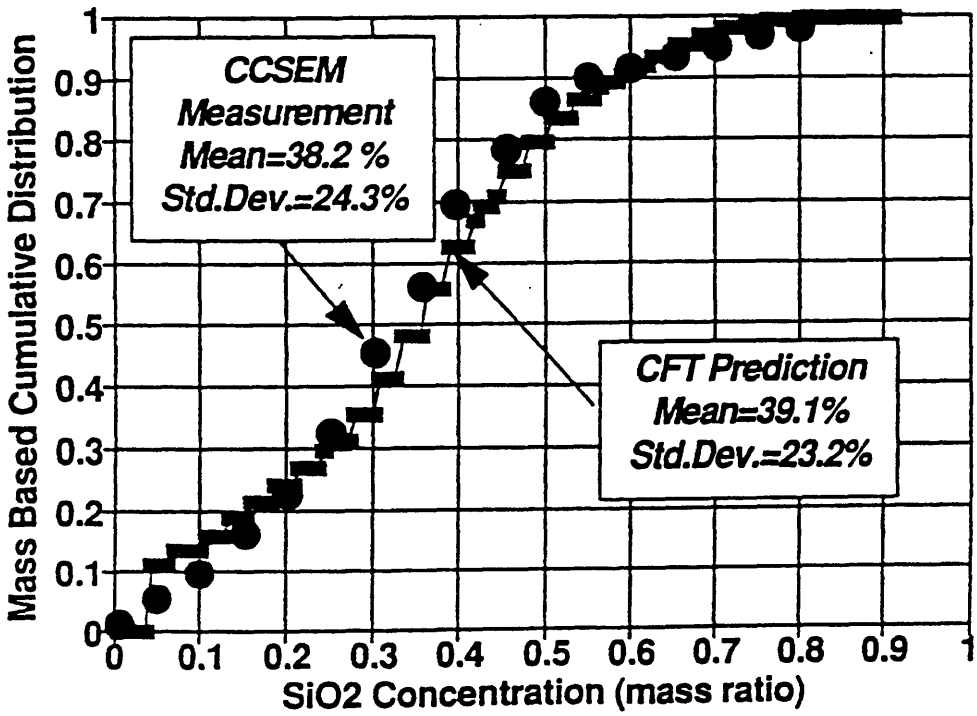

Figure 94. **SiO_2 Content Distribution Prediction *vs.* Experiment:** Wyoming Lignite

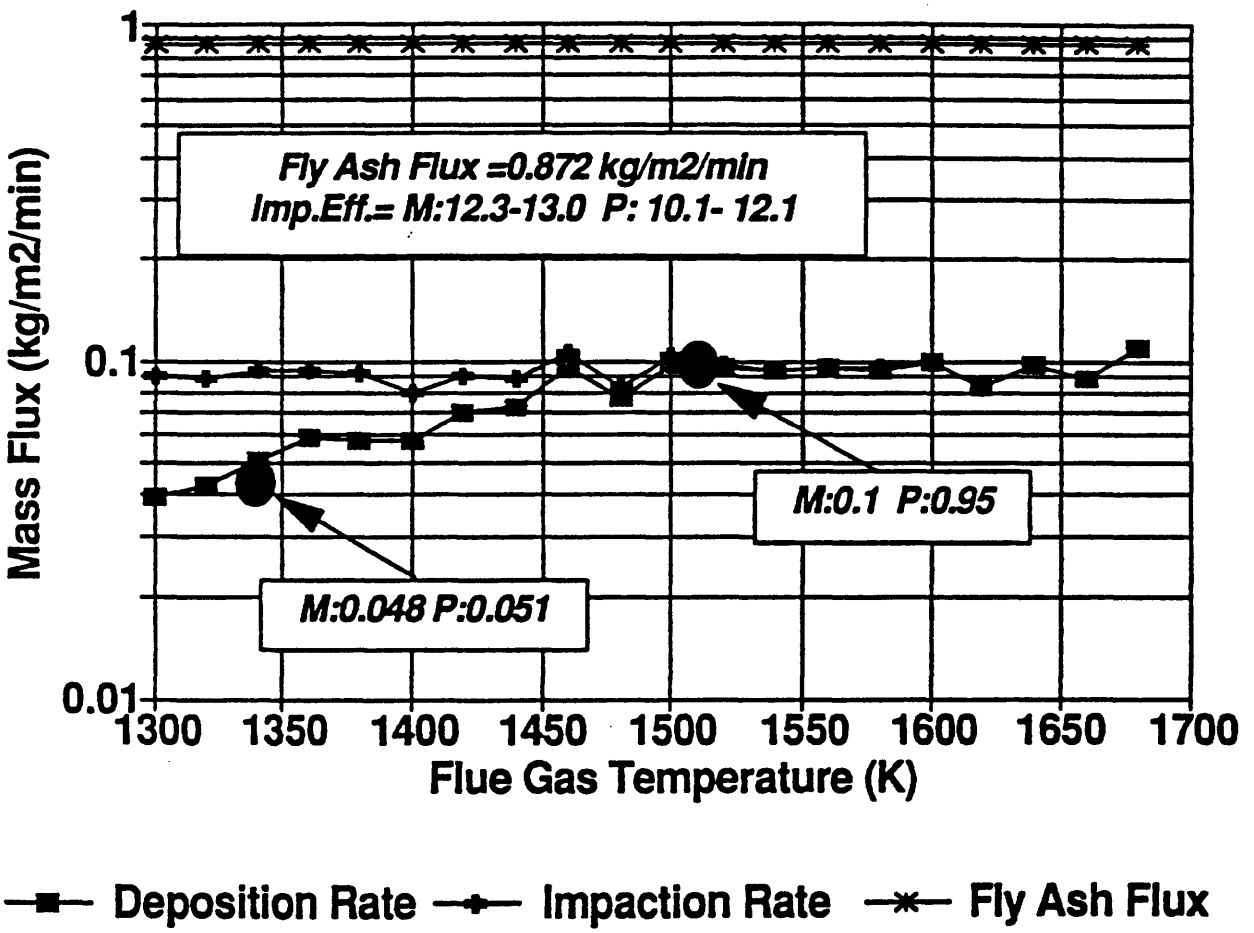

Figure 95. **Fly Ash Behavior Predictions *vs.* Experiments:** Wyoming Lignite

M : measured P:predicted

Table 27.
CFT Model Predictions for CRF Coals

Coals		Key Input Parameters				CFT Model Predictions											
						Size Distribution				SiO_2 Content				η_{imp}		Deposition Rates	
						Mean		Std.d.		Mean		Std.d.					
		N_{coal}	P_{ratio}	δ	η_{crit}	M	P	M	P	M	P	M	P	M	P	M	P
Wyom.	L	3	50	0.26	5.1	12.6	11.6	7.0	6.5	38.1	39.1	24.3	23.1	12.3	10.1	0.048	0.051
	H													13.0	12.1	0.102	0.095
Blend	L	3	60	0.24	5.2	16.1	15.2	14.1	13.2	44.0	43.2	21.1	18.2	20.1	18.1	0.042	0.039
	H													21.2	20.0	0.152	0.149
Mapco	L	3	50	0.27	5.2	10.1	12.0	6.0	7.2	47.5	46.1	16.6	15.3	9.8	14.7	0.007	0.009
	H													10.4	15.2	0.083	0.05
Island Creek	L	4	50	0.28	5.3	12.8	11.3	15.5	12.2	48.0	47.3	17.2	16.5	24.1	20.1	0.011	0.031
	H													25.1	21.4	0.129	0.114
Jader	L	3	50	0.24	5.1	15.4	16.2	15.1	12.0	49.4	47.5	14.4	13.3	24.1	23.6	0.029	0.085
	H													25.2	24.1	0.179	0.156

N_{coal}: the number of coal size class,
P_{ratio}: the ratio of the standard deviation and mean value of the total number of inclusion particles,
δ: the ratio of the transition radius and the coal radius,
η_{crit}: the critical viscosity value in log(poise),

η_{imp}: the impaction efficiency,
Deposition Rates: the fly ash deposition rates, kg/m²/min,
M,P: abbreviations for "Measured" and "Predicted", respectively,
L,H: abbreviations for "Low Temperature" and "High Temperature".

Results for the Blend fly ash are shown in Figures 96 - 98. Also, good agreement was found between the CFT predictions and the measured data. Due to coarser size distribution of the Blend coal, its fly ash was also coarser in comparison with the Wyoming fly ash. As a consequence of this result, higher impaction efficiency was predicted and measured for the Blend fly ash (Figure 98). The SiO_2 distribution in the Blend fly ash had a smaller standard deviation than the Wyoming fly ash which, in turn, resulted in narrower viscosity distribution for the Blend fly ash as well. It follows, therefore, that the deposition rate of fly ash of blend coal was more sensitive to flue gas temperature in comparison with that of the Wyoming fly ash. This prediction was experimentally validated as shown in Figure 98.

The predictions for the Island Creek fly ash can be seen in Figures 9 - 101. The Island Creek coal had the coarsest size distribution among the examined coals with a mean size of 60.3 μm and a standard deviation of 127.8 μm. The mineral matter was present in this coal as inclusions with the finest size distribution. Consequently, a high degree of coalescence was expected during particle burning. It manifested in the highest increase of mean size and standard deviation (Figure 99). The small standard deviation of SiO_2 content distribution shown in Figure 100 was also a good indicator for the intensive inclusion coalescence. The CFT model followed the changes in the properties of mineral matter caused by the inclusion random coalescence. The used input conditions for the transformation radius and for the sticking efficiency can be seen in Table 27. The increase of deposition rate of fly ash due to temperature rise was also predicted by the CFT model as shown in Figure 101.

The Jader coal contained about 10 wt% extraneous mineral matter. The size distribution of the mineral inclusions was the coarsest of the coals examined, with a mean size of 5.3 μm and a standard deviation of 4.7 μm. However, the size distribution of the coal was fine. Therefore, a moderate rate of inclusion coalescence was predicted by the CFT code. The predicted size distribution of the fly ash is shown in Figure 102. The increase of mineral size can be seen, although the rate of size change is smaller than that shown in the previous case. There is a small difference between the predicted and the measured size distribution functions at the two ends of the size range, which is possible the result of uncertainty of size measurements for these size ranges. The distribution of SiO_2 content is shown in Figure 103. The fit between the CFT prediction and the measurements is acceptable. However, a sharp increase in the deposition rate of the fly ash particles was not totally predicted by the CFT code (Figure 104), which may be an indication of the possible chemical interaction between the fly ash particles produced by the extraneous mineral matter with those produced by the inclusion coalescence. This effect may alter the sticking fraction of the deposit surface.

The Mapco coal contained its mineral matter in the form of inclusions. Due to inclusion coalescence, the size distribution of the inclusions was changed. The mean size and standard deviation doubled during the coal particle burnout. The prediction of the CFT model can be seen in Figure 105. The distribution of the chemical concentration was also modified. The measured and predicted distribution functions of SiO_2 content are plotted in Figure 106. Due to random inclusion coalescence, the standard deviation of SiO_2 distribution was decreased, consequently the distribution of the particle viscosity also had a smaller standard deviation,

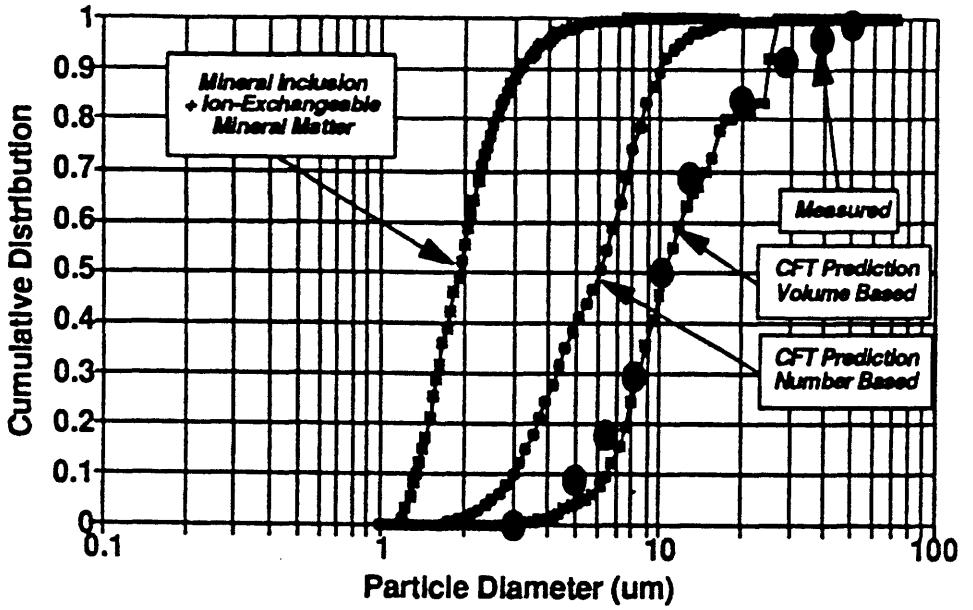

Figure 96. **Fly Ash Size Distribution Predictions and Correlation with Measurements:** Blend Coal

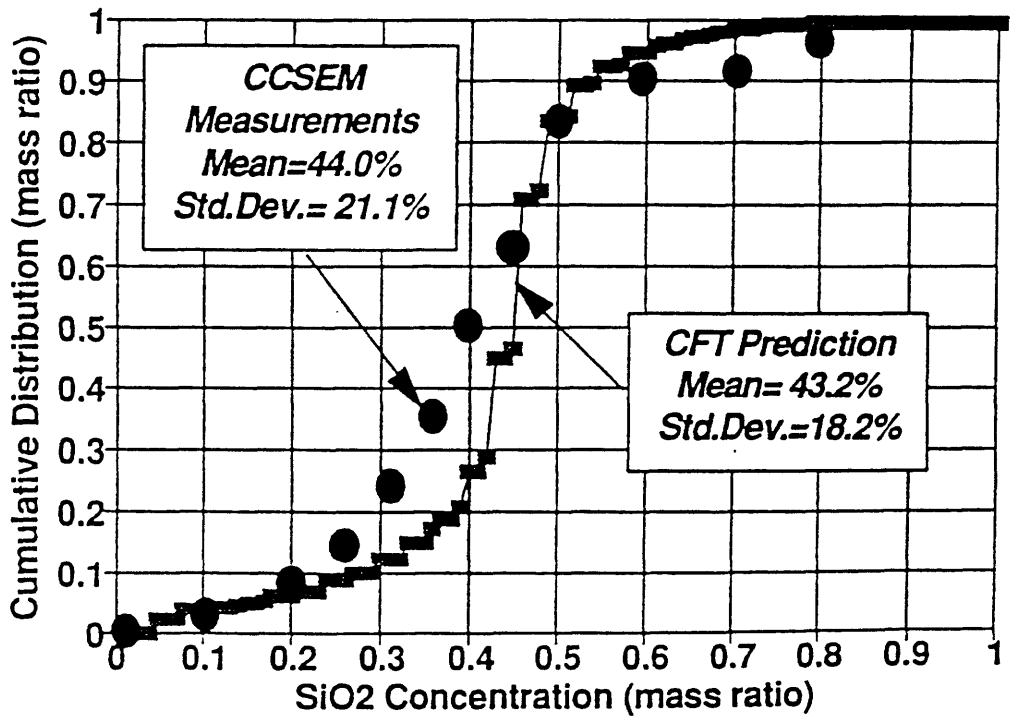

Figure 97. **SiO_2 Content Distribution Prediction *vs.* Experiment:** Blend Coal

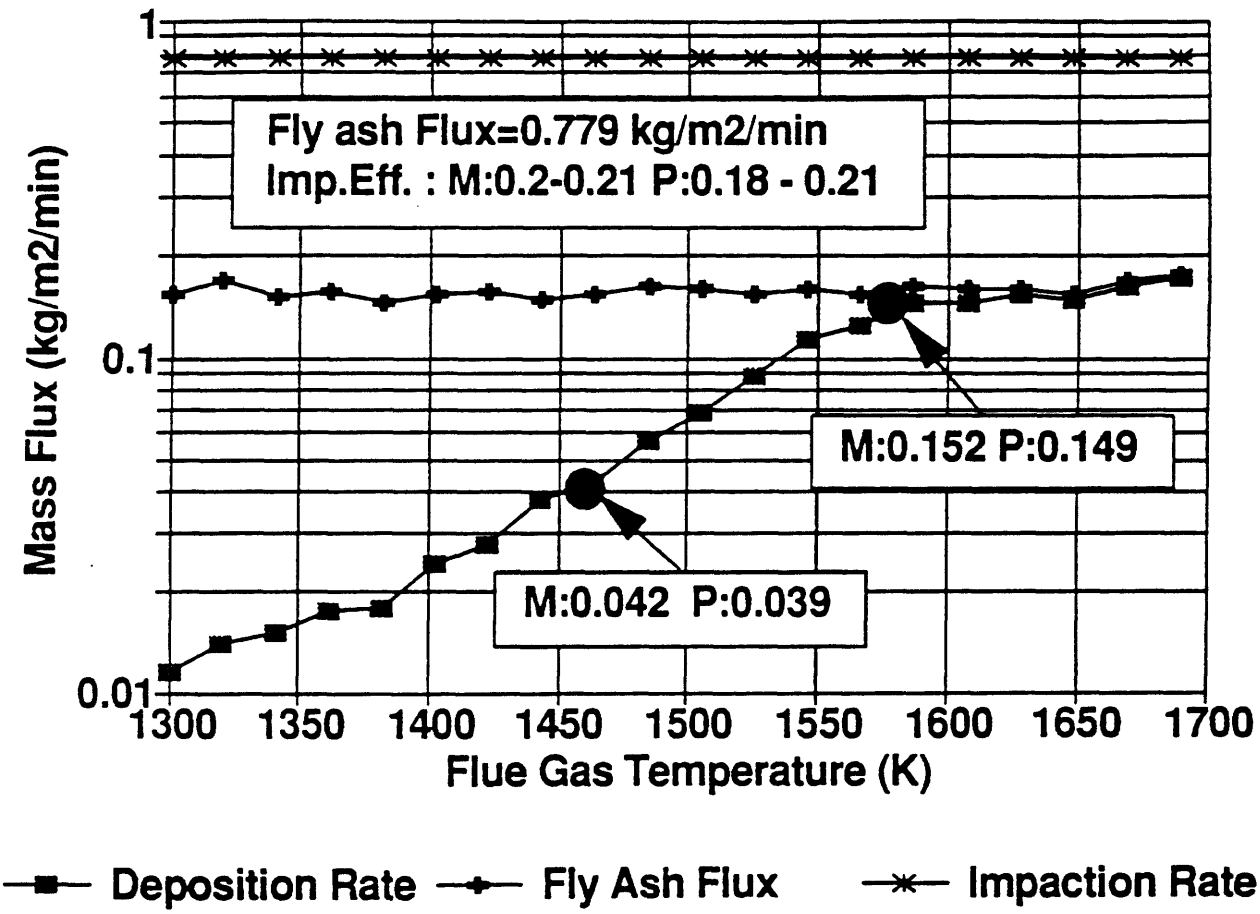

Figure 98. **Fly Ash Behavior Predictions *vs.* Experiments:** Blend Coal

M: measured P: predicted

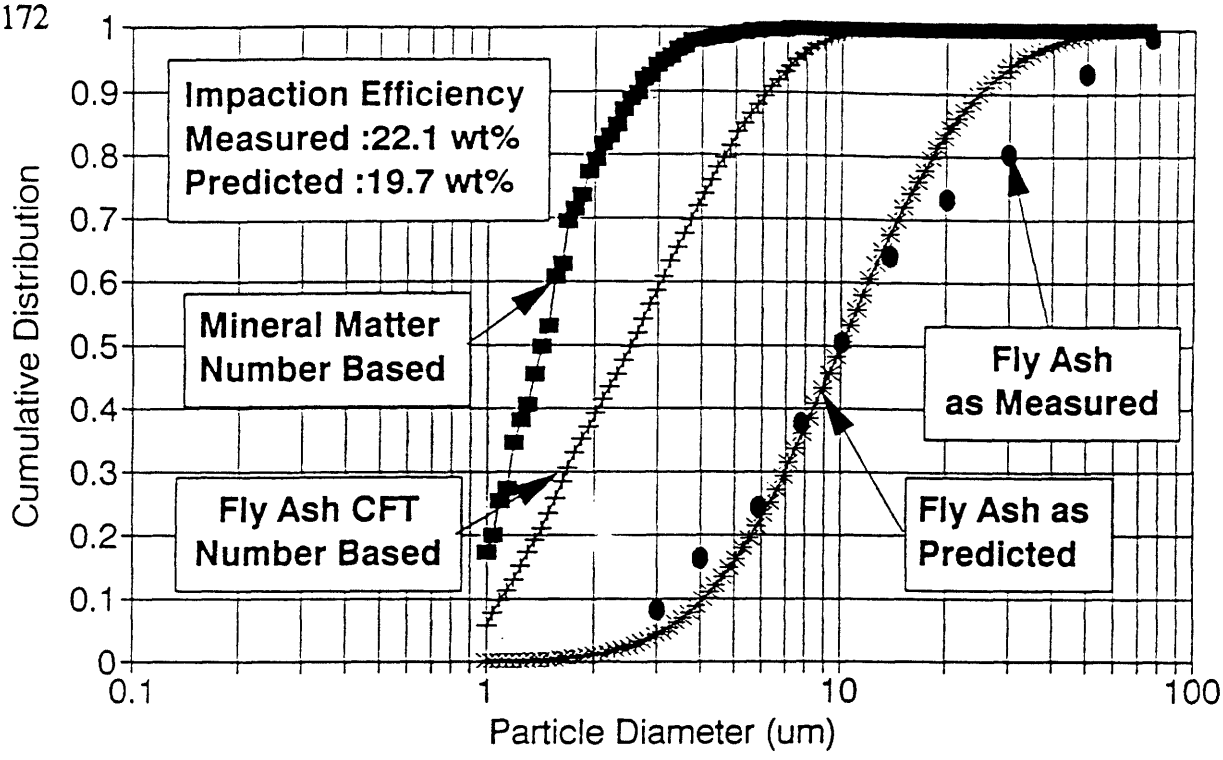

Figure 99. **Fly Ash Size Distribution Predictions and Correlation with Measurements:** Island Creek Coal

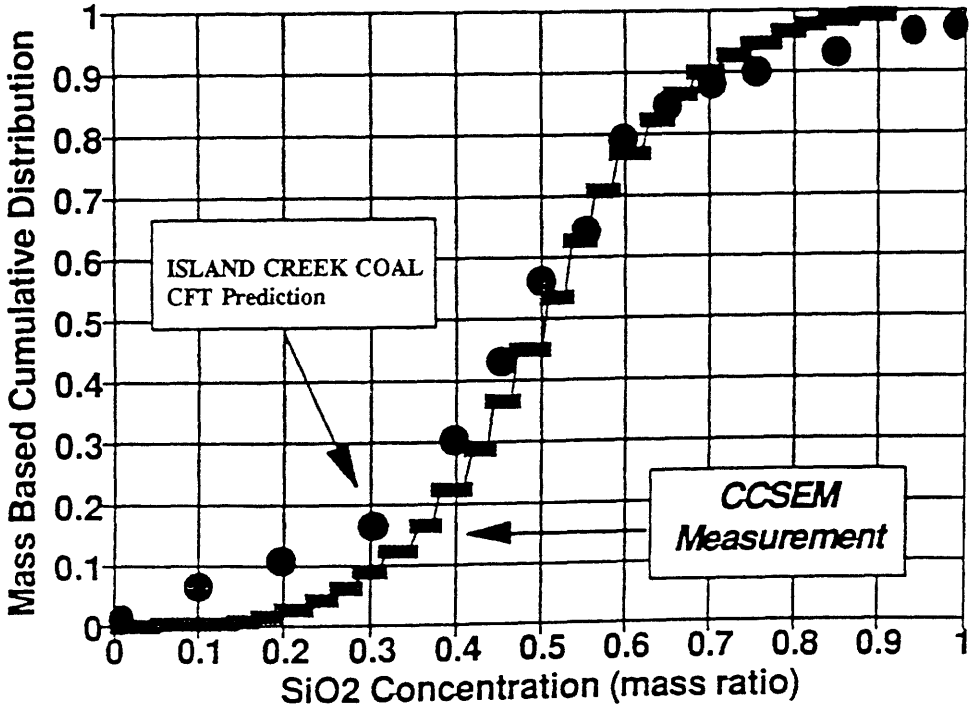

Figure 100. **SiO_2 Content Distribution Prediction *vs.* Experiment:** Island Creek Coal

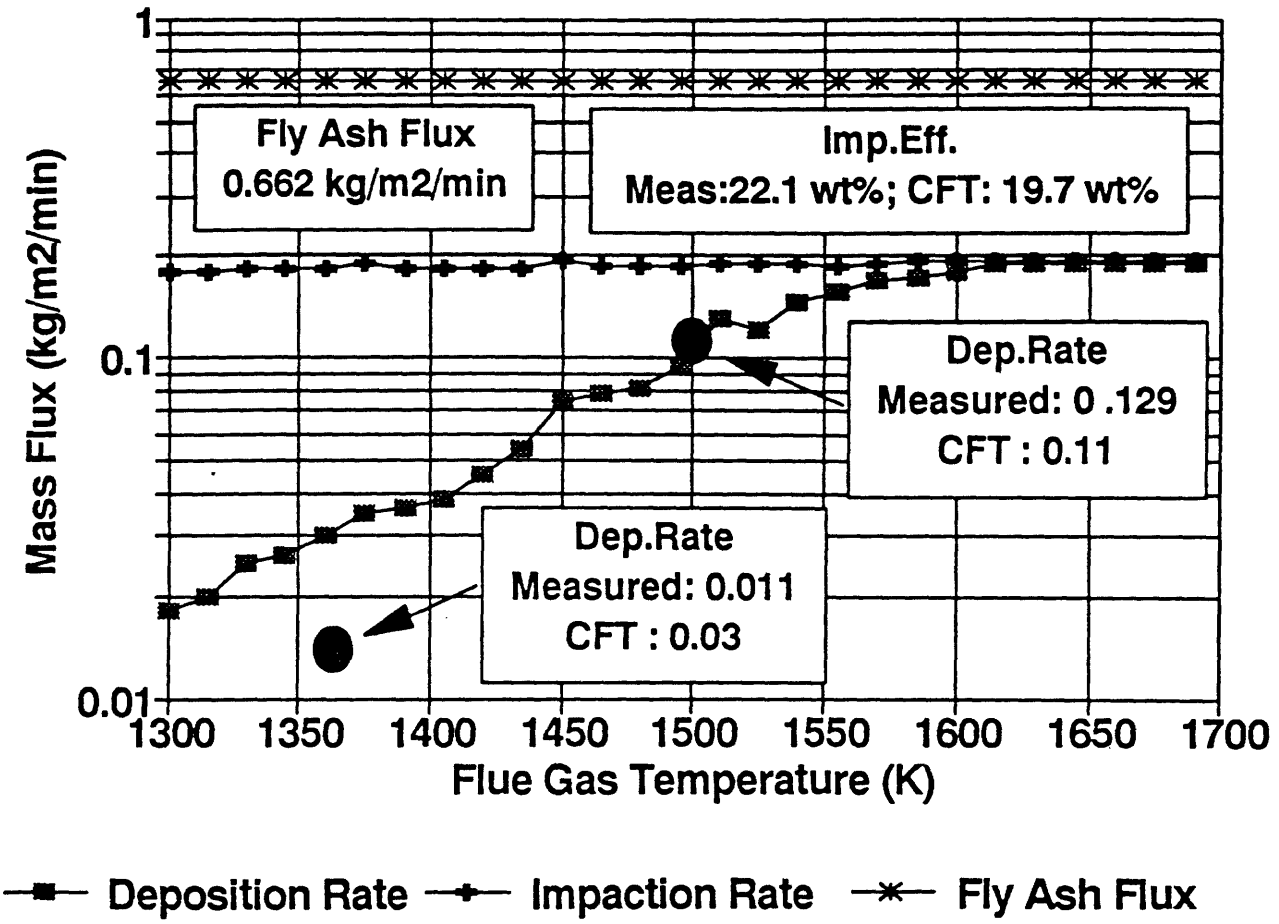

Figure 101. **Fly Ash Behavior Predictions *vs.* Experiments:** Island Creek Coal

M: measured P: predicted

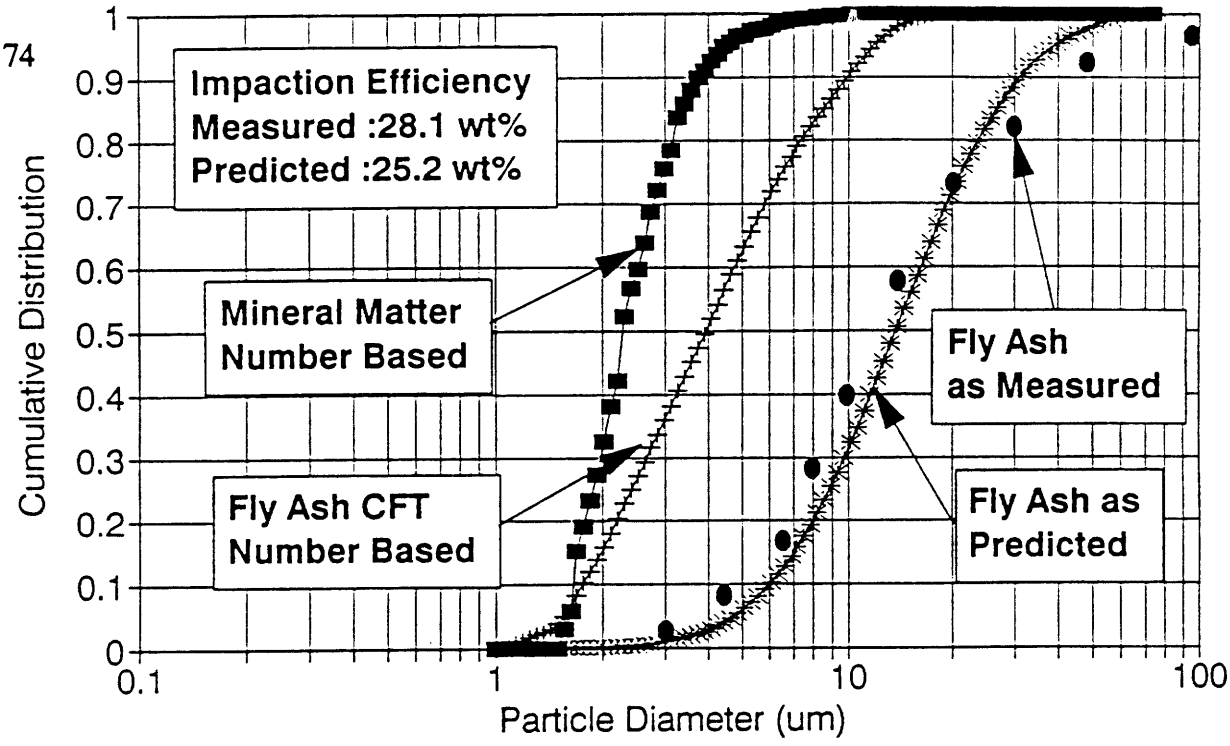

Figure 102. **Fly Ash Size Distribution Predictions and Correlation with Measurements:** Jader Coal

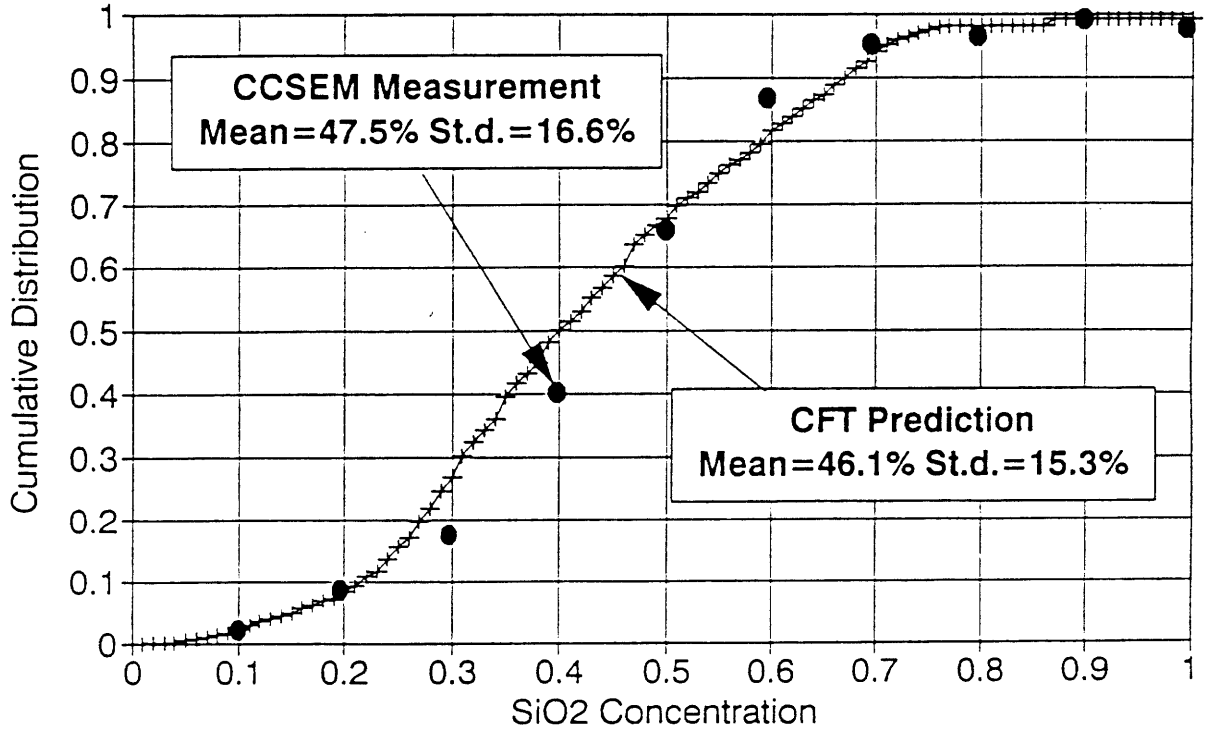

Figure 103. **SiO_2 Content Distribution Prediction *vs.* Experiment:** Jader Coal

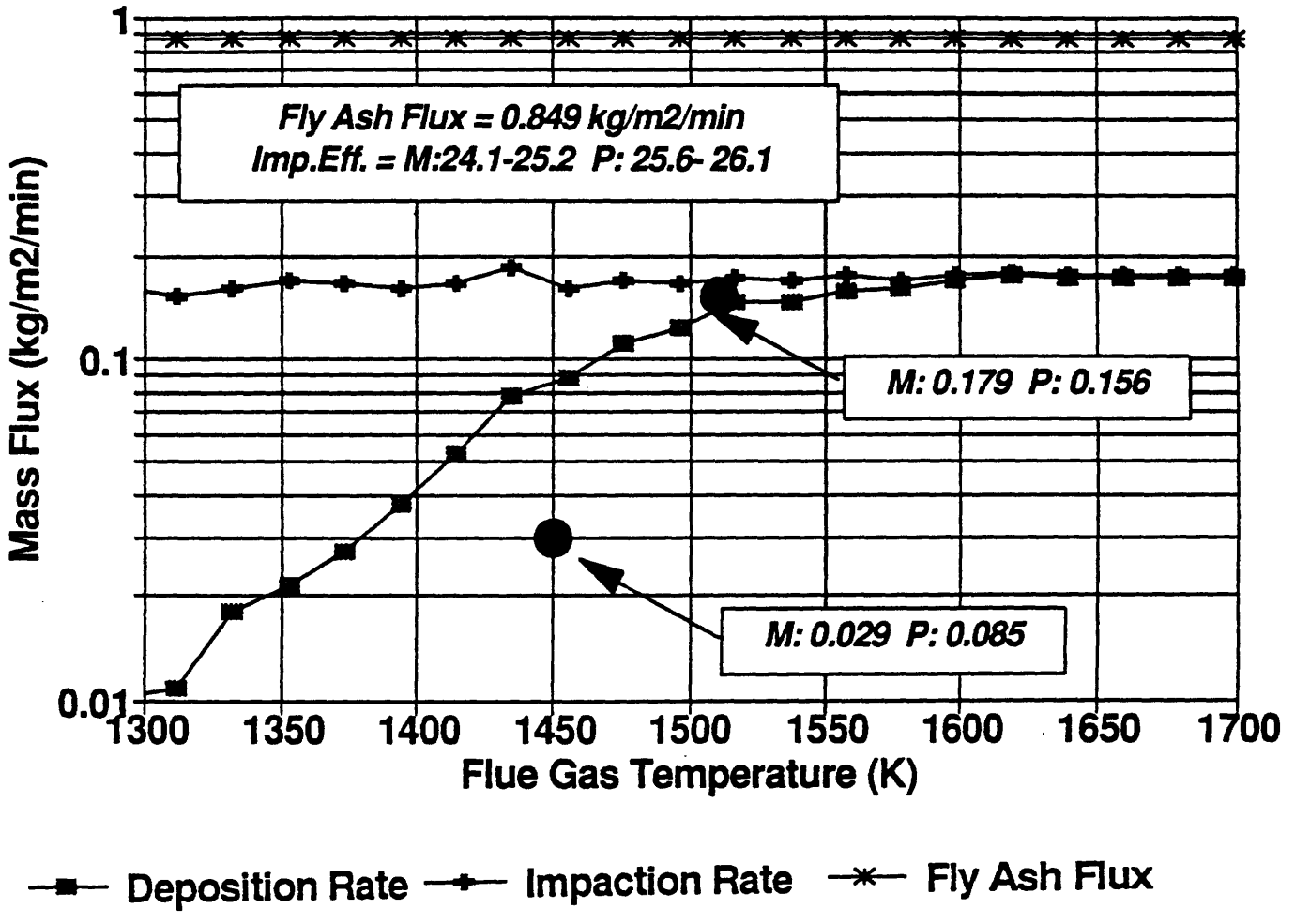

Figure 104. **Fly Ash Behavior Predictions *vs.* Experiments:** Jader Coal

M: measured P: predicted

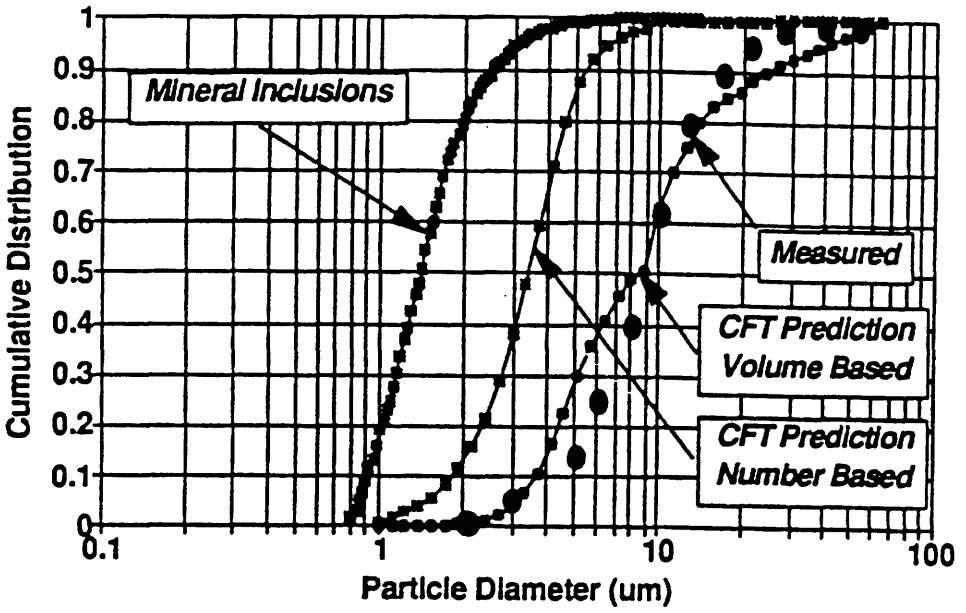

Figure 105. **Fly Ash Size Distribution Predictions and Correlation with Measurements:** Mapco Coal

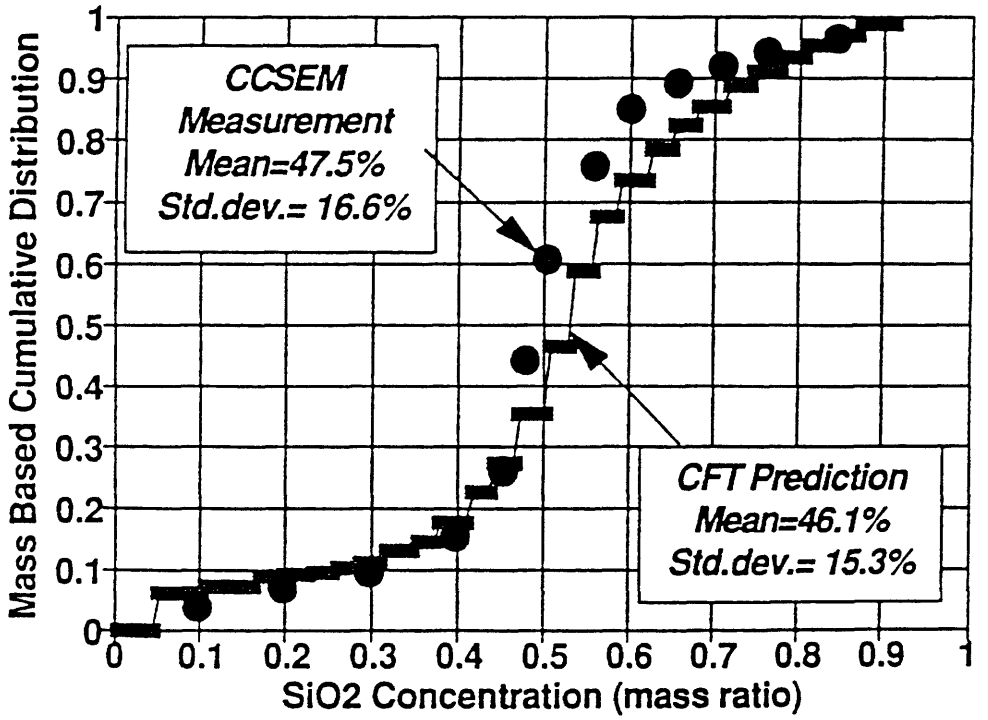

Figure 106. **SiO_2 Content Distribution Prediction *vs.* Experiment:** Mapco Coal

making the fly ash deposition rate more sensitive to the flue gas temperature. The measured and the predicted deposition rates are plotted in Figure 107.

A summary of the CFT predictions can be given by comparing the measured and predicted mean values and the standard deviations of the fly ash size and chemical composition distributions. The results can be seen in Figure 108. A correlation coefficient of 0.96 was calculated for these distributions. Also, good correlation was reached between the calculated and predicted impaction efficiencies (Figure 109). However, a slightly lower confidence limit was obtained for the fly ash deposition rates (Figure 110, correlation coefficient of 0.9).

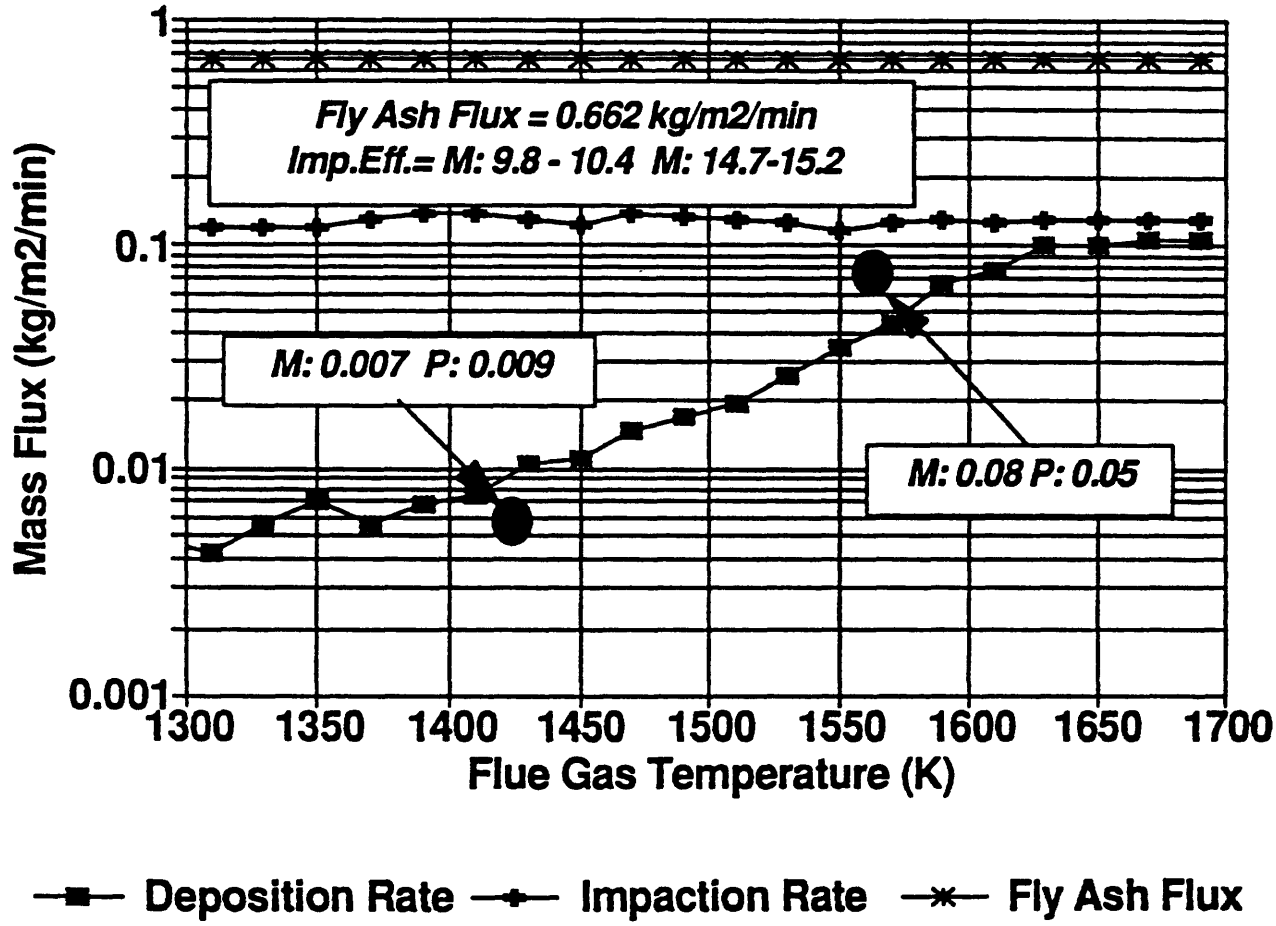

Figure 107. **Fly Ash Behavior Predictions *vs.* Experiments:** Mapco Coal

M: measured P: predicted

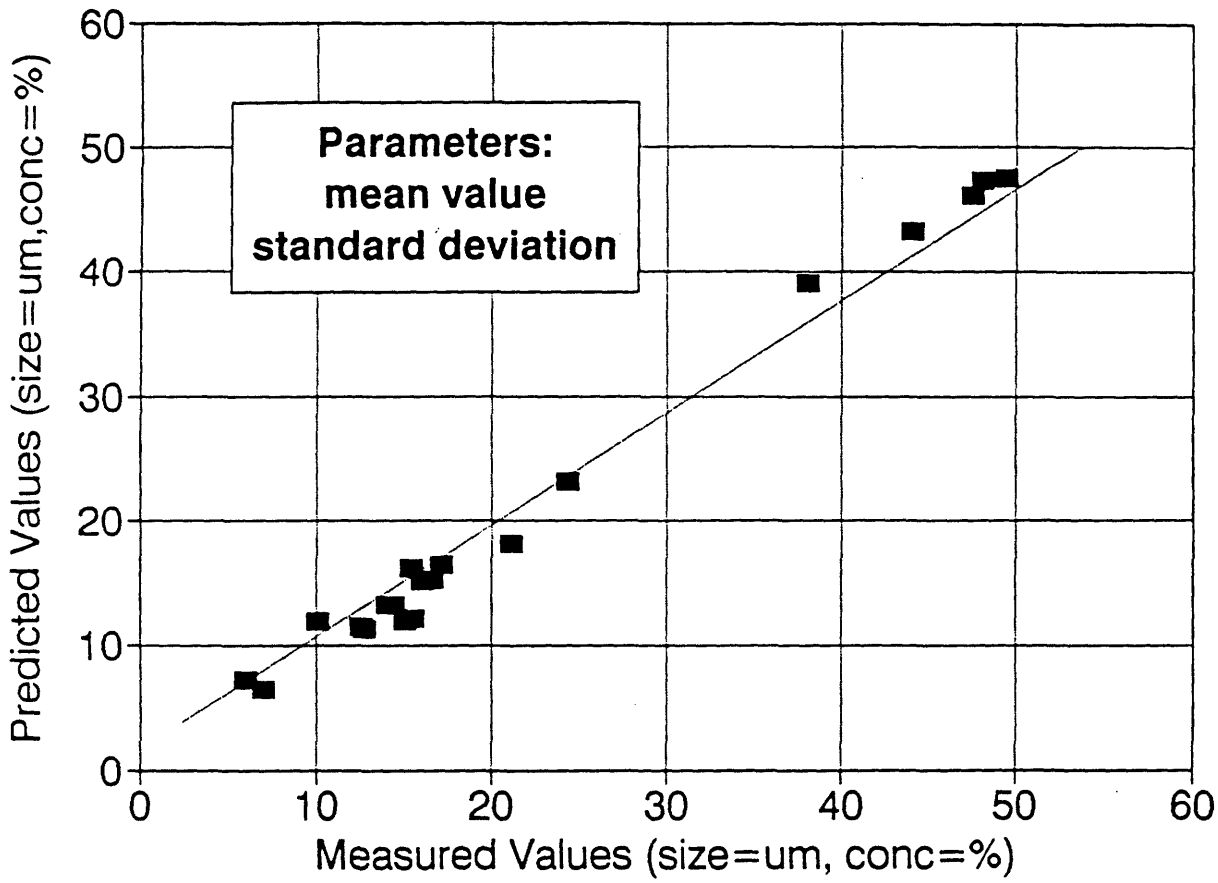

Figure 108. **Summary: CFT Predictions *vs.* Measurements** Fly Ash Size Parameters and SiO_2 Content for CRF Coals

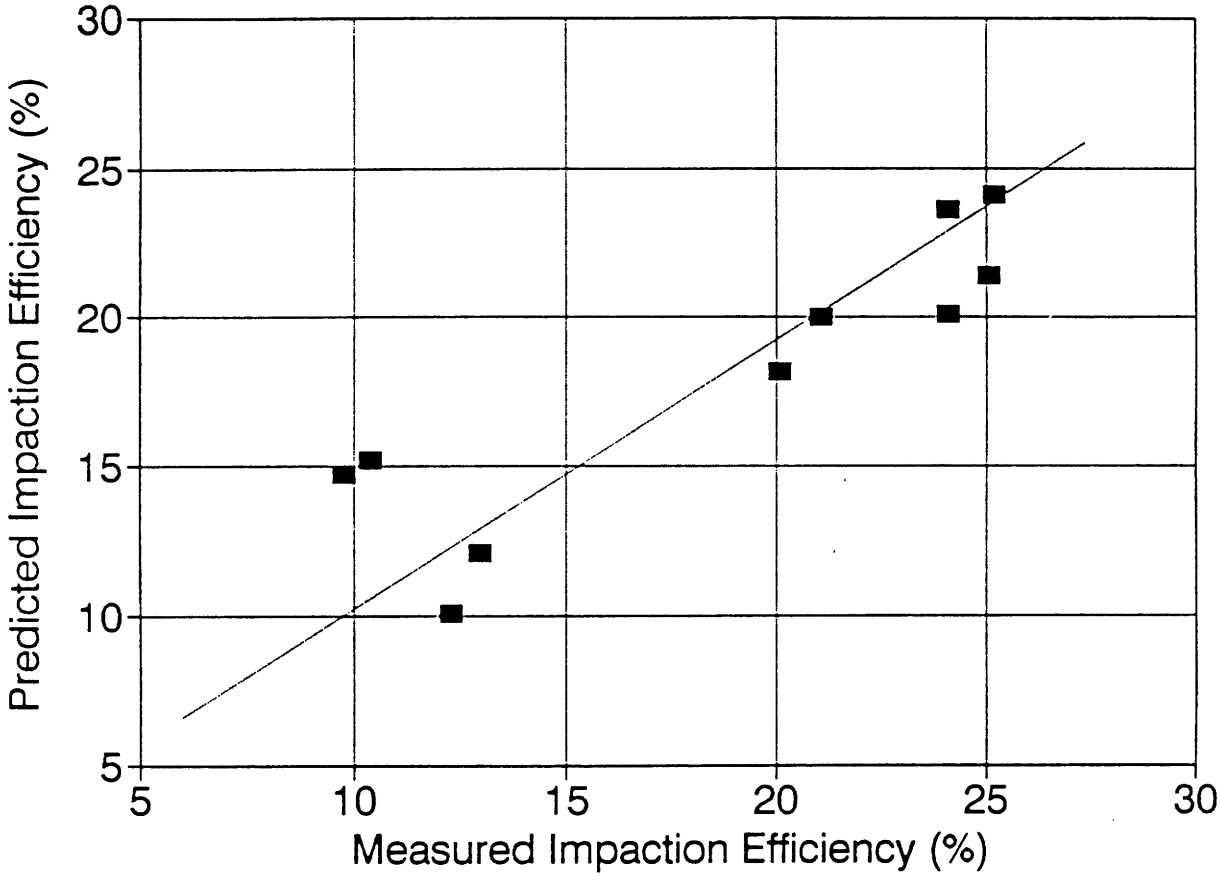

Figure 109. **Summary: CFT Predictions *vs.* Measurements**
Fly Ash Impaction Efficiencies for CRF Coals

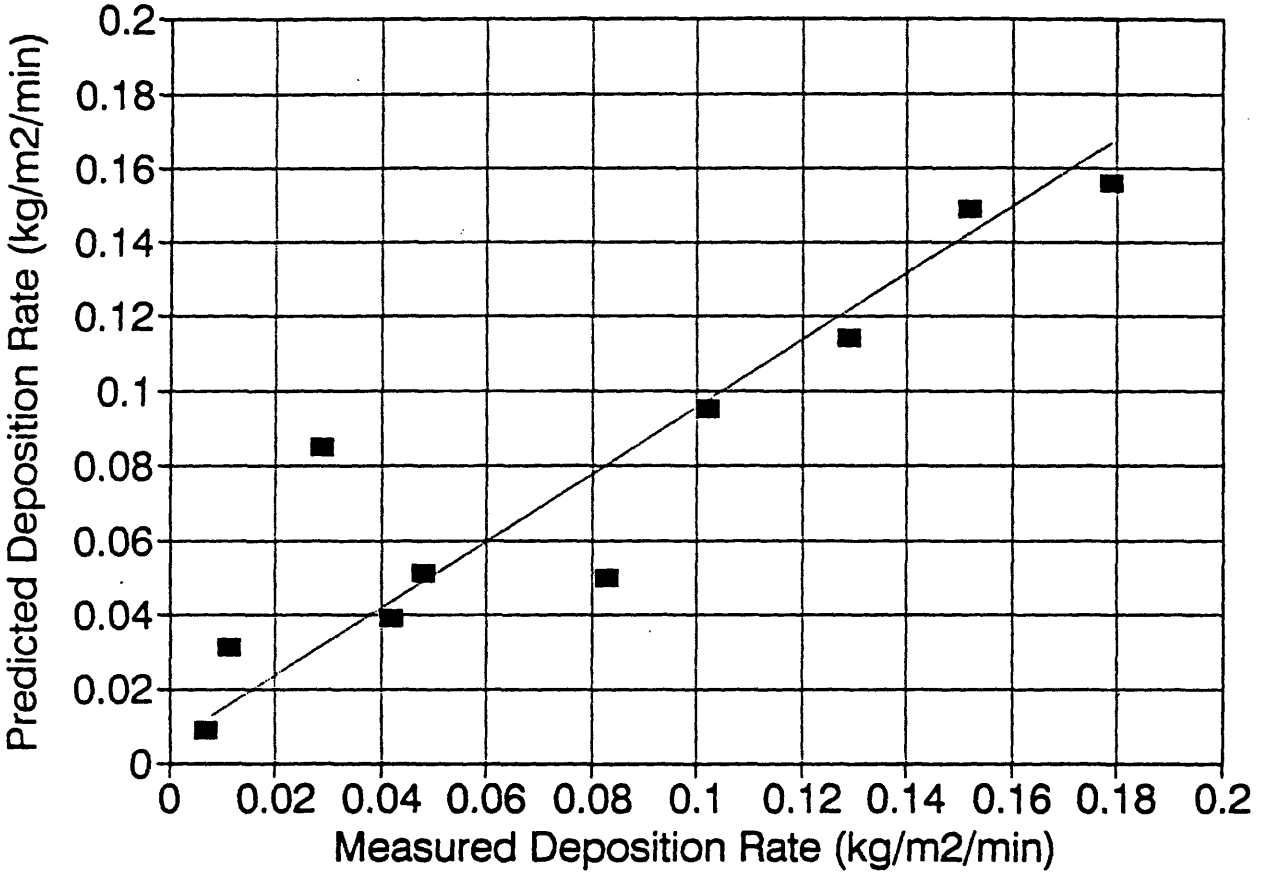

Figure 110. **Summary: CFT Predictions *vs.* Measurements**
Fly Ash Deposition Rates for CRF Coals

SECTION 6

RELATIVE FOULING TENDENCY OF TEST COALS

The objective of defining a relative fouling tendency value is to obtain a meaningful order for different coals with respect to the deposition behavior of their fly ashes *in a given combustion system or boiler.* One of the most important predictions of the CFT model is the fly ash deposition rate as a function of flue gas temperature. The coal fouling tendency is defined as the accumulation rate of deposit mass per unit heat input, as measured or calculated at some appropriate temperature, and this temperature must be defined for each coal and for the specific combustion system. A natural choice for the comparison temperature would be to use the flue gas temperature in the convective section of the boiler. This temperature is dependent on boiler design. Therefore, in our case it is approximated by taking a certain fraction (say 62%) of the adiabatic flame temperature. The basis of this definition of the *"comparison flue gas temperature"* relies on the recognition that, in all boiler designs, a certain fraction of the thermal heat input has to be extracted in the radiative section of the furnace.

The adiabatic flame temperature is calculated by the following equation:

$$T_{adiab} = \frac{H_i + A_t * c_{p\ air} * \Delta T_{air}}{V_t * c_{p\ flue\ gas}}$$

where H_i is the inferior calorific value of coal (kJ/kg),
A_t is the total air mass/fuel mass (kg_{air}/kg_{coal}),
V_t is the total flue gas mass/fuel mass ($kg_{flue\ gas}/kg_{coal}$),
ΔT_{air} is the air temperature (K),
$c_{p\ air}$ & $c_{p\ flue\ gas}$ are the heat capacity of air and flue gas, respectively (kJ/kg-K).

6.1 Coals Tested in the CRF

The necessary data such as the mass of air and flue gas per unit mass of coal were obtained by using the elemental analyses of coals. The results of calculations can be seen in Table 28. The adiabatic flame temperature for each coal was calculated with an excess air ratio of 1.4. The combustion air was preheated to 523 K in all cases. The results indicated that the adiabatic temperatures for bituminous coals were higher than those for the lignite and the Blend coal. The calculated flue gas temperature at the convective section is plotted in Figure 111. The comparisons of coal fouling tendencies were made by taking the deposition rate of each coal for the case of 1 MW thermal input at the corresponding flue gas temperature. The results are shown in Table 29. The Mapco coal was found to be the best in this ranking, due to its homogeneous inclusions (clay mineral) and its low impaction efficiency, which was the result of very fine inclusion size distribution. The homogeneous mineral matter had a narrow chemical composition distribution, and, in turn, a narrow viscosity distribution which made the deposition rate very sensitive to the flue gas temperature. However, in the case of the Mapco coal, most

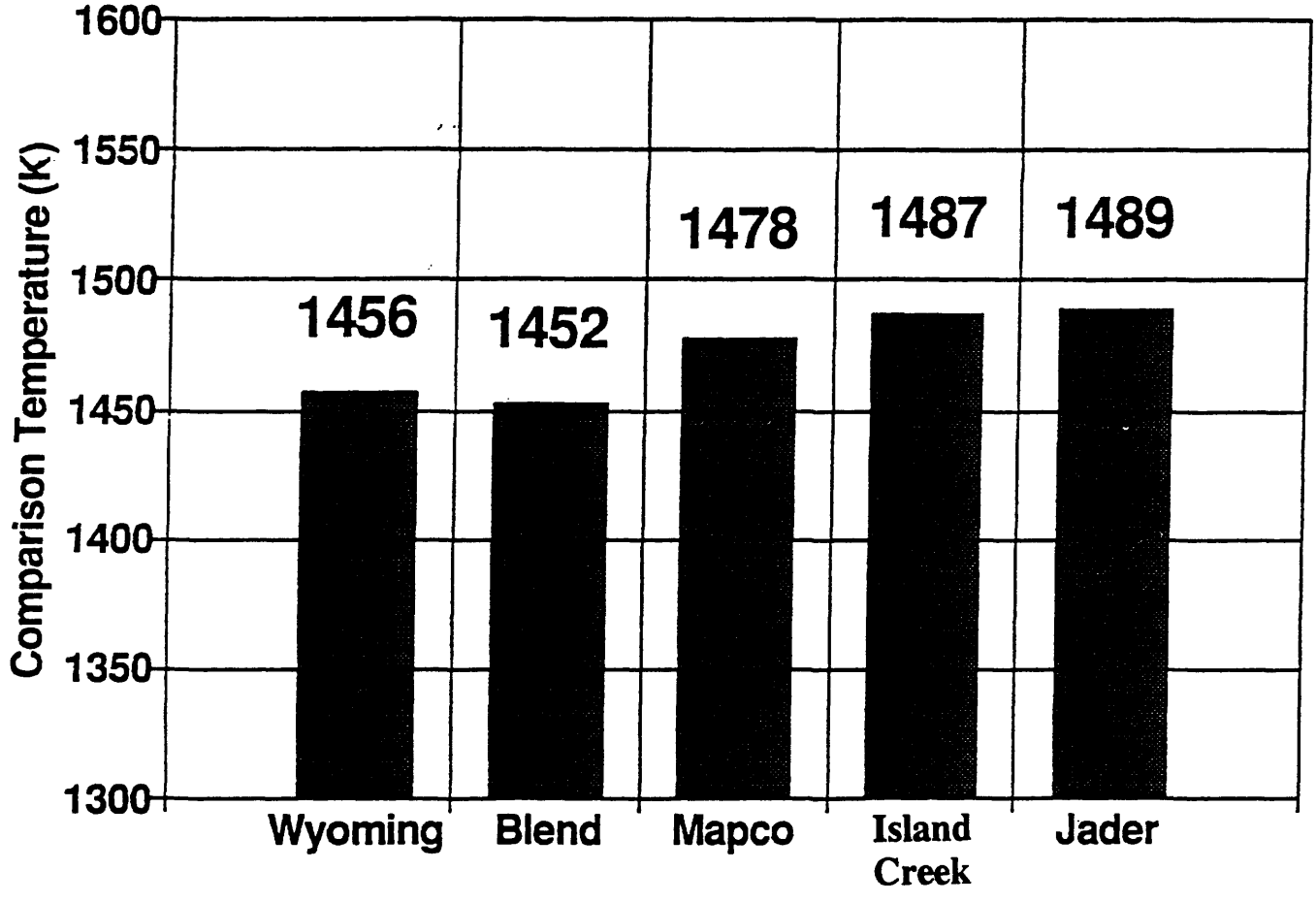

Figure 111. **Flue Gas Temperatures for Comparison of Coals Tested in CRF**

Table 28.
Calculation of Flue Gas Temperatures for Comparison of CRF Coals

Parameters	Wyoming	Blend	Mapco	Island Creek	Jader
Carbon	0.618	0.646	0.760	0.711	0.731
Hydrogen	0.046	0.046	0.051	0.048	0.049
Sulfur	0.005	0.006	0.008	0.030	0.029
Nitrogen	0.009	0.014	0.016	0.015	0.016
Oxygen	0.171	0.148	0.086	0.094	0.072
Ash	0.073	0.069	0.068	0.068	0.088
Moisture	0.076	0.070	0.011	0.032	0.015
Excess Air	1.4	1.4	1.4	1.4	1.4
Air (kg_{air}/kg_{coal})	11.14	11.72	14.19	13.37	13.84
Flue Gas (kg_{gas}/kg_{coal})	11.56	12.12	14.48	13.67	14.11
H_i (KJ/kg)	25167	26136	31489	30053	30963
T_{air} (K)	523	523	523	523	523
$T_{adiab.}$ (K)	2348	2342	2384	2399	2403
$T_{conv.}$ (K)	1456	1452	1478	1487	1489

Table 29.
CFT Ranking of CRF Coals

Coal	62% of Adiabatic Temperature (K)	Measured Deposition Rate ($kg/m^2/min$) (linearly interpolated)	Deposition Rate ($kg/m^2/min$) CFT Predictions	Ranking of Coal Fouling Tendencies
Mapco	1478	0.030	0.016	1
Blend	1452	0.036	0.039	2
Wyoming	1456	0.084	0.088	3
Island Creek	1487	0.117	0.108	4
Jader	1489	0.129	0.124	5

of the fly ash particles were not sticky at the calculated flue gas temperature at the convective section.

6.2 Coals from Italy

In addition to the five coals tested in the CRF, samples were provided of several coals used in boilers in Italy by ENEL S.p.A. CFT model calculations were made for the following coals, in an attempt to predict their relative order with respect to their deposition behavior in boilers:

- Sud Africano
- Sulcis 1
- Polacco
- Russia
- Columbiano.

The characteristics of these ENEL coals are given in Table 30. It can be seen that the Sulcis coal was a low grade coal of high volatile and ash content and low calorific value. Its sulfur content was also high, 8%. The Sud Africano, Polacco and Columbiano samples were of bituminous coals with high heating value and fixed carbon. Their ash content varied between 6.4% and 16%. The Russia sample was an anthracite with very high fixed carbon and low volatile content. From comparison of their deformation temperatures, the Sulcis coal was expected to be worst from the point of view of fly ash deposition. This conclusion was supported also by the viscosity approximation shown in the last row of Table 30. The CFT model, however, predicted a different result.

The CFT model predictions were made as if all of these coals had been tested in the CRF. In this way, a direct comparison could be made with the previously tested coals, too. For each coal sample the CCSEM data were obtained for a specific size cut, 45-90 μm. The most important output of the CFT modeling was the fly ash deposition rates as functions of temperature. These calculations indicated the effect of flue gas temperature on the fly ash deposition rate. The results are plotted in Figures 112 - 116. Legend boxes in each figure indicate the low and high deposition rates corresponding to the temperature extremes (1300 K, 1680 K) used in the calculations. Figure 113 shows that the Sud Africano coal was the most sensitive coal to flue gas temperature because its mineral matter was a very homogeneous clay material with a fixed melting point. The deposition rate of the Polacco fly ash, however, showed a very weak temperature dependence.

As described earlier in this Section, the comparison flue gas temperature necessary to obtain a fly ash deposition rate is calculated by the use of the adiabatic flame temperature. The results of such calculations for the Italian coals are shown in Table 31, and the comparison flue gas temperatures are plotted in Figure 117. Due to its high heating value, the Polacco coal had the highest flue gas temperature and the Sulcis coal had the lowest. By calculating the corresponding deposition rate for each coal, the relative order of these coals could be obtained.

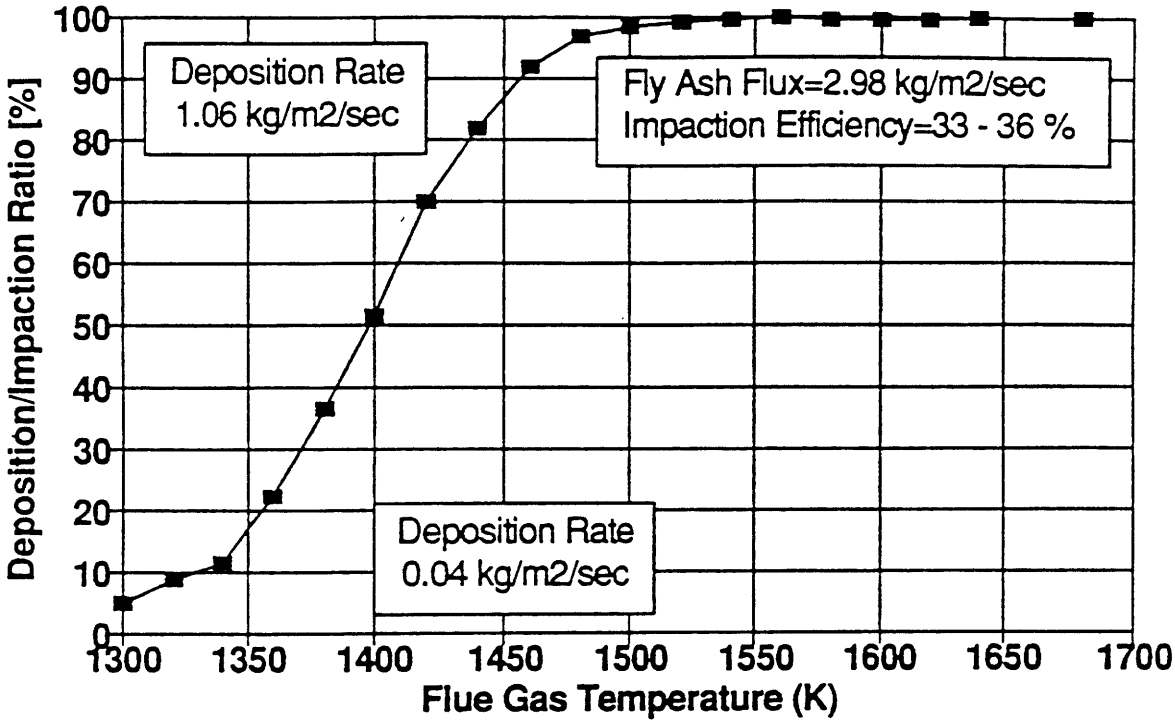

Figure 112. **Predicted Fly Ash Deposition for Sulcis Coal**

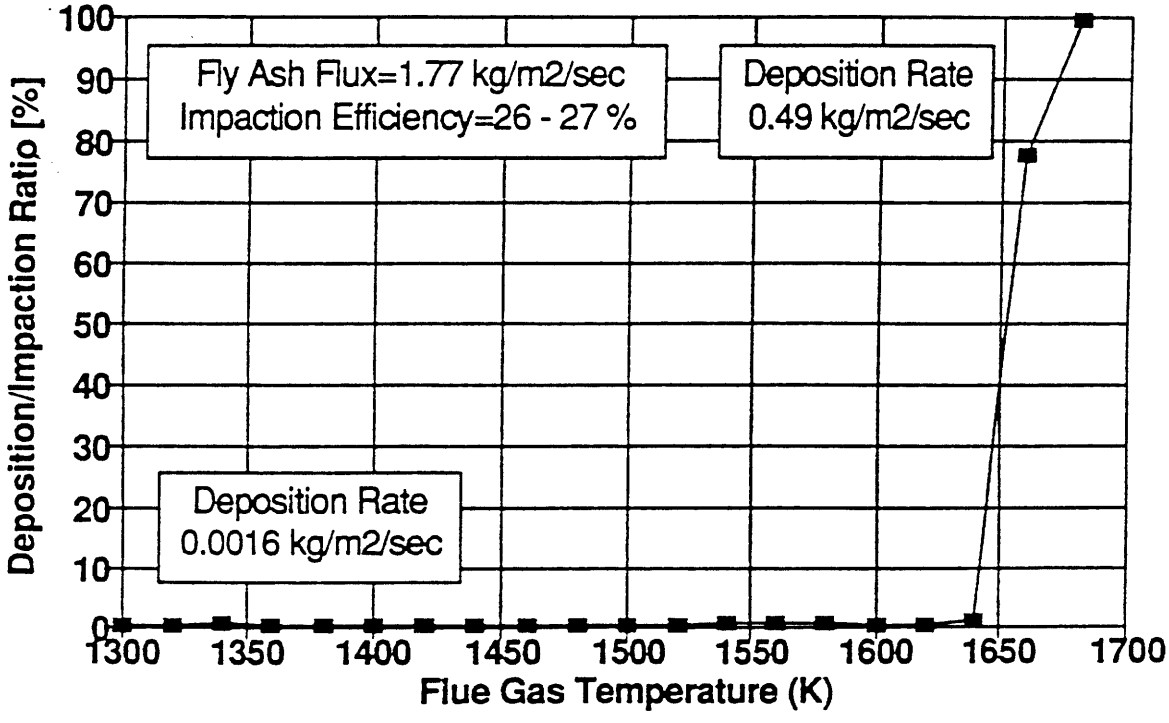

Figure 113. **Predicted Fly Ash Deposition for Africano Coal**

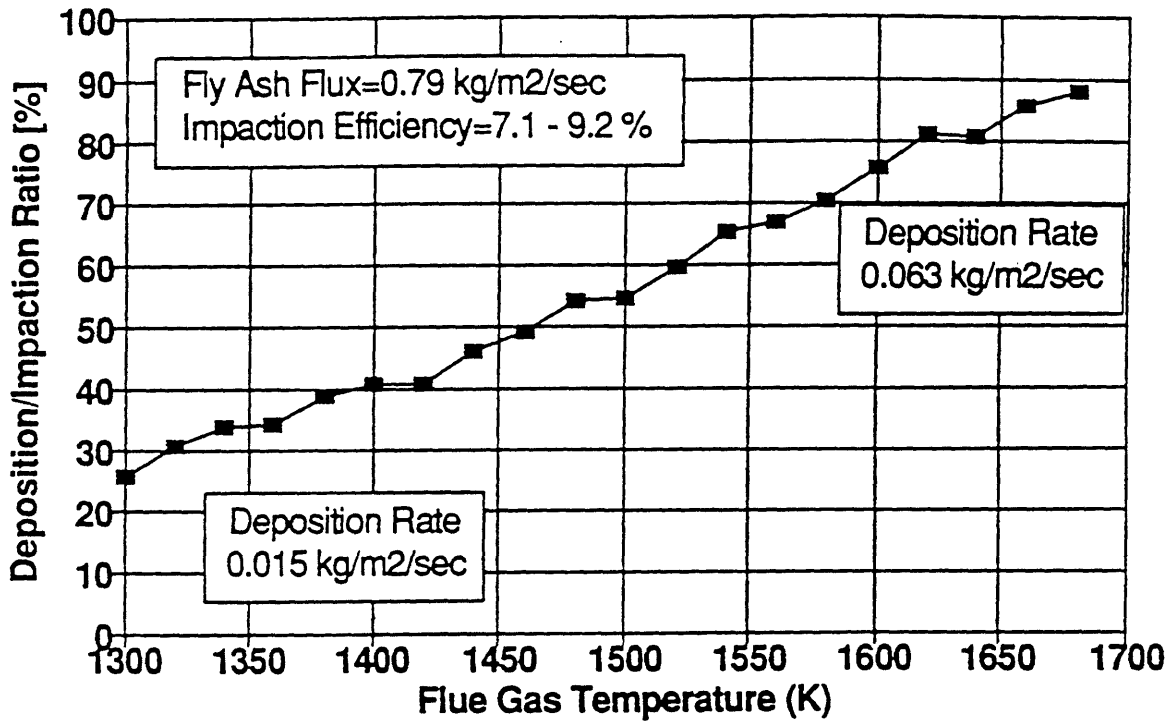

Figure 114. **Predicted Fly Ash Deposition for Russia Coal**

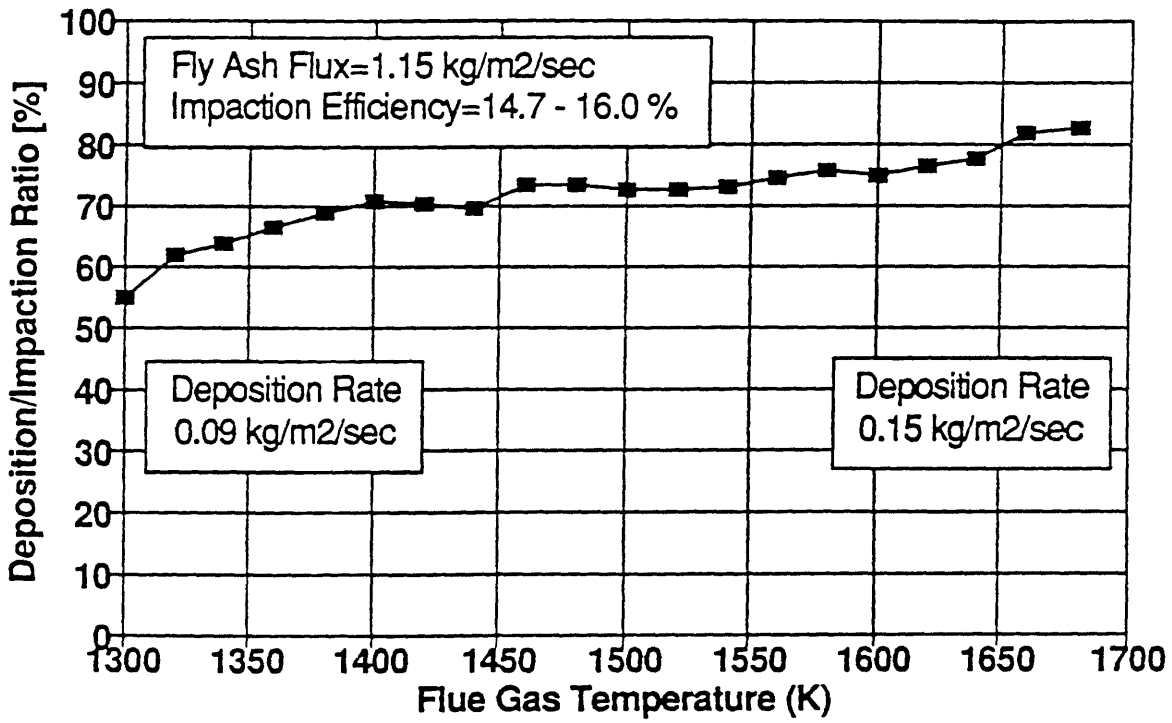

Figure 115. **Predicted Fly Ash Deposition for Polacco Coal**

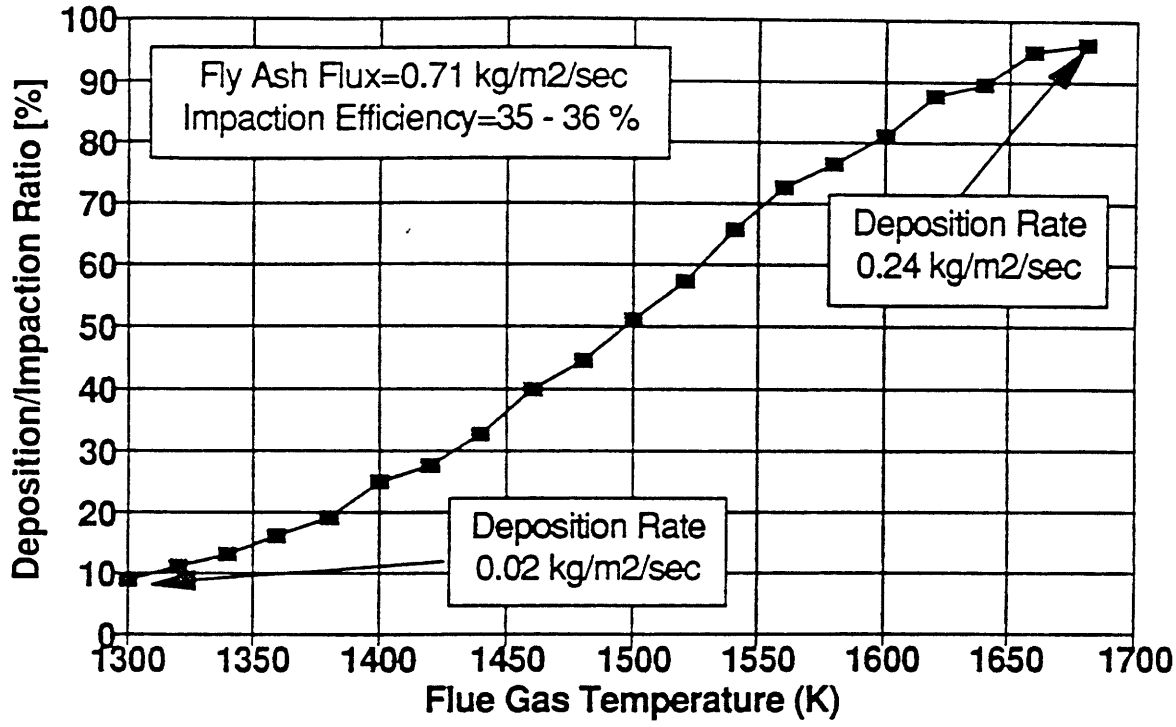

Figure 116. **Predicted Fly Ash Deposition for Columbiano Coal**

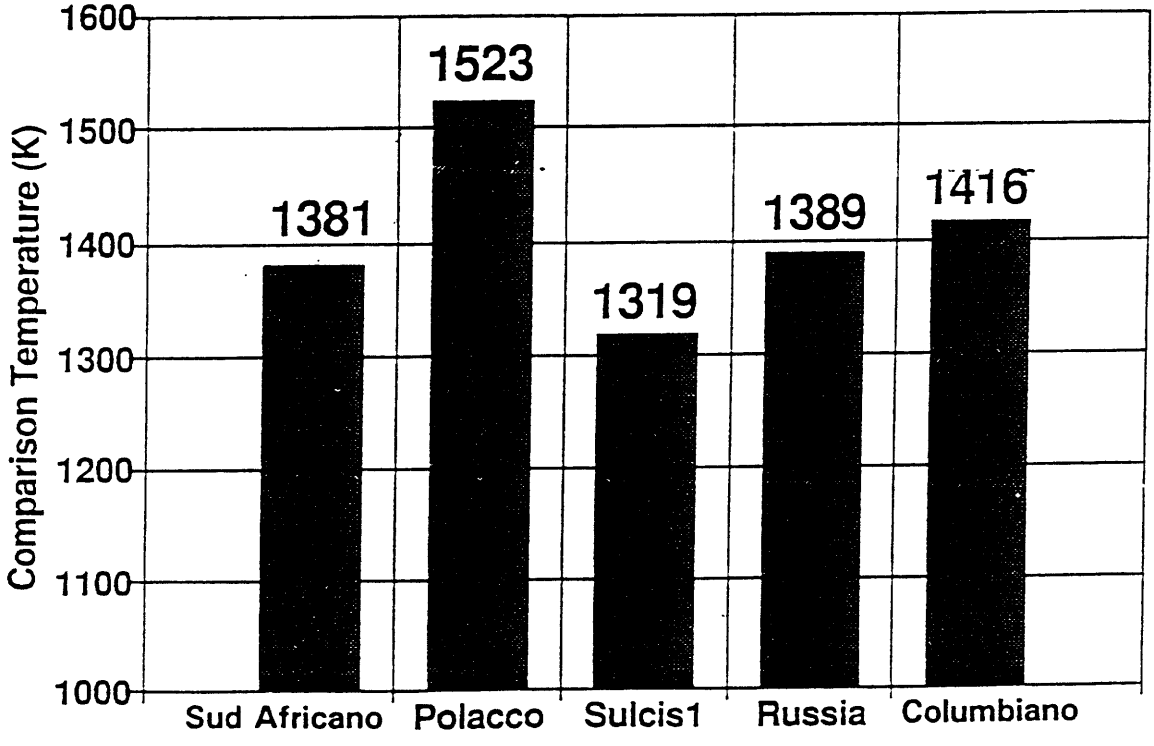

Figure 117. **Flue Gas Temperatures for Comparison of ENEL Coals**

Table 30.
Summary: Characteristics of ENEL Coals

Quantity	Sud-Africano	Sulcis 1	Polacco	Russia	Columbiano
Moisture wt%	2.8	6.2	2.4	4.2	1.6
Volatile Matter wt.%	25.2	42.4	29.9	9.1	27.6
Fixed Carbon wt.%	60.6	37.2	58.5	82.2	66.0
Ash wt.%	16.0	24.1	12.5	9.7	6.4
Heating Value MJ/kg	27.57	22.31	32.95	29.33	32.64
Total Sulfur wt.%	0.46	8.1	0.6	0.89	0.83
IDT K	n.d.	n.d.	n.d.	n.d.	n.d.
ST K	n.d.	n.d.	n.d.	n.d.	n.d.
HT K	n.d.	n.d.	n.d.	n.d.	n.d.
FT K	1733	1483	1573	1583	1633
Ash SiO_2 wt.%	60.1	44.5	54.01	44.3	50.6
Ash Al_2O_3 wt.%	34.4	13.2	25.6	23.5	21.9
Ash Fe_2O_3 wt.%	1.23	15.2	7.98	4.95	12.1
Ash CaO wt.%	1.13	4.65	5.83	13.8	3.23
Other Flux Comp. wt.%	3.14	22.45	6.58	13.45	12.17
Viscosity $\log_{10}$ Poise, 1500 K	4.74	2.5	3.79	3.0	3.3

Table 31.
Calculation of Flue Gas Temperatures for Comparison of ENEL Coals

Parameters	Polacco	Sulcis	Russia	Columb.	Africa
Carbon	0.747	0.530	0.838	0.711	0.721
Hydrogen	0.047	0.041	0.017	0.049	0.041
Sulfur	0.006	0.075	0.008	0.007	0.004
Nitrogen	0.011	0.011	0.007	0.014	0.013
Oxygen	0.042	0.053	0.003	0.093	0.054
Ash	0.122	0.226	0.083	0.069	0.138
Moisture	0.024	0.062	0.042	0.056	0.028
Excess Air	1.4	1.4	1.4	1.4	1.4
Air (kg_{air}/kg_{coal})	14.01	10.6	14.31	13.25	13.24
Flue Gas (kg_{gas}/kg_{coal})	14.25	10.9	14.42	13.59	13.48
H_i (KJ/kg)	32098	20771	27992	28207	26727
T_{air} (K)	523	523	523	523	523
$T_{adiab.}$ (K)	2457	2127	2241	2284	22228
$T_{conv.}$ (K)	1523	1319	1389	1416	1381

The results are shown in Table 32. Sud Africano coal was ranked the best since its fly ash particles were not sticky under 1650 K, and the flue gas temperature at the convective section was lower than this value, 1381 K. The Polacco coal was ranked as the worst since the flue gas temperature at the convective section was high, 1523 K, so the fly ash contained a high proportion of sticky particles. The Russian coal was the second. Its fly ash was very fine which resulted in low impaction efficiency. The Sulcis and the Columbian coals were similar from the point of view of their deposition behavior. The Sulcis fly ash had a high impaction efficiency, but the flue gas temperature at the convective section was low (1319 K), therefore the sticking efficiency of the fly ash was small. The flue gas temperature for the Columbian coal was higher by 100 K, but its fly ash mass flux was low due to its low ash content. Consequently, these effects led to a relatively small difference between the deposition rates of these two coals.

Table 32.
CFT Ranking of ENEL Coals
(Based on 45-90 μm Size Cut from Samples)

Coal	62% of Adiabatic Temperature (K)	Deposition Rate ($kg/m^2/min$)	Ranking of Coal Fouling Tendencies
Sud Africa	1337	0.002	1
Russia	1389	0.021	2
Sulcis 1	1319	0.041	3
Columbiano	1416	0.049	4
Polacco	1523	0.122	5

SECTION 7

CONCLUSIONS AND RECOMMENDATIONS

7.1 Conclusions

Results of a mathematical modeling and experimental study of coal mineral matter transformation and deposition in pulverized coal combustion are reported. The research objectives were:

a) to develop a model (computer code) of fly ash deposition in pulverized coal-fired boilers to be used for predicting the relative fouling tendency of different coal types and blends;
b) to follow, under well-controlled experimental conditions in 1 to 2 MW pulverized coal flames, the transformation of coal mineral matter to fly ash, and the deposition of the resultant fly ash on heat transfer surfaces, for the effect of different coal types and blends; and
c) to use the experimental information to test and validate the Coal Fouling Tendency (CFT) model with sufficient rigor for a range of coal types.

A key feature of the CFT model is that it requires input data only of the chemical composition of the coal, and the size and chemical composition distributions of the mineral matter in the coal provided by Computer Controlled Scanning Electron Microscope (CCSEM) analysis. In the report, mass-based distributions of coal mineral size, chemical compounds and viscosity are given in terms of their mean values and standard deviations for the individual coals. The significance of such calculations is that they help to establish relationships between the CCSEM measurements of coal minerals and the properties of the fly ash such as size and chemical composition as affected by the mode of coal particle burnout. The fly ash size distribution provides the basis for the fly ash impaction calculation. The chemical composition distribution gives information on viscosity and hence the sticking probability of the impacted fly ash. ***The fly ash deposition rate as a function of flue gas temperature is used for determining the coal relative fouling tendency.***

In the course of the experimental investigation, five test coals were used, namely: the Wyoming lignite, the blend of 70% Wyoming lignite with 30% Oklahoma bituminous, and the Jader, Island Creek and Mapco bituminous coals. Some of these were specially chosen to render the results relevant to a major EPRI-DOE study. It was also considered important to select coals with a wide variety of certain properties such as coal burning behavior, and size and chemical composition of mineral matter.

Results of density separation and acid leaching of the pulverized ***Wyoming lignite*** showed that one-fourth of the mineral matter was ion-exchangeable, with high CaO content. However, CCSEM measurements indicated that the included minerals consisted mainly of alumina-silicates of very different SiO_2 content. The chemical composition and melting behavior of these

minerals were considerably different from each other, which resulted in very wide distribution of mineral particle viscosity. The coal burnout, however, changed the distribution of particle viscosity by the modification of the distribution of chemical composition. Mineral inclusions within a coal particle received a certain fraction of the ion-exchangeable mineral matter of different chemical composition during the burnout of a coal particle. Further random coalescence occurred between the inclusion particles resulting in a coarser distribution of particle size and a distribution of chemical composition of lower variance, and consequently in a particle viscosity distribution of lower variance. The significance of the variance of the particle viscosity distribution is that it determines the sensitivity of fly ash deposition rate to the flue gas temperature.

It was measured by CCSEM that the values of the mean and of the standard deviation of the fly ash size distribution were 2.9 and 1.8 times larger, respectively, than those of the included mineral matter. However, those of the particle viscosity distribution decreased by 50% and 25%, respectively. These changes in the mineral matter properties are in accordance with the CFT model predictions, and the predicted distribution functions gave good agreement with the measured data.

Fly ash deposition behavior was studied by changing the flue gas temperature while the target tube initial temperature was kept constant. It was found that the mass of deposit increased linearly with time independently of the flue gas temperature, and that the deposition rate was decreased from 0.1 $kg/m^2/min$ to 0.048 $kg/m^2/min$ by reducing the flue gas temperature from 1509 K to 1339 K. Both values of deposition rates were predicted by the CFT model with a high degree of accuracy. The results indicated low sensitivity of the fly ash deposition rate to the flue gas temperature, unlike the ASTM analysis of the lignite ash which showed a very sensitive sticking behavior of the ash between 1426 and 1454 K.

The fouling tendency of coals is given on the basis of calculating the fly ash deposition rate at the flue gas temperature in the convective section of a given boiler. For the Wyoming lignite, the appropriate temperature was calculated as 1456 K by taking a certain fraction, 62% of the lignite adiabatic flame temperature. The fly ash deposition rate at 1456 K was predicted by the CFT model as 0.088 $kg/m^2/min$.

The ***Blend coal*** was a mixture of 70 wt% Wyoming lignite and 30 wt% Oklahoma bituminous coal. The purpose of blending these coals was to lower the sulfur content of the bituminous coal and to increase the heating value of the lignite. Our investigation was focused on the comparison of the fouling behavior of the pure lignite and Blend fly ash. The ASTM ash analysis showed that the Blend coal ash behaved very similarly to that of the lignite ash. However, CCSEM measurements indicated the mineralogy of the lignite was changed by blending. The illite content of the Blend coal was increased from 36 wt% to 43 wt%. No significant differences were measured between the size distributions of the included mineral matter of the coals. The mean particle size of the Blend coal was higher by 7.9 μm and the standard deviation by 14 μm. The higher coal particle size increased the number of inclusions within a coal particle, causing a higher degree of inclusion coalescence, and resulting in a Blend

coal fly ash of coarser size distribution and a viscosity distribution of lower standard deviation. Coarser fly ash size distribution gave higher impaction efficiency, which eliminated the advantage of lower fly ash mass flux of the Blend coal. The viscosity distribution of lower standard deviation for the Blend coal fly ash made its deposition rate more sensitive to flue gas temperature. The Blend fly ash deposition rate was increased from 0.042 $kg/m^2/min$ to 0.152 $kg/m^2/min$ by increasing the flue gas temperature from 1458 K to 1573 K. The calculations showed that the deposition sensitivity of the lignite ash was increased from 3.06 $kg/m^2/min/K$ to 9.56 $kg/m^2/min/K$ by blending due to higher illite content of the mineral matter and coarser size distribution of the Blend coal. The CFT model followed these changes and gave good approximations for the size and chemical composition of fly ash and predicted more sensitive fly ash deposition behavior for the Blend coal. The fouling tendency of the Blend coal was evaluated by calculating the fly ash deposition rate at the flue gas temperature in the convective section of a boiler. The flue gas temperature was calculated as 1452 K at which the fly ash deposition rate was estimated as 0.039 $kg/m^2/min$. This rate was lower than that of the lignite fly ash ***indicating a superior fouling behavior of the Blend fly ash as compared to that of the lignite fly ash.***

The coal fouling tendency is expected to be a parameter which can be generally applied for different kinds of coals. In addition to the Wyoming lignite and Blend coal discussed above, our investigation was extended to bituminous coals of different mineralogy. Two of the three bituminous coals, ***the Island Creek and the Jader,*** contained similarly high Fe_2O_3. However, ASTM measurements of their ash indicated superior melting behavior for the Jader ash since it contained 20 wt% more non-melting material such as quartz, as measured by CCSEM. In addition, 50 wt% of the iron in the Jader coal was found in the extraneous mineral matter, which did not coalesce with alumina-silicates of inclusion type to form low melting point compounds. Despite these observations, which were based only on the properties of coal mineral matter, ***the deposition behavior of Jader fly ash was found inferior to that of the Island Creek coal fly ash by our experiments.*** One of the reasons of this result was the high fly ash mass flux in the convective section of the MIT-CRF for the Jader coal, which was a consequence of high ash content per unit heating value. Also, higher impaction efficiency was calculated for the Jader fly ash due to the coarse size distribution of extraneous mineral matter. The flue gas temperature at the convective section was also slightly higher for the Jader coal due to its higher heating value. All these effects contributed to the higher fly ash deposition rate of the Jader fly ash. Predictions of the CFT model for the distributions of size and SiO_2 content were good, as were the fly ash deposition rates at the higher temperatures. At lower temperatures, the calculated deposition rates were higher than in the experiments. In the low temperature range it is possible that our prediction of the viscosity of particles with high iron content is inaccurate. This must be considered a topic for further investigation.

For the ***Mapco bituminous coal,*** results of density separation and acid leaching of the pulverized coal showed that the mineral matter was mainly composed of inclusions of high illite content as measured by CCSEM. The homogeneity of the Mapco mineral matter was further increased by random inclusion coalescence, which was confirmed by CCSEM measurements of the resulting fly ash. The mean value and standard deviation of the viscosity distribution of the

mineral inclusions decreased by 15% and 28%, respectively. The CFT prediction for the increase of mean particle size and standard deviation was also confirmed by the experiment. They were 2.4 and 1.8 times larger, respectively, than those of the included mineral matter. The deposition rate of the fly ash increased with the flue gas temperature. It was found that by decreasing the flue gas temperature from 1563 K to 1423 K, the fly ash deposition rate was reduced by an order of magnitude, from 0.0825 kg/m^2/min to 0.0069 kg/m^2/min, indicating that the Mapco fly ash is highly sensitive to the flue gas temperature. Low ash content/heating value ensured a low fly ash mass flux in the convective section. Also, low impaction and sticking efficiency resulted in a very low value of fly ash deposition rate even at high calculated flue gas temperature, which led to a conclusion: ***the deposition behavior of the Mapco fly ash was the most superior*** among the fly ashes investigated.

In accord with one of our objectives, the CFT code can provide us with predictions of high confidence level for the distributions of the fly ash particle size and chemical composition and for the fly ash deposition rate as a function of flue gas temperature, without expensive pilot-scale experiments. Based on ultimate coal analyses together with CCSEM measurements of the mineral matter, comparisons of coals or coal blends can be assessed from the point of view of their fouling behavior in a given boiler. ***The following coals were provided by ENEL S.p.A., and were investigated by the CFT code without any pilot-scale experiment: Sulcis lignite, Sud Africano, Polacco and Columbiano bituminous coals and Russia anthracite.*** Calculations were made as if they had been tested at MIT in the CRF. Ultimate analyses of these coals were provided, and additional CCSEM data were acquired on the mineral matter of each coal. The most important output of the CFT calculations was the fly ash deposition rate as a function of flue gas temperature. This function, together with the calculated flue gas temperature, determined the fly ash deposition rate, which was used as the basis for the comparison of these coals. The Sud Africano fly ash was ranked the first due to its very low sticking efficiency at the calculated flue gas temperature. The Russia coal was selected as the second due to the fine size distribution of its fly ash, which resulted in low impaction efficiency. The Sulcis and Columbiano coals were ranked third and fourth; however, the difference between them was minor. The Sulcis fly ash had high impaction efficiency but its sticking efficiency was predicted to be small due to the low calculated flue gas temperature (low heating value). This temperature was higher for the Columbiano coal, but its fly ash mass flux was lower. High sticking efficiency was predicted for the Polacco coal due to its high flue gas temperature, which was the main reason to rank this coal as the fifth among the five ENEL coals investigated.

In summary, the results show that the CFT code is a powerful tool for prediction of fly ash particle size and viscosity distributions, as well as deposition behavior. The code has successfully amalgamated the individual probabalistic sub-models for mineral matter distribution in coal, for mineral matter coalescence, and for impaction and sticking efficiencies.

It should be noted that the interpretation of the results of the CFT model calculations is useful not only for the assessment of the relative fouling behavior of a coal or a coal blend in a given boiler plant, but also as a source of guidance regarding the dependence of fouling upon operating variables such as the fineness of coal grind. This capability can be a valuable asset in dealing with day-to-day problems or in evaluating strategic decisions.

However, such assessments or predictions must be accompanied by confidence limits which are established by selective validation experiments. There is a continual need for expansion of the range of achievable validation by testing more coals of different characteristics. The data-base can also be augmented by comparing other experimental results - obtained from utilities or research companies - with CFT predictions.

Throughout this report we have dealt solely with non-swelling coals, and have used a "shrinking sphere" combustion sub-model within the CFT code. This sub-model has one coal-dependent parameter which has not yet been subjected to critical assessment, and that is the particle size (diameter) at which the diffusion-controlled "shrinking sphere" mode of combustion should be halted and superseded by the kinetically-limited mode. A critical char particle size is assumed, below which the combustion proceeds with constant size but increasing porosity. Under the CFT model assumptions, this is the point at which coalescence ceases, with eventual fragmentation of the residual char causing each surviving mineral inclusion to become an individual fly ash particle. More information on the validity of choice of this critical core size, and the dependence of the choice on coal type, could be obtained from the expanded data-base mentioned above, or could be gained from specific bench-scale experiments.

An alternative sub-model for cenospheric particle burning (appropriate for swelling coals) has been documented by Monroe (1989), validated over a limited range of coal types. Expansion of the data-base mentioned above may call for CFT calculations that make more frequent use of the cenospheric particle burning sub-model.

More tests would also help in development of new sub-models which could be merged into the existing code. These sub-models include slagging, tube corrosion, mineral matter evaporation, and sintering of deposits. Expansion of the CFT model in such directions, with concomitant increasing complexity of the code, would make the use of faster machines (e.g. DEC 5000/250) more desirable. Compatibility problems may then prompt revisions to the CFT code in order to develop a version suitable for computers using the Ultrix operating system.

7.2 Recommendations

Future research activity in this area of coal combustion should address the issues raised in the closing paragraphs of the above summation. The first steps taken could include the following:

1) Expansion of the coal data-base, and validation of CFT predictions by comparison with the newer experimental results.

2) Assessment of the choice of critical char size for different coal types.

3) Development of sub-models for sintering, and acquisition of a data-base on hardened deposits for comparison with CFT predictions that include sintering.

4) Extension of the measurement temperature range, to obtain experimental data at temperatures where slagging becomes the ash-behavior problem of interest.

8. REFERENCES

Barta, L.E., G. Vámos, M.A. Toqan, J.D. Teare, J.M. Beér and A.F. Sarofim; "A Statistical Investigation on Particle-to-particle Variation of Fly ash Using SEM-AIA-EDAX Technique". MATERIALS RESEARCH SOCIETY, 1989. Fall Meeting, Boston, Paper W1.6.

Barta, L.E., F. Horváth, J.M. Beér and A.F. Sarofim; Mineral Matter Distribution in Individual Pulverized Coal Particles; Application of the "URN" model. Presented at the "Twenty-third International Symposium on Combustion". Orléan, France July 22-27, 1990.

Barta, L.E. and J.M. Beér; "Distribution Functions of Chemical Compounds and Viscosity of Fly Ash Originated from Monosize Coal Particles in the Case of Total Mineral Coalescence", Internal Report, MIT Cambridge, MA, June, 1990.

Barta, L.E., Toqan M.A., Beér and Sarofim A.F;" Transformation of Mineral Matter during Combustion of Parent and Beneficiated Upper Freeport Coal". 16th International Conference of Coal and Slurry Technologies. US-DOE Clearwater, FL. Apr. 22-25, 1991.

Barta, L.E., M.A. Toqan, J.M. Beér and A.F. Sarofim; " Prediction of Fly Ash Size and Chemical Composition Distribution; the Random Coalescence Model". Twenty-Fourth International Symposium on Combustion. Sydney, Australia, July 5-10, 1992.

Beér, J.M., L.S. Monroe, L.E. Barta and A. S. Sarofim, "From Coal Mineral Properties to Fly Ash Deposition Tendencies: A Modeling Route". Seventh Annual International Pittsburgh Coal Conference, U.S. DOE, Pittsburgh, PA, Sept. 1990.

Beér, J.M., A.F. Sarofim and L.E. Barta; "From Properties of Coal Mineral to Deposition Tendencies of Fly Ash - A Modelling Route", Journal of Institute of Energy, pp. 55-62, March 1992.

Borio, R.W. and R.R. Narciso; "The Use of Gravity Fractionation Techniques for Assessing Slagging and Fouling Potential of Coal Ash, Transactions of the ASME", Journal of Engineering for Power, Vol. 101, pp. 500-505, October, 1979.

Bryers, R.W. and T.E. Taylor; "An Examination of the Relationship Between Ash Chemistry and Ash Fusion Temperatures in Various Coal Size and Gravity Fractions Using Polynomial Regression Analysis", Transactions of the ASME, Journal of Engineering for Power, pp. 528-539, October, 1976.

Charon, O., A.F. Sarofim and J.M. Beér; "Distribution of Mineral Matter in Pulverized Coal".Progress in Energy and Combust. Sci.. vol. 16, pp. 319-326, 1990.

Dinger, D.R.; "New Stereological Methods for Obtaining 3-Dimensional Grain Size Distributions and Shape Factors from Planar Section: Application to Characterization of Mineral Matter in Coal", Ph.D. Thesis, Pennsylvania State University, November 1975.

Field, M.A., Gill, D.W., Morgan, B.B., and Hawksley. P.G.W.: "Combustion of Pulverized Coal", Published by the British Coal Utilization Research Association, Leatherhead, Surrey, England, p. 155, 1967.

Huffman, G.P. and F.E. Huggins; "Analysis of the Inorganic Constituents in Low-Rank Coals", In: H.H. Schobert, Ed., The Chemistry of Low-Rank Coal, ACS Advances in Chemistry Series, American Chemical Society, Washington, DC., pp. 159-174, 1984.

Horváth F. Personal communication, 1989.

Huggins, F.E., D.A. Kosmack, G.P. Huffman and R.J. Lee; "Coal Mineralogies by SEM Automated Image Analysis, Scanning Electron Microscopy", 1980, Vol. 1., pp. 531-540.

Israel, R. and D.E. Rosner; "Use of a Generalized Stokes Number to Determine the Aerodynamic Capture Efficiency of Non-Stokesian Particles from a Compressible Gas Flow, Aerosol Science and Technology, 2, pp. 45-51, 1983.

Kang, Shin-Gyoo, J.J. Helble, A.F. Sarofim and J.M. Beér; "Time Resolved Evolution of Fly Ash During Pulverized Coal Combustion". Twenty-Second Symposium (International) on Combustion. The Combustion Institute 1988, pp. 231-238.

Kerstein, A.R. and S. Niksa, "Prediction and Measurement of the Critical Porosity for Fragmentation During Char Conversion", Proceedings of the 1983 International Conference on Coal Science, International Energy, Pittsburgh, PA, 743, 1983.

King, R.P.; "Determination of the Distribution of Size of Irregularly Shaped Particles from Measurements of Sections or Projected Areas", Powder Technology, 32, pp. 87-100, 1982.

Klyachko, L., Otopl i. ventil., No. 4, 1934, Cited by N.A. Fuchs in The Mechanics of Aerosols, Pergamon Press/Macmillan, NY, 1964, p. 33.

Langmuir, I. and K. Blodgett; "A Mathematical Investigation of Water Droplet Trajectories", Tech. Rep. No. 5418, Air Material Command, Army Air Forces, Feb. 1946.

Lee, R.J. and J.F. Kelly; "Overview of SEM-Based Automated Image Analysis, Scanning Electron Microscopy", 1980, Vol. 1, pp. 303-510.

Loehden, D.O., P.M. Walsh, A.N. Sayre, J.M. Beér and A.F. Sarofim, "Generation and deposition of fly ash in the Combustion of Pulverized Coal". Journal of the Institute of Energy. June 1989, pp. 119-127.

Loehden, D.O.; "The Formation of Fouling and Slagging Deposits in Pulverized Coal Combustion", M.S. Thesis, Department of Mechanical Engineering, MIT, 1988.

Monroe, L.S.; "An Experimental and Modeling Study of Residual Fly Ash Formation in Combustion of a Bituminous Coal", Ph.D. Thesis, MIT, 1989.

Moza, A.K., L.G. Austin, and G.C. Johnson, Jr.; "Inorganic Element Analysis of Coal Particles Using Computer Evaluation of Scanning Electron Microscopy Images, Scanning Electron Microscopy", 1979, Vol. 1, pp. 473-476.

Srinivasachar, S., M.A. Toqan and J.M. Beér; "Percolation Model for Coal Char Particle Combustion and Fragmentation", Combustion Sci. and Tech., 57, Nos. 1-3, pp. 55-79, 1988.

Watt, J.D. and F. Fereday; "The Flow Properties of Slags Formed from the Ashes of British Coals: Part 1. Viscosity of Homogeneous Liquid Slags in Relation to Slag Composition". Journal of the Institute of Fuel. March 1969.

Wibberly, L.J.; "Alkali Ash Reactions and Deposit Formation in Pulverized Coal Fired Boilers", Ph.D. Thesis, Department of Chemical Engineering, University of Newcastle, N.S.W., Australia, 1980.

8.1 Prior Reports on "Coal Mineral Matter" Project

Walsh, P.M., D. Loehden, A.N. Sayre, L.S. Monroe, J.V. Gobbell, J.M. Beér and A.F. Sarofim; "Comprehensive Studies of Coal Mineral Matter Behavior During Combustion", EP84-12, The Energy Laboratory, Massachusetts Institute of Technology, Cambridge, MA, April 24, 1987.

Walsh, P.M., L.E. Barta, J.M. Beér and A.F. Sarofim, "The Transformation of Minerals during Coal Combustion: Effects on Fouling and Slagging", Final Report of Massachusetts Institute of Technology, Cambridge, MA, July 20,1989.

Walsh, P.M., A.N. Sayre, J.M. Beér, and A.F. Sarofim, "Effects of Coal Type and Combustion Oxidations of Fouling and Slagging", EP87-31, The Energy Laboratory, Massachusetts Institute of Technology, Cambridge, MA, May 1989.

Appendix A. Calculation of Fly Ash Properties

Fly Ash Size Distribution

During the burnout of a coal particle, random coalescence of mineral inclusions takes place which reduces the number of inclusions. In the description of a model of the coalescence process two groups of mineral particles can be distinguished. One of these consisting of "n" particles is named the "acceptor" group, and the other in which there are "Δn" inclusions is called the "captured" group. The particles in these groups are referred to as "acceptor" and "captured" inclusions, respectively. Both groups of particles have the same size and chemical composition distributions. This reduction in the number of inclusions can be given as:

$$n_o = n + \Delta n \qquad (1)$$

where

n_o : *the number of inclusions before coalescence,*

n : *the number of inclusions after coalescence,*

Δn: *the number of captured inclusions.*

The captured particles are distributed randomly onto the acceptor particles of size x_i ; the number of acceptor particles with size x_i is n_i. The probability of coalescence between these two groups can be given as the fractional surface area ($p(x_i)$) of the particles with size x_i in the acceptor group.

The above formulation of the problem renders it amenable to the application of the "urn" model. This method of probability distributions has been discussed by Barta et al, 1990 in an application of determining the distributions of mineral inclusion particles in pulverized coal. In the present case, we consider the distribution of $\Delta n * p(x_i)$ particles having a size distribution of f(x) onto n_i acceptor particles. The total volume of captured particles that an acceptor particle can receive can be expressed as a gamma random variable with a mean value and variance as given by the equations below.

$$E(v_i) = \Delta n * p(x_i) * \frac{1}{n_i} * M_3 * \frac{\pi}{6} \qquad (2)$$

$$Var(v_i) = \Delta n * p(x_i) * \frac{1}{n_i} * M_6 * (\frac{\pi}{6})^2 \qquad (3)$$

$$p(x_i) = \frac{n_i * x_i^2}{n * M_2}$$

where

v_i : *volume of captured inclusions coalesced with acceptor inclusions of size* x_i;

M_2 : *the second moment of the size distribution of the captured inclusions;*

M_3 : *the third moment of the size distribution of the captured inclusions;*

M_6 : *the sixth moment of the size distribution of the captured inclusions;*

The fly ash size distribution emerging from the above allocation of the captured particles can be obtained by determining the distribution of the total volume of a fly ash particle after coalescence. The total volume of a single fly ash particle can be given as:

$$v_i^T = \frac{x_i^3 * \pi}{6} + v_i \qquad (4)$$

where

v_i^T : *the total volume of a fly ash particle after the coalescence of the captured inclusions with the acceptor particles of size* x_i ;

The distribution function of the random variable ν_i^T can be obtained directly from the distribution function of ν_i. Let γ_i be the size of a fly ash particle after the coalescence of acceptor particles of size x_i with the captured particles. The cumulative distribution of γ_i can be obtained by determining the probability of the event ($\gamma_i < y$), which equals that of ($\nu_i^T < y^3 * \pi/6$):

$$Prob.(\gamma_i<y)=Prob.(v_i^T<\frac{y^3*\pi}{6}) \qquad (5)$$

By substituting the Equation (4) into Equation (5), the following is obtained:

$$Prob.(\gamma_i<y)=Prob.(\frac{x_i^3*\pi}{6}+v_i<\frac{y^3*\pi}{6}) \qquad (6)$$

and

$$Prob.(\gamma_i<y)=Prob.(v_i<\frac{\pi}{6}*(y^3-x_i^3)) \qquad (7)$$

It was shown by Barta et al. (1990), that ν_i is a compound Poisson variable, which can be approximated by a gamma distribution. Its mean value and variance are given by the Equations 2 and 3, respectively. It follows that the probability specified by Equation (7) can be calculated by the following equation:

$$Prob.(\gamma_i<y)=\begin{pmatrix} 0 & if\ y<x_i \\ \Gamma^*(\alpha(x_i),\lambda*\frac{\pi}{6}*(y^3-x_i^3)) & if\ y\geq x_i \end{pmatrix} \qquad (8)$$

The final size distribution of the fly ash is calculated by the weighted integral of the distribution functions of γ_i for every value of "i". The final result is given by Equations (9,10 and 11):

$$F_{size}(y) = \int_0^y f(x)*\Gamma^*(\alpha(x),\lambda*\frac{\pi}{6}*(y^3-x^3))\,dx \qquad (9)$$

where

$$\alpha(x)=\frac{\Delta n*x^2*M_3^2}{n*M_2*M_6} \qquad (10)$$

$$\lambda=\frac{6*M_3}{\pi*M_6} \qquad (11)$$

Γ^* : *the incomplete gamma function;*

Fly Ash Chemical Composition Distribution

In the derivation of the chemical composition distribution, a similar procedure to that for size distribution is followed, except that in this case a joint size-chemical concentration distribution, f(x,c) is used.

The random coalescence of mineral particles is described in the following by using the urn model and the concept of acceptor and captured particles.

The number of acceptor particles of size y and chemical content c is designated by n(y,c). The probability that the captured particles coalesce with acceptor particles of size y and chemical compound concentration c, is given by the area fraction of these particles: p(y,c) ($= n(y,c)*y^2/n/M_2$). The captured particles of chemical content c_i are distributed randomly onto acceptor particles of size y and chemical compound concentration c. The total volume of captured particles coalesced with acceptor inclusions of size y and concentration c, is approximated by a gamma random variable (μ_i). Its mean value and variance can be given by:

$$E(\mu_i) = \Delta n * f(c_i) * \Delta c_i * \frac{n(y,c)*y^2}{n*M_2} * \frac{1}{n(y,c)} * M_3 * \frac{\pi}{6} \qquad (12)$$

$$Var(\mu_i) = \Delta n * f(c_i) * \Delta c_i * \frac{n(y,c)*y^2}{n*M_2} * \frac{1}{n(y,c)} * M_6 * (\frac{\pi}{6})^2 \qquad (13)$$

Where

μ_i = *the volume of captured inclusions coalesced with acceptor inclusions of size y and concentration c*

$f(c_i)$ = *the number-based frequency function of a chemical compound.*

When an acceptor and a captured particle coalesce, the chemical composition of the emerging fly ash particle can be different from that of its parents. By taking into account the coalescence of the captured particles with all their possible chemical composition (μ_i ,i=1...), the concentration τ, of a chosen chemical compound in a fly ash particle can be given as:

$$\tau = \frac{c*\frac{y^3*\pi}{6} + \sum_i^{\infty} c_i*\mu_i}{\frac{y^3*\pi}{6} + \sum_i^{\infty} \mu_i} \qquad (14)$$

The distribution of τ can be obtained from convolution theory by using the distribution functions of μ_i ($i=1\ldots\infty$).The cumulative distribution function of τ defined by the Equation 14 is calculated by determining the probability of the event ($\tau<t$):

$$Prob.(\tau<t)=Prob.\left(\frac{c*y^3*\pi/6+\sum_i^{\infty} c_i*\mu_i}{y^3*\pi/6+\sum_i^{\infty}\mu_i}<t\right) \qquad (15)$$

To calculate this probability, Equation (15) is rearranged:

$$Prob.(\tau<t)=Prob.(\kappa_1+\kappa_2<\frac{y^3*\pi}{6}*(t-c)) \qquad (16)$$

where

$$\kappa_1=-\sum_1^{j}(t-c_i)*\mu_i \qquad (17)$$

$$\kappa_2=\sum_j^{\infty}(c_i-t)*\mu_i \qquad (18)$$

and

$$c_j=t \qquad (19)$$

κ_1 and κ_2 are random variables. κ_1 can take only negative values while κ_2 is always positive. The distribution function of their convolution specified in Equation (16) can be given by the convolution integral:

$$Prob.(\tau<t)=\int_{-\infty}^{\infty} f_2(x)\int_{-\infty}^{y^3*\pi/6*(t-c)} f_1(u-x)\,du\,dx \qquad (20)$$

where $f_1(x)$ and $f_2(x)$ are the distribution functions of κ_1 and κ_2, respectively. From the definitions of κ_1 and κ_2 (Equations 17 and 18),, it can be seen that they are given by the convolution of the random variables μ_i ($i=1\ldots\infty$). It follows therefore that it is possible to obtain the distributions of κ_1 and κ_2 by using the distribution functions of μ_i ($i=1\ldots\infty$). The distribution function of μ_i is approximated by a gamma distribution and the same approximation is applied for κ_1 and κ_2. The functional forms for $f_1(x)$ and $f_2(x)$ can be given as follows:

$$f_1(x)=\begin{pmatrix} \frac{\lambda_1^{\alpha_1}}{\Gamma(\alpha_1)}(-x)^{\alpha_1-1}e^{\lambda_1 x} & \text{if } x\le 0 \\ 0 & \text{if } x>0 \end{pmatrix} \qquad (21)$$

and

$$f_2(x)=\begin{pmatrix} 0 & \text{if } x\le 0 \\ \frac{\lambda_2^{\alpha_2}}{\Gamma(\alpha_2)}x^{\alpha_2-1}e^{-\lambda_2 x} & \text{if } x>0 \end{pmatrix} \qquad (22)$$

The parameters of the distribution functions such as α_1, α_2, λ_1 and λ_2 are given by using the equations 23-26.

$$\lambda_1=\frac{\int_0^t f(c)*(t-c)*M_3(c)*\frac{\pi}{6}\,dc}{\int_0^t f(c)*(t-c)^2*M_6(c)*(\frac{\pi}{6})^2\,dc} \qquad (23)$$

$$\alpha_1=\frac{\Delta n*y^2}{n*M_2}*\lambda_1*\int_0^t f(c)*(t-c)*M_3(c)*\frac{\pi}{6}\,dc \qquad (24)$$

$$\lambda_2=\frac{\int_t^1 f(c)*(c-t)*M_3(c)*\frac{\pi}{6}\,dc}{\int_t^1 f(c)*(c-t)^2*M_6*(\frac{\pi}{6})^2\,dc} \qquad (25)$$

$$\alpha_2=\frac{\Delta n*y^2}{n*M_2}*\lambda_2*\int_t^1 f(c)*(c-t)*M_3(c)*\frac{\pi}{6}\,dc \qquad (26)$$

where $\frac{\Delta n}{n}$ *is the captured particles as a fraction of the number of acceptors.*

The convolution integral of τ (Equation 20) is calculated by introducing a new variable $z=\lambda_1*(x-u)$:

$$\int_{-\infty}^{y^3\pi/6*(t-c)} f_1(u-x)\,du = \int_{\lambda_1(x-y^3\pi/6*(t-c))}^{\infty} \frac{1}{\Gamma(\alpha_1)} z^{\alpha_1-1} e^{-z}\,dz \qquad (27)$$

which equals to

$$= \begin{pmatrix} 1 & \text{if } x \le y^3\pi/6*(t-c) \\ 1-\Gamma^*(\alpha_1,\lambda_1(x-y^3\pi/6*(t-c)) & \text{if } x > y^3\pi/6*(t-c) \end{pmatrix} \qquad (28)$$

Since $f_2(x)$ equals zero if $x <= 0$ then the convolution integral can simplified by considering the following four cases:

	$x \ge 0 \cap x \le y^3\pi/6(t-c)$	$x \ge 0 \cap x \ge y^3\pi/6(t-c)$
$(t-c) \le 0$	$\varnothing$	$x \ge 0$
$(t-c) \ge 0$	$0 \le x \le y^3\pi/6(t-c)$	$x \ge y^3\pi/6(t-c)$

The convolution integral (Equation 20) is evaluated for each of these regimes, and the integral finally yields the following form:

$$\begin{pmatrix} \int_0^{\infty} f_2(x)*[1-\Gamma^*(\alpha_1,\lambda_1(x-y^3\pi/6(t-c)))]\,dx & \text{if } (t-c)\le 0 \\ \int_0^{y^3\pi/6(t-c)} f_2(x)\,dx + \int_{y^3\pi/6(t-c)}^{\infty} f_2(x)*[1-\Gamma^*(\alpha_1,\lambda_1(x-y^3\pi/6(t-c)))]\,dx & \text{if } (t-c)>0 \end{pmatrix} \qquad (29)$$

By rearranging this equation, the final result can be given as shown in Equations 30 and 31.

$$F_{chem}(t) = \int_0^1 \int_0^{\infty} f(y,c)*g(c,y,t)\,dydc \qquad (30)$$

in which the cumulative distribution of a chemical species after capture by acceptor inclusions of a given size and concentration is expressed as:

$$g(c,y,t) = Prob.(\tau<t) = \qquad (31)$$

$$= \begin{cases} 1 - \int_0^{\infty} \frac{\lambda_2^{\alpha_2}}{\Gamma(\alpha_2)} * x^{\alpha_2-1} * e^{-\lambda_2 * x} * \Gamma^*(\alpha_1, \lambda_1 * (x - \frac{y^3 * \pi}{6} * (t-c))) \, dx & when \quad t \le c \\ 1 - \int_{\frac{y^3 * \pi}{6} * (t-c)}^{\infty} \frac{\lambda_2^{\alpha_2}}{\Gamma(\alpha_2)} * x^{\alpha_2-1} * e^{-\lambda_2 * x} * \Gamma^*(\alpha_1, \lambda_1 * (x - \frac{y^3 * \pi}{6} * (t-c))) \, dx & when \quad t > c \end{cases}$$

Appendix B. Example of an Input Data File

```
 1  CCSEM_FILE_NAME
 2  blend.prb
 3  CCSEM_END_OF_INFO
 4  COAL_SIZE_DISTRIBUTION
 5  NUMBER_OF_DIVISION
 6  7
 7  2.00 0.00
 8  10.00 0.25
 9  20.0  0.48
10  40.0  0.70
11  55.0 0.80
12  85.0 0.90
13  100.0 1.00
14  COAL_SIZE_END_OF_INFO
15  COAL_DENSITY_G/CM3
16  1.35
17  END_OF_INFO
18  TRANSITION_RADIUS_RATIO
19  0.35
20  END_OF_INFO
21  INCLUSION_CONTENT_OF_COAL
22  0.0576
23  END_OF_INFO
24  IONEXCHANGEABLE_MINERAL_CONTENT_OF_COAL
25  0.0227
26  END_OF_INFO
27  POISSON_VARIATION_RATIO
28  1
29  NUMBER OF TRY OF JOINT SIZE AND CHEMICAL COMPOUND
30  10
31  NUMBER OF INTEGRAL DIVISION FOR CHEM>COMPOUND
32  500
33  INTEGRAL MAXIMUM VALUE t<C AND MAXIMUM VALUE t>c
34  5 5000
35  END_OF_INFO
36  CHEMICAL_COMP_OF_IONEXCHANGEABLE
37  COMPOUND__CONC_%
38  NA2O
39  5.0
40  MGO
41  15.0
42  AL2O3
43  00.00
44  SIO2
45  00.00
46  P2O2
47  00.00
48  SO3
49  00.00
50  CL
```

```
00.00
K2O
00.00
CAO
80.0
TIO2
00.00
FEO
00.00
CR2O3
00.00
BAO
00.00
SRO
00.00
MNO
00.00
END_OF_INFO
DEPO_INFO
AIRVELOCITY (m/s)
0.5
TUBE_INNER_RADIUS (m)
0.00635
TUBE_OUTER_RADIUS (m)
0.0127
AIR_INLET_TEMPERATURE (K)
293
INIT_ TUBE_ TEMP__MIN and MAX_ FLUE_GAS_TEMP__DIVISION
1073 1300 1600 20
FLUE_GAS_VELOCITY (m/s)
8.7
DEPOSIT_HEAT_CONDUCTIVITY (W/K/m)
0.5
TUBE_HEAT_CONDUCTIVITY (W/K/m)
45
LENGTH OF TUBE (m)
0.2
TIMEINCREMENT (sec)
2
MAXIMUM_TIME (sec)
10
FLYASH_MASS_FLUXinFLUEGAS (kg/m2/sec)
0.0146
DEPOSIT_DENSITY (kg/m3)
1200
EROSION_FACTOR(number_of_dry_eroded_particle/impacted_dry_particle)
1
MINIMUM _SIZE(um)   MAXIMUM_SIZE (um)
1 40
NUMBER_OF_TIMES_THE_SIZE_VALUE_INCREASE
40
CRITICAL_STICKING_EFFICIENCY_in_log_POISE
5
END_OF_INPUT_FILE
```

Appendix C. Example of an Output Data File

```
"RESULTS"
1   "SIZE DISTRIBUTION"
2   "TOTAL MINERAL MATTER"
3   "SIZE "                  " NUM_BASED"
4   " [um] "                 " [ratio]"
5   9.75786358906101E-0001   1.04728127087744E-0002
6   1.00495389272605E+0000   3.52367390819609E-0002
7   1.03499328237938E+0000   6.20643297400010E-0002
8   1.06593058878020E+0000   8.12961488298463E-0002
9   1.09779265183755E+0000   1.01283441325903E-0001
10  1.13060711374052E+0000   1.27161860949662E-0001
11  1.16440244293950E+0000   1.46081705495667E-0001
12  1.19920795884418E+0000   1.76659682415089E-0001
13  1.23505385725984E+0000   2.05036859014847E-0001
14  1.27197123658401E+0000   2.45372307141914E-0001
15  1.30999212478608E+0000   2.88957902692083E-0001
16  1.34914950719344E+0000   3.15050694271139E-0001
17  1.38947735510817E+0000   3.53987240939350E-0001
18  1.43101065527913E+0000   3.84680903784264E-0001
19  1.47378544025496E+0000   4.12504164950640E-0001
20  1.51783881964446E+0000   4.41480882781818E-0001
21  1.56320901231127E+0000   4.76159919327232E-0001
22  1.60993537953099E+0000   5.10715538654368E-0001
23  1.65805845913937E+0000   5.37150530647510E-0001
24  1.70762000070121E+0000   5.74025647442665E-0001
25  1.75866300173057E+0000   5.99860997819169E-0001
26  1.81123174499357E+0000   6.28147626389278E-0001
27  1.86537183692629E+0000   6.54862503846980E-0001
28  1.92113024720098E+0000   6.92972181351551E-0001
29  1.97855534947499E+0000   7.26224421537099E-0001
30  2.03769696335771E+0000   7.39831231056508E-0001
31  2.09860639763201E+0000   7.54477027087843E-0001
32  2.16133649476753E+0000   7.76167880269806E-0001
33  2.22594167676464E+0000   7.96584342004377E-0001
34  2.29247799236866E+0000   8.15080282226503E-0001
35  2.36100316569540E+0000   8.27477704388969E-0001
36  2.43157664631019E+0000   8.47959777502534E-0001
37  2.50425966080381E+0000   8.62001300387954E-0001
38  2.57911526591016E+0000   8.72806251676385E-0001
39  2.65620840321156E+0000   8.87159400408139E-0001
40  2.73560595547942E+0000   8.98434115303524E-0001
41  2.81737680469887E+0000   9.10354530118513E-0001
42  2.90159189182791E+0000   9.16424281168393E-0001
43  2.98832427834278E+0000   9.23293780457629E-0001
44  3.07764920962308E+0000   9.31399096580977E-0001
```

45	3.16964418023147E+0000	9.39713424578830E-0001
46	3.26438900114468E+0000	9.44654440055333E-0001
47	3.36196586899421E+0000	9.52032281597913E-0001
48	3.46245943737668E+0000	9.55431287760262E-0001
49	3.56595689029569E+0000	9.60355833650578E-0001
50	3.67254801779904E+0000	9.63957118176845E-0001
51	3.78232529387680E+0000	9.67823862960005E-0001
52	3.89538395668787E+0000	9.73073791647582E-0001
53	4.01182209118460E+0000	9.74906376449728E-0001
54	4.13174071420720E+0000	9.78085966541596E-0001
55	4.25524386212168E+0000	9.80497162123388E-0001
56	4.38243868107745E+0000	9.82494707895127E-0001
57	4.51343551996284E+0000	9.84439358763851E-0001
58	4.64834802613916E+0000	9.86642123663372E-0001
59	4.78729324403635E+0000	9.87866605654216E-0001
60	4.93039171669587E+0000	9.89351981574830E-0001
61	5.07776759034873E+0000	9.91954015778820E-0001
62	5.22954872211961E+0000	9.92796125814853E-0001
63	5.38586679095027E+0000	9.93612573581348E-0001
64	5.54685741183874E+0000	9.94400794151297E-0001
65	5.71266025349316E+0000	9.95173698992499E-0001
66	5.88341915950251E+0000	9.95670175614798E-0001
67	6.05928227312926E+0000	9.95913166288893E-0001
68	6.24040216583227E+0000	9.96384519605813E-0001
69	6.42693596963134E+0000	9.96838642551394E-0001
70	6.61904551342844E+0000	9.97727361907527E-0001
71	6.81689746340359E+0000	9.97727361907527E-0001
72	7.02066346760748E+0000	9.97936459783177E-0001
73	7.23052030487614E+0000	9.98137509122285E-0001
74	7.44665003819681E+0000	9.98137509122285E-0001
75	7.66924017265814E+0000	9.98897569291874E-0001
76	7.89848381812179E+0000	9.99270183490102E-0001
77	8.13457985675638E+0000	9.99270183490102E-0001
78	8.37773311557937E+0000	9.99270183490102E-0001
79	8.62815454415634E+0000	9.99270183490102E-0001
80	8.88606139761202E+0000	9.99435306169632E-0001
81	9.15167742511169E+0000	9.99435306169632E-0001
82	9.42523306397660E+0000	9.99435306169632E-0001
83	9.70696563960171E+0000	9.99435306169632E-0001
84	9.99711957134921E+0000	9.99435306169632E-0001
85	1.02959465845966E+0001	9.99578836353377E-0001
86	1.06037059291229E+0001	9.99578836353377E-0001
87	1.09206646040230E+0001	9.99578836353377E-0001
88	1.12470975893450E+0001	9.99710016262604E-0001
89	1.15832880846510E+0001	9.99710016262604E-0001
90	1.19295277547096E+0001	9.99831946362621E-0001
91	1.22861169825315E+0001	9.99831946362621E-0001
92	1.26533651299699E+0001	9.99831946362621E-0001
93	1.30315908061090E+0001	9.99831946362621E-0001
94	1.34211221436766E+0001	9.99831946362621E-0001
95	1.38222970837180E+0001	9.99831946362621E-0001
96	1.42354636687795E+0001	9.99831946362621E-0001
97	1.46609803448552E+0001	9.99831946362621E-0001
98	1.50992162723605E+0001	9.99831946362621E-0001
99	1.55505516463993E+0001	9.99831946362621E-0001

100	1.60153780266058E+0001	9.99831946362621E-0001
101	1.64940986768453E+0001	9.99919938011604E-0001
102	1.69871289150686E+0001	9.99919938011604E-0001
103	1.74948964736247E+0001	9.99919938011604E-0001
104	1.80178418703435E+0001	1.00000000000000E+0000
105	"FLY ASH"	
106	"SIZE "	" NUM_BASED" " VOL_BASED"
107	" [um] "	" [ratio]" " [ratio]"
108	1.00000000000000E+0000	4.44693638180574E-0003 1.19689721191016E-0006
109	1.09660822712431E+0000	2.37046779583460E-0002 7.18091725549896E-0006
110	1.20254960379680E+0000	4.48447114759270E-0002 1.58432058488924E-0005
111	1.31872578904949E+0000	7.71679841199219E-0002 3.33091750022959E-0005
112	1.44612554959167E+0000	1.05893159126828E-0001 5.37793288921109E-0005
113	1.58583317513694E+0000	1.35854375036146E-0001 8.19347546452536E-0005
114	1.73903770670222E+0000	1.67074098636690E-0001 1.20622243001430E-0004
115	1.90704305644977E+0000	1.98158287722248E-0001 1.71420737328159E-0004
116	2.09127910518146E+0000	2.27067353975169E-0001 2.33721525005215E-0004
117	2.29331387195634E+0000	2.55729515187128E-0001 3.15177512157961E-0004
118	2.51486685936470E+0000	2.83697367579509E-0001 4.19992971197093E-0004
119	2.75782368810178E+0000	3.11969482229830E-0001 5.59722206556542E-0004
120	3.02425214533287E+0000	3.42097043696431E-0001 7.56076893027855E-0004
121	3.31641978347034E+0000	3.75108451252520E-0001 1.03980141822649E-0003
122	3.63681321914919E+0000	4.07971405287570E-0001 1.41227377819272E-0003
123	3.98815929663397E+0000	4.46555171962232E-0001 1.98896828744499E-0003
124	4.37344829577341E+0000	4.84612058717645E-0001 2.73908780292619E-0003
125	4.79595938204875E+0000	5.26313220635268E-0001 3.82301037791626E-0003
126	5.25928851530625E+0000	5.66334293819238E-0001 5.19482367071865E-0003
127	5.76737905470509E+0000	6.03010481722754E-0001 6.85266610890425E-0003
128	6.32455532033782E+0000	6.31538210363888E-0001 8.55318643046818E-0003
129	6.93555939718499E+0000	6.61701525183017E-0001 1.09242781285562E-0002
130	7.60559149466280E+0000	6.90332634130763E-0001 1.38922637744268E-0002
131	8.34035420519649E+0000	7.13137436331380E-0001 1.70097467464168E-0002
132	9.14610103855375E+0000	7.36942883098193E-0001 2.13012408680325E-0002
133	1.00296896449872E+0001	7.51064053493104E-0001 2.46582939374616E-0002
134	1.09986401801871E+0001	7.64640877155676E-0001 2.89146666404910E-0002
135	1.20611993087805E+0001	7.74597736163455E-0001 3.30310738723264E-0002
136	1.32264103909984E+0001	7.89326989777727E-0001 4.10613580094307E-0002
137	1.45041904500831E+0001	8.02883658413372E-0001 5.08080687493752E-0002
138	1.59054145753471E+0001	8.26295606939196E-0001 7.30052139322678E-0002
139	1.74420084791491E+0001	8.40381653080877E-0001 9.06169739871486E-0002
140	1.91270499957900E+0001	8.54976939454271E-0001 1.14681711856893E-0001
141	2.09748803860275E+0001	8.71116616358301E-0001 1.49774481236563E-0001
142	2.30012263942626E+0001	8.87697024258214E-0001 1.97315978842395E-0001
143	2.52233340978855E+0001	9.06565859878533E-0001 2.68663170440995E-0001
144	2.76601156872639E+0001	9.30578000108644E-0001 3.88397142891752E-0001
145	3.03323104258452E+0001	9.47825181252621E-0001 5.01809146299713E-0001
146	3.32626611606684E+0001	9.62913642993135E-0001 1.00000000000000E+0000

147 "CUMULATIVE CHEMICAL COMPOUND DISTRIBUTIONS"

148 " CONC." " MgO" " Al2O3" " SiO2" " CaO" " FeO"

lines 149-248 - 6 numbers per line to show cumulative distributions of the above compounds

249 DEPOSITION RATE

250 "GasTemp" "Dep_Rate" " Imp_Rate" "Ash_Rate" "Stck_Eff" " Imp_Eff"
251 " [K]" "kg/m2/mn" "kg/m2/mn" "kg/m2/mn" " [wt%]" " [wt%]"

lines 252-271 - 6 numbers per line, to list Gas Temperature, Deposition Rate, Impaction Rate, Ash Flux & Sticking Efficiency